The Genomic Loci *Cer-za* and *Cer-ye* Contribute to Cuticular Wax Biosynthesis in *Hordeum vulgare*

Dissertation

zur

Erlangung des Doktorgrades (Dr. rer. nat.)

der

Mathematisch-Naturwissenschaftlichen Fakultät

der

Rheinischen Friedrich-Wilhelms-Universität Bonn

vorgelegt von

Yannic Müller

aus

Oberhausen

Bonn, April 2022

Angefertigt mit Genehmigung der Mathematisch-Naturwissenschaftlichen Fakultät der
Rheinischen Friedrich-Wilhelms-Universität Bonn

1. Gutachter: Prof. Dr. Peter Dörmann
2. Gutachter: Prof. Dr. Lukas Schreiber
Tag der Promotion: 23.06.2022
Erscheinungsjahr: 2022

Table of contents

List of abbreviations

AA	Amino acid
ACP	Acyl carrier protein
APS	Ammonium persulfate
A. thaliana	*Arabidopsis thaliana*
A. tumefaciens	*Agrobacterium tumefaciens*
ATP	Adenosine triphosphate
AVG	Average
BSR-Seq	Bulked segregant RNA-Seq
BSTFA	*N,O*-Bis(trimethylsilyl)trifluoroacetamide
CA	Contact angle [°]
cDNA	Complementary deoxyribonucleic acid
cds	Coding sequence
cer	*Eceriferum*
CoA	Coenzyme A
CTAB	Cetyltrimethylammonium bromide
dH_2O	Deionized water
ddH_2O	Double-deionized water
DNA	Deoxyribonucleic acid
DPW	Defective pollen wall
DSA	Drop shape analyser
E. coli	*Escherichia coli*
EDTA	Ethylenediaminetetraacetic acid
EPS	Extracellular polymeric substances
ER	Endoplasmic reticulum
EtOH	Ethanol
EW	Epicuticular waxes
FAE	Fatty acid elongase
FAME	Fatty acid methyl ester
FAR	Fatty acyl-CoA reductase
FAS	Fatty acid *de novo* synthesis
FID	Flame ionisation detector
g	Gravitational force equivalent
g_{min}	Minimal leaf water conductance
GC	Gas chromatography
GFP	Green fluorescent protein
gDNA	Genomic deoxyribonucleic acid
HEPES	2-(4-(2-Hydroxyethyl)-1-piperazineethanesulfonic acid
H. vulgare	*Hordeum vulgare*
IW	Intracuticular waxes
IPTG	Isopropyl-β-D-thiogalactopyranoside

KCS	β-Ketoacyl-CoA synthase
m/z	Mass-to-charge
MCS	Multiple cloning site
MES	2-(*N*-morpholino)ethanesulfonic acid
ML	Maximum-Likelihood
MS	Mass spectrometry
MS medium	Murashige and Skoog medium
NAD	Nicotinamide adenine dinucleotide
NADPH	Nicotinamide adenine dinucleotide phosphate
N. benthamiana	*Nicotiana benthamiana*
NGS	Next generation sequencing
OD600	Optical density at a wavelength of 600 nm
ORF	Open reading frame
P_{min}	Minimal water leaf permeability
PAM	Pulse amplitude modulation
PBS	Phosphate-buffered saline
PCR	Polymerase chain reaction
RNA	Ribonucleic acid
rpm	Revolutions per minute
RT	Room temperature
RT-PCR	Reverse transcriptase polymerase chain reaction
RWD	Residual water deficit
S. cerevisiae	*Saccharomyces cerevisiae*
SD	Standard Deviation
SDS	Sodium dodecyl sulfate
Seq	Sequencing
SNP	Single nucleotide polymorphism
SPE	Solid-phase extraction
t	Time
TA	Tilt angle [°]
TEMED	Tetramethylethylenediamine
TM	Transmembrane
TMS	Trimethylsilyl
Tris	Tris(hydroxymethyl)aminomethane
UTR	Untranslated region
VLCFA	Very long-chain fatty acid
v/v	Volume-per-volume
w/v	Weight-per-volume
WT	Wild-type

1 Introduction

By 2090s, it is predicted that the percentage of global surface area exposed to prolonged drought will increase from currently 1-3% to up to 30%, causing the loss of potential arable land concomitant with a predicted loss of up to 30% crop yield until 2025 (Burke, Brown, and Christidis 2006; Zhang and Cai 2011). At the same time, the world population is exponentially increasing and is expected to count approximately nine and a half billion people in 2050, requiring an increase of the current crop yield by up to 70% (Godfray *et al.* 2010). Consequently, the regard of farmers, breeders and scientists is currently shifted to plants which are more adapted to these new circumstances. Former breeding strategies mainly prioritised easily selectable traits related to an increased yield and customer requirements, but at the same time, this strategy was driven at the expense of genetic variability which can provide benefits under varying environmental conditions. Xue *et al.* (2017) already concluded that the identification of novel genes involved in the biosynthesis of cuticular waxes may improve the accessible genetic resources to allow the breeding of more resilient crop plants. *H. vulgare* is the fourth most important crop in terms of global yield. Newton *et al.* (2011) highlighted the increasing relevance of barley for the world's food production in the long-term, based on its ability to adapt to a wide range of stress factors and its worldwide distribution. Accessing novel genetic resources for enhanced stress resilience in common cultivars and wild barley variants has increasingly moved into focus of researchers (Zhao *et al.* 2010; Mansour *et al.* 2018).

1.1 The cuticle – crucial interface between terrestrial plants and their environment

Drought stress causes a broad range of physiological responses. This involves the development of a deep root system (Chloupek *et al.* 2010), adjustment of the water-balance by osmotic changes (Turner 2017) as well as the deposition of cuticular waxes or the cutinisation of leaf surfaces (Srivastava and Wiesenberg 2018). While most of these responses take place on a cellular level, the cuticle as extracellular hydrophobic barrier covering aerial plant tissue forms a direct interface between the plant and its environment. The macrostructure of the cuticle evolved 450 million years ago as a crucial adaptation to enable the colonisation of the terrestrial environment (Graham 1993; Kenrick and Crane 1997; Niklas, Cobb, and Matas 2017). While conditions in a marine environment are rather stable, terrestrial plants are exposed to large temperature fluctuations during the day-and-night and the seasonal cycles, strongly increased UV radiation, and the need to handle highly restricted water availability (Cai *et al.* 2017; Chen *et al.* 2017). The occurrence of cuticles is not just restricted to Spermatophyta, but predecessors of different complexity already occur in algae, mosses and lycophytes (Xue *et al.* 2017). Ancient liverworts did not develop stomata, but their surface was already covered by a hydrophobic cuticle (Chen *et al.* 2017); however, these early extant

species are generally less resistant to drought (Edwards, Abbott, and Raven 1996) and their habitats are often limited to humid and shadowed areas.

1.2 Cuticular macrostructure

The cuticle seals the surface of a plant with a strongly hydrophobic and impermeable barrier composed of different highly structured elements (Figure 1, Schreiber and Schönherr 2009). Its matrix is established by cutin, a biopolymer, synthesized from sn-2 mono(oxygenated)acyl-glycerols (Yeats *et al.* 2014). Carbohydrates extend from the epidermal cell wall and connect the polymer to the underlying cell layer (Segado, Domínguez, and Heredia 2016). This matrix is embedded (intracuticular) and superimposed (epicuticular) with a heterogeneous mixture of cuticular waxes (Riederer and Müller 2008). Depending on the biochemical composition, epicuticular waxes often form crystalline structures in numerous varieties which spike the surface and may establish the well-known Lotus Effect (Barthlott and Neinhuis 1997). Waxes are mainly composed of very long-chain fatty acid (VLCFA) derivatives with chain lengths commonly of C_{20}-C_{34}. The waxes cover a broad range of substance classes dominated by acids, alkanes, alcohols, aldehydes, and exceptionally long-chain esters (C_{38}-C_{70}), but ketones, diols and further metabolites occur in several plant groups as well (Bernard and Joubès 2013; Lai, Kunst, and Jetter 2007). Aliphatic monomers are commonly supplemented with cyclic compounds e.g. flavonoids, sterols or pentacyclic triterpenoids (Walton 1990; Jetter and Schäffer 2001). The cuticular wax composition differs strongly between different plant species, even if they share the same habitat. In addition, wax coverage and composition often differ between different plant organs or organ ontogeny (von Wettstein-Knowles and Netting 1976; Wang *et al.* 2015). The cuticle is a highly dynamic structure, which adapts to changes in environmental conditions including temperature, humidity and light-intensity (Kosma and Jenks 2007; Xu *et al.* 2009; Lee and Suh 2015; Riederer and Schreiber 2001). Individuals of the same species can differ significantly in the biochemical composition of their cuticular waxes in strong dependency of their growth conditions. The wax load of most species was narrowed down to 10-100 µg per cm² surface area, packed to a very thin layer of 10-100 nm thickness (Schreiber and Riederer 1996). Several models for a detailed cuticular macrostructure have been proposed over the past 170 years, but even widely accepted models are still frequently developed today (von Mohl 1874; Jeffree 1986, 2006; Fernández *et al.* 2016).

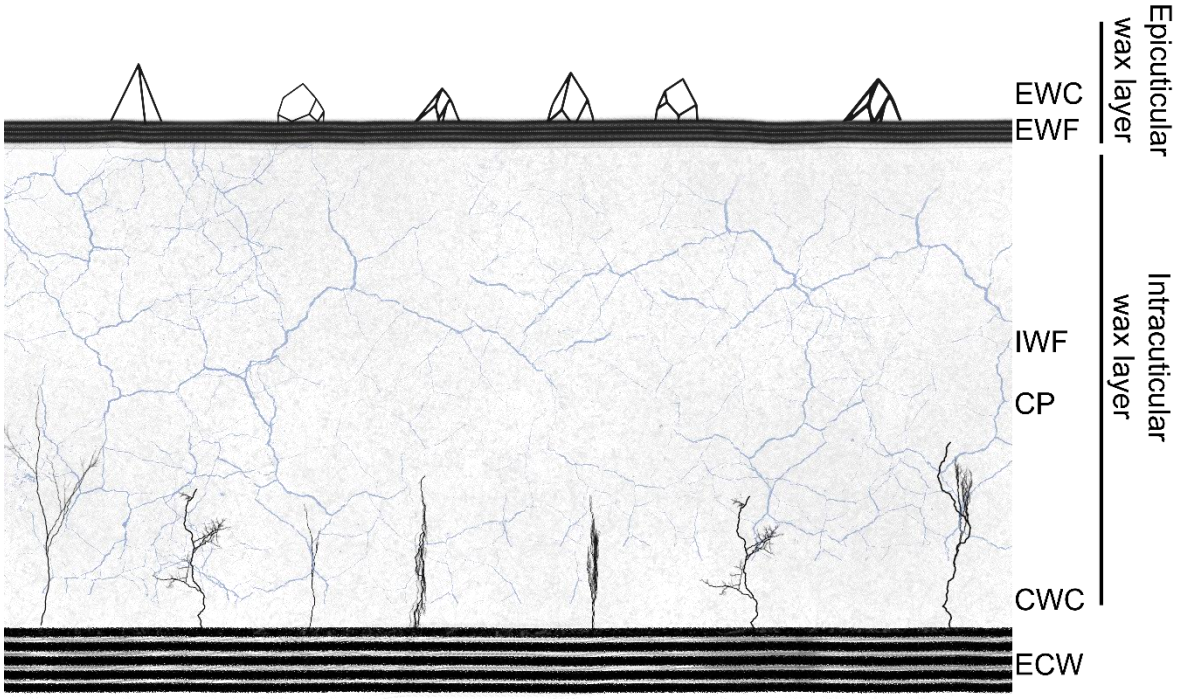

Figure 1: Schematic diagram of the cuticular macrostructure. Structural parameters strongly differ between plant species. The cuticle covers the outer epidermal cell wall (ECW) and is connected by cell-wall anchored carbohydrates (CWC, black). The intracuticular wax layer is built on a cutin matrix (CP, blue) which is embedded with intracuticular waxes (IWF, grey dotted). An epicuticular wax film (EWF) is overlaid, and eventually forms epicuticular wax crystals (EWC) as indicated.

1.3 Biosynthesis pathway of cuticular waxes

1.3.1 Fatty acid *de novo* synthesis

C_{16} and C_{18} acyl-CoAs serve as substrates for the biosynthesis of cuticular waxes. They are derived from the plastidial fatty acid *de novo* synthesis (FAS, Type II; Schultz and Ohlrogge 2002). During fatty acid *de novo* synthesis, acyl chains are elongated by C_2 units in repetitive cycles until palmitoyl-ACP is generated. The C_{16} moiety can undergo one more elongation step to generate stearyl-ACP, most of which is desaturated to oleoyl-ACP by stearoyl-CoA 9-desaturase. The generated acyl-ACPs are further modified either in a plastidial (“prokaryotic”) or a non-plastidial (“eukaryotic”) pathway (Browse and Somerville 1991). The plastidial pathway leads to the generation of phosphatidic acid that is used to generate glycoglycerolipids or phosphatidylglycerol. Acyl chains can be desaturated by fatty acid desaturases (FAD, Ohlrogge and Browse 1995; Mekhedov *et al.* 2000). Alternatively, acyl-ACPs can be hydrolysed by fatty acid thioesterases (FAT) to release the acyl chain and enable the export of the free fatty acids from the plastid (Harwood 2005). Two commonly occurring FATs are well described: while FATA is rather specific for oleoyl-ACP, saturated fatty acids, mostly palmitic acid, are mainly released by FATB (Salas and Ohlrogge 2002; Bonaventure *et*

al. 2003; Serrano-Vega, Garcés, and Martínez-Force 2005). Free fatty acids can be exported from the plastid by FAX1 (fatty acid export 1), or they can cross the plastidial membrane via flip-flop barriers (Cupp, Kampf, and Kleinfeld 2004). Afterwards, acyl-chains are esterified to coenzyme A by long-chain acyl-CoA synthetase (LACS). LACS1, LACS2 and LACS3 have all been associated with the development of a functional cuticle (Pulsifer, Kluge, and Rowland 2012). Acyl-CoAs are imported to the ER where a certain proportion is transesterified to generate phosphatidic acid as precursor for the generation of different phospholipids and storage lipids (Ohlrogge and Browse 1995; Mekhedov *et al.* 2000). Alternatively, acyl-CoAs can be elongated by the fatty acid elongation complex (Joubès *et al.* 2008).

1.3.2 Synthesis of long-chain aliphatic cuticular wax compounds

Acyl-CoAs can be imported to the endoplasmic reticulum (ER). An ER-membrane localised set of fatty acid elongation enzymes (FAEs) catalyses the extension of the C_{16} and C_{18} acyl-CoAs to very long-chain fatty acyl-CoAs (Figure 2, VLCFA-CoAs). Each cycle of reactions adds a C_2 unit to a growing acyl-chain (Joubès *et al.* 2008; Joubès and Domergue 2018). Unlike the FAS reaction of de novo synthesis in the plastid, CoA instead of ACP is used as acyl carrier during the elongation cycle, and malonyl-CoA is employed as carbon source. Each individual FAE consists of a β-ketoacyl-CoA synthase (KCS), β-ketoacyl-CoA reductase (KCR), β-hydroxyacyl-CoA dehydratase (HCD) and an enoyl-CoA reductase (ECR, Millar and Kunst 1997). KCS catalyses the condensation reaction of malonyl-CoA with an acyl-CoA to form a β-ketoacyl-CoA. KCR mediated reduction of the intermediate generates β-hydroxyacyl-CoA, which is converted into enoyl-CoA by β-hydroxyacyl-CoA dehydratase. The final reduction of enoyl-CoA results in an acyl-CoA elongated by two CH_2 units (Joubès and Domergue 2018). Lundqvist and von Wettstein-Knowles (1982) proposed the existence of several FAE complexes with distinct chain length specificities. Correspondingly, an average of 20 KCS members were identified in gymnosperms, 21 in Arabidopsis and 33 in *H. vulgare* and *O. sativa* each (Haslam and Kunst 2013; Guo *et al.* 2016; Lei *et al.* 2021; Tong *et al.* 2021). Several *KCS* genes have been described and were confirmed to be involved in the elongation of fatty acids as precursors for cuticular waxes. Some of the KCS gene products showed partially overlapping functions but distinct chain length specificities, and the activities of some KCS enzymes are mediated by environmental factors (Joubès *et al.* 2008; Haslam and Kunst 2013; Hegebarth and Jetter 2017). The substrate specificity of the overall FAE complex is determined by the incorporated KCS, while KCR, HCD and ECR accept a broad substrate spectrum and are shared by a broad range of the FAE complexes (Kunst and Samuels 2009). *KCS* genes additionally are highly relevant for a wide range of physiological processes. While ectopic organ fusion in the Arabidopsis *fiddlehead 1* mutant indicates a crucial role of *KCS* genes for organ development, knock-out mutations of *KCS2* and *KCS20* lead to the accumulation of C_{20}

acyl-CoAs affecting the biosynthesis of cuticular waxes and suberin (Lee *et al.* 2009; Voisin *et al.* 2009). Although many KCS enzymes have been well characterized, protein-protein interactions between different KCS have rarely been described. Haslam *et al.* (2012) highlighted that none of the characterised enzymes were able to generate VLCFA with chain lengths longer than C_{28}. CER6 was described to be involved in the biosynthesis of VLCFA up to C_{28} for cuticular waxes and root development (Millar *et al.* 1999). Co-expression of CER6 with CER2 and CER2-LIKE enzymes caused a promoting effect and resulted in the synthesis of longer-chained acyl-CoAs (Haslam and Kunst 2020). The mechanism is still unknown, but the authors suggested a stabilising effect of CER2 that enhances the range of accepted substrates by the FAE complex and thereby allows the synthesis of acyl-CoAs with chain lengths above C_{30}.

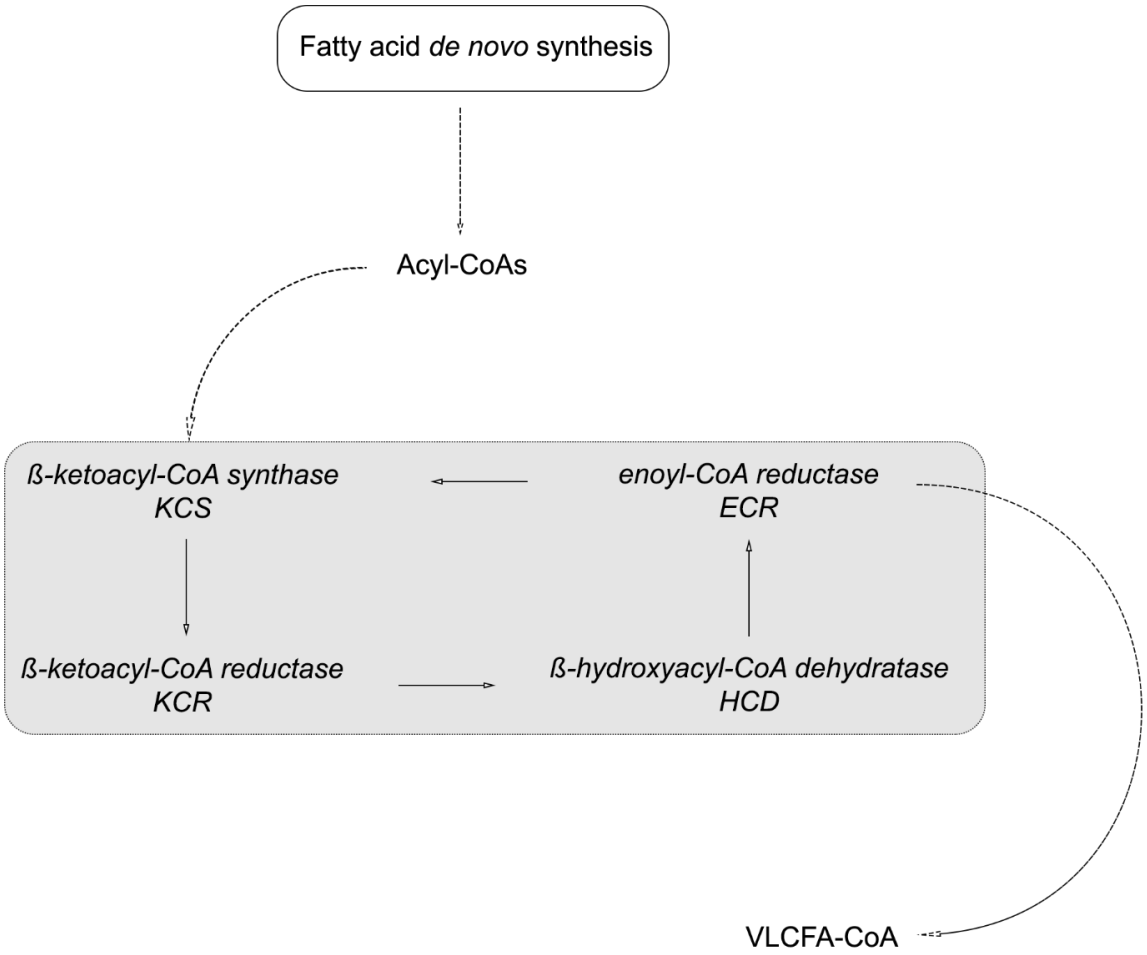

Figure 2: Schematic illustration of the fatty acid elongation complex (FAE). The FAE (grey framed) is composed of four individual proteins. Each cycle expands the acyl-CoAs by C_2 units derived from malonyl-CoA to generate very long-chain fatty acyl-CoAs (VLCFA-CoA).

1.3.3 Synthesis of VLCFA derivatives and export of cuticular wax precursors

During cuticular wax synthesis, VLCFA-CoAs are further modified in two separate pathways: they can either be decarbonylated (decarbonylation pathway) or reduced (reduction pathway, Figure 3). The decarbonylation pathway leads to the generation of odd-chained alkanes, secondary alcohols and ketones (Bernard and Joubès 2013). Initially, CER1 and CER3 form a heterodimer protein complex and catalyse the synthesis of alkanes from VLCFA-CoAs during which an intermediate aldehyde is formed, but not released. Co-expression in recombinant systems showed that CYTB5 acts as redox factor and enhances the catalytic activity of the complex (Bernard *et al.* 2012), while CER1 is an alkane forming enzyme, and the role of CER3 remains unclear. Alkanes are further processed by CYP96A15, a midchain alkane hydroxylase (MAH1). MAH1 forms secondary alcohols and ketones by consecutive oxidation reactions (Greer *et al.* 2007). After formation of the first hydroxyl group, a second germinal hydroxyl group is introduced to the same carbon atom, and after dehydration, the keto group is formed. On the other hand, the reduction pathway mainly generates primary alcohols and alkyl esters (Li *et al.* 2008). In a first step, a fatty acyl-CoA reductase (FAR) synthesises a free primary alcohol from a VLCFA-CoA in an NADPH-dependent reaction with formation of an intermediate aldehyde. In Arabidopsis, the FAR family is composed of eight orthologous genes which show homology to well-characterised FARs from jojoba and wheat (Metz *et al.* 2000; Wang *et al.* 2015). CER4 was the first FAR sequence characterized in Arabidopsis after heterologous expression in *S. cerevisiae* by Rowland *et al.* (2006). CER4 produces C_{24} and C_{26} alcohols. Doan *et al.* (2009) expressed six *At*FAR proteins, including CER4, in *E. coli* and confirmed a reductive activity for five of the enzymes. Most of the *At*FARs are involved in the cuticular wax biosynthesis, but *At*FAR2, encoded by *MALE STERILITY 2* (*MS2*), is crucial for the synthesis of sporopollenin. Sporopollenin contributes to the outer pollen wall and its loss results in a strongly reduced fertility (Aarts *et al.* 1997). The plastidial localised *At*FAR6 protein produces aldehydes instead of primary alcohols and does not contribute to cuticular wax accumulation (Doan *et al.* 2012). After the initial reduction, the alcohols can be esterified to fatty acids by wax ester synthases *WSD*. A family of eleven *WSD* genes was identified in *A. thaliana*. WSD1 is the dominant enzyme in the synthesis of wax esters in shoots and leaves (Li *et al.* 2008; Patwari *et al.* 2019). Since aldehydes are not released from the corresponding enzymes in both the reductive and the decarbonylation pathways, and subsequently used for the next synthesis steps, the existence of an aldehyde forming reductase that contributes to the cuticular wax formation was postulated (Bernard *et al.* 2012; Rowland and Domergue 2012). Also, a portion of acyl-CoAs must be hydrolysed to release free fatty acids by an unknown ER located thioesterase (Joubès and Domergue 2018). The export of the wax compounds to the surface of the leaf or stem is just briefly discussed here. Recent studies indicate a vesicle mediated transport via the ER-Golgi-interface followed by the transit to the plasma membrane

via the trans-Golgi network (McFarlane, Döring, and Persson 2014). Several ATP-binding cassette transporters (ABC), including ABCG11, ABCG12 and ABCG13, were described to be involved in the transport of cuticle precursors across the epidermal membrane (Pighin *et al.* 2004; Bird *et al.* 2007; Panikashvili *et al.* 2011). Further, LTPG1 and LTPG2 (Lipid Transfer Protein; Suh *et al.* 2005; Lee *et al.* 2009; Kim *et al.* 2012) are associated with the export of cuticular wax monomers to the epidermal surface.

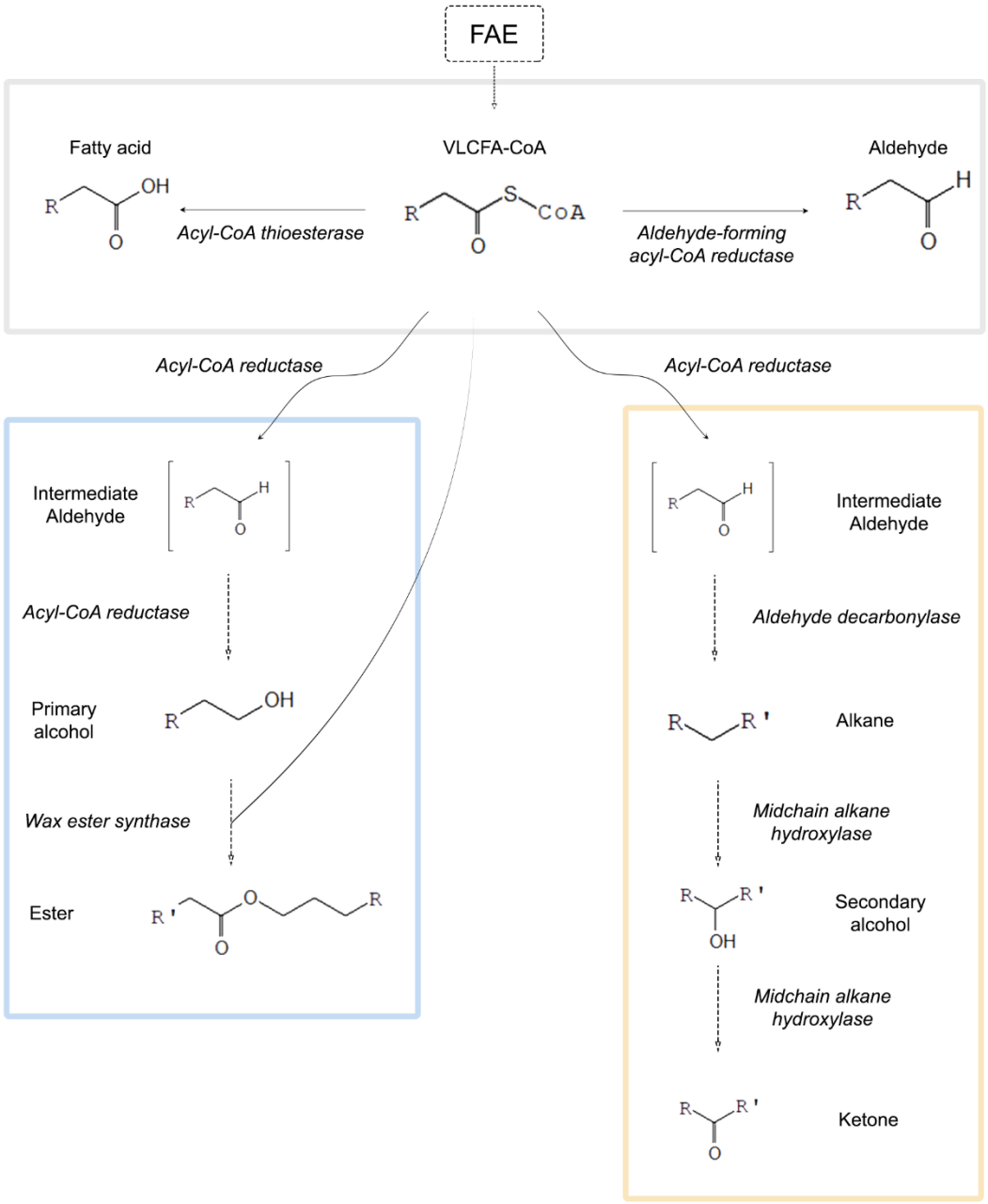

Figure 3: Biosynthesis pathway of cuticular wax monomers. Very long-chain fatty acyl-CoAs (VLCFA) derive from the fatty acid elongation complex (FAE). Acyl chains can either be released or reduced to free aldehydes. Alternatively, VLCFA-CoAs can be modified in the reductive pathway (blue) or in the decarbonylation pathway (orange) to generate different fatty acid derivatives.

1.4 Barrier functions of cuticular waxes

Apoplastic barriers like the cuticle evolved as adaptation to a wide variety of abiotic and biotic stress conditions. Several studies highlighted its essential role in the reduction of non-stomatal water-loss (Riederer and Schreiber 2001; Lee and Suh 2015; Zhang *et al.* 2015), the importance of its macrostructure under high UV radiation (Krauss, Markstädter, and Riederer 1997; Fukuda *et al.* 2008) as well as its ability to provide a self-cleaning effect, commonly known as Lotus effect (Barthlott and Neinhuis 1997). Especially the microorganism-cuticle interactions gained more attention over the last decade and revealed some insights into the relevance of the cuticle for plant pathogen resistance (Vorholt 2012).

1.4.1 Reduction of non-stomatal water-loss

Terrestrial plants are under a constant pressure to monitor, regulate and adapt their transpiration rate to survive in a dehydrating environment. This can be done actively by opening and closing of stomata, but the predominant water-loss occurs across the aerial surface area as the result of an extreme humidity gradient between the plant tissue and the relatively arid atmosphere. The hydrophobic cuticle is capable to drastically decrease this physically driven water-loss (Schönherr and Riederer 1989; Schreiber and Schönherr 2009). Cuticular transpiration rates depend strongly on the ambient temperature, humidity, and light-intensity (Riederer and Schreiber 2001; Schreiber 2005). While the cutin matrix was shown to be highly permeable for water and soluble molecules, the ability of cuticular waxes to establish a hydrophobic barrier was confirmed in several studies (Schönherr 1976; Schreiber and Schönherr 2009). Questions about the functional division of epi- and intracuticular waxes remain still open. While some studies reported a functional barrier dominantly established by intracuticular waxes for several plant species (Zeisler and Schreiber 2016; Zeisler-Diehl, Müller, and Schreiber 2018), others suggested a shared contribution in some species (Jetter and Riederer 2016). Different authors highlighted significant correlations between the wax content, drought tolerance and finally an impact on yield for a broad variety of crop plants including sorghum, barley and wheat (Jordan *et al.* 1984; Richards, Rawson, and Johnson 1986; Febrero *et al.* 1998). Drought conditions were reported to cause an increase of the wax content and thickness as well as compositional changes for several species including Arabidopsis and *Tritium* (Kosma *et al.* 2009; Seo and Park 2011; Zhang *et al.* 2015). Nevertheless, several studies indicated that the cuticular wax thickness itself is not directly correlated with drought tolerance, but rather the biochemical composition (Schreiber and Riederer 1996; Vogg *et al.* 2004). Due to the complexity and variety of the cuticle, detailed knowledge about the interplay of different wax monomers is still missing. An increase in long-chain alkanes was correlated with enhanced drought tolerance (Panikashvili *et al.* 2007; Kosma *et al.* 2009). Further, Patwari *et al.* (2019) suggested a contribution of wax esters to the

transpiration barrier. It is reasonable to assume that especially the implementation of non-polar substances in the cuticular composition can control the formation of penetration pathways of water and solubles through the wax layer. In 1976, Schönherr proposed the existence of 'polar pores'. Since then, several structural models were developed which implemented the formation of polar paths close to hydrophilic domains (Schönherr and Schreiber 2004; Schreiber 2005). A recent study raised the term 'dynamic aqueous continuum' and proposed a continuous network of dendritic aqueous connections mainly formed by hydrophilic domains of epidermal polysaccharides, cutin and trichomes (Fernández *et al.* 2017).

1.4.2 Reduction of UV-radiation

Photosynthesis evolved as a life-forming mechanism to convert energy in form of photons into biochemical energy. Concurrently, enhanced radiation, especially with increased UV-B levels (280-315 nm), can transiently or permanently affect ribulose-1,5-bis-phosphate carboxylase (RuBisCo) activity, inhibit active centres of photosystem II as well as of ATP hydrolysis, decrease the photosynthetic activity and depress plant growth (Barnes, Flint, and Caldwell 1987; Greenberg *et al.* 1989; Tevini and Teramura 1989; Strid, Chow, and Anderson 1990; Jordan *et al.* 1992). It can further affect stomatal gas exchange, and cause severe mutations of the DNA (Saito and Werbin 1969; Pang and Hays 1991). Besides epidermal localised mechanisms, a response in the cuticular wax synthesis evolved to prevent damage caused by radiation (Day, Martin, and Vogelmann 1993; Fukuda *et al.* 2008). These photoprotective cuticular mechanisms are based on the reflection of light by three-dimensional epicuticular wax crystals, and on the accumulation of UV-B absorbing compounds (UACs, Batt *et al.* 1960; Reicosky and Hanover 1978; Krauss, Markstädter and Riederer 1997); thereby, the cuticle enables plants to exclude UV light and reduce the window of radiation to the useable wavelengths of 400-800 nm (Jacobs, Koper, and Ursem 2007). Under high radiation, an increase up to 28% in cuticular wax contents of cucumber, bean and barley was reported by Steinmüller and Tevini (1985). Rozema *et al.* (2009) and Krauss, Markstädter and Riederer (1997) described the accumulation of *p*-coumaric acid and ferulic acid, which are co-polymerised to the cutin polymer, under high radiation levels. This mechanism was already present in extant and fossil trees and was further shown for the ancient *Gingko biloba* (Rozema *et al.* 2001; Blokker *et al.* 2006). Flavonoids can additionally be accumulated in the wax layer. The flavonoids harbour free electron pairs in their conjugated ring structures, which quench a portion of the photon flux. Some authors restrict the relevance of the cuticle as UV photoprotective barrier primarily to heavily glaucous plants. Studies with glaucous and non-glaucous *Picea pungens* species concluded advantages and disadvantages of the reflective properties of epicuticular waxes in strong dependence on the environmental conditions (Reicosky and Hanover 1978; Solovchenko and Merzlyak 2003).

1.4.3 Shaping of superhydrophobic plant surfaces by epicuticular waxes

Dust, biofilms, and water accumulation inhibit gas-exchange and photosynthetic activity of a leaf or can increase the chance of pathogen infections. Nano- and microstructures of a plant surface can curb these threats by formation of low-adhesive surfaces (Gorb *et al.* 2005; Koch and Barthlott 2009). Mainly cell shapes and epicuticular waxes determine the properties of a surface which can range from superhydrophilicity to superhydrophobicity. Barthlott and Neinhuis (1997) analysed the surfaces of a wide spectrum of several hundred species and linked the structural characteristics to the level of water repellence. They described commonly hierarchical structures, based on convex papillose epidermal cells, which are heavily covered with three-dimensional wax crystals and create a superhydrophobic surface. Further, the authors classified the occurring epicuticular waxes and grouped them into 23 different crystal types and subtypes (Barthlott *et al.* 1998). These crystal types ranged from 0.2-100 µm in size (Reynhardt and Riederer 1994; Schreiber, Kirsch, and Riederer 1997) and are formed by self-assembly (Jeffree, Baker, and Holloway 1975; Jetter and Riederer 1994; Koch and Barthlott 2009). A coherence of plant surfaces and their wetting properties was already suggested by Holloway in the early 1980s (Holloway 1969; 1971). Their wetting properties are a result of the balance between adhesive forces, between the liquid and the plant surfaces, and cohesive forces, between the water molecules (Adamson 1990; Israelachvili 1992). On superhydrophobic surfaces, the energy ratio is strongly shifted to the side of enlargement caused by entrapped air in the cavities of the different domains. Water droplets adopt spherical shapes on these surfaces, with a strongly reduced surface adhesion and a consequently very high contact angle above 150° (CA; Extrand 2005; Bhushan and Jung 2008; Nosonovsky and Bhushan 2008). Contact angles are a common measure for the wettability of a surface and were consensually used by several authors to define stages of hydrophobicity (Bhushan and Jung 2007; Koch, Bhushan, and Barthlott 2008; Roach, Shirtcliffe, and Newton 2008). Besides the CA, the tilt angle (TA) is another common measure and describes at which angle of a leaf a liquid rolls off. Plants with a Lotus Effect generally show a TA below 4° (Koch *et al.* 2009). During the roll-off procedure, strong capillary forces drive the admission of particles by the droplets (Pitois and Chateau 2002; Reyssat *et al.* 2008). This self-cleaning property has become a role model for the subject of biomimetics (Forbes 2008; Genzer and Marmur 2008) which resulted in the invention of several surface coatings in industrial scale, that are not just focused on self-cleaning but on the reduction of water resistance. At date of this work, *Salvinia molesta* is under investigation as role model to develop a novel coating which is expected to drastically decrease fuel-consumption and air pollution of industrial ship traffic (Barthlott *et al.* 2010; Oeffner *et al.* 2020).

1.4.4 Microbe-plant contact site

The surface area of the terrestrial mainland was determined as 148.300.000 km². In comparison, the cuticle covered surface area of all leaves was estimated to create a total area 6.8 times larger than that, corresponding to roughly one billion km² (Coble *et al.* 1987, Vorholt 2012). The entirety of aerial wax-covered plant organs was unified as phyllosphere (Ruinen 1961). The phyllosphere provides a habitat for a tremendous amount of epiphyllic bacteria and fungi. Lindow and Brandl (2003) estimated that a single leaf can be densely covered by 10^6 to 10^7 bacteria per cm², even considering that the phyllosphere was categorised as very harsh and unfavourable environment. It can be exposed to high UV radiation, heavily fluctuating temperatures and humidity gradients due to the diurnal cycle (Zeisler-Diehl, Barthlott, and Schreiber 2020). The colonisation on the surface can strongly differ and is rather structured as aggregated biofilms (Kinkel 1997; Morris, Monier, and Jacques 1998; Tecon and Leveau 2012). These aggregates form in particular near trichomes, guard cells and anticlinical cell walls, since those areas offer an enhanced nutrient supply due to an increased leaching of molecules from the leaf interior through the cuticular permeability barrier (Schreiber *et al.* 2005; Schönherr 2006). The overall density of epiphyllic microorganisms was shown to strongly correlate with the leaf surface wettability which strongly depends on the epicuticular macrostructure (Knoll and Schreiber 1998). Several epiphyllic microorganisms evolved the ability to synthesise biosurfactants to enhance their own fitness (Bunster, Fokkema, and Schippers 1989; Bhardwaj, Sharma, and Chauhan 2013; Burch *et al.* 2014). These extracellular polymeric substances (EPS) are generally composed of carbohydrates and increase the wettability of a leaf surface (Lindow and Brandl 2003; Baldotto and Olivares 2008; Vorholt 2012). Many organisms, e.g. the plant pathogen *Pseudomonas syringae*, produce EPS to protect themselves from rapid dehydration and UV radiation (Lindow, Andersen, and Beattie 1993; Hirano and Upper 2000; Morris and Monier 2003). Other plant pathogens adapted to their host's specific cuticles and utilise characteristic compounds as recognition sites. Germination and penetration of *Blumia graminis* was reported to be triggered by very long-chain C_{26} aldehydes and alcohols which belong to the main compounds of the cuticular wax fraction of *H. vulgare* (Zabka *et al.* 2008; Hansjakob *et al.* 2010; Hansjakob, Riederer, and Hildebrandt 2011). Studies correlated a reduction of these VLCFAs in *H. vulgare* cuticular wax fractions with decreased germination rates of powdery mildew (Weidenbach *et al.* 2014; Li *et al.* 2018).

1.5 *A. thaliana* and *H. vulgare* as model systems for cuticular wax studies

The dicotyledonous *Brassicaceae* plant *Arabidopsis thaliana* has been the preferred model plant for many researchers over decades. Its relatively small and diploid nuclear genome (125 megabases) was sequenced in course of the Arabidopsis Genetic Initiative (AGI) in 2000. The genome harbours relatively few repetitive DNA sequences and contains approximately 25,500 genes, localized to five chromosomes. A short reproductive cycle of 6-8 weeks and its easy genetic mutability make it a time-efficient system for fundamental studies on genetics and molecular biology of flowering plants (The Arabidopsis Genome Initiative 2000). This also applies to studies on the synthesis of cuticular waxes. Mutagenetic approaches generated at least 120 cuticular wax mutants and allowed the identification of over 30 wax-related loci (Jennks, Eigenbrode, and Lemieux 2002). This large genetic resource has enabled researchers to widely clarify the biosynthetic pathway of the cuticle in Arabidopsis by characterization of key enzyme families and to generate knowledge that can be transferred to economical relevant species. The *Pooideae* plant barley (*Hordeum vulgare*) is the globally fourth most relevant cereal crop species in terms of yield after wheat (*Triticum aestivium)*, rice (*Oryza sativa)* and maize (*Zea mays*) (Langridge 2018). Barley is a diploid organism and has seven chromosomes with a haploid genome size of 5.3 gigabases (Monat *et al.* 2019). Its diploidity makes it a simpler model for genetic studies compared to the closely related hexaploid *Tritium aestivium*. Due to these benefits, barley is considered one of the best cereal systems for various research fields, and its genome has been fully sequenced (Gubatz *et al.* 2007, Sreenivasulu *et al.* 2008b). Currently, the best barley genome assembly data are available for the Morex cultivar with a coverage of 97.1% of full-length cDNAs (Morex V2, Monat *et al.* 2019). However, barley was already used to study cuticular wax synthesis long before its genome sequence became available (Richardson *et al.* 2005). Its leaf wax composition is heavily dominated by 1-hexacosanol (26:0-ol alcohol) that accounts for up to 75% of the total wax load in some cultivars and forms distinct epicuticular crystals. The cuticular wax composition was reported to differ between leaves and reproductive organs; especially striking is the replacement of 1-hexacosanol by hentriacontane-14,16-dione in spike cuticular waxes (Mikkelsen 1979).

1.6 *Eceriferum* mutants in *H. vulgare*

Secreted cuticular waxes represent a major barrier between plants and their environment. Over decades, scientists investigated the underlying biosynthetic genetic mechanism mainly utilizing *A. thaliana*. A changing climate increasingly challenges researchers to move their focus to economically relevant crop plants to improve our understanding for stress factors with the goal to develop new breeding strategies. In this regard, widely accessible genetic collections are a valuable source for researchers world-wide. One of these collections goes back to the Scandinavian mutation program, which reached its peak back in the 1950s to 1970s. Under direction of the Swedish researchers H. Nilsson-Ehle and A. Gustafsson, an impressive collection of over 10,000 different mutants was created by using radiation and different mutagenetic chemicals (Lundqvist 2014). The Scandinavian researchers categorised the mutants into sub-collections. The largest one is the group of *eceriferum* (wax-less, glossy) mutants, harbouring 1580 different alleles localized with genetic markers to 79 loci. Unfortunately, the use of a high number of cultivars with different genetic backgrounds during mutagenesis impeded the direct comparison of the original mutagenized plants. Druka *et al.* (2011) aimed to overcome this issue with the creation of a Near Isogenic Line (NIL) population containing a NIL for each mutation. The 'Bowman NILs' collection is derived from marker-supported, recurrent backcrosses of the original mutant plant to the American cultivar Bowman. It contains 881 backcrossed NILs of different genetic complexity, reaching from F1 inbreds to ten times backcrossed lines. The plants were grouped according to their phenotypes. The second largest category are the *eceriferum* (*cer*) lines with 93 wax mutants associated to different loci. Some of the *cer* lines were used to identify key genes contributing to the cuticular wax pathway in barley, e.g. genes coding for key enzymes as diketone synthase (*Cer-c*), lipase/carboxyl transferase (*Cer-q*), or P450 enzymes (*Cer-u*, Schneider *et al.* 2016). More recently, *Cer-zh* was shown to encode a β-ketoacyl CoA-synthase (Li *et al.* 2018).

In a previous work, approximately 20 of these Bowman *eceriferum* (*cer*) mutant lines were screened for conspicuities in their cuticular wax compositions (Patwari 2019). Part of these efforts was the visualisation of surface structures via scanning electron microscopy; thereby, significant reductions of crystalline structures were observed for some of the investigated *cer* lines (Figure 4). Finally, this approach moved the two lines *cer*-za.227 and *cer*-ye.267 to the centre of the present study. These two lines are originally derived from ethylene imine induced mutational events in the barley cultivar Foma, and for both, *cer*-za.227 and *cer*-ye.267, seven-times backcrossed Bowman NILs are available. For *cer*-za, 54 alleles in various cultivars were originally pre-mapped based on SNP markers, while for *cer*-ye just four further alleles were annotated (Barley Genetic Newsletter Vol. 48).

Figure 4: Adaxial leaf surfaces of the cultivar Bowman and the *cer* lines za.227 and ye.267 of *H. vulgare* (NILs in Bowman background) visualised with a scanning electron microscope. A reduction in crystalline structures becomes visible in comparison to the Bowman cultivar. Scale bar: 10 µm. Photos were modified from Patwari (2019).

1.7 Aim of the study

The two *eceriferum* loci *cer-za* and *cer-ye* were suggested to be involved in the biosynthesis of cuticular waxes (Patwari 2019), but the identities of the genes *Cer-za* and *Cer-ye* as well as their function remained unclear. Following on from this, three overarching objectives were addressed in the present study; initially, it was aimed to identify the gene responsible for the origin of the *eceriferum* phenotypes. In this process, a bulked segregant analysis combined with next generation sequencing was performed to map mutational events and finally identify genes of interest. Bioinformatical resources were utilised to predict both, mutational impact as well as gene products and putative functions. Additionally, a wide spectrum of biological databases was employed to classify phylogenetic relationships and evolutionary events. Protein prediction tools were used supportively to set up experiments to confirm the roles of presumed gene products during wax synthesis. This included subcellular localization studies, allelism tests as well as analytical approaches after heterologous expression in recombinant host organisms. Besides, detailed biochemical analyses allowed to narrow down the impact of the affected gene product on the composition of the cuticular wax fractions. Since changes in wax composition can strongly affect the structure and barrier properties of the cuticle, physiological experiments were performed to determine the impact on the protective properties in the *cer* lines. Overall, this study aims to contribute to the knowledge about the biosynthesis of cuticular waxes in *H. vulgare* as well as about the functional impact of structural details of the wax layer.

2 Material and Methods

2.1 Lists of materials

2.1.1 List of consumables

Trade name	Specifications	Supplier
96-well plate		Applied Biosystems™ / Thermo Fisher Scientific Inc., Waltham, US
Autoclave tape		Labomedic GmbH, Bonn, DE
Centrifuge tubes	15 mL	SARSTEDT AG & Co. KG, Nürnbrecht, DE
	50 mL	
Cryo Vials	1.8 mL	STARLAB GmbH, Hamburg, DE
Disposable glass vials	100x12 mm	Assistant™ Fisher Scientific GmbH, Schwerte, DE
ED73 soil		Nitsch & Sohn GmbH, Kreuztal, DE
Electroporation cuvettes	1 mm	Bio-Budget Technologies GmbH, Krefeld, DE
Glass inlets	conical	VWR International GmbH, Darmstadt, DE
	flat	
Glass Pasteur pipettes	145 mm	BRAND GmbH & Co., Wertheim, DE
	225 mm	
Glass beads		Sigma-Aldrich Chemie GmbH, Taufkirchen, DE
Glass vials	12x100 mm	Kimble® DWK Life Sciences, Wertheim, DE
Semi micro cuvettes	1.6 mL	Greiner Bio-One GmbH, Frickenhausen, DE
Leukotape	1.25 cm	Duchefa Biochemie B.V., Haarlem, NL
	2.5 cm	
Lids		VWR International GmbH, Darmstadt, DE
MCE membrane	0.025 µM	Merck KGaA, Darmstadt, DE
Nematodes (*Steinernema feltiae*)		Katz Biotech AG, Baruth, DE
Nitril gloves, M		Th. Geyer GmbH & Co. KG, Renningen, DE
Nitrocellulose blotting membrane	0.45 µm, 300 mm x 4 m	Amersham™Protran™, GE Healthcare GmbH, Solingen, DE
Paper bags	25 x 10 cm	Baumann Saatzuchtbedarf, Waldenburg, DE
Parafilm PM-996	4 inx125 ft.	Sigma-Aldrich Chemie GmbH, Taufkirchen, DE
PCR tubes		LABC-Labortechnik Zillger KG, Hennef, DE
Petri dishes	94x16 mm	Greiner Bio-One GmbH, Frickenhausen, DE
	145x20 mm	
Pipette tips	0.1-1 mL	
	10-200 µL	Greiner Bio-One GmbH, Frickenhausen, DE
	0.1-10 µL	
	0.5-5 mL	SARSTEDT AG & Co. KG, Nürnbrecht, DE

Planoclips	140x9 mm	Baumann Saatzuchtbedarf, Waldenburg, DE
Plant pots	10x7.5 cm	Rolfs Gärtner-Einkauf GmbH&Co KG, Siegburg, DE
	13x8 cm	Nitsch & Sohne GmbH, Kreuztal, DE
Reaction tubes	1.5 mL	SARSTEDT AG & Co. KG, Nürnbrecht, DE
	2.0 mL	
Screw neck vials	1.5 mL	VWR International GmbH, Darmstadt, DE
SPE columns	1 mL	Phenomenex Ltd., Aschaffenburg, DE
	6 mL	
Sterile filter	0.22 µm, 25 mm	Labomedic GmbH, Bonn, DE
Syringe	5 mL	Labomedic GmbH, Bonn, DE
	10 mL	
	20 mL	Terumo Corporation, Tokio, JP
	50 mL	
Teflon inlets	13.3 mm	Schmidlin AG, Affoltern, CH
	22.4 mm	
Vermiculite		Hoffman WDT, Teutschenthal, DE
Whatman paper	3 mm, 58x68 mm	Sigma-Aldrich Chemie GmbH, Taufkirchen, DE

2.1.2 List of enzymes und enzymatic buffers

Product designation	Art. Nr.	Provider
BamHI-HF	R3136S	New England Biolabs GmbH, Frankfurt am Main, DE
Bovine serum albumin	B9000S	New England Biolabs GmbH, Frankfurt am Main, DE
BbsI-HF	R3539S	New England Biolabs GmbH, Frankfurt am Main, DE
BsaI-HFv2	R3733S	New England Biolabs GmbH, Frankfurt am Main, DE
CutSmart® Buffer (5x)	B7204S	New England Biolabs GmbH, Frankfurt am Main, DE
DCSPol DNA Polymerase	DPT500	DNA Cloning Service e.K., Hamburg, DE
DCS Reaction Buffer (10x)		DNA Cloning Service e.K., Hamburg, DE
EcoRI-HF	R3101S	New England Biolabs GmbH, Frankfurt am Main, DE
MluI-HF	R3198S	New England Biolabs GmbH, Frankfurt am Main, DE
T4 DNA Ligase	M0202S	New England Biolabs GmbH, Frankfurt am Main, DE
T4 DNA Ligase Reaction Buffer (10x)	B0202A	New England Biolabs GmbH, Frankfurt am Main, DE
Q5® High-Fidelity DNA Polymerase	M0491S	New England Biolabs GmbH, Frankfurt am Main, DE
Q5® Reaction Buffer (5x)	B9027S	New England Biolabs GmbH, Frankfurt am Main, DE
Q5® High GC Enhancer (5x)	B9028A	New England Biolabs GmbH, Frankfurt am Main, DE
SalI-HF	R3138S	New England Biolabs GmbH, Frankfurt am Main, DE

SmaI	R0141S	New England Biolabs GmbH, Frankfurt am Main, DE
XhoI-HF	R0146S	New England Biolabs GmbH, Frankfurt am Main, DE

2.1.3 List of kits

Product designation	Art. Nr.	Provider
CloneJET PCR Cloning Kit	K1231	Thermo Fisher Scientific Inc., Waltham, US
NucleoSpin Gel and PCR Clean-up kit	740609.50	MACHEREY-NAGEL, Düren, DE
NucleoSpin Plasmid, Mini kit	740588.50	MACHEREY-NAGEL, Düren, DE
RevertAid First Strand cDNA Synthesis Kit	K1621	Thermo Fisher Scientific Inc., Waltham, US
RNeasy® Plant Mini Kit	74904	Qiagen N.V., Hilden, DE
TURBO DNA-free Kit	AM1907	Thermo Fisher Scientific Inc., Waltham, US

2.1.4 List of chemicals

Trade name	Formula	Provider
Acetic acid, glacial	CH_3CO_2H	VWR Chemicals, Darmstadt, DE
Acetonitrile	CH_3CN	VWR Chemicals, Darmstadt, DE
Acetosyringone	$C_{10}H_{12}O$	Sigma-Aldrich Chemie GmbH, Taufkirchen, DE
Adenine hemisulfate	$C_{10}H_{12}N_{10}O_4S$	AppliChem GmbH, Darmstadt, DE
Agarose	$C_{24}H_{38}O_{19}$	VWR Chemicals, Darmstadt, DE
Agarose, granulated bacteriological grade		Formedium™, Norfolk, UK
Ammonium acetate	$C_2H_7NO_2$	Carl Roth GmbH + Co. KG, Karlsruhe, DE
Ammonium nitrate	NH_4NO_3	AppliChem GmbH, Darmstadt, DE
Ammonium persulfate	$(NH_4)_2S_2O_8$	AppliChem GmbH, Darmstadt, DE
N,O-Bis(trimethylsilyl)-trifluoracetamide (BSTFA)	$C_8H_{18}F_3NOSi_2$	Chromatographie Service GmbH, Langerwehe, DE
Boric acid	BH_3O_3	AppliChem GmbH, Darmstadt, DE
Bovine serum albumin		Sigma-Aldrich Chemie GmbH, Taufkirchen, DE
Brij® 4	$(C_{20}H_{42}O_5)n$	Sigma-Aldrich Chemie GmbH, Taufkirchen, DE
Bromophenol blue, sodium salt	$C_{19}H_{10}Br_4O_5S$	SERVA Electrophoresis GmbH, Heidelberg, DE
Calcium chloride dihydrate	$CaCl_2.2H_2O$	AppliChem GmbH, Darmstadt, DE
Cetyl trimethylammonium bromide	$C_{19}H_{42}BrN$	Carl Roth GmbH + Co. KG, Karlsruhe, DE
Chloroform	$CHCl_3$	VWR Chemicals, Darmstadt, DE
Collodion solution, 4-8% in EtOH		Sigma-Aldrich Chemie GmbH, Taufkirchen, DE

Coomassie Brilliant Blue R-250	$C_{45}H_{44}N_3NaO_7S_2$	AppliChem GmbH, Darmstadt, DE
Danklorix		CP GABA GmbH, Hamburg, DE
Deoxyribonucleic acid sodium salt, from herring testis		Sigma-Aldrich Chemie GmbH, Taufkirchen, DE
3,6-Dichloro-2-methoxybenzoic acid	$C_8H_6Cl_2O_3$	Duchefa Biochemie B.V., Haarlem, NL
Diethylether	$C_4H_{10}O$	Sigma-Aldrich Chemie GmbH, Taufkirchen, DE
Dimethylsulfoxide	C_2H_6OS	Sigma-Aldrich Chemie GmbH, Taufkirchen, DE
Disodium hydrogen phosphate dihydrate	$Na_2HPO_4.2H_2O$	Supelco® / Merck KGaG, Darmstadt, DE
Ethanol absolute	C_2H_6O	Sigma-Aldrich Chemie GmbH, Taufkirchen, DE
Ethylenediaminetetraacetic acid (EDTA)	$C_{10}H_{16}N_2O_8$	Carl Roth GmbH + Co. KG, Karlsruhe, DE
Formic acid	H_2CO_2	AppliChem GmbH, Darmstadt, DE
Glucose anhydrous	$C_6H_{12}O_6$	Formedium™, Norfolk, UK
Glycerol	$C_3H_8O_3$	Fisher Scientific GmbH, Schwerte, DE
1-Heptadecanol, 98%	$C_{17}H_{36}O$	Sigma-Aldrich Chemie GmbH, Taufkirchen, DE
n-Hexane	C_6H_{14}	VWR Chemicals, Darmstadt, DE
Hydrochloric acid (37%)	HCl	VWR Chemicals, Darmstadt, DE
2-[4-(2-Hydroxyethyl)piperazin-1-yl]ethane-1-sulfonic acid	$C_8H_{18}N_2O_4S$	AppliChem GmbH, Darmstadt, DE
Isopropanol	C_3H_8O	Fisher Scientific GmbH, Schwerte, DE
Isopropyl β-d-1-thiogalactopyranoside	$C_9H_{18}O_5S$	Formedium™, Norfolk, UK
Lithium acetate	$C_2H_3LiO_2$	AppliChem GmbH, Darmstadt, DE
Lysogenic broth Lennox		AppliChem GmbH, Darmstadt, DE
Magnesium chloride hexahydrate	$MgCl_2.6H_2O$	Carl Roth GmbH + Co. KG, Karlsruhe, DE
Magnesium sulfate heptahydrate	$MgSO_4.7H_2O$	AppliChem GmbH, Darmstadt, DE
β-Mercaptoethanol	C_2H_6OS	AppliChem GmbH, Darmstadt, DE
Methanol	CH_4O	Fisher Scientific GmbH, Schwerte, DE
Metribuzin	$C_8H_{14}N_4OS$	Bayer AG, Leverkusen, DE
Midori Green Advance		NIPPON Genetics GmbH, Düren, DE
2-Morpholino-4-ylethanesulfonic acid monohydrate (MES)	$C_6H_{13}NO_4S$	ChemCruz™ / Bio-Connect B.V., Huissen, NL

Murashige and Skoog Basal Salt Mixture		Duchefa Biochemie B.V., Haarlem, NL
1-Pentadecanal	$C_{15}H_{30}O$	Tokyo Chemical Industry, Zwijndrecht, BN
Peptone		Formedium™, Norfolk, UK
Phyto Agar		Duchefa Biochemie B.V., Haarlem, NL
Polyethylene glycol 4000	$C_{2n}H_{4n}+2O_{n+1}$	Carl Roth GmbH + Co. KG, Karlsruhe, DE
Potassium chloride	KCl	Carl Roth GmbH + Co. KG, Karlsruhe, DE
Potassium dihydrogen phosphate	KH_2PO_4	Carl Roth GmbH + Co. KG, Karlsruhe, DE
Potassium iodide	KI	Honeywell Fluka™, Charlotte, US
Potassium nitrate	KNO_3	Supelco® / Merck KGaG, Darmstadt, DE
Pyridine	C_5H_5N	Sigma-Aldrich Chemie GmbH, Taufkirchen, DE
Rotiphorese®Gel 40 (29:1)		Carl Roth GmbH + Co. KG, Karlsruhe, DE
Silwet® Gold		General Electric Company, Friendly, US
Sodium chloride	NaCl	Th. Geyer GmbH & Co. KG, Renningen, DE
Sodium dodecyl sulfate	$C_{12}H_{25}NaSO_4$	AppliChem GmbH, Darmstadt, DE
Sodium hydroxide	NaOH	Honeywell Fluka™, Charlotte, US
Sodium hypochlorite	NaOCl	Carl Roth GmbH + Co. KG, Karlsruhe, DE
Sodium molybdate dihydrate	$Na_2MoO_4.2H_2O$	Merck KGaG, Darmstadt, DE
D-Sorbitol	$C_6H_{14}O_6$	Carl Roth GmbH + Co. KG, Karlsruhe, DE
Sucrose	$C_{12}H_{22}O_{11}$	Duchefa Biochemie B.V., Haarlem, NL
Tetracosane	$C_{24}H_{50}$	Sigma-Aldrich Chemie GmbH, Taufkirchen, DE
Tetramethylethylenediamine	$C_6H_{12}N_2$	Carl Roth GmbH + Co. KG, Karlsruhe, DE
Thimerosal	$C_9H_9HgNaO_2S$	AppliChem GmbH, Darmstadt, DE
Toluene	C_7H_8	Sigma-Aldrich Chemie GmbH, Taufkirchen, DE
Tris(hydroxymethyl)aminomethane (Tris)	$C_4H_{11}NO_3$	AppliChem GmbH, Darmstadt, DE
Triton-X 100	$C_{14}H_{22}O(C_2H_4O)_n$	Carl Roth GmbH + Co. KG, Karlsruhe, DE
Water, HPLC grade	H_2O	VWR Chemicals, Darmstadt, DE
Yeast extract power		Formedium™, Norfolk, UK
Yeast nitrogen base, without amino acids		Formedium™, Norfolk, UK
Zinc sulfate heptahydrate	$ZnSO_4.7H_2O$	Supelco® / Merck KGaG, Darmstadt, DE
Amino acids		
L-Arginine	$C_6H_{14}N_4O_2$	Duchefa Biochemie B.V., Haarlem, NL
L-Aspartate	$C_4H_7NO_4$	Duchefa Biochemie B.V., Haarlem, NL
L-Cysteine	$C_3H_7NO_2S$	Duchefa Biochemie B.V., Haarlem, NL
L-Glutamate sodium salt	$C_5H_8NO_4Na$	Duchefa Biochemie B.V., Haarlem, NL
L-Glutamine	$C_5H_{10}N_2O_3$	Duchefa Biochemie B.V., Haarlem, NL

L-Glycine	$C_2H_5NO_2$	Duchefa Biochemie B.V., Haarlem, NL
L-Histidine	$C_6H_9N_3O_2$	Duchefa Biochemie B.V., Haarlem, NL
L-Leucine	$C_6H_{13}NO_2$	Duchefa Biochemie B.V., Haarlem, NL
L-Lysine	$C_6H_{14}N_2O_2$	Duchefa Biochemie B.V., Haarlem, NL
L-Methionine	$C_5H_{11}NO_2S$	Duchefa Biochemie B.V., Haarlem, NL
L-Phenylalanine	$C_9H_{11}NO_2$	Duchefa Biochemie B.V., Haarlem, NL
L-Proline	$C_5H_9NO_2$	Duchefa Biochemie B.V., Haarlem, NL
L-Serine	$C_3H_7NO_3$	Duchefa Biochemie B.V., Haarlem, NL
L-Threonine	$C_4H_9NO_3$	Duchefa Biochemie B.V., Haarlem, NL
L-Tryptophane	$C_{11}H_{12}N_2O_2$	Duchefa Biochemie B.V., Haarlem, NL
L-Tyrosine	$C_9H_{11}NO_3$	Duchefa Biochemie B.V., Haarlem, NL
L-Valine	$C_5H_{11}NO_2$	Duchefa Biochemie B.V., Haarlem, NL
Antibiotics		
Ampicillin	$C_{16}H_{19}N_3O_4S$	Duchefa Biochemie B.V., Haarlem, NL
Carbenicillin	$C_{17}H_{18}N_2O_6S$	Duchefa Biochemie B.V., Haarlem, NL
Gentamicin	$C_{21}H_{43}N_5O_7$	Duchefa Biochemie B.V., Haarlem, NL
Kanamycin	$C_{18}H_{36}N_4O_{11}$	Duchefa Biochemie B.V., Haarlem, NL
Rifampicin	$C_{43}H_{58}N_4O_{12}$	Duchefa Biochemie B.V., Haarlem, NL
Spectinomycin	$C_{14}H_{24}N_2O_7$	Duchefa Biochemie B.V., Haarlem, NL
Streptomycin	$C_{21}H_{39}N_7O_{12}$	Duchefa Biochemie B.V., Haarlem, NL

2.1.5 List of instruments

Instrument	Model/Serial Nr.	Supplier
ChemiDoc MP Imaging System		Bio-Rad Laboratories GmbH, Feldkirchen, DE
Drop shape analyser	DSA25S	KRÜSS GmbH, Hamburg, DE
Electrophoresis Power Supply	EPS 301	Amersham Pharmacia Biotech Inc., Buckinghamshire, UK
Gel documentation system	FastGene FAS-DIGI PRO	Nippon Genetics EUROPE GmbH, Düren, DE
Homogeniser	Precellys 24	Bertin Technologies SAS, Montigny-le-Bretonneux, FR
Incubator		
Junior Pam system		
Light table	2 RE	Palmed GmbH, Blaustein, DE
MicroPulser™	411BR	Bio-Rad Laboratories GmbH, Feldkirchen, DE
Mixing Block	MB-102, 40 x 1.5 mL/ 40 x 2.0 mL	BIOER Technology Co. Ltd., CN
NanoDrop	1000 Spectrophotometer	PEQLAB Biotechnologie GmbH, DE

Nucleic acid electrophoresis system		Laborgeräte Beranek GmbH, Nußloch, DE
pH Electrode	ino®Lab pH Level 1	Xylem Analytics Germany GmbH & Co. KG, DE
Photospectrometer	SPECORD 205	Analytik Jena AG, DE
Plant growth chambers	SIMATIC OP17	York International, Mannheim, DE
Plant tissue culture chamber	SE41-CU5cLED	Percival Scientific, Perry, US
PowerPac™	Basic	Bio-Rad Laboratories GmbH, Feldkirchen, DE
Protein electrophoresis system	Mighty small II, 8x7cm gels	GE Health Care Bio-Sciences Corp., Piscataway, US
Scanlaf Mars	1200 Runner	LaboGene ApS, Frederiksborg, DK
Sonorex	RK106	Bandelin electronic GmbH & Co. KG, Berlin, DE
Thermocycler	T-Personal 48	Analytik Jena AG, Jena, DE
Trans-Blot SD Semi-Dry transfer cell		Bio-Rad Laboratories GmbH, Feldkirchen, DE
Quantus™ Fluorometer	E6150	Promega GmbH, Walldorf, DE
Ultrapure Water System	OmniaLab ED40	stakpure GmbH, Niederahr, DE
Vortex Genie	2	Scientific Industries™ Inc., Bohemia, US
Centrifuges		
Eppendorf centrifuge	5417 R, F45-30-11	Eppendorf AG, Hamburg, DE
Eppendorf centrifuge	5810 R, A-4-62	Eppendorf AG, Hamburg, DE
Sorvall centrifuge	RC 5B Plus, GS3	Kendro Laboratory Products, Osterode am Harz, DE
Fluorescence microscopy system		
Confocal microscope	IX71	Olympus Optical Co. Ltd., Tokyo, JP
Linear laser system	400 Series	Oxford Instruments GmbH, Wiesbaden, DE
Filter wheel changer	Lambda 10-3	Sutter Instrument, Novato, US
Confocal scanner unit		Yokogawa Electric Corporation., Tokio, JP
Analytical instruments		
GC/FID	6890N	Agilent Technologies Inc., Santa Clara, US
	DB-1, 30 m x 0.32 mm, 0.1 µm	Agilent Technologies Inc., Santa Clara, US

GC/FID	7890A	Agilent Technologies Inc., Santa Clara, US
	SP™-2380, 30 m x 0.53 mm x 0.2 µm	Supelco® / Merck KGaA, Darmstadt, DE
GC/MS	6890N/5973 MS	Agilent Technologies Inc., Santa Clara, US
	DB-1MS, 30 m x 0.32 mm, 0.1 µm	Agilent Technologies Inc., Santa Clara, US
GC/MS	7890A, 5975C inert XL MSD	Agilent Technologies Inc., Santa Clara, US
	HP-5MS, 30 m x 0.25 mm x 0.25 µm	Agilent Technologies Inc., Santa Clara, US
Pipettes		
Research® Plus	0.1-1.5 µL	Eppendorf AG, Hamburg, DE
	1-10 µL	Eppendorf AG, Hamburg, DE
	10-200 µL	Eppendorf AG, Hamburg, DE
	100-1000 µL	Eppendorf AG, Hamburg, DE
	0.5-5 mL	Eppendorf AG, Hamburg, DE
Acura® manual 835	0.2-2 mL	Socorex Isba SA, Ecublens, CH

2.2 Cultivated plant species

Barley seeds were obtained from the Nordic Genetic Resource Center (NordGen). Additional segregating generations were provided by Chiara Campoli (University of Dundee). *A. thaliana* *cer*4-3 seed material was kindly offered by Gillian Dean (University of Vancouver).

Allele/Ecotype	Species	Origin	Background	Mutagen	Source of supply	NGB Number
Bonus	*H. vulgare*	-	-	-	NordGen	14657
Bowman	*H. vulgare*	-	-	-	NordGen	22812
Foma	*H. vulgare*	-	-	-	NordGen	14659
cer-ye.267$_{BC7}$	*H. vulgare*	Foma	Bowman	Ethylene imine	NordGen	20542
cer-ye.267$_{BC8}$	*H. vulgare*	Foma	Bowman	Ethylene imine	Chiara Campoli	
cer-ye.582	*H. vulgare*	Foma	-	Ethylene imine	NordGen	111470
cer-ye.792	*H. vulgare*	Bonus	-	Ethylene imine	NordGen	111680
cer-ye.1395	*H. vulgare*	Bonus	-	Ethylene imine	NordGen	112283
cer-za.173	*H. vulgare*	Bonus	-	Ethylene imine	NordGen	111059
cer-za.227$_{BC7}$	*H. vulgare*	Foma	Bowman	Ethylene imine	NordGen	21989
cer-za.227$_{BC8}$	*H. vulgare*	Foma	Bowman	Ethylene imine	Chiara Campoli	
cer-za.232	*H. vulgare*	Foma	-	Ethylene imine	NordGen	111119
cer-za.318	*H. vulgare*	Foma	-	Ethylene imine	NordGen	111205
cer-zh.54	*H. vulgare*	Bonus	Bowman	X-ray induced	NordGen	110938
Col-0	*A. thaliana*	-	-	-	-	
*cer*4-3	*A. thaliana*	Col-0		T-DNA insertion SALK_038693	Gillian Dean	
*cer*4-3+CER-ZA	*A. thaliana* *N. benthamiana*	Col-0		T-DNA insertion		

2.3 Cultivation methods for plants

2.3.1 Cultivation of *H. vulgare*

Moistened filter paper was placed in sealable chambers. Barley seeds were slightly embedded on the prepared tissue layers. The chambers were sealed with leukotape and incubated in the dark at RT for 3 d. Germinated seedlings were transferred to pots filled with a composite of ED73 soil and Vermiculite mixed in a ratio of 3:1. Plants were cultivated in growth chambers (SIMATIC OP17) at 21°C with 55% relative humidity and 16 h of light (150 µE) until harvest.

Pots were occasionally watered with a nematode (*Steinernema feltiae*) suspension (1 g/L) to reduce the infestation by gnats.

2.3.2 Vapor-phase sterilisation of *A. thaliana* seeds

The vapor-phase sterilisation method is widely used and allows the efficient simultaneous treatment of several different seed batches while retaining a stable seed germination rate (Lindsey *et al.* 2017). A thin layer of seeds was filled into 1.5 mL microfuge tubes. Up to 20 tubes were placed in an desiccator (DN 150, 2.4 L) sealed with lubricant. Under the fume hood, 1 mL of 37% HCl were quickly added to 25 mL of bleach (DanKlorix) to adjust to a final concentration of 6-7% chlorine gas in the enclosed atmosphere. The container was subsequently airtight closed, and seeds were incubated for up to 3 h. Finally, the desiccator was opened under the fume hood, reaction tubes were quickly closed and stored until usage.

2.3.3 Cultivation of *A. thaliana*

A. thaliana seeds were vapor-phase sterilized (2.3.2) prior to germination. Surface sterilized seeds were evenly distributed on freshly prepared MS medium (Murashige and Skoog 1962) and stratified at 4°C under exclusion of light for 24-72 h. Stratified seeds were incubated under long-day conditions (16 h of light, 8 h of night) at 22°C with 55% relative humidity in plant tissue culture chambers (Percival SE41-CU) for two to three weeks. Grown plants were transferred to a mixture of ED73 soil:Vermiculite (3:1) soaked with 1 mM boric acid (pH 8) and grown at 21°C under long-day conditions (150 µmol m^{-2} s^{-1}). The first watering was performed with a nematode suspension (1 g/L) to prevent pests. For seed harvest, primary shoots were cut to improve the number of secondary shots and consequently the number of flowers. Plants were covered with paper bags as soon as the first siliques ripened to avoid seed loss and continued to be watered until all seeds were visibly drying. After harvest, sieved seeds were additionally dried in a closed desiccator with silica gel for up to one week prior to long-term storage at 4°C.

MS medium	
MS Salts (including vitamins)	0.4405 g/L
Sucrose	1% (w/v)
MES	0.213 g/L
Phyto agar	0.8% (w/v)
	Adjusted to pH 6.0 with KOH.

2.3.4 Cultivation of *N. benthamiana*

N. benthamiana seeds were directly sown to pots containing a mixture of ED73 soil and Vermiculite (3:1) which was initially soaked with 1 mM boric acid (pH 8). Cultivation was carried out in growth chambers (21°C, 55% relative humidity, 150 µmol m^{-2} s^{-1}) under long-day conditions (16 h of light, 8 h of night). After one week, seedlings were separated to individual pots and frequently watered with tab water until usage. For seed propagation, plants were additionally fertilised at least once a month.

2.4 Crossing of *H. vulgare*

H. vulgare was grown for eight to twelve weeks until the first row of ears was developed. A spike of the female parent was carefully opened when the seed coat became clearly developed and the anthers were still greenish. The three upper and lower rows of flowers were removed with fine, disinfected forceps. Lemma and palea were opened carefully to emasculate the spikes by removal of the unswollen anthers without damaging the peduncle. Afterwards, the spike was carefully re-wrapped in the sheath leaf, bagged, and left for stigma development for 6-10 d. The bag was removed frequently to control the developmental state of the prepared flowers. Developed flowers harboured an extended stylus with a whitish stigma, while undeveloped flowers were removed. Fertile flowers were pollinated with pollen from the intentional father plant. To do so, yellowish but unopened anthers were obtained from the flowers, warmed to trigger the pollen release, and tapped on the exposed stigma. Finally, the spike was wrapped again and left until harvest. The detailed procedure was described by Harwood (2019).

2.5 List of cultivated microorganisms

Different prokaryotic and eukaryotic microorganisms were cultivated during this project. *Escherichia coli* was used for cloning procedures, and, *E. coli* as well as *Saccharomyces cerevisiae*, served as recombinant host organisms. *Agrobacterium tumefaciens* strains were applied for the transformation of *A. thaliana* and *N. benthamiana*. Details about utilised strains and IMBIO stock numbers are listed below.

Species	Strain	Provider	Plasmid	Stock number
E. coli	Rosetta DE3	Novagen/Merck Chemicals GmbH	pET-15b	Bn1451
			pET-15b-CER-ZA	Bn1452
	ElectroSHOX	Bioline/Meridian Life Science, Inc.		Bn1017
			pLH9000	Bn1176
			pLH9000-CER-ZA	Bn1470
		Hölzl, unpublished	pBin-35s-GG-DsRed	Bn1370
			pBin-CER4Prom-CER-ZA-CER4Term	Bn1444
A. tumefaciens	GV3101	Per Hofvander	pMP90	Bn76
			pMP19	Bn856
	GV3101	AG Menzel, University of Bonn	pCB-DsRed-HDEL	Bn545
S. cerevisiae	BY4741	Euroscarf/SRD GmbH		Bn1446
			pDR196-CER-ZA	Bn1469
		AG Rentsch, University of Bern	pDR196	Bn1470

2.6 Cultivation methods for microorganisms

2.6.1 Cultivation of *E. coli*

Two *E. coli* strains were used. Electrocompetent ElectroSHOX were applied for cloning strategies due to their high efficiency in electroporation-based transformation. The expression of pET-15b based constructs required the Rosetta DE3 strain as recombinant host due to presence of the T7 expression system. Commonly, *E. coli* cultures were incubated at 37°C over-night. Lysogeny broth (LB) served as preferred medium for the cultivation. Antibiotics were sterile filtrated and added according to the tolerated concentrations.

Lysogenic broth (LB)	
Lysogeny broth	20.0 g
Bacto agar (optional)	15.0 g
ddH_2O	ad 1000 mL
Adjusted to pH 7.2 with NaOH.	

Antibiotic concentrations for *E. coli*

Antibiotic	Stock concentration [mg/mL]	Dissolved in	Final concentration [µg/mL]
Ampicillin	100	ddH_2O	100
Carbenicillin	50	ddH_2O	50
Chloramphenicol	30	DMSO	30
Kanamycin	25	ddH_2O	25
Spectinomycin	75	ddH_2O	75
Streptomycin	150	ddH_2O	150

Antibiotic stock solutions were sterile filtrated and stored at -20°C.

2.6.2 Cultivation of *A. tumefaciens*

A. tumefaciens GV3101 was used to transform *A. thaliana* and *N. benthamiana*. YEP broth was chosen as nutrient medium for the cultivation of all *Agrobacteria* strains. Antibiotics were added according to the specific requirements of the experiments. *Agrobacteria* were cultivated at 28°C for 48-72 h.

YEP broth

Peptone	10.0 g
Yeast extract	10.0 g
NaCl	5.0 g
Bacto agar (optional)	15.0 g
dH2O	ad 1000 mL

Adjusted to pH 7.2 with NaOH.

Antibiotic concentrations for *A. tumefaciens*

Antibiotic	Stock concentration [mg/mL]	Dissolved in	Final concentration [µg/mL]
Ampicillin	200	ddH_2O	200
Carbenicillin	150	ddH_2O	150
Gentamycin	50	ddH_2O	50
Kanamycin	50	ddH_2O	50
Rifampicin	60	DMSO	60
Spectinomycin	150	ddH_2O	150

Antibiotic stock solutions were sterile filtrated and stored at -20°C.

2.6.3 Cultivation of *S. cerevisiae*

S. cerevisiae BY4741 was used as heterologous expression system. The strain lacks the *URA3* gene and is therefore not capable of expressing orotidine-5-phosphate decarboxylase, a protein required to produce uracil. This enables the efficient selection of transformed cells on uracil-deficient medium. Untransformed yeast cells were cultivated with YPD medium at 30°C for 48-72 h.

YPD medium

Yeast extract	10.0 g
Peptone	20.0 g
Glucose	20.0 g
Bacto agar (optional)	20.0 g
dH_2O	ad 1000 mL

Adjusted to pH 7.2 with KOH.

2.7 Molecular biological methods

2.7.1 Genomic DNA isolation from plants with CTAB buffer

Leaf or shoot material was harvested in 2 mL reaction tubes containing glass beads, and subsequently frozen in liquid nitrogen. Samples were homogenised (Precellys 24; 6500 rpm, 10 s, 3x), afterwards 1 mL cetyltrimethylammonium-bromide (CTAB) buffer was added to the powder and thoroughly mixed. Incubation at 65°C for 10 min was followed by addition of 0.4 mL chloroform. Samples were briefly vortexed and centrifuged at 1000 *g* for 5 min. The DNA-containing aqueous phases were transferred to fresh reaction tubes and mixed with 700 µL cold isopropanol. DNA precipitation was enhanced by incubation on ice for at least 20 min or at -20°C over-night. The DNA was pelleted by centrifugation for 5 min at 11,000 *g*. Supernatants were discarded, and DNA was washed with 500 µL of cold 75% EtOH. Pellets were dried, and DNA was resuspended in 30 µL of ddH_2O. Samples were stored at -20°C until use.

CTAB buffer

Sorbitol	140 mM
Tris-HCl, pH 8	220 mM
EDTA	22 mM
NaCl	800 mM
CTAB	0.8%

2.7.2 RNA isolation from plants for cDNA synthesis

Leaf sections of 4 cm length from two weeks old *H. vulgare* plants, or two to three shoot sections of 2 cm length from three weeks old *A. thaliana* plants, were harvested in 2 mL reaction tubes containing glass beads and frozen in liquid nitrogen. Plant material was homogenised with a Precellys 24 (4 x 6500 rpm, 15 s). Thawing of the samples was avoided between the homogenization cycles by intermediate cooling in liquid nitrogen. RNA was extracted from the fine-ground powder using the NucleoSpin RNA Plant Kit. The on-column DNA digest was skipped and DNA was instead digested with the TURBO DNA-free Kit. The quality of the extracted RNA was monitored on an agarose gel and the purity was determined by absorption ratios measured with a NanoDrop (1000 Spectrophotometer). Purified RNA was subsequently utilised for the generation of cDNA (2.7.3).

2.7.3 Synthesis of cDNA

cDNA was synthesised from freshly extracted RNA (2.7.2) with the RevertAid First Strand cDNA Synthesis Kit. The synthesis was performed according to the manufacturer's instruction. 500 ng of freshly isolated template RNA were sufficient for the reverse transcription. The reaction was carried out at 42°C for one hour and stopped by heat-inactivation at 70°C for 5 min. Synthesised cDNA was stored at -20°C for up to four weeks.

2.7.4 Identification of candidate genes with the BSR-Seq strategy

The combination of the bulked segregant analysis method with modern next-generation-sequencing (NGS) offers a powerful tool for the mapping and identification of genes of interest based on measurable traits. This method was shown to be highly efficient in several studies, even on small population sizes (Barua *et al.* 1993; Liu *et al.* 2012; Dong *et al.* 2018; Wu *et al.* 2018), and was applied here to identify the loci of mutational events in the *H. vulgare cer*-za and *cer*-ye alleles.

2.7.4.1 Sampling for RNA-Seq

Seeds of the segregating F2 generation of the two *eceriferum* lines, eight-times backcrossed to Bowman (BC_8), were provided by Chiara Campoli (University of Dundee, Scotland). A screening population of 250 plants was grown in the greenhouse for 14 d. After 10 d, plants were screened for the characteristic *eceriferum* phenotype by spraying with water (see paragraph 3.1). Plants with a high water-repellence were considered as wild-type-like, while those showing an increased hydrophily were recorded as *cer*-like. For the sampling, pieces of 2 cm were cut from the second leaf of each plant. The area was chosen in 2-3 cm distance from the point of emergence to cover an area of enhanced cuticular wax biosynthesis activity

(Richardson *et al.* 2007b). A total of roughly 250 leaf samples per segregating line were immediately frozen in liquid nitrogen and stored at -80°C until RNA extraction (2.7.4.2).

2.7.4.2 Bulking of samples and isolation of RNA for NGS

A set of twelve different bulks was created for the following RNA-Seq approach (Table 1). Leaf material from wild-type-like and *cer*-like plants was each bulked to generate two pools from the segregating F2 lines for both *cer*-za and *cer*-ye. Samples for the homozygous allelic *cer* lines *cer*-za.173, *cer*-za.232 and *cer*-za.318, as well as *cer*-ye.582, *cer*-ye.792 and *cer*-ye.1395 were also created. Since the mutations were originally generated in the cultivar Foma, and all backcrossing steps were performed in Bowman background, both cultivars were included in the analysis. Frozen tissue was ground to a very fine powder using cleaned and autoclaved mortars and pestles. Liquid nitrogen was added frequently to prevent the material from thawing. 100 mg of the powder were weighed in and transferred to RNAse free 2 mL reaction tubes. RNA isolation was performed with the RNeasy® Plant Mini Kit according to the manufacturer's instructions. The final elution was done with 40 µL of RNAse-free water. 1 µL was used for concentration and purity determination (NanoDrop 1000 Spectrophotometer). Samples were stored at -80°C until they were shipped for NGS.

Table 1: Pools prepared for the BSR-Seq approach. Each sample pool contained bulked leaf samples from several individual plants. The state of inheritance and sample sizes [n, number of plants] of each pool are listed.

Sample Nr.	Pool	Genotype	[n]
1	Wild-type-like *cer*-za.227, F2 generation	homozygous/heterozygous	40
2	Wild-type-like *cer*-ye.267, F2 generation	homozygous/heterozygous	19
3	*cer*-za.173	homozygous	5
4	*cer*-za.232	homozygous	3
5	*cer*-za.318	homozygous	4
6	*cer*-ye.582	homozygous	4
7	*cer*-ye.792	homozygous	5
8	*cer*-ye.1395	homozygous	5
9	*cer*-like *cer*-za.227, F2 generation	homozygous/heterozygous	38
10	*cer*-like *cer*-ye.267, F2 generation	homozygous/heterozygous	7
11	Bowman	homozygous	4
12	Foma	homozygous	4

2.7.4.3 Transcriptome analysis by RNA-Seq

Purified samples were shipped on dry ice for sequencing to the West German Genome Center (WGGC, Cologne). The RNA-Seq strategy included a Ribo depletion method to reduce the required sequencing depth and enhance the exonic coverage. 80 million reads were requested to achieve the aimed sequencing depth and resolution. The sequencing was performed paired-end and adjusted to 2x100bp sequencing frames on a NextSeq 1000 Sequencing system (Illumina Inc, USA). Sequence string libraries were available after six weeks.

2.7.4.4 Data evaluation

Datasets were processed by Tyll Stöcker and Heiko Schoof (INRES, University of Bonn). Prior to data preparation, the basic quality of the raw files was controlled using FastQC (Version 0.11.9) to avoid any irregularities in the data sets. After quality confirmation, genetic adapter sequences, required for the RNA sequencing, and low-quality nucleotides were trimmed of retrieved reads (Trimmomatic, Version 0.39), again followed by an additional quality control step utilising FastQC. Overexpressed sequences were identified via BLAST and turned out to be dominantly related to the chloroplast biosynthesis. These sequences were treated as contaminations and cleared using BBDuk (Version 38.71). Remaining filtered and trimmed reads were aligned to the common reference genome derived from the *H. vulgare* Morex (Morex_v2.0, GCA_902498975.1) cultivar by STAR (Version 2.7.8a). Resulting datasets were edited, organised and converted to SAM format with Picard Toolkit (Version 2.24.2) and Samtools (Version 1.12) for the further data evaluation performed with the Genome Analysis Toolkit (GATK, Version 4.2.0.0). As first GATK tool SplitNCigarReads was utilised to compensate for alignment gaps returned as Ns, e.g. resulting from splicing events, by hard clipping the original reads and generation of new reads according to the number of false alignment events. Novel created reads were added to the library by AddReadGroupID. Afterwards a first SNP calling was performed running HaplotypeCaller comparing the wild-type cultivars Bowman and Foma to the Morex genome to identify naturally occurring polymorphisms. In course of the sequencing itself, the machine produces quality scores for the different bases. These underlie technical errors which can lead to a distortion of the estimated quality score for each base. To correct these factors, a Base Quality Score Recalibration (BQSR) was performed by first applying the BaseRecalibrator Tool, producing a report based on machine learning, which can be used in a second step to recalibrate the scores via ApplyBQSR with a BAM file as output. A second variant calling was performed with the recalibrated file again using HaplotypeCaller. Prior to processing the resulting genomic variant calling files (GVCFs) for a joint calling approach with GenotypeGVCFs, the GVCFs had to be consolidated into a single file by GenomicsDBImport.

2.7.5 Sequencing of genomic DNA sections via Sanger sequencing

The Sanger sequencing service GATC (Eurofins Genomics Germany GmbH, Ebersberg, DE) was employed to sequence up to 1000 bp long double-stranded DNA sections, derived from PCR products or plasmids. The enhanced sequencing error rate over the flanking 100 bp areas were considered in course of the primer design. Whole genes were sequenced by creating overlapping DNA sections of 400 bp in length covered by different primer pairs (7.2). Resulting FASTA files were proceeded with Chromas and MEGA X. Overlapping ends were trimmed and joined to receive a continuous sequence.

2.7.6 Quantitative PCRs

gDNA and cDNA fragments of interest were amplified using the Q5® High-Fidelity DNA Polymerase system. The enzyme is characterised by low error rates and was therefore chosen for cloning and sequencing. Annealing temperatures were calculated using the T_m calculator (version 1.13.0) provided by the supplier and the reaction settings were adjusted according to the manufacturer's instruction (Table 2). Q5® High GC Enhancer (5x) was added for amplification of regions with high GC contents. A Hot Start was performed according to the provider's recommendation.

(1x) Q5® Polymerase reaction mixture	
Template DNA	< 1000 ng
dNTPs (2.5 mM)	1 µL
Forward primer (10 µM)	2.5 µL
Reverse primer (10 µM)	2.5 µL
Q5® Reaction Buffer (5x)	10 µL
Q5® High-Fidelity DNA Polymerase	0.5 µL
ddH_2O	ad 50 µL

Table 2: Thermocycler program applied for quantitative PCRs with the Q5® Polymerase.

Step	**Temperature [°C]**	**Time [min]**	**Cycles**
Denaturation	98	0:30	
Denaturation	98	0:30	
Hybridisation	T_A	0:30	35x
Elongation	72	1:00/2000 bps	
Elongation	72	2:00	
Cool down	10	-:-	

2.7.7 Qualitative PCRs

Qualitative PCRs were performed for control and screening applications. The DCSPol DNA Polymerase was utilised for this purpose. The reaction mixture was consistent for all applications; in case of colony PCRs the DNA template was replaced by a sample of the cells picked from the plate. The PCR settings were adjusted to the requirements of the polymerase and the annealing temperature (T_A) of the individual primer pair (Table 3).

(1x) DCSPol reaction mixture	
Template DNA/Cell material	< 1000 ng
Forward Primer (10 µM)	1.5 µL
Reverse Primer (10 µM)	1.5 µL
DCS Reaction Buffer (10x)	1.5 µL
$MgCl_2$ (10 mM)	1.5 µL
dNTPs (2.5 mM)	0.3 µL
DCSPol DNA Polymerase	0.2 µL
ddH_2O	ad 15 µL

Table 3: Thermocycler program applied for qualitative PCRs with the DCSPol DNA Polymerase.

Step	**Temperature [°C]**	**Time [min]**	**Cycles**
Denaturation	98	0:30	
Denaturation	98	0:30	
Hybridisation	T_A	0:30	35x
Elongation	72	1:00/1000 bps	
Elongation	72	2:00	
Cool down	10	-:-	

2.7.8 Preparation of plasmid DNA

4 mL cultures were grown at 37°C over-night. Plasmids were either harvested using the NucleoSpin® Plasmid Kit following the manufacturer's instructions, or by manual preparation. For the latter, cultures were harvested by centrifugation at 20,000 *g* for 2 min. Collected cell pellets were resuspended in 200 µL BF buffer mixed with 10 µL of lysozyme (20 mg/mL). The lids of the reaction tubes were pricked to avoid overpressure, afterwards the samples were incubated at 100°C for one minute to break the cells, followed by incubation on ice for 1 min. Supernatant and cell debris were separated by centrifugation at 20,000 *g* for 20 min. Supernatants were transferred to fresh reaction tubes and mixed with 480 µL of IS mix by inverting, followed by another twelve minutes of centrifugation. Resulting pellets were washed with 500 µL ethanol (20,000 *g*, 6 min). Finally, harvested plasmids were dried and resuspended in 50 µL of ddH_2O supplemented with 0.05% of RNAse (10 units/mL).

BF buffer	
Triton-X 100	0.5% (v/v)
Sucrose	8% (w/v)
EDTA, pH 8	14.612 g
Tris-HCl	1.211 g
ddH_2O	ad 1000 mL

IS mix	
Isopropanol	40 mL
5 M Ammonium acetate	8 mL

2.7.9 Restriction digests

Restriction digests were performed either to control isolated plasmids or to prepare and harvest DNA fragments for further cloning applications. For control digests, 100-500 ng of DNA were used for each 10 µL reaction volume, in dependence of the number of expected fragments. Reaction mixtures were incubated at the enzyme specific optimal temperature for 45 min. For cloning applications, 500-2000 ng of DNA were used for each reaction assay. The reaction setup was adjusted to the enzyme-specific working temperatures for 60-90 min. Enzymes supplied by NEB were utilised according to the manufacturer's instruction. Afterwards DNA fragments were separated and visualised by gel electrophoresis. Fragments of interest were cut from the gel and either stored at -20°C or directly eluted (2.7.12) for further downstream procedure.

(1x) Reaction setup for qualitative digests	
DNA	100–500 ng
CutSmart Buffer (5x)	1 µL
Enzyme	0.1 µL/100 ng DNA
ddH_2O	ad 10 µL

(1x) Reaction mixture for quantitative digests	
DNA	500 – 2000 ng
(5x) CutSmart Buffer	10
Enzyme	1 µL/1 µg DNA
ddH_2O	ad 50 µL

2.7.10 Ligation reactions

A successful ligation depends strongly on the precise determination of the proper ratio of the ligation fragments. Concentrations of the DNA fragments were determined with the QuantiFluor® ONE dsDNA system and adjusted to a final insert to vector ratio of 3:1. 1 µL of sample was mixed with 200 µL of the included dye and incubated under light exclusion for 5 min. The fluorescent dye binds to double-stranded DNA, and this allows the indirect measurement of the DNA concentration by measuring the light emission of the bound dye (504 nm excitation/531 nm emission) with the Quantus™ Fluorometer. The returned amount in ng/µL was converted to pmol/µL.

$$\mathrm{c\ [pmol/\mu L]} = \mathrm{ng/\mu L\ [Sample]\ x} \left(\frac{\mathrm{pmol}}{660\ \mathrm{pg}}\right) \mathrm{x} \left(\frac{10^6\ \mathrm{pg}}{1\ \mathrm{ng}}\right) \mathrm{x}\left(\frac{1}{\mathrm{N}}\right)$$

Ligations were catalysed by the T4 DNA Ligase from NEB. Blunt end ligations were incubated for 16°C for 1 h, while sticky end ligations were conducted at RT for 12 min. As an exception, the CloneJET PCR Cloning Kit was used following the manufacturer's instructions. Reaction mixtures were transferred to a semipermeable membrane filter floating on ddH_2O for at least 60 min prior to transformation. The osmotically driven desalting process stopped the reaction and enhanced the efficiency of transformation by electroporation (2.7.15).

(1x) Ligation mixture

Insert DNA	0.060-0.150 pmol
Vector DNA	0.020-0.050 pmol
T4 DNA Ligase Reaction Buffer (10x)	1 µL
T4 DNA Ligase	0.5 µL
ddH_2O	ad 10 µL

2.7.11 Golden Gate cloning procedure

Golden Gate ligations were set up in PCR tubes kept on ice. All involved PCR fragments and plasmids were adjusted to reach similar molarities in the final reaction mixture. Restriction enzymes were added as required. Golden Gate reactions were performed in a thermocycler (Table 4).

(1x) Ligation mixture for Golden Gate cloning

Bovine serum albumin (10x)		2 µL
T4 Ligase Buffer		2 µL
T4 DNA Ligase		1 µL
n x	Restriction enzyme(s)	1 µL/1 µg target DNA
n x	DNA Template(s)	250 nM
ddH_2O		ad 20 µL

Table 4: Thermocycler program applied for Golden Gate cloning approaches. Temperatures were adjusted according to the manufacturer's recommendations for ligation and restriction enzymes.

Step	Temperature [°C]	Time [min]	Cycle
Restriction digest	37	2:00	26x
Ligation	16	5:00	
Inactivation of	50	5:00	
enzymes	80	5:00	

Finally, ligation mixtures were desalted (2.7.10) and the generated DNA was electroporated into the target host strain of *E. coli* (2.7.15).

2.7.12 Separation, visualisation, and purification of linearised nucleic acids via gel electrophoresis

Linear nucleic acid fragments were separated on 1.2% (w/v) agarose gels via gel electrophoresis using 1x TAE as buffer system. 2.5 µL Midori Green Advance were freshly added per 50 mL gel volume. The dye binds to nucleic acids and can be visualised on a Blue/Green LED transilluminator (FastGene FAS-DIGI PRO, Nippon Genetics) that emits light at a wavelength band of 470-520 nm. Depending on the size of the gel chamber, 100-120 V with 25 mA were applied for gel electrophoresis.

(50x) TAE buffer

Tris	40 mM
Acetic acid, glacial	20 mM
EDTA, pH 8	1 mM

(1.2%) Agarose gel

1x TAE buffer	400 mL
Agarose	4.8 g

Concentrated nucleic acid bands were documented using a Canon 250D camera with a 18-55 mm lens (Canon, Japan), equipped with a FastGene Amber Lens Filter (Nippon Genetics). Bands of interest were cut from the gel and eluted using the NucleoSpin Gel and PCR Clean-up kit for further downstream applications.

2.7.13 Cloning strategies

Several vector systems were applied for the expression in different recombinant host organisms. Expression of CER-ZA from *H. vulgare* in *E. coli* was performed under an inducible T7 promotor (pET-15b) for high expression levels. pDR196 was used to express proteins in *S. cerevisiae* as eukaryotic host. pBin-35S-DsRed and pLH9000 were included to realise the expression of CER-ZA in the plants *A. thaliana* and *N. benthamiana*.

2.7.13.1 Cloning of the *E. coli* expression vector pET-15b-CER-ZA

The coding sequence of *HORVU5Hr1G089230.1* was amplified from *H. vulgare* cDNA (bn4206, bn4161) and subcloned into pJET1.2. Following the transformation into ElectroSHOX cells, selected colonies were screened by PCR. Plasmids from positive colonies were control digested and sequenced. Afterwards the inserts were cut (XhoI, BamHI) and ligated into pET-15b (XhoI, BamHI). Selected colonies were screened by PCR (bn4176, bn4060), control digested and sequenced. A confirmed construct was electroporated (2.7.15.1) into *E. coli* Rosetta DE3 cells for protein expression.

2.7.13.2 Cloning of the *S. cerevisiae* expression vector pDR196-CER-ZA

Expression of CER-ZA in *S. cerevisiae* was realised using the pDR196 vector (Meyer *et al.* 2006). The coding sequence of CER-ZA was amplified from cDNA using bn4277 and bn4171. The amplicon was subcloned into pJET1.2 and transformed into ElectroSHOX. Selected colonies were screened via PCR. Plasmids were isolated from positive clones and control digested. Inserts were cut from confirmed plasmids (EcoRI, SalI) and ligated into the multi cloning site of pDR196 (EcoRI, SalI). Again, selected colonies were screened via PCR (bn4174, bn4175) and positive ones were inoculated to isolate plasmids. Constructs were tested by control digest and sequencing. Confirmed plasmids were transformed into competent *S. cerevisiae* BY4741 (2.7.16). Colonies received on the plate were transferred to reference plates, briefly heated in the microwave and confirmed via PCR.

2.7.13.3 Cloning of the plant expression vector pBin-CER4PROM-CER-ZA-CER4TERM-DsRed

CER-ZA was expressed in the wax-deficient mutant *A. thaliana cer*4-3 to prove the function of CER-ZA *in planta*. The expression was under control of the endogenous CER4 promotor and terminator regions to target the expression to the epidermis. The regulatory units were amplified from *A. thaliana* Col-0 gDNA using bn3957/bn3958 to generate the promotor region (2159 bps) and bn3959/bn3960 to amplify the terminator region (439 bps, Rowland *et al.* 2006). The open reading frame of CER-ZA was amplified using bn3955/bn3956 from *H. vulgare* leaf cDNA. All three amplicons carried BsaI restriction sites and were designed for Golden Gate cloning. The acceptor vector pBin-35S-DsRed was cut with SmaI/MluI to remove the 35S promotor. The linearised vector was purified by gel electrophoresis and used for the final assembly (2.7.11). The ligated construct was transferred into *E. coli*, and colonies obtained on the plate were screened via PCR (2.7.15.1). Plasmids were control digested and confirmed by sequencing, followed by the electroporation into *A. tumefaciens* GV3101 pMP90 (2.7.15.2).

2.7.13.4 Cloning of the GFP-fusion construct pLH9000-CER-ZA

A GFP-tag was fused to the N-terminal site of the CER-ZA sequence to localise the protein on subcellular level after expression in *N. benthamiana*. The ORF of CER-ZA was amplified using bn4045 and bn4046 from freshly generated *H. vulgare* leaf cDNA. The amplicon was subcloned into pJET1.2 and transformed into ElectroSHOX cells. Next, colonies were screened via PCR and control digested. The coding sequence was cut from a positive plasmid with BamHI/SalI and purified, afterwards it was ligated into pLH9000 (BamHI/SalI) and transformed into ElectroSHOX. Colonies were screened via PCR, control digested and sequenced prior to the further electroporation into *A. tumefaciens* GV3101 pMP90.

2.7.14 Preparation of electrocompetent cells

2.7.14.1 Preparation of electrocompetent *E. coli*

A 10 mL preculture of the respective *E. coli* strain was grown over-night at 37°C. The cells were transferred to 400 mL of SOB medium and incubated at 37°C until the culture reached an OD600 of 0.5 to 0.8. Cell activity was inhibited by incubation on ice for at least 30 min. All following steps were performed on ice or with pre-cooled instruments. In addition, all solutions were kept cool and sterile. Cells were harvested by centrifugation at 3500 *g* for 10 min. The resulting pellet was washed with 50 mL of 0.5 M HEPES buffer to remove residual medium, followed by centrifugation at 4°C and 2400 *g* for 7 min. The buffer was discarded and two washing steps with ddH_2O were applied (2500 *g*, 4°C, 7 min) to remove remaining salts. Cells

were resuspended in 20 mL of 20% glycerol, followed by another centrifugation step (2500 *g*, 4°C, 7 min). Finally, the washed pellet was resuspended in 1-5 mL of 10% glycerol in dependence on the size of the remaining pellet. 50 µL aliquots were prepared, immediately frozen in liquid nitrogen, and stored at -80°C until transformation.

SOB medium

Peptone	20.0 g
Yeast extract	5.0 g
NaCl	0.6 g
KCl	0.18 g
dH_2O	ad 1000 mL
	Adjusted to pH 7.0 with NaOH.
	Separately filter sterilised and added after autoclaving:
1 M $MgCl_2$	2 mL
1 M $MgSO_4$	2 mL

2.7.14.2 Preparation of electrocompetent *A. tumefaciens*

20 mL liquid culture of the respective *A. tumefaciens* strain was grown for two days at 28°C in YEP medium with the corresponding antibiotics. The preculture was used to inoculate 200 mL of a main culture which was grown to an OD600 of 0.8 at 21°C overnight. The culture was transferred to sterile centrifugation retainers and kept on ice for 30 minutes to reduce the cell activity. All following steps were performed with precooled equipment and liquids to keep the bacteria cold at any time. Cells were pelleted by centrifugation at 3500 *g* for 15 min. The medium was removed, cells were resuspended in 50 mL cold water and transferred to 50 mL centrifugation tubes before they were centrifuged at 3200 *g* for 10 min. Washing of the cell pellet was performed two more times with 15 min of incubation time on ice between each single step. Finally, pellets were resuspended in 1-3 mL 10% glycerol and partitioned into 50 µL aliquots which were immediately frozen in liquid nitrogen and stored at -80°C until transformation.

2.7.15 Transformation of electrocompetent cells

2.7.15.1 Transformation of electrocompetent *E. coli*

A 50 µL aliquot of frozen electrocompetent *E. coli* was thawed on ice. A desalted ligation mixture or a low-concentrated, purified plasmid were added and mixed with the cells. The suspension was transferred to a pre-cooled electroporation cuvette. Application of 1.25 kV using a MicroPulser™ led to pore widening and enabled the transfer of plasmids across the

cell membranes. 300 µL of antibiotic-free LB medium were added and finally the cells were regenerated for 30 min at 37°C prior to being plated on selection medium.

2.7.15.2 Transformation of electrocompetent *A. tumefaciens*

Thawed cell aliquots were mixed with the plasmid of interest and incubated on ice for 30 min. Afterwards, the suspension was transferred into a precooled cuvette and electroporated by application of 1.25 mA. 500 µL of antibiotic-free YEP medium were added to the cells subsequently. Transformed bacteria were selected to solid medium supplemented with antibiotics at 28°C after 2 h of regeneration and afterwards further incubated for 48-72 h.

2.7.16 Preparation and transformation of chemically competent *S. cerevisiae*

Chemically competent *S. cerevisiae* cells were always freshly prepared and subsequently transformed according to (Gietz and Schiestl 2007) with implemented modifications by Gabriel Schaaf and Dominique Loque (INRES, University of Bonn).

2.7.16.1 Preparation of chemically competent *S. cerevisiae* cells

A freshly grown colony was used to inoculate 5 mL of liquid YPD medium and the culture was incubated under shaking at 180 rpm and at 28°C over-night. 200 µL of the over-night cultures were transferred to 4 mL of fresh YPD medium and grown to an OD600 of 0.8 over four to six hours. Cells were harvested in 2 mL reaction tubes by centrifugation at 1700 *g* for 1 min. Supernatants were discarded and the cell pellets were washed four times (1700 *g*, 2 min) with 500 µL TE/LiAc buffer at RT. Finally, cell pellets were resuspended in 150 µL of TE/LiAc Buffer and kept on ice until transformation.

(10x) TE buffer	
Tris-HCl	100 mM
EDTA	10 mM
	Adjusted to pH 7.5 with NaOH.

TE/LiAc buffer	
10x TE Buffer	5 mL
1 M Li acetate	5 mL
ddH_2O	ad 50 mL

2.7.16.2 Transformation of chemically competent *S. cerevisiae* cells with the lithium acetate method

Transformation mixtures were set up in PCR tubes and the heated incubation steps were performed in a thermocycler. The mixtures were pipetted in the following order. 3.5 µL of carrier

DNA (8 mg/mL) were added to each tube, warmed up and denaturated at 95°C. Afterwards, the tube was cooled on ice for 2 min. 200-500 ng plasmid DNA were added to the mixtures, followed by 30 µL of freshly prepared competent cells. 200 µL PEG/LiAc Buffer were added and tubes were incubated on a shaker at 500 rpm for 40 min. The heat-shock was performed at 42°C for 20 min, and resuspension of the cells in 800 µL sterile ddH_2O stopped the transformation. Cells were harvested by brief centrifugation at 1700 *g* for 1 min and resuspended in 60 µL sterile ddH_2O. Recombinant cells were selected on uracil-deficient medium after incubation at 28°C for 24-72 h.

PEG 4000 [50% (w/v)]

Polyethylene glycol 4000	40 g
Add ddH_2O to a volume of 70 mL, dissolved by heating.	
ddH_2O	ad 80 mL

PEG/LiAc buffer

1 M LiAc	10 mL
10x TE Buffer	10 mL
PEG 4000 [50% (w/v)]	ad 80 mL

Single-stranded carrier DNA

Salmon Sperm DNA	400 mg
TE/LiAc Buffer	ad 50 mL
Incubated at 4°C for 24-48 h under continuous shaking prior to long-time storage at -20°C.	

Glucose [20% (w/v)]

Glucose	20 g
ddH_2O	ad 100 mL

Uracil Dropout powder

Adenine hemisulfate	2.5 g
L-Arginine	1.2 g
L-Aspartate	6 g
L-Glutamate sodium salt	6 g
L-Lysine	1.8 g
L-Methionine	1.2 g
L-Phenylalanine	3 g
L-Serine	22.5 g
L-Threonine	12 g
L-Tyrosine	1.8 g
L-Valine	9 g

Histidine, Leucine and Tryptophan stock solutions

L-Histidine	100 mM
L-Leucine	100 mM
L-Tryptophan	40 mM
ddH_2O	ad 50 mL

NaOH was added in traces to enhance solubility.

Sterile filtrated and stored at 4°C.

Yeast selective uracil-deprivation medium

Uracil Dropout powder	1.16 g
Yeast Nitrogen Base (with ammonium sulfate, without amino acids)	6.7 g
Bacto-Agar (optional)	2 g
ddH_2O	ad 880 mL

Adjusted to pH 5.9 with NaOH.

Autoclaved, cooled down to 55°C:

Sterile Glucose solution [20% (w/v)]	100 mL
L-Histidine Stock	8 mL
L-Leucine Stock	8 mL
L-Tryptophan Stock	8 mL
Sterile ddH_2O	ad 1000 mL

2.7.17 Transformation of *A. thaliana* by floral dipping

Freshly transformed *A. tumefaciens* cells were used to inoculate a 200 mL liquid culture in YEP medium containing the required antibiotics. Cells were harvested by centrifugation at 3200 *g* at 4°C for 10 min. The pellet was resuspended in 200 mL dipping solution required to maintain a balanced osmotic gradient and enhance the surface application. In a first attempt, a brush was used to apply the bacterial solution directly to the flowers and slightly damage the tissue to induce the infection, followed by the direct dipping of the flowers into the bacterial solution for 10 s. Transformed plants were regenerated in the dark for 24 h. The treatment was repeated after five to seven days to increase the yield of transformed seeds.

Dipping solution

Sucrose	50 g
SILWET® Gold	1 mL
Tab water	at 1000 mL

After ripening of siliques, seeds were harvested and screened for DsRed expression under the fluorescent binocular microscope indicating a successful transformation. The T1 generation was grown and screened for their morphological and biochemical phenotype via GC/FID. Lines of interest were cultivated and T2 seeds were harvested. These seeds were screened for homozygous descendants which were used for the final cuticular wax analyses via gas chromatography.

2.7.18 Transient transformation of *N. benthamiana* for confocal microscopy

Three to five weeks old *N. benthamiana* plants were transformed by leaf infiltration with transgenic *Agrobacteria* (Wood *et al.* 2009). Electrocompetent *A. tumefaciens* GV3101 pMP90 cells were transformed (2.7.15.2) with pLH9000-CER-ZA and cultivated on YEP medium. Additional strains carrying the pMP19 vector and an DsRed-fused ER marker were simultaneously cultivated on selective medium. The P19 protein, originating from the Tombusvirus, mediates the suppression of RNA-silencing in the plant cell (Qiu, Park, and Scholthof 2002). Precultures were grown at 28°C for 2 d. 100 µL were used to induce main cultures of 10 mL volume. 20 h incubation at 28°C were followed by addition of acetosyringone to a final concentration of 1 mM to induce the virulence genes. Cultures were further incubated for 3 h. Meanwhile, *N. benthamiana* plants were well-watered and placed in the dark to stimulate the opening of the stomata and improve the infiltration with *Agrobacteria*. After incubation, bacterial cultures were harvested by centrifugation at 3200 *g* for 10 min. Pelleted cells were resuspended in 5 mL of infiltration solution. OD600 values for all cultures were determined and dilutions with a final OD600 of 0.4 were prepared. Same volumes of the

different strains were mixed, and 3 mL of the suspension were drawn up into a 5 mL plastic syringe. Since the stomata density is higher on the abaxial site of the leaf. The infiltration was done on this leaf side by gently pressing the suspension into the mesophyll tissue. After three days of incubation, leaf discs were produced with a hole drill and taped to a microscope carrier. Samples were analysed with a confocal microscope (IX71) equipped with a linear laser system (400 Series) and a DSU filter turret (Lambda 10-3). DsRed was excited with a laser wavelength of 561 nm, and emitted light was filtered over an emission band of 598-625 nm with a centre wavelength of 607.36 nm. Excitation of GFP at 488 nm caused GFP emission detected over a wavelength band of 502.5-537.5 nm with a centre wavelength of 525.3 nm. Z stacks were created to cover a depth of 290 nm in 30 planes.

***A. tumefaciens* infiltration solution**

$MgCl_2$	5 mM
MES	5 mM
Acetosyringone	100 µM
	Adjusted to pH 5.7 with NaOH.

2.8 Biochemical methods

2.8.1 Synthesis of fatty acid methyl esters

Fatty acids were derivatised by transesterification with methanol to mask the carboxy groups. This step to improves the volatility for the analysis via gas chromatography on the one hand and allows the separation of free fatty acids from other lipid classes on the other hand. Initially, analytes were resuspended in 1 mL of 1 M methanolic HCl. The acid-catalysed reaction took place by incubation at 80°C for 30-60 min (Figure 5). Lipids were extracted with 1 mL of n-hexane and 1 mL 1 M NaCl. Samples were briefly vortexed and centrifuged at 1700 *g* for 5 min. The organic solvent phase was transferred into a cleaned glass vial, evaporated under nitrogen flow and the methyl esters dissolved in n-hexane for the final analysis.

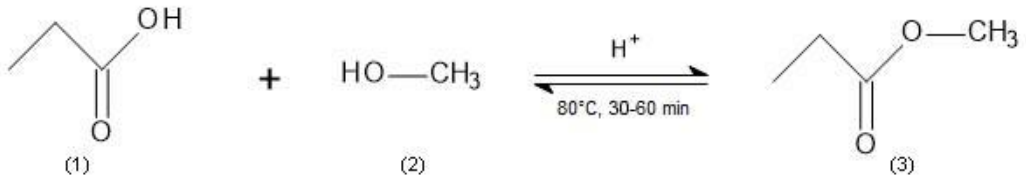

Figure 5: Derivatisation reaction scheme of fatty acids (1) with methanolic HCl (2). Fatty acyl methyl esters are formed by transesterification (3).

2.8.2 Extraction of total cuticular wax fractions from barley leaves

The second leaves of 14 d old barley plants were cut in 2 cm distance from the stem. Harvested leaves were dipped into 40 mL of chloroform for 10 s under continues movement. Subsequently, 10 µg of tetracosane were added to the sample as internal standard, and the leaf surface was scanned to enable the later normalisation via the surface area. Wax extracts were concentrated under nitrogen flow to a volume of 200 µL. 20 µL each of pyridine and BSTFA were added to individual samples for the derivatisation step (2.8.6). Finally, derivatised samples were transferred to analytic vials and measured by gas chromatography (2.8.5).

2.8.3 Cuticular wax analyses of *A. thaliana* stems

Two stems per plant were collected from four weeks old, transformed *A. thaliana cer*4-3 plants. The corresponding wild-type Columbia-0 (Col-0) and the untransformed *cer*4-3 line were included as controls. Leaves and flower buds were cut with a clean scissor. The tailored shoots were dipped into chloroform for 10 s to extract the cuticular waxes. 10 µg of tetracosane were added as internal standard. The leaf sections were scanned to allow surface area calculations. Extracts were evaporated to a volume of 200 µL under nitrogen flow and derivatised with BSTFA (2.8.6). Derivatised extracts were transferred into analytic vials and compounds quantified via GC/FID (2.8.5).

2.8.4 Extraction of intra- and epicuticular wax fractions from *H. vulgare* leaves

Epicuticular wax fractions were isolated with collodion according to Zeisler & Schreiber (2016). Collodion does not create artifacts and is non-soluble in chloroform thus simplifying the later analyses. First, chloroform-cleaned magnets were used to delimit defined areas of 2 cm length along the leaf blades of 14 d old *H. vulgare* plants. A drop of collodion was carefully applied to the section without touching the surface area. After drying, the nitrocellulose strip was transferred to a glass vial. The procedure was repeated for both sides of the leaves, afterwards the stripped leaf area was cut from the magnets and dipped into chloroform for 10 s. Surface areas were scanned for later surface area determination. 5 mL chloroform were added to the strips to dissolve wax compounds. 10 µg tetracosane were added to each sample subsequently. Extracts were derivatised with BSTFA. Finally, wax compounds were analysed by gas chromatography (2.8.5).

2.8.5 Quantification of cuticular wax components via GC/FID

The composition of extracted cuticular waxes was determined using a GC/FID system composed of a gas chromatograph 6890N and a connected flame ionisation detector (FID). Samples were separated according to their molecular mass, structure and polarity on a column composed of polysiloxane (DB-1) with a defined temperature program (Table 5). Hydrogen

served as mobile phase. Nitrogen was used to mask the oxyhydrogen flame utilized to ionise separated analytes.

Table 5: Temperature program for the analyses of total cuticular wax fractions via GC/FID. Samples were separated on a DB-1 GC column.

Step	Gradient [°C/min]	Step [°C]	Hold [min]
Injection		50	
Hold		50	2
Rise	40	200	
Hold		200	2
Rise	3	310	
Hold		310	30

2.8.6 Derivatisation of polar groups with BSTFA

Polar functional groups like hydroxy, carboxy or amino groups of analytes can interact with each other as well as with the polysiloxane based column polymer utilised for the sample separation in course of the gas chromatography. These groups should be masked to prevent the interactions which would cause peak tailing in the final chromatogram. N,O-Bis(trimethylsilyl)-trifluoracetamid (BSTFA) was used as donor for substitutional trimethylsilyl (TMS) groups (Figure 6). The resulting TMS derivatives are more volatile thus improving the analyses by gas chromatography. The reaction was incubated at 70°C for 45 min in the presence of pyridine as catalyst.

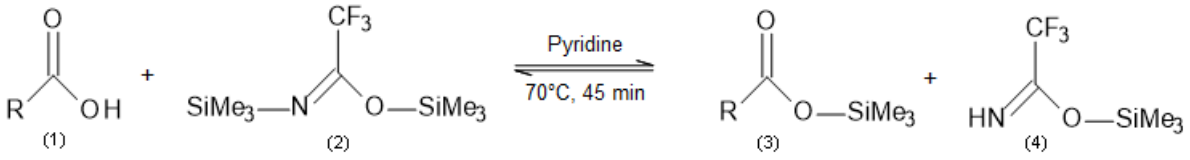

Figure 6: Derivatisation of polar groups (1) with BSTFA (2) catalysed with pyridine. A trimethylsilyl-(TMS) group is transferred to generate TMS-derivatives (3). Me, methyl.

2.8.7 Expression of the putative acyl-CoA reductase CER-ZA in *E. coli*

Colonies of freshly transformed cells, harbouring the pET-15b-CER-ZA vector, were used to inoculate 2 mL precultures. 1 mL bacteria solution was transferred to 1.5 mL reaction tubes and briefly centrifuged (4°C, 11,000 *g*, 3 min). Pellets were washed with PBS buffer to remove remaining medium. Centrifugation was repeated and cells were resuspended in fresh LB medium with antibiotics. 200 mL main cultures were inoculated with the suspensions and grown at 37°C to an OD600 of 0.5. Application of 0.5 mM IPTG induced the activity of the

regulative T7 promotor. Induced cultures were further incubated at 37°C for 5 h to allow the protein accumulation. Afterwards the bacterial activity was stopped by incubation at 4°C for 30 min. Cells were pelleted by centrifugation at 3200 *g* for 10 min at 4°C, and pellets were washed with 10 mL PBS buffer. The OD600 was determined in a 1:100 dilution for normalisation. 500 µL aliquots, prepared for latter protein isolation (0), were frozen in liquid nitrogen and stored at -80°C. Remaining cell suspensions were transferred into pre-cleaned glass vials for lipid extraction. Cell suspensions were centrifuged at 1700 *g* for 25 min or until all cells were pelleted, and the cell pellet was washed with ddH_2O. Remaining water was fully removed before the cell pellet was resuspended in 4 mL chloroform. In addition, 10 µg heptadecanol were added as internal standard. The extraction was either performed at 4°C over-night or at RT for 15 min under gentle shaking. Afterwards, samples were centrifuged again to remove the cell debris (1700 *g*, 25 min). Extracts were transferred to fresh glass vials, evaporated under nitrogen flow, and resuspended in 1 mL 1 M methanolic HCl. FAMEs were synthesised by incubation of the samples at 80°C for 1 h (2.8.1). 1 mL 0.9% NaCl and 1 mL n-hexane were added to stop the reaction and isolate lipids. The vials were briefly vortexed and centrifuged at 1700 *g* for 5 min. The organic solvent phases were transferred to new vials and evaporated under nitrogen flow. Lipids were dissolved in 1 mL fresh n-hexane and purified via solid phase extraction (SPE). The performed steps allowed to separate free alcohols from methylated acids (hexane, hexane:diethylether 99:1, 95:5 , and 92:8). The 92:8 fraction, containing free alcohols, was evaporated and dissolved in 200 µL chloroform. Samples were silylated with BSTFA (2.8.6) and transferred to analytic vials for measurement via gas chromatography (2.8.9).

Phosphate-buffered saline (PBS)

NaCl	137 mM
KCl	2.7 mM
Na_2HPO_4	8.1 mM
KH_2PO_4	1.76 mM

Adjusted to pH 7.2 with NaOH.

2.8.8 Expression of the putative acyl-CoA reductase CER-ZA in *S. cerevisiae*

Colonies transformed with pDR196-CER-ZA were used to grow 200 mL cultures at 30°C for 72 h. Cell pellets were harvested by centrifugation at 3500 *g* for 10 min. Pellets were resuspended in 5 mL of dH_2O and transferred to glass vials. After another centrifugation step (2500 *g*, 10 min), cell pellets were resuspended in 1 mL of methanol. 10 µg of heptadecanol were added as internal standard. Samples were incubated under continuous shaking for 5 min. 2 mL of chloroform were added followed by another 5 min of incubation. 1 mL of 0.9% NaCl was added prior to centrifugation at 2500 *g* for 15 min. The solvent fractions were transferred

to fresh glass vials and completely evaporated. Analytes were resuspended in 150 µL of chloroform and silylated with BSTFA (2.8.6). Afterwards, samples were analysed by GC/MS (2.8.9).

2.8.9 Measurements of primary alcohols

Extracted and derivatised primary alcohols were analysed by gas chromatography. Samples derived from *E. coli* (2.8.7) and *S. cerevisiae* (2.8.8) extracts were measured with by GC/MS using a 7890A GC system coupled to a 5975C inert XL MSD Triple-Axis Detector (Agilent Technologies). Separation of trimethylsilyl derivatives was achieved on an HP-5MS (5%-phenyl)-methylpolysiloxane column (Table 6). The lipids extracted from *E. coli* were silylated and quantified with a GC/FID system (7890A) equipped with a SP™-2380 capillary column (Table 7). Very long-chain primary alcohol were extracted from *S. cerevisiae*, silylated and quantified by GC/MS (Table 8) since no sufficient separation was achievable by the applied GC/FID.

Table 6: GC/MS program for the separation of primary alcohols from *E. coli*. Carrier gas flow rate was constantly hold at 2.18 mL/min. The split-splitless inlet was heated to 250°C with a septum purge flow of 3 mL/min. Injection volume was 1 µL.

Step	Gradient [°C/min]	Step [°C]	Hold [min]
Injection		80	
Rise	4	210	
Hold		210	4
Decrease	20	80	

Table 7: GC/FID program for the separation of primary alcohols from *E. coli*. Carrier gas flow rate was constantly hold at 7.0 mL/min. The split-splitless inlet was hold at 250°C with a septum purge flow of 3 mL/min. 2 µL of each sample was injected.

Step	Gradient [°C/min]	Step [°C]	Hold [min]
Injection		100	
Hold		100	2
Rise	5	200	
Hold		200	10
Decrease	20	100	

Table 8: GC/MS program for the separation of primary alcohols from *S. cerevisiae*. Carrier gas flow rate was constantly hold at 1.05 mL/min. The split-splitless inlet was hold at 250°C with a septum purge flow of 3 mL/min. Injection volume was 1 µL.

Step	Gradient [°C/min]	Step [°C]	Hold [min]
Injection		120	-
Hold		120	2
Rise	10	180	-
Hold		180	2
Rise	5	310	-
Hold		310	10
Decrease	20	120	-

2.8.10 Isolation of proteins from *E. coli*

Cell pellets stored in PBS buffer were centrifuged at 11,000 *g* for 2 min. Supernatants were removed, and the pellets were resuspended in 4x Laemmli reduction buffer (Laemmli 1970) and water according to their OD600 (50 µL 4x Laemmli reduction buffer x OD600; 80 µL ddH_2O x OD600) by vigorous vortexing. The samples were sonicated for 15 min and incubated at 95°C for 5 min. Protein extracts were briefly vortexed and sonicated for another 15 min to degrade released DNA and carbohydrates. Finally, samples were centrifuged at 11,000 *g* for 5 min. Protein-containing supernatants were transferred to new 1.5 mL reaction tubes without stirring the pellets and placed on ice.

(5x) Laemmli stock buffer		**(4x) Laemmli reduction buffer**	
Tris	100 mM	Laemmli stock buffer (5x)	80% (v/v)
SDS	2% (w/v)	β-Mercaptoethanol	10% (v/v)
Glycerol	10% (w/v)	ddH_2O	10% (v/v)
EDTA	1 mM		
Bromophenol blue	0.005% (w/v)		

2.8.11 Separation of proteins via SDS-PAGE

Isolated proteins were separated in an electric field by sodium dodecyl sulfate polyacrylamide gel electrophoresis (SDS-PAGE) (Laemmli 1970). The separating gel was filled into the glass carrier to approximately 70% of capacity. The gel was flattened by adding isopropanol and left for 45 min to allow the polymerisation. Next, the stacking gel was prepared and added on top of the separation gel after removal of isopropanol. A comb was placed, and the gel was left for another 45 min to polymerise. SDS-PAGE gels could be stored for up to three weeks in 1x tank buffer at 4°C. For electrophoresis, gels were clamped on both sites of the gel running

chambers. The chambers were filled with 1x tank buffer before the comb was removed and 10 µL of each sample were filled to the slot. 3 µL protein standard (Color Prestained Protein Standard, Broad Range 10-250 kDa, NEB) were mixed with 7 µL 4x Laemmli buffer and added into one slot as molecular weight marker. Unloaded slots were filled with 10 µL 4x Laemmli buffer to ensure an even load and reduce the 'smiling' effect. The power supply was adjusted to 25 mA and 150 V and the electrophoresis performed for approximately 30 min until the samples aligned at the separation gel. Afterwards the amperage was increased to 35 mA and run until the sample front reached the bottom end of the gel. Finished gels were either stained with Coomassie Blue (2.8.11.1) or processed for Western Blot (2.8.11.2).

(10%) SDS-PAGE gel

Separating gel (10%)		**Stacking gel (4%)**	
ROTIPHORESE Gel 40 (29:1)	17 mL	ROTIPHORESE Gel 40 (29:1)	2.66 mL
1.5 M Tris-HCl, pH 8.8	12.5 mL	0.5 M Tris-HCl, pH 6.8	5 mL
SDS, 10%	0.5 mL	SDS, 10%	0.2 mL
TEMED	20 µL	TEMED	10 µL
APS, 10% (w/v)	0.3 mL	APS, 10% (w/v)	0.2 mL
dH_2O	20 mL	dH_2O	12 mL

(1x) SDS tank buffer

Tris	25 mM
Glycine	192 mM
SDS	0.1% (w/v)

2.8.11.1 Visualisation of proteins by Coomassie Blue staining

Separated proteins in the gel were visualised with Coomassie Blue. The stacking gel was removed with a razor blade after disassembling the protein gel chamber and the separation gel, harbouring the proteins, was placed in a glass container and overlaid with Coomassie Blue staining solution. The stain was briefly heated in the microwave oven until cooking and incubated on a shaker for 5 min. The staining solution was removed, and the gel was washed with dH_2O before the de-stain solution was added. The gel was heated in the de-stain solution again in the microwave oven. Afterwards, it was incubated under continues shaking for at least 15 min. The de-stain solution was exchanged, and the procedure repeated three to five times until the gel was completely transparent again. After the final step, the gel was rinsed with dH_2O and photographed on a light table using a D700 camera and a 105 mm F2.8 D macro lens (Nikon Corporation).

Coomassie Blue staining solution	
Ethanol (95%)	50% (v/v)
Acetic acid, glacial	7.2% (v/v)
Coomassie® R-250	0.25% (w/v)
dH_2O	42.55% (v/v)

SDS-Page de-stain solution	
Glycerol	5% (v/v)
Acetic acid, glacial	7.5% (v/v)
dH_2O	87.5% (v/v)

2.8.11.2 Visualisation of His-tagged proteins by Western Blot

The Western Blot was performed according to Towbin, Staehelin and Gordon (1979). An SDS-PAGE gel was removed from the electrophoresis chamber and the stacking gel was cut using a razor blade. The gel was incubated in Towbin transfer buffer for at least 5 min. Whatman Filter Paper (0.8 mm thick) and a nitrocellulose membrane (0.45 µm pore size) were cut to the gel size and shortly soaked with Towbin transfer buffer. Three layers of filter paper were placed in the middle of the blotting device. The nitrocellulose membrane was placed on top, layered by the SDS-PAGE gel and three additional layers of filter paper. Air bubbles were avoided and, if enclosed, removed by rolling out with a glass tube. The blotting device's lid (Trans-Blot SD) was properly pressed on, and the power supply was adjusted to 15 V and 70 mA. After 90 min, the nitrocellulose membrane was removed from the sandwich and transferred to 20 mL TBSTXSB buffer supplemented with 2% BSA to block unspecific binding sites. The membrane was incubated on a shaker at RT for 1 h or at 4°C over-night. 1 µL HisDetector Nickel-HRP (SeraCare) was added to the blocking solution prior to 1 h of incubation at RT under continuous shaking. Afterwards, the membrane was washed three times with TBSTXSB buffer for 15 min each step and rinsed with dH_2O in between. Finally, the membrane was constantly wetted with 1 mL Peroxide- and 1 mL Luminol-Enhancer solution (Pierce® ECL Western Blotting Substrate, ThermoScienfitic) for 10 min before it was exposed (Chemidoc MP).

Towbin transfer buffer	
Tris-HCl	3.03 g
Glycine	14.4 g
Methanol	200 mL
SDS (10%, w/v)	10 mL
dH_2O	ad 1000 mL

Adjusted to pH 8.3 with NaOH.

TBSTXSB buffer	
1 M Tris-HCl, pH 8	10 mL
NaCl	9 g
Triton X-100	1 mL
SDS	0.5 g
Thimerosal	0.1 g
Bovine serum albumin (BSA)	1 g
dH_2O	ad 1000 mL

Adjusted to pH 7.4 with NaOH.

2.9 Physiological Methods

2.9.1 Determination of cuticular wetting properties

A Drop Shape Analyser (DSA25S) was used to compare the contact angels of a water droplet on the leaf surface between different genotypes. The instrument determines the α and β angles between a determined baseline and the droplet. The average of both angles represents the finally determined contact angle. First, leaf segments of 3 cm length were tapped to a microscope slide while kept as flat as possible. Three water droplets of 20 µL were placed in equal distance onto each leaf. Contact angles of each drop were measured three times to create an average and reduce the methodical error caused by atmospheric movements. Further the values of all three droplets were averaged and the standard deviations calculated.

2.9.2 Gravimetrical determined water-loss of cut leaves

The described experiment was performed by Prof. Lukas Schreiber's working group. Five biological replicates for Bowman, *cer*-za.227 and *cer*-ye.267 plants were grown to the three-leaf stage. Stomatal transpiration rates were measured for the second leaf of well-watered plants at RT with a porometer. Afterwards, leaves were cut and incubated in a container harbouring silica gel to adjust for a low humidity. The loss of weight over time was frequently documented for the later calculations of the stomatal transpiration as well as the cuticular permeability rate.

2.9.3 Permeability of a photosynthetic inhibitor across the cuticular barrier

Cuticular barrier properties of Bowman, *cer*-za.227 and *cer*-ye.267 were recorded utilising the photosynthetic inhibitor Metribuzin. Therefore, the photosynthetic quantum yield (Y(II)) of photosystem II was monitored with a pulse-amplitude modulation (PAM) fluorometer, as the fluorescence parameter Y(II) provides information about the excitation energy flux of photosynthesis, and thus about the penetration of the photosynthetic inhibitor into the leaf (Genty, Briantais, and Baker 1989; Kramer *et al.* 2004). Data were collected in 5 min intervals after treatment for 3 h. The second leaf of individual plants was pressure sprayed over the whole leaf-length for three seconds with a suspension of 50 µmol Metribuzin in 0.1% of Brij 4. The detergent was required to achieve homogenous distribution of the applied suspension over the leaf surfaces since the wetting properties of the three genotypes strongly differ (3.1).

2.10 Software-based methods

2.10.1 Databases

A variety of databases and prediction tools for protein properties was consulted in course of this study (Table 9). For the investigated *cer* lines, protein and DNA sequences were searched and extracted from NCBI and EnsemblePlants. BLAST was used for nucleotide-protein translation as well as for the similarity search in genomes of interest. Protein models were constructed using Phyre2 and displayed with the NGL viewer. Further, transmembrane helixes were predicted by TMHMM and proteins localisations estimated by TargetP and DeepLoc, and peptide sequences were screened for targeting domains. Finally, cofactor binding sites and functional domains were predicted by the Cofactory and Pfam algorithms.

Table 9: List of databases and web services used in course of this study.

Platform	Purpose	Version	Hyperlink
BLAST	Sequence and similarity search	-	https://blast.ncbi.nlm.nih.gov
Cofactory	Cofactor binding sites	1.0	http://www.cbs.dtu.dk/services/Cofactory/
DeepLoc	Localisation	1.0	http://www.cbs.dtu.dk/services/DeepLoc/
EnsemblePlants	DNA and protein sequences	-	https://plants.ensemble.org
NCBI	DNA and protein sequences	-	https://www.ncbi.nlm.nih.gov
NGL Viewer	Protein model display	-	https://nglviewer.org/
Pfam	Functional domain homology	34.0	https://pfam.xfam.org/
Phyre2	Protein modelling based on homology	2.0	http://www.sbg.bio.ic.ac.uk/phyre2
SignalP	Signal peptides	5.0	http://www.cbs.dtu.dk/services/SignalP/
TargetP	Localisation	2.0	http://www.cbs.dtu.dk/services/TargetP/
TMHMM	Prediction of transmembrane regions	2.0	https://www.cbs.dtu.dk/services/TMHMM

2.10.2 Software

Cloning strategies were designed and developed with Clone Manager (Sci Ed Software, US) and SnapGene (GSL Biotech LLC, CA). Sequencing files were visualised with Chromas (Technelysium Pty Ltd, AU). Further, sequencing alignments and trimmings were done with MEGA X, ClustalX2 and ClustalW2 (EMBL-EBI, UK). Analytical data from GC analyses were evaluated with Instrument One (Agilent Technologies, US). The further processing of datasets was done with Microsoft Excel (Microsoft Corporation, US), and figures were additionally created with SigmaPlot (Systat Software GmbH, DE). Photos were modified with Adobe Photoshop 2020 (Adobe Inc., USA). Besides, chemical formulas were created with Strukturformel-Editor (Buchholz Wengst GbR, DE).

2.10.3 Generation of phylogenetic trees

Peptide sequences from proteins of interest were extracted from NCBI and aligned with ClustalW. Processed datasets were converted to MEGA X format and used to generate bootstrap consensus trees. Phylogenetic trees inferred from 500 replicas were calculated based on the Maximum Likelihood method (ML) to predict the evolutionary developed clusters between the genes of interest and a selection of species from different angiosperm families. Further, pBLAST was employed and the closest orthologs were added to the phylogenetic analysis. Trees were rooted to ancestral proteins from the protists *Euglenia gracilis* and *Trypanosoma brucei*.

3 Results

3.1 Leaves of the *cer*-za.227 and *cer*-ye.267 mutants show a reduced hydrophobicity

A previous study from Patwari (2019) reported a strong decrease of cuticular wax crystals on the leaf surface of the investigated *eceriferum* mutants. This reduction was observed concomitant with a decreased hydrophobicity. Leaves of 14 d old *H. vulgare* plants were wetted with a fine water sprayer to visualise this leaf hydrophobicity (Figure 7). An accumulation of droplets on the leaves of the two *cer* lines was noticed while the water was strongly repelled from the leaves of the Bowman cultivar.

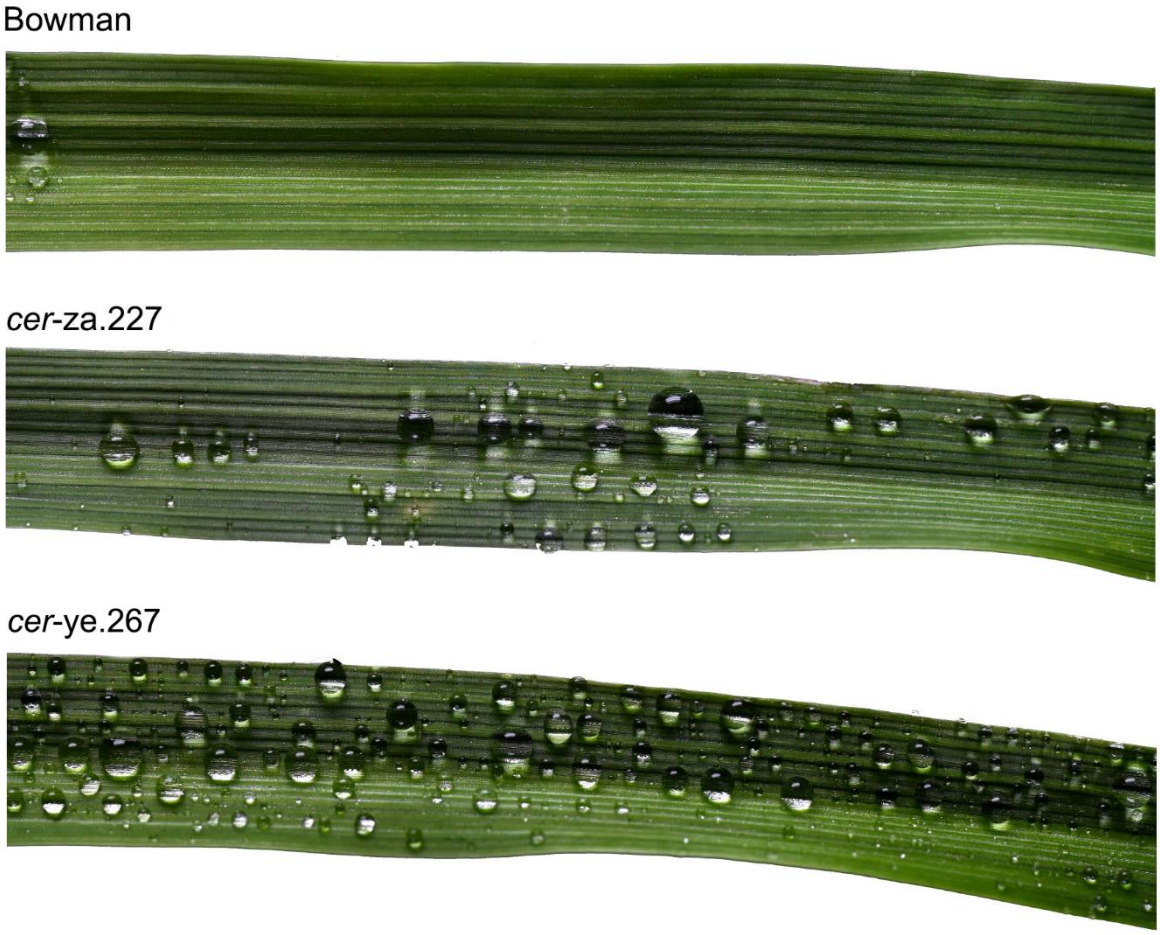

Figure 7: Water-repellent phenotypes of the leaves of the barley *cer*-za and *cer*-ye mutants are different from Bowman control. After spraying with water, droplets were repelled and rolled off immediately from the leaves of the cultivar Bowman (top), while large drops were spread on the surfaces of the barley mutant lines *cer*-za.227 (middle) and *cer*-ye.267 (bottom). Second leaves of 14 d old barley plants were sprayed with water and photos taken with a Nikon D850 and a Nikon AF 105mm f/2.8 D Micro-Nikkor lens.

To quantify the reduction of surface hydrophobicity, the contact angles of water droplets with a defined volume situated on the surface of flattened and fixed leaf sections were determined with a Drop Shape Analyser. Striking differences became already visible during the

experimental procedure since droplets rolled off almost immediately from Bowman samples. The leaf surface of the cultivar Bowman was determined as superhydrophobic (> 150°). In contrast, the two *eceriferum* lines were less hydrophobic: contact angles of 122.25 ± 2.61° were determined for *cer*-za.227, and 119.96 ± 7.36° for *cer*-ye.267. The reduced water repellence properties were used to screen for the *cer* phenotype in the following experiments. To quantify the reduction of surface hydrophobicity, a Drop Shape Analyser was applied to determined contact angles of water droplets with a defined volume situated on the surface of flattened and fixed leaf sections. Striking differences became already visible during the experimental procedure since droplets rolled off almost immediately from Bowman samples. The leaf surface of the cultivar Bowman was determined as superhydrophobic (> 150°). In contrast, the two *eceriferum* lines were less hydrophobic: contact angles of 122.25 ± 2.61° were determined for *cer*-za.227 and 119.96 ± 7.36° for *cer*-ye.267. The reduced water repellence properties were used to screen for the *cer* phenotype in the following experiments.

3.2 Cuticular wax accumulation is strongly affected in leaves of the *cer*-za.227 and *cer*-ye.267 mutants

Altered cuticular wax crystals on the surface of the two *cer* lines *cer*-za.227 and *cer*-ye.267 compared to Bowman were already reported by Patwari (2019). The increased leaf surface hydrophilicity strongly indicates macrostructural changes of the cuticular waxes and raised the question about possible variations in the biochemical composition. Consequently, cuticular waxes were extracted and analysed by gas chromatography.

3.2.1 *cer*-za.227 is deficient in primary alcohols and esters

Besides the analysis of the total cuticular waxes from leaves of the *cer*-za.227 mutant, epicuticular and intracuticular fractions were isolated and their compositions were measured. Overall, a striking decrease in the total wax load by approximately 60% (2.39 ± 0.46 µg/cm²) compared to Bowman (6.08 ± 1.12 µg/cm², Figure 8A) was noticed. The individual wax components were grouped into corresponding substance classes (Figure 8B). The predominant primary alcohols showed a significant reduction from 4.87 ± 0.80 µg/cm² to 1.51 ± 0.32 µg/cm² in *cer*-za.227, corresponding to a decrease by 70%. A significant decrease of roughly 40% was observed for esters from 0.94 ± 0.11 µg/cm² in Bowman to 0.58 ± 0.12 µg/cm² in *cer*-za.227. The amounts of aldehydes were slightly reduced with high standard deviations. While the contents of acids were not affected, the contribution of alkanes to the total wax load increased significantly from 0.04 ± 0.01 µg/cm² in Bowman to 0.13 ± 0.02 µg/cm² in *cer*-za.227. Consequently, alterations in individual substance classes affect the compositions of the wax fractions (Figure 9A). While the Bowman cuticular waxes are dominated by alcohols which make up 80%, this proportion decreased to 63% in *cer*-

za.227. Concomitantly, the percentage of alkanes in *cer*-za.227 increased from 0.8% to 5.3%. Although the absolute amounts of esters were decreased, their relative proportion increased from approximately 15% to 25%. When considering the chain length distribution across all lipids (Figure 9B), the strongest decreases were detected for C_{24}-C_{28}, as well as for C_{44}-C_{48}, while a significant increase was recorded for C_{33}. Since cuticular lipids with chain lengths of C_{24}-C_{28} are dominated by primary alcohols, and lipids with C_{44}-C_{48} correspond to the most dominant ester groups, these results are in agreement with the previous observation. Lipids with the chain length of C_{33} correspond to the only detected alkane in the wax fraction. Epicuticular waxes were removed with collodion, and both fractions, epi- and the remaining intracuticular waxes, were individually analysed. The epicuticular waxes made up 9.14 ± 0.87 µg/cm² (79.5%) of the total wax load in Bowman, while merely 2.34 ± 0.33 µg/cm² (21.5%) were found in the intracuticular fraction. In comparison, 1.78 ± 0.25 µg/cm² of epicuticular waxes were removed from the surface of *cer*-za.227, while 1.41 ± 0.23 µg/cm² remained in the intracuticular fraction (Figure 10A). The ratio of intracuticular (44.4%) to epicuticular (55.6%) waxes was consequently strongly shifted in *cer*-za.227. The reduction in total lipids in both fractions was mostly caused by a decrease in alcohols (Figure 10B), but while the amounts of alcohols were decreased to 50% in the intracuticular wax fraction (1.93 ± 0.26 µg/cm² to 0.89 ± 0.22 µg/cm²), the removed epicuticular waxes from *cer*-za.227 were seven-times less abundant compared with Bowman (7.88 ± 0.78 µg/cm² to 1.12 ± 0.15 µg/cm²). Esters decreased from 1.04 ± 0.11 µg/cm² to 0.49 ± 0.09 µg/cm² in the epicuticular fraction of *cer*-za.227, while alkanes and aldehydes contributed significantly more to the intracuticular wax fraction of *cer*-za.227. In the chain length distributions (Figure 11), significant decreases for lipids of C_{24}-C_{28} and C_{38}-C_{50} were noticed. These changes were particularly striking for C_{24}-C_{28} and C_{38}-C_{50} lipids between the epicuticular wax fractions which are strongly reduced in *cer*-za.227 compared to Bowman, while intracuticular waxes were less affected. In summary, the cuticular waxes in *cer*-za.227 are strongly reduced compared to the cultivar Bowman. This reduction is especially observed for alcohols and esters. Effects on the chain lengths are particularly distinctive in epicuticular waxes which are more strongly affected than the intracuticular fraction. Consequently, the reduction of different compound classes results in a shift of the relative composition of the wax fractions. Most prominent is the strong increase of alkanes in both, absolute and relative amounts, which is more significant in the intracuticular wax fraction.

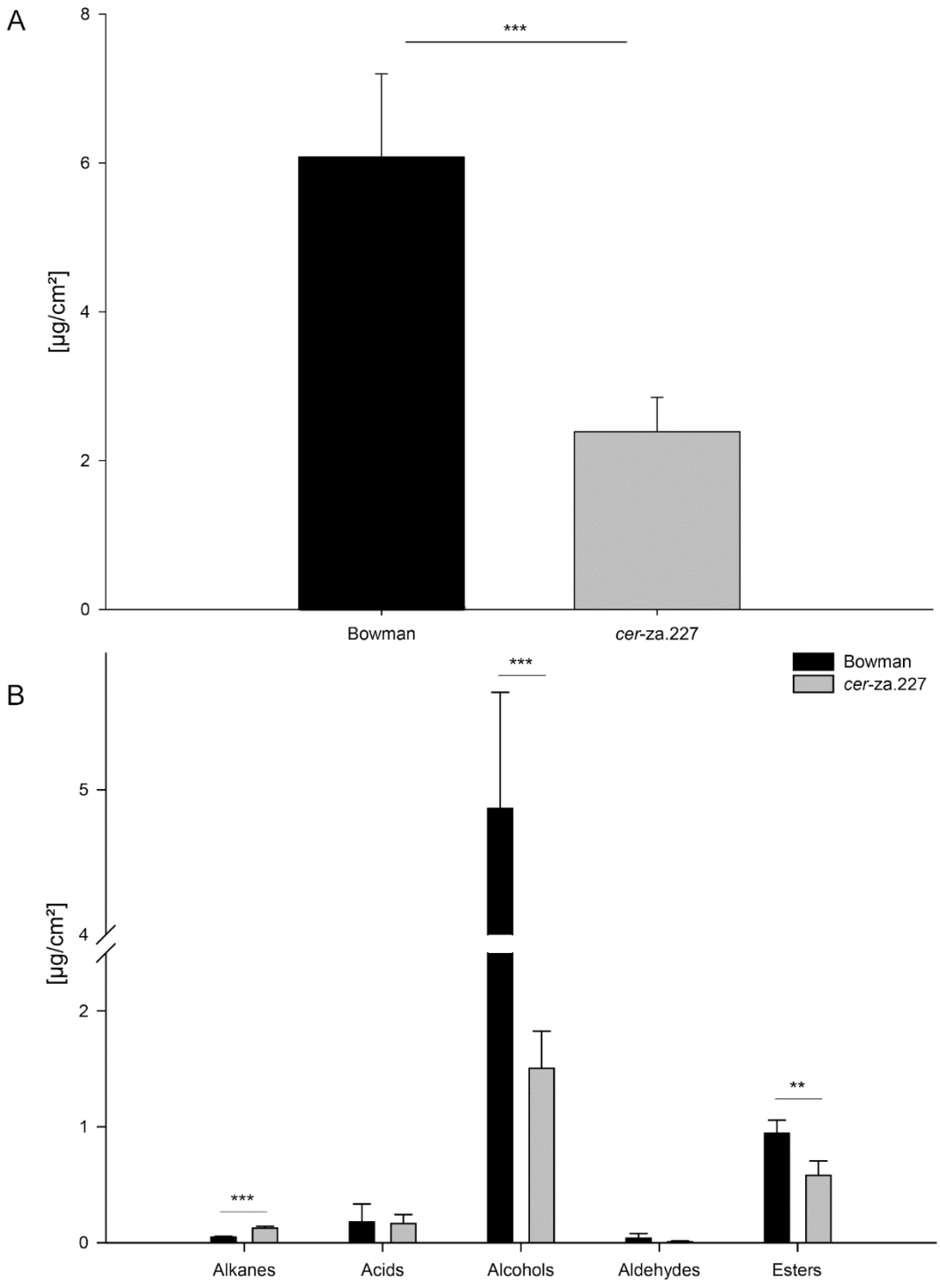

Figure 8: Cuticular waxes extracted from the second leaves of 14 d old *H. vulgare* Bowman and *cer*-za.227 were quantified by GC/FID. A: Total wax load. B: Distribution of aliphatic substance classes. n = 9. Student's *t*-test; $p^{***} \leq 0.01$. $p^{**} \leq 0.03$. $p^{*} \leq 0.05$.

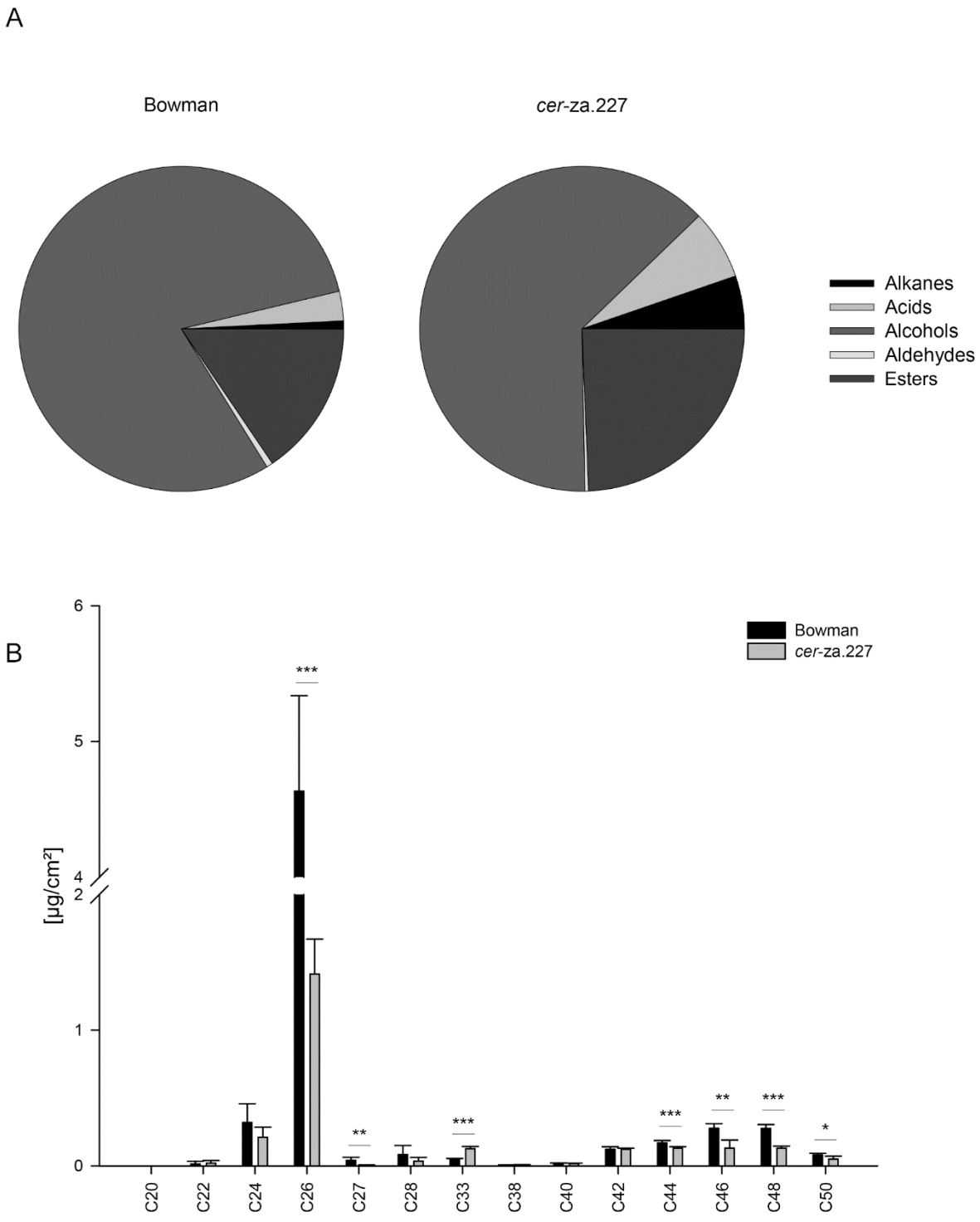

Figure 9: Cuticular waxes extracted from the second leaves of 14 d old *H. vulgare* Bowman and *cer*-za.227 were quantified by GC/FID. A: Relative substance class composition. B: Distribution according to chain lengths. n = 9. Student's *t*-test; $p^{***} \leq 0.01$. $p^{**} \leq 0.03$. $p^{*} \leq 0.05$.

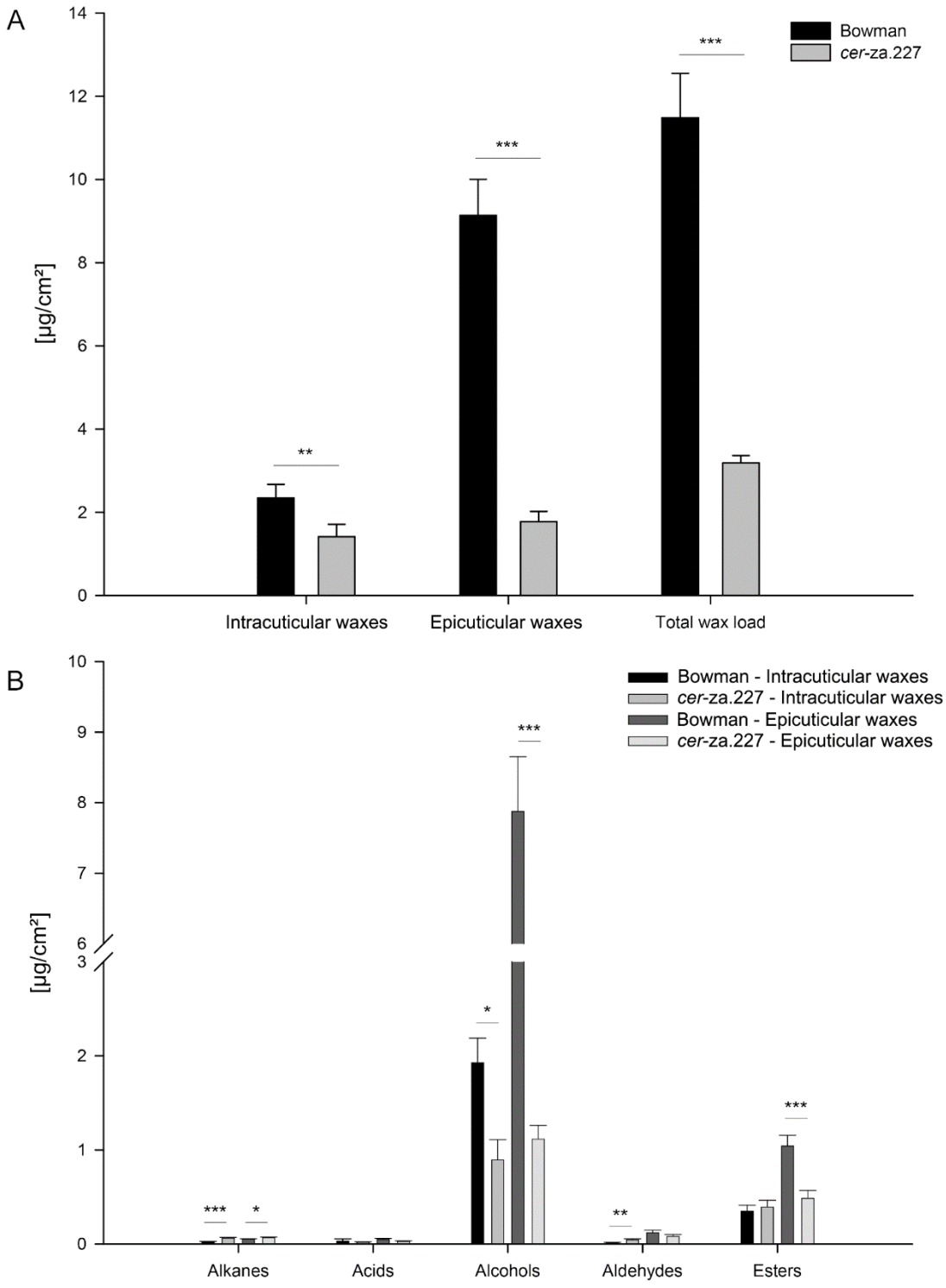

Figure 10: Analysis of epi- and intracuticular wax fractions isolated from leaves of Bowman and *cer*-za.227. A: Total wax load in the individual fractions. Both fractions were summed up to generate the total wax load. B: Substance class distributions in each fraction. n = 5. Student's *t*-test was applied to statistically compare the individual fractions of *cer*-za.227 with the Bowman cultivar; $p^{***} \leq 0.01$. $p^{**} \leq 0.03$. $p^{*} \leq 0.05$.

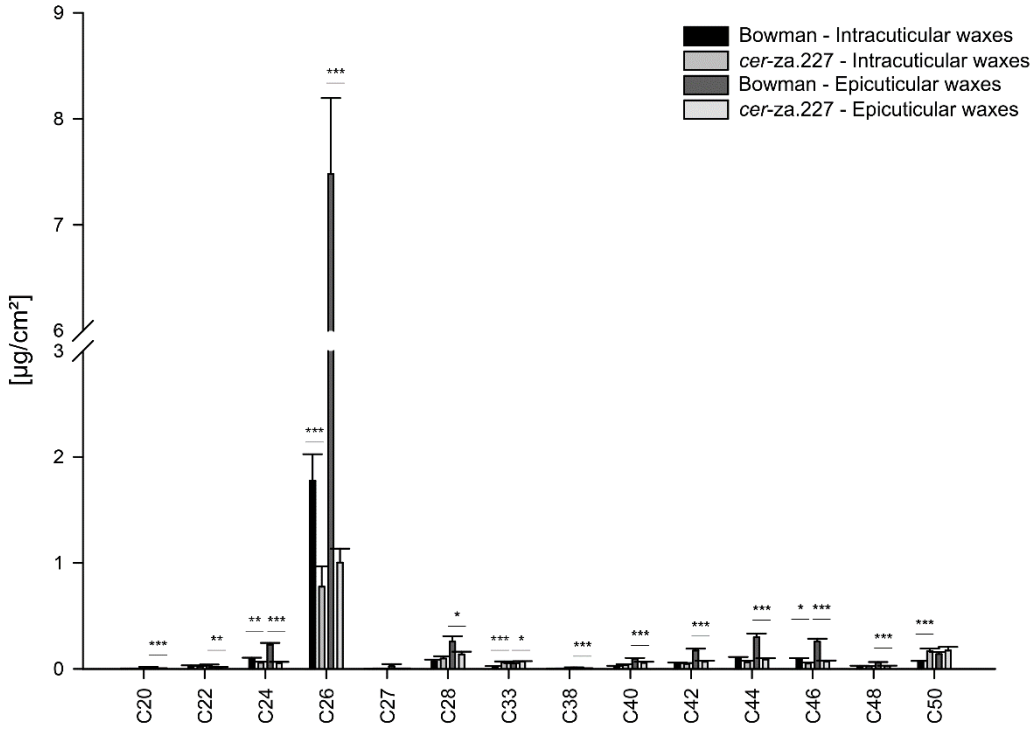

Figure 11: Chain length composition of cuticular wax fractions from Bowman and *cer*-za.277 according to their distribution into epi- and intracuticular waxes. Samples were quantified with GC/FID. n = 5. Student's *t*-test was applied to statistically compare the individual fractions of *cer*-za.227 with the Bowman cultivar; $p^{***} \leq 0.01$. $p^{**} \leq 0.03$. $p^{*} \leq 0.05$.

3.2.2 Three additional *cer*-za alleles show alterations in lipid composition analogous to *cer*-za.227

Three additional *cer*-za lines, *cer*-za.173, *cer*-za.232 and *cer*-za.318, which had previously been characterized as *cer*-za alleles by allelism test, are available at the Nordic Genetic Resource Center. In the present study, the three *cer*-za lines were biochemically characterised by comparison with the cuticular wax composition of *cer*-za.227. In all measurements, the three additional *cer*-za alleles showed very similar and statistically homogenous lipid composition. Therefore, in the following, only the data for one line, *cer*-za.173 are discussed, but the results of all three additional cer-za lines are shown in the figures. First noticeable was an overall reduction of the general wax load across the *cer*-za lines in a range from 3.29 ± 0.67 µg/cm² and 2.66 ± 1.12 µg/cm² for *cer*-za.173, *cer*-za.232 and *cer*-za.318 compared to 13.05 ± 3.02 µg/cm² in Bowman (Figure 12).

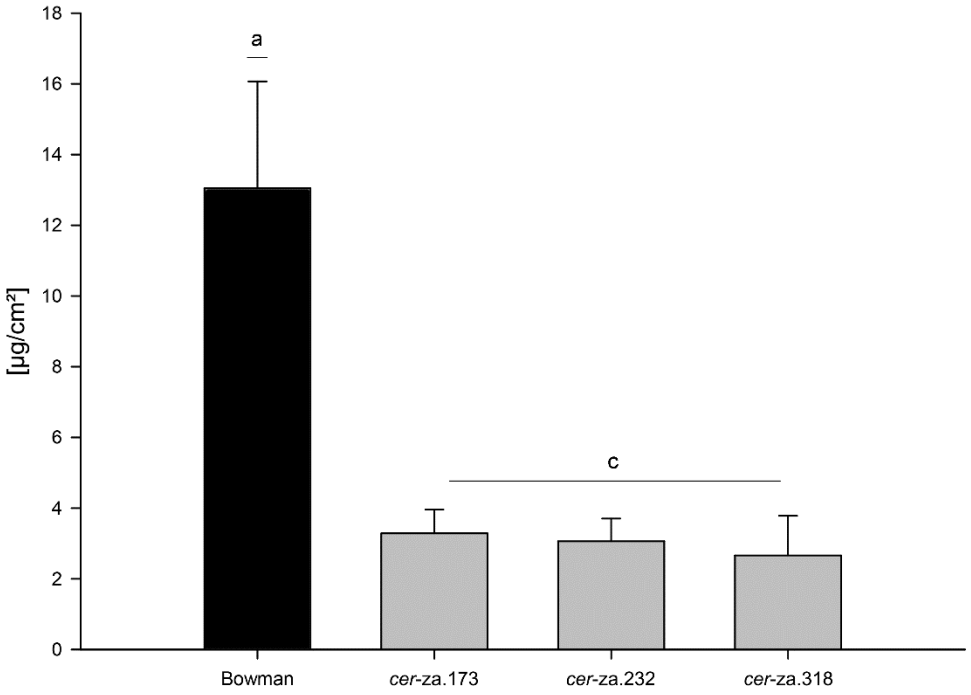

Figure 12: Total cuticular wax load from leaves of Bowman and additional *cer*-za alleles. Lipids were quantified with GC/FID. n = 5. ANOVA; $p_c \leq 0.01$.

The strongest impact was caused by the decrease of alcohols from 10.55 ± 2.22 µg/cm² in Bowman to 2.18 ± 0.54 µg/cm² in *cer*-za.173 (Figure 13A). The amount of lipids with C_{26} chain lengths, as dominant primary alcohol species, was reduced to 2.10 ± 0.49 µg/cm² in *cer*-za.173 compared to 10.84 ± 2.42 µg/cm² in Bowman. Substantial reductions were also observed for aldehydes (0.89 ± 0.35 µg/cm² to 0.17 ± 0.04 µg/cm²) and esters (1.38 ± 0.37 µg/cm² to 0.62 ± 0.06 µg/cm²), while acids and alkanes were not significantly altered. Consequently, the chain length compositions were also affected (Figure 13B). Besides, significant reductions were observed for lipids with the chain length range of C_{44}-C_{48} which represent esters.

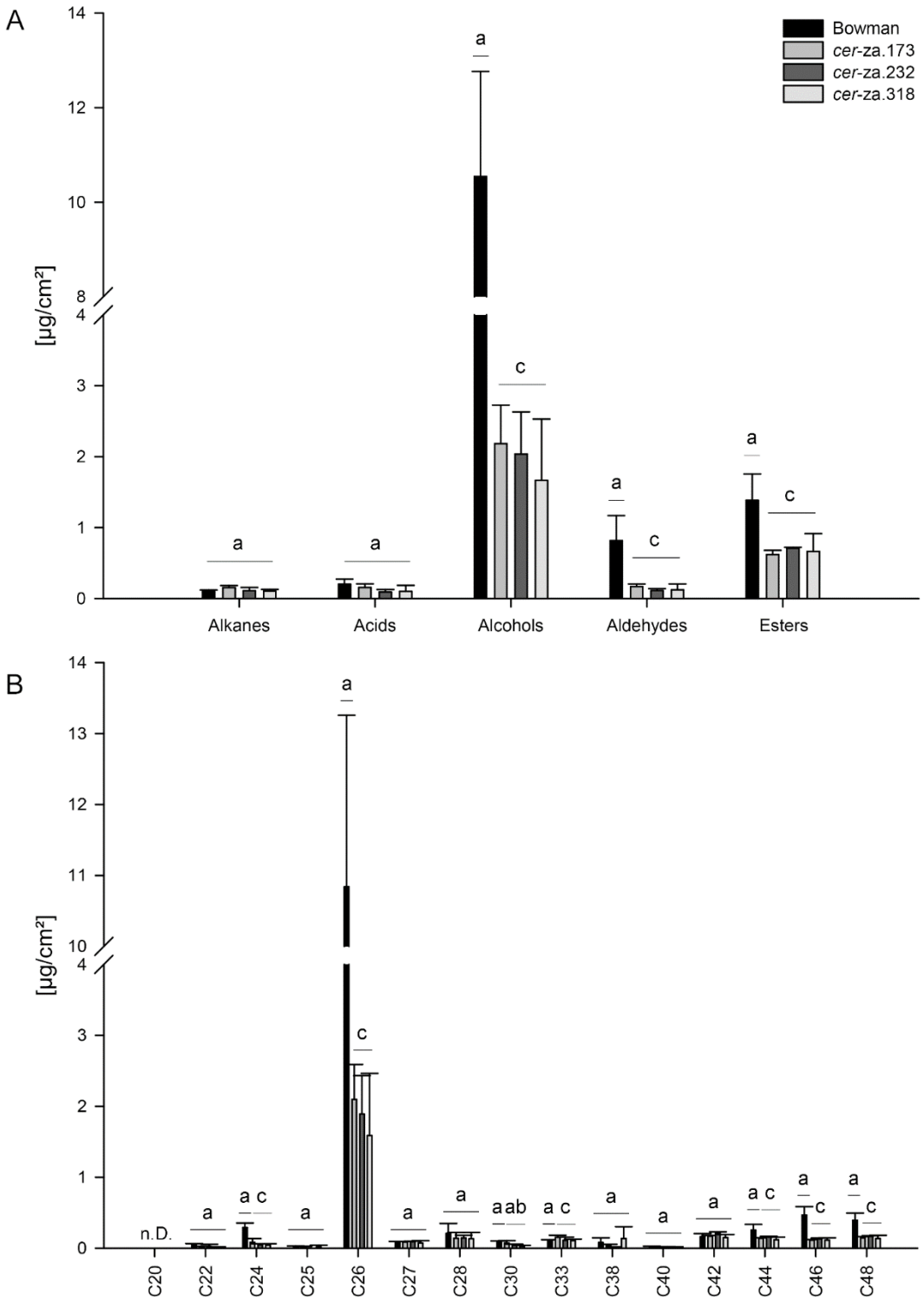

Figure 13: Composition of cuticular wax fractions from Bowman and *cer*-za alleles quantified by GC/FID. A: Distribution of aliphatic substance classes. B: Distribution with regard to the chain length pattern. n = 5. ANOVA; $p_c \leq 0.01$. $p_b \leq 0.03$. $p_{ab} \leq 0.05$.

3.2.3 The *cer*-ye.267 mutant is affected in cuticular lipids with a wide range of chain lengths

The lipids of *cer*-ye.267 were analysed in the total cuticle, and after separation, in the epicuticular and intracuticular wax fractions. A strong reduction to 37.7% of the total wax load was recorded for *cer*-ye.267 (3.28 ± 0.41 µg/cm²) in comparison to Bowman (8.67 ± 1.01 µg/cm², Figure 14). Nearly all substance classes were strongly affected (Figure 15A), with a decrease to 35.1% in alcohols (7.84 ± 0.90 µg/cm² to 2.76 ± 0.38 µg/cm²) and to 58.9% in aldehydes (0.24 ± 0.03 µg/cm² to 0.14 ± 0.07 µg/cm²). The amounts of esters were just slightly shifted and showed high standard deviations (Figure 15A/B). The broad reduction across nearly all substance classes was in line with the results shown for the chain length spectrum. Lipids with chain lengths of C_{24}-C_{33} and C_{42}-C_{50} were significantly affected and reduced to 20-40% of the wild-type wax load (Figure 16). Concomitantly, cuticular lipids with chain lengths between C_{38} and C_{40}, were slightly increased.

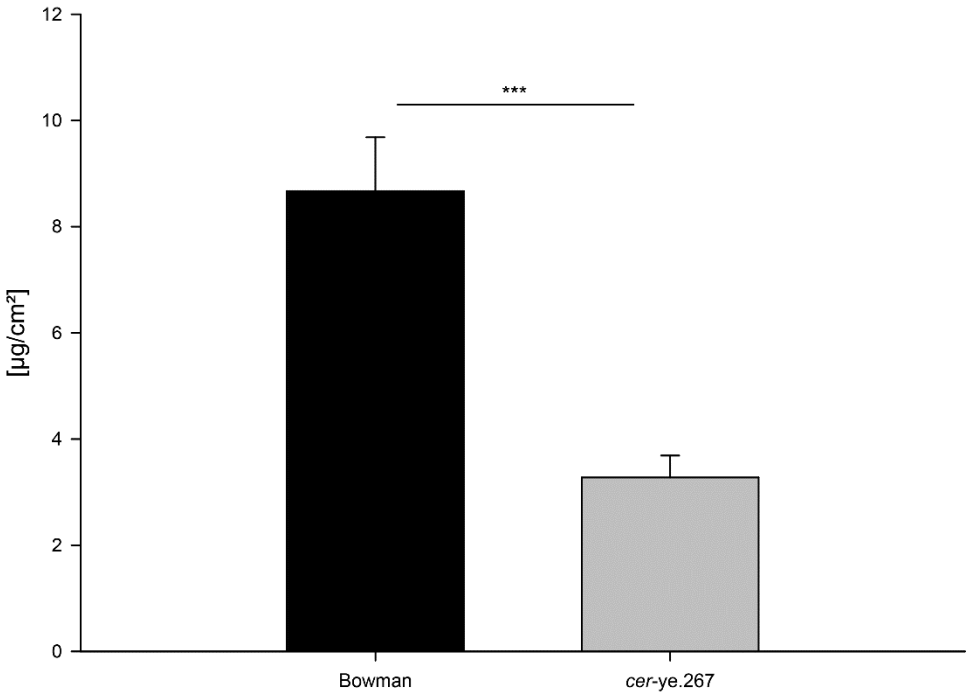

Figure 14: Total cuticular waxes from the second leaves of Bowman and *cer*-ye.267. Individual aliphatic compounds were quantified via GC/FID and summed up to calculate the total amount. n = 5. Student's *t*-test; *p**** ≤ 0.01. *p*** ≤ 0.03. *p** ≤ 0.05.

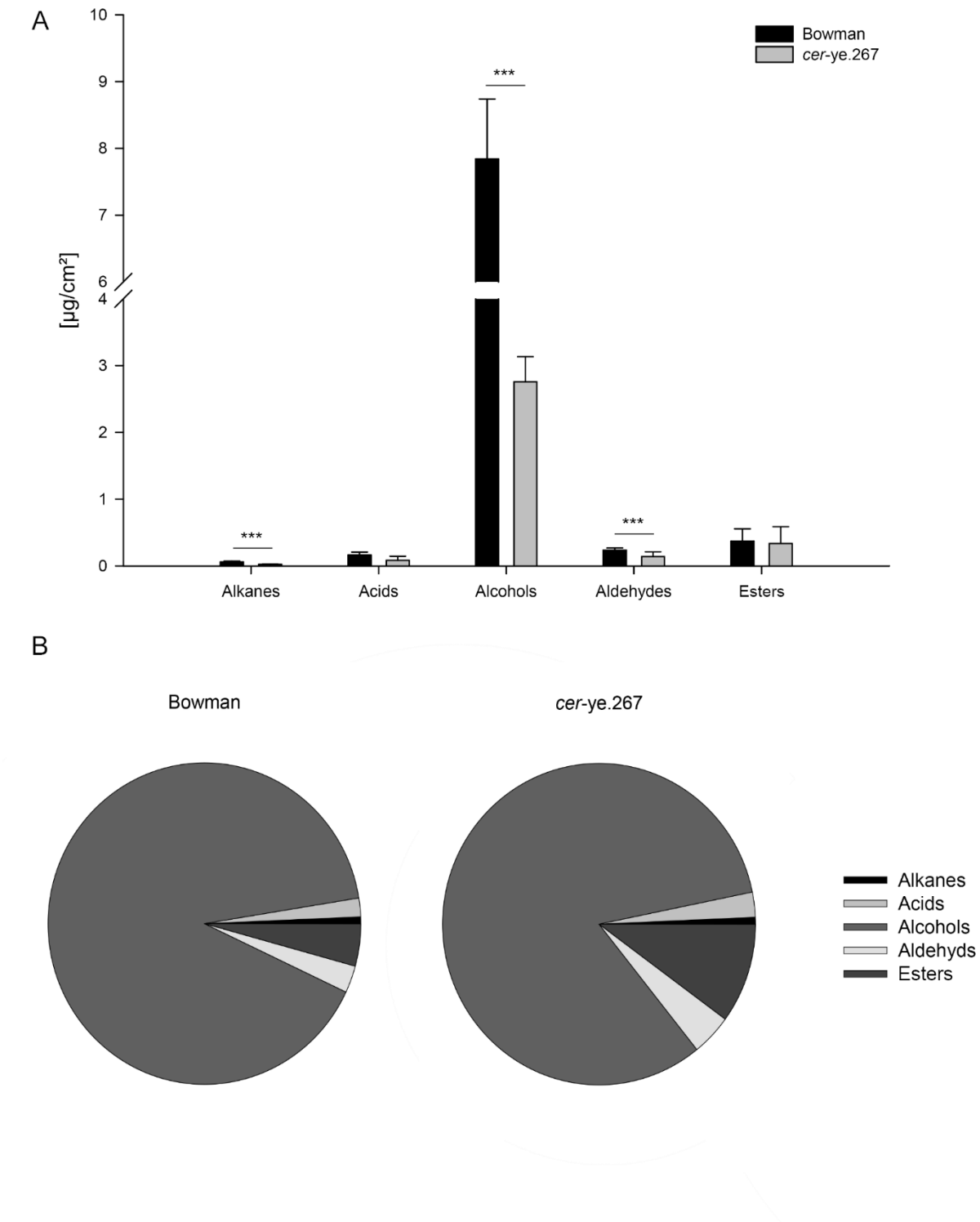

Figure 15: The composition of cuticular waxes from Bowman and *cer*-ye.267 was quantified via GC/FID. A: Substance class distribution. B: Relative substance class distribution. n = 5. Student's *t*-test; $p^{***} \leq 0.01$. $p^{**} \leq 0.03$. $p^{*} \leq 0.05$.

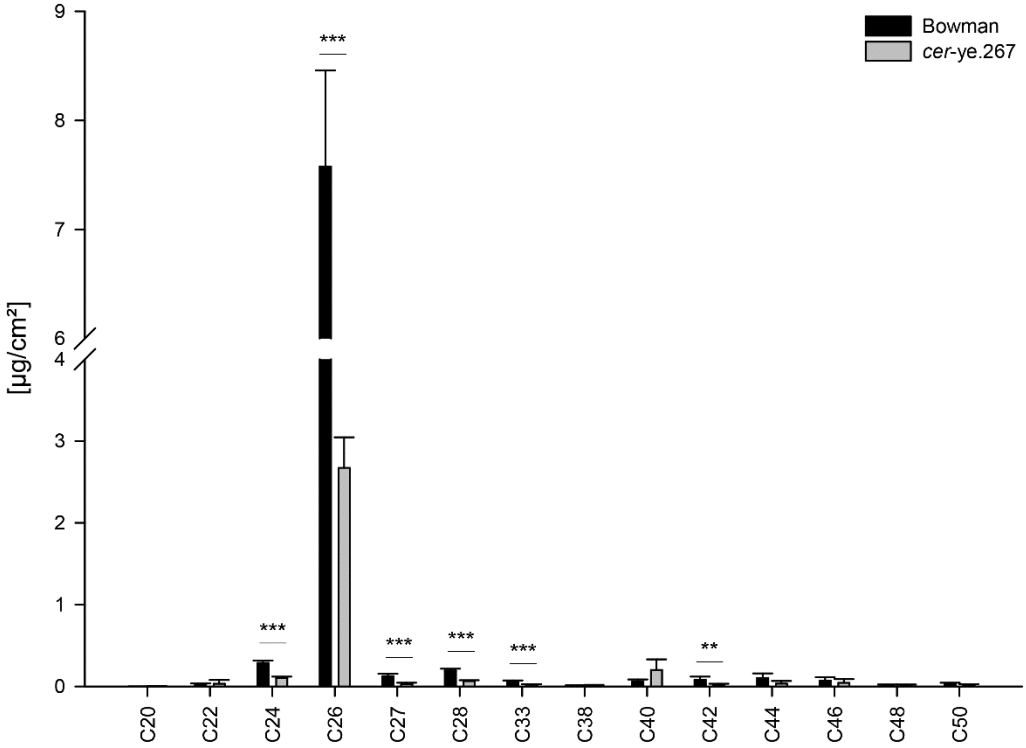

Figure 16: Chain length distribution of lipids in cuticular waxes from Bowman and *cer*-ye.267. Lipids were quantified with GC/FID. n = 5. Student's *t*-test; $p^{***} \leq 0.01$. $p^{**} \leq 0.03$. $p^{*} \leq 0.05$.

Epicuticular waxes were isolated to take a closer look on the impact of the mutation on the separated wax fractions. A reduction of 44.1% (2.34 ± 0.33 µg/cm² to 1.08 ± 0.17 µg/cm²) was recorded for the intracuticular waxes, while the total amount of epicuticular waxes in *cer*-ye.267 dropped to 25.7% (9.14 ± 0.87 µg/cm² to 2.35 ± 0.34 µg/cm²) of the Bowman levels (Figure 17A). Despite this strong reduction, the ratio of epi- and intracuticular waxes was just slightly shifted between Bowman (79.6/20.4) and *cer*-ye.267 (68.6/31.4). Like the previously described effect on individual substance classes, alkanes and alcohols were significantly reduced in both fractions. Epicuticular esters were additionally affected (Figure 17B). With regard to the chain length distribution, cuticular lipids with chain lengths of C_{20}, C_{24}, C_{26}, C_{28} and C_{33}, as well as C_{42}-C_{50} were strongly reduced. On the other hand, C_{40} containing lipids were concomitantly increased in epicuticular and intracuticular fractions (Figure 18). In conclusion, the cuticular waxes of *cer*-ye.267 were similarly affected in a broad range of components over the complete spectrum of chain lengths. Thereby, intra- and epicuticular fractions were affected in a similarly strong extent. Consequently, only a slight shift in the ratio of the two fractions was observed.

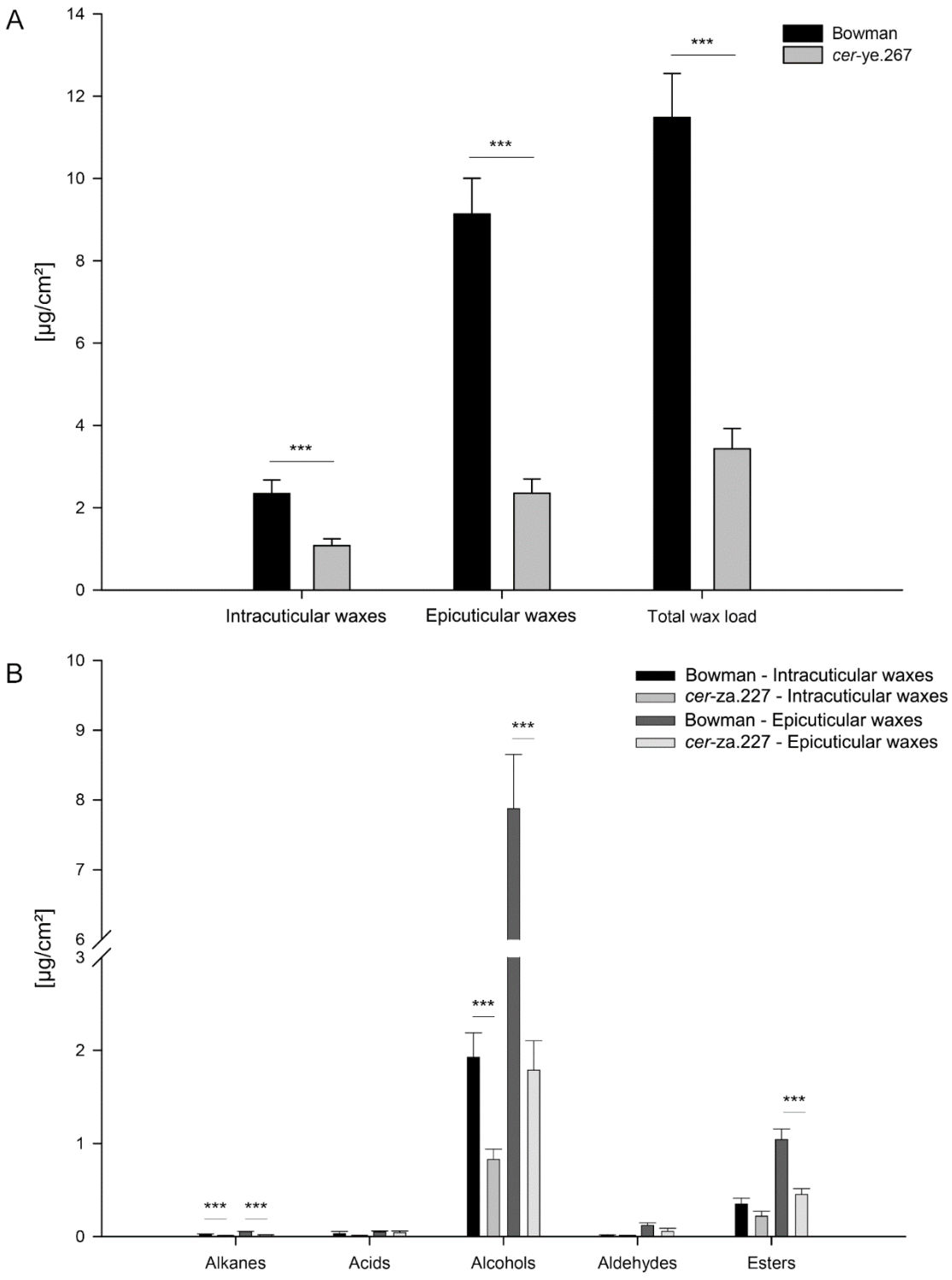

Figure 17: Analysis of epi- and intracuticular wax fractions from leaves of Bowman and *cer*-ye.267 quantified by GC/FID. A: Total wax load in the individual wax fractions. The lipids stripped from the leaves (epicuticular) and remaining (intracuticular) fractions were summed up to calculate the total wax load. B: Substance class distribution. Student's *t*-test was applied to statistically compare the individual fractions of *cer*-ye.267 with the Bowman cultivar; $p^{***} \leq 0.01$. $p^{**} \leq 0.03$. $p^{*} \leq 0.05$.

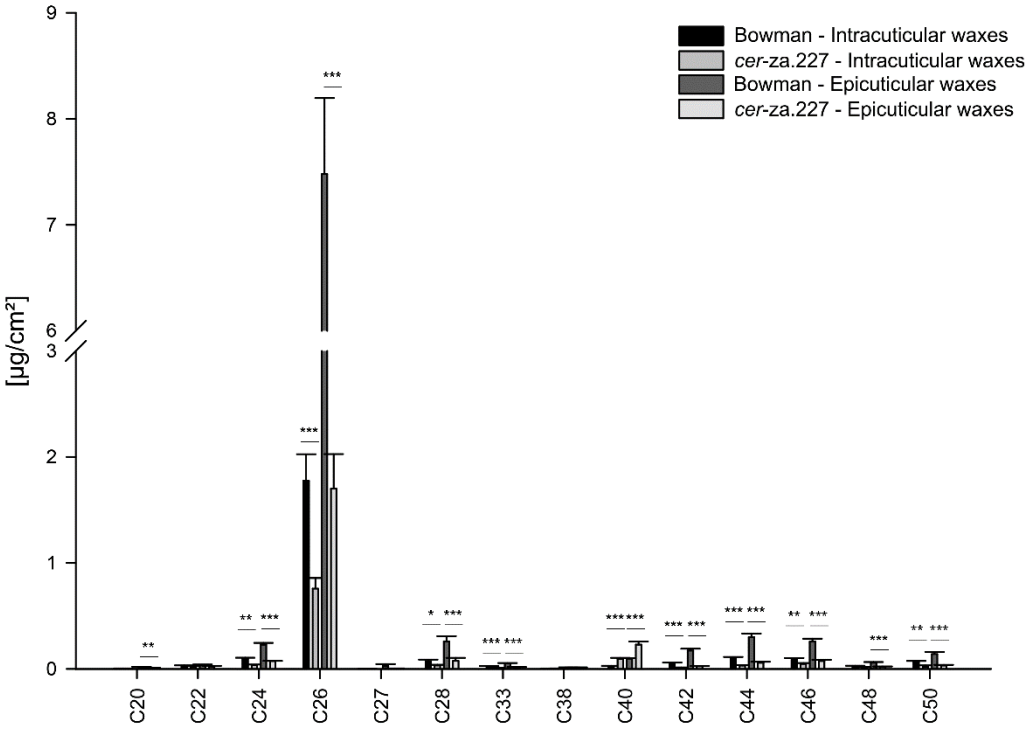

Figure 18: Chain length distribution of cuticular wax fractions extracted from Bowman and *cer*-ye.267 separated into epi- and intracuticular wax fractions and quantified with GC/FID. Student's *t*-test was applied to statistically compare the individual fractions of *cer*-ye.267 with the Bowman cultivar; $p^{***} \leq 0.01$. $p^{**} \leq 0.03$. $p^{*} \leq 0.05$.

3.2.4 Additional *cer*-ye lines reveal a cuticular lipid composition similar to *cer*-ye.267

The preliminary mapping of *cer* lines by Druka *et al.* (2011) suggested that three additional cer-ye mutations (*cer*-ye.582, *cer*-ye.792 and *cer*-ye.1395) might be located close to the *cer*-ye.267 mutation. In addition, these three mutants were previously annotated as alleles of *cer*-ye.267 after marker-based analysis (Lundqvist 2014). We therefore selected the three lines to confirm the results obtained for *cer*-ye.267. The cuticular wax load of all *cer*-ye lines was significantly decreased compared to Bowman, but the absolute numbers differed slightly between the lines (Figure 19). While 12.95 ± 1.75 µg/cm² of total cuticular waxes were extracted from the Bowman control, the amounts dropped to a range of 3.67 ± 0.09 µg/cm² in *cer*-ye.582 and to 6.32 ± 1.15 µg/cm² in *cer*-ye.1395. In particular, the group of alcohols was affected (Figure 20A). While Bowman contained 10.57 ± 1.24 µg/cm² of alcohols, only 2.417 ± 0.064 µg/cm² were found for *cer*-ye.582. Besides, significant reductions were recorded for the other aliphatic substance classes. As an exception, the alkanes in *cer*-ye.582 did not significantly differ from the Bowman levels. Results became less uniform between the allelic

mutants when looking at the chain length distribution. Strong and significant reductions in all three *cer* lines were confirmed for C_{22}, C_{24}, C_{26} and C_{27}, as well as for C_{46} containing lipids. Further, C_{33} and C_{38} lipids were decreased in *cer*-ye.792 and *cer*-ye.1395. The cuticular lipids with chain lengths in the range of C_{40}-C_{48} showed increased standard deviations (Figure 20B). In conclusion, all tested *cer*-ye lines were strongly reduced in their cuticular wax load, including all aliphatic substance classes and the entire spectrum of chain lengths.

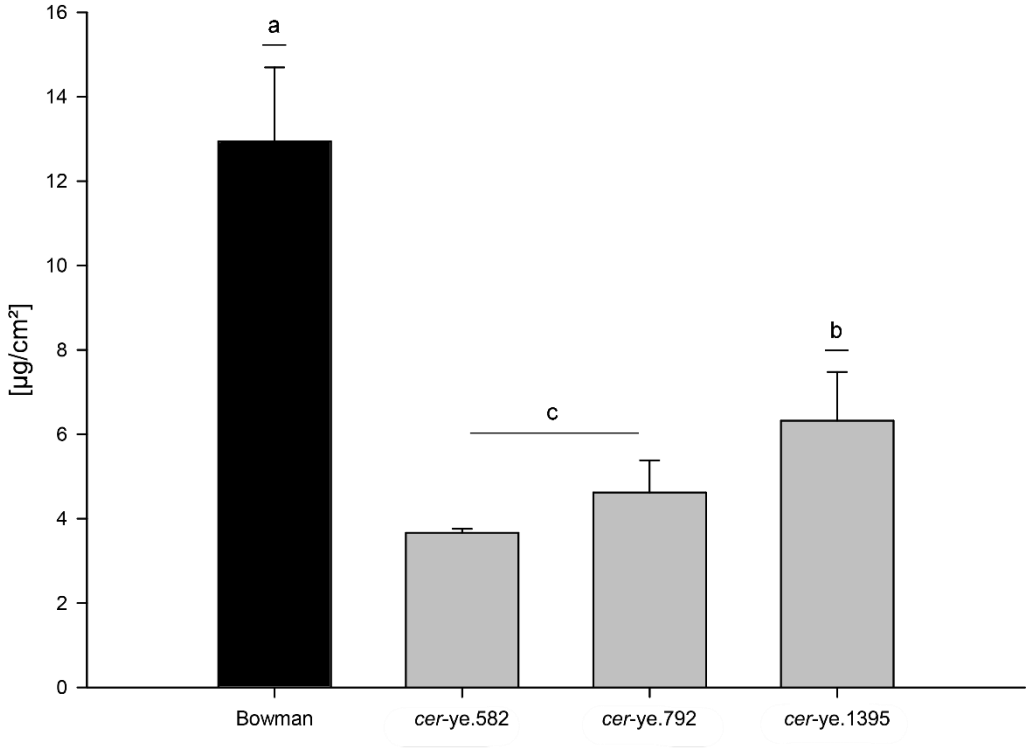

Figure 19: Total wax load from leaves of Bowman and different *cer*-ye alleles. n = 5. ANOVA; $p_c \leq 0.01$. $p_b \leq 0.03$. $p_{ab} \leq 0.05$.

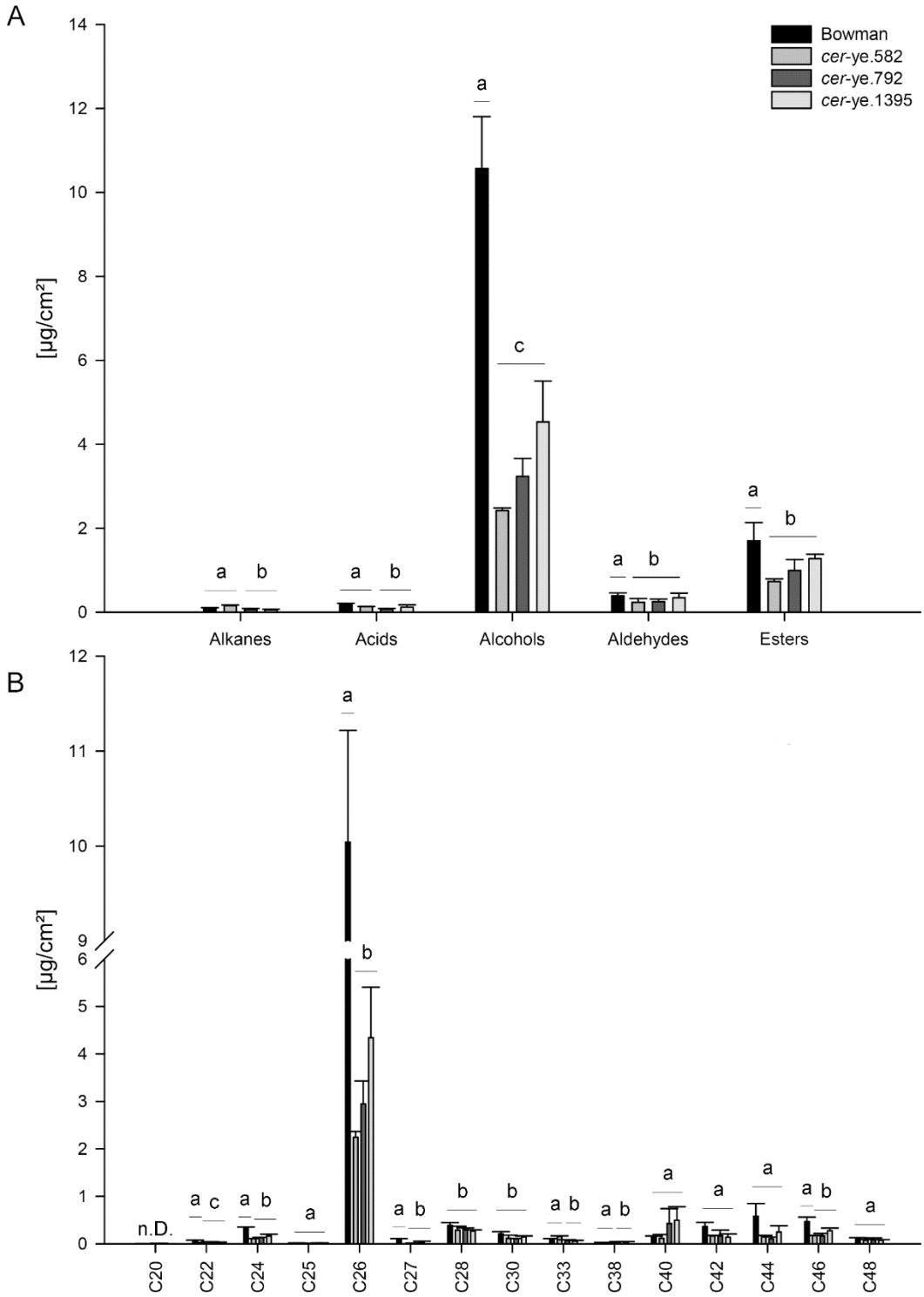

Figure 20: Cuticular wax fractions from leaves of Bowman and *cer*-ye alleles. A: Substance class distribution of aliphatic monomers. B: Chain length distribution of aliphatic compounds. n = 5. ANOVA; $p_c \leq 0.01$. $p_b \leq 0.03$. $p_{ab} \leq 0.05$.

3.3 Identification of candidate genes by bulked segregant RNA-Seq analysis

The establishment of NGS methods provided a boost for the development of new sequencing strategies and approaches. The bulked segregant RNA-Seq (BSR-Seq) analysis is a powerful tool for the identification of variations in gene expression between different pools of RNA. It allows precise SNP mapping to track mutation events restricted to DNA areas of transcription. Read libraries, generated during the sequencing process, can be aligned to a reference genome, or compared between different samples to highlight variations. At the time of this study, the best full genome sequence data were available for the barley cultivar Morex (morex_v2.0, GCA_902498975.1). Consequently, this genome was used as reference for the mapping approach. RNA samples from the barley cultivars Foma, Bonus and Bowman were included in the RNA-Seq analysis since these cultivars represent the genetic origins and backgrounds of the investigated *cer* lines. In the course of this study, data evaluation was performed in collaboration with Heiko Schoof and Tyll Stöcker (INRES, University of Bonn).

3.3.1 The *cer-za* alleles carry a mutation in the gene *HORVU5Hr1G089230*

Samples from 38 individual plants showing the *eceriferum* phenotype were harvested from the segregating F2 generation of a cross of an eight-times backcrossed *cer*-za.227 plant to Bowman, and combined into one heterogeneous pool for RNA-Seq analysis. Next, expression data from this pool were compared to a pool of 40 plants derived from the same cross, showing the wild-type phenotype to identify a set of candidate genes. Read mapping and SNP calling pointed out ten possible mutational events in the sequence from *HORVU5Hr1G089230* of *cer*-za.227 compared with Morex, which could cause the dysfunction of the gene product (Figure 21). The gene *HORVU5Hr1G089230* is located on chromosome 5 (chr5H:584524108-584528253) and contains 10 exons with 7 possible splicing variants. The genomic locus of *HORVU5Hr1G089230* of *cer*-za.227 was sequenced via Sanger sequencing to confirm the ten mutational events predicted by variant calling from the BSR-Seq analysis. All ten predicted variations of *cer*-za.227 compared with the Morex genome were confirmed (Table 10). Some of the SNPs were suspected to be rather based on naturally occurring variations between the cultivars of Morex and Foma; therefore, the sequences of Foma and Morex were compared. This approach showed that the Foma gene variant, the donor of the *cer*-za.227 locus, differed from the one in Morex. Nine out of ten SNPs, derived from the BSR-Seq analysis between Morex and *cer*-za.227 (Table 10, #1-4/6-10) were shown the be natural variances between Morex and Foma. Only one genetic variant on position 584526708 was confirmed as a deletion of a guanine in exon 4 between *cer*-za.227 and Morex/Foma (Table 10, #5).

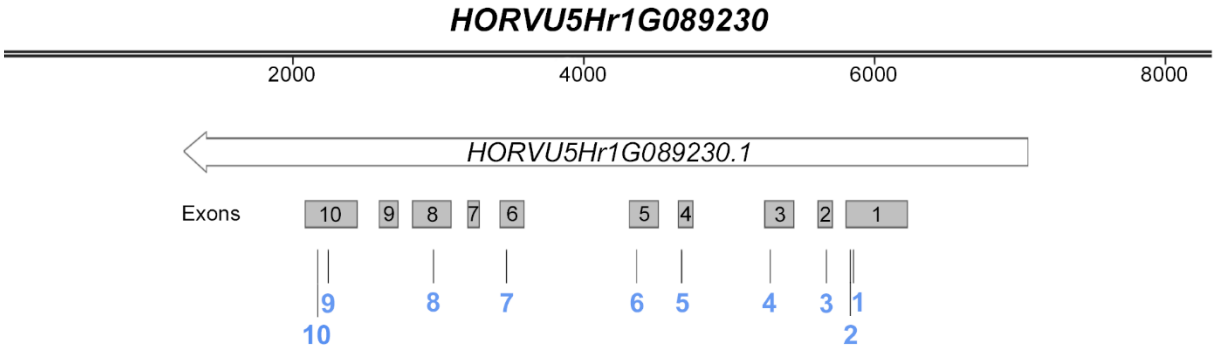

Figure 21: Gene map of *HORVU5Hr1G089230* indicating the predicted mutational events of *cer*-za.227 based on the performed BSR-Seq analysis. The *HORVU5Hr1G089230.1* sequence was indicated (arrow). The mutational events were aligned to the exon structure (1-10, grey) and consecutively numbered (1-10, blue). Corresponding events are depicted in Table 10.

Table 10: Results of the BSR-Seq approach for *cer*-za.227. Based on the comparison with the reference genome from Morex, ten genetic variations were detected in the exon sequences. Comparison to the Foma cultivar, the genetic donor of *cer*-za.227, were drawn to identify natural variations. Exact positions of the SNPs as well as the positions relative to the exons are given. The fifth SNP (blue) was identified as deletion of guanine uniquely mapped to the *HORVU5Hr1G089230* locus in *cer*-za.227.

			SNP/Deletion			
Gene-ID	**SNP**	**Position**	**Morex**	**Foma**	***cer*-za.227**	**Localisation**
HORVU5Hr1G089230	1	584527893	C	T	T	Exon 1, cds
	2	584527874	T	C	C	Exon 1, cds
	3	584527706	T	C	C	Exon 2, cds
	4	584527323	A	G	G	Exon 3, cds
	5	584526708	AG	AG	A	Exon 4, cds
	6	584526402	A	G	G	Exon 5, cds
	7	584525508	C	G	G	Exon 6, cds
	8	584525002	G	A	A	Exon 8, cds
	9	584524278	T	A	A	Exon 10, UTR
	10	584524206	C	T	T	Exon 10, UTR

Beside *cer*-za.227, RNA-Seq samples were prepared for *cer*-za.173, *cer*-za.232 and *cer*-za.318. Since these lines have not been backcrossed, the genetic background is substantially less purified; therefore, data produced from these lines were rather used as supportive controls; again, unique SNPs were clearly identified in the gene *HORVU5Hr1G089230* in all three lines (Table 11).

Table 11: Results of the BSR-Seq approach for *cer*-za.173, *cer*-za.232 and *cer*-za.318. Based on the comparison with the reference genome from Morex, one mutational event was clearly identified for each line. Exact positions of the SNPs as well as the position relative to the exons were given.

			SNP/Deletion		
Gene-ID	**Allele**	**Position**	**Morex/Foma**	***cer*-za**	**Localisation**
HORVU5Hr1G089230	*cer*-za.173	584526341	C	A	Exon 8, cds
	cer-za.232	584525054	T	A	Splicing region, exon 5 to intro 5
	cer-za.318	584526708	AG	A	Exon 4, cds

In Table 11, the natural variations between Foma and Morex were excluded from the analysis from the outset, and only the variations between the mutant lines and Foma were considered. In case of *cer*-za.173, a base exchange of cytosine to adenine was identified in position 584525054 in exon 8. For *cer*-za.232 a SNP from thymine to adenine was confirmed in position 584526341. The affected region was identified as splicing region between exon and intron 5 (Figure 22). The *cer*-za.318 line showed a deletion of a guanine in the exact same position in exon 4 as already described for the *cer*-za.227 locus (Table 11).

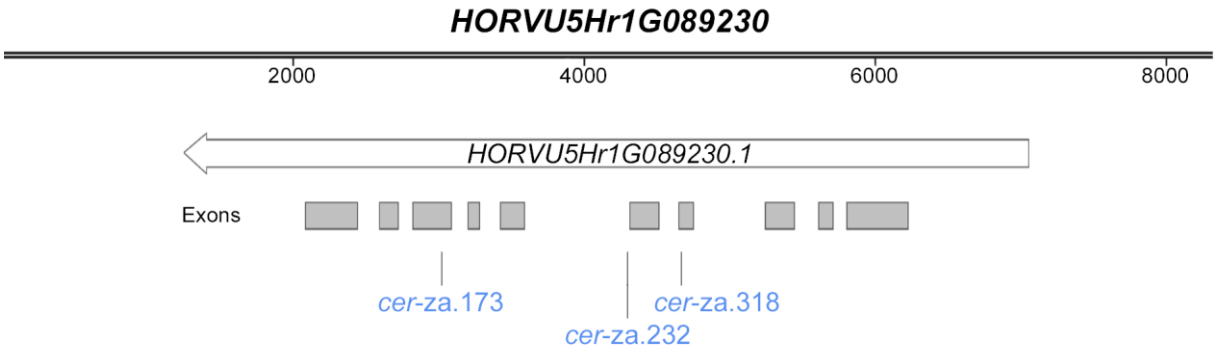

Figure 22: Localisation of the individual sites of mutational events (Table 11) for the investigated *cer*-za alleles *cer*-za.173, *cer*-za.232 and *cer*-za.318 on the gene map of *HORVU5Hr1G089230*. The *HORVU5Hr1G089230* sequence was indicated (arrow). The mutations are highlighted in blue, exons are indicated in grey.

3.3.2 Protein predictions and structural modelling of CER-ZA variants

Changes in the nucleotide sequence were transferred to the amino acid sequence based on the Morex reference genome sequence to determine the impact on the protein product (Table 12). Since the same deletion of a guanine was found in *cer*-za.227 and in *cer*-za.318, both lines shared the same frame shift (Figure 23, 2/3) which was predicted to cause a premature stop codon shortly after the mutation occurs. Consequently, the translated gene products are predicted to be truncated to 153 instead of 498 AAs.

Table 12: Overview of the amino acid changes caused by SNPs in *cer*-za lines. The Morex genome sequence served as reference.

		Nucleotide exchange		Amino acid exchange		
Genotype	**Position [AA]**	**Morex**	***cer-za***	**Morex**	***cer-za***	**Peptides**
cer-za.227	152	G	Deletion	P	Frame shift	Premature stop codon after 153 AA
cer-za.173	138	C	A	A	S	498
cer-za.232	230	T	A	R	Splicing site	Premature stop codon after 253 AA
cer-za.318	152	G	Deletion	P	Frame shift	Premature stop after 153 AA

Another premature stop codon was determined for the sequence of *cer*-za.232. The base pair shift from thymine to adenine caused the AA exchange of arginine by tryptophane. This SNP is located to the splicing site between exon 5 and intron 5, presumably affecting splicing. Parts of the intron sequence would consequently be included into the transcript. This SNP does not just alter the sequence starting from position 229, but also induces an early stop codon at position 254 (Figure 23, 5). For *cer*-za.173, just a single base-pair exchange from cytidine to adenine causing an amino acid exchange from alanine to serine at position 138 was observed (Figure 23, 4); the two amino acids differ strongly in their biochemical properties, because alanine is non-polar, and serine carries a polar hydroxyl group. Conclusively, strongly altered polypeptide structures were expected for all *cer*-za lines.

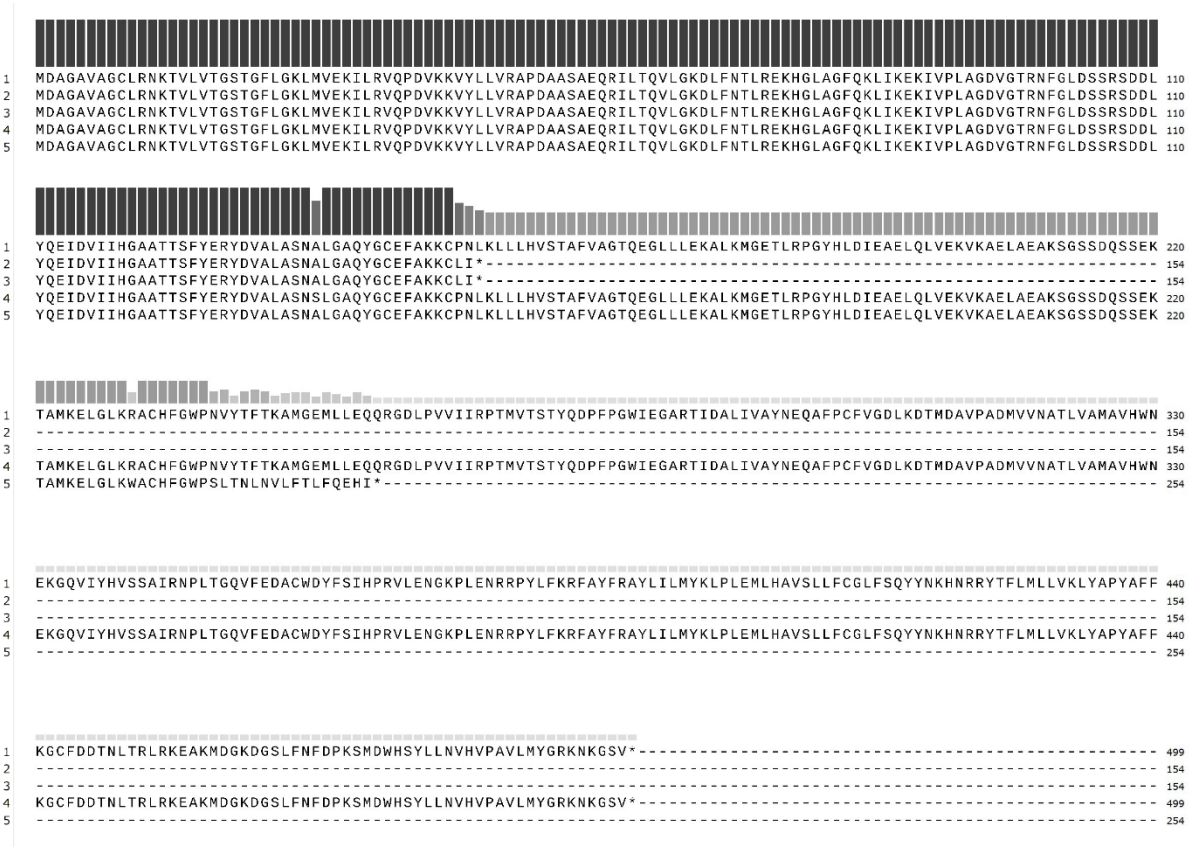

Figure 23: Alignment of the *HORVU5Hr1G089230* protein sequences for the four different *cer*-za alleles to the reference protein sequence from Morex. The level of consensus is indicated by grey bars. 1: Reference sequence Morex. 2: *cer*-za.227. 3: *cer*-za.318. 4: *cer*-za.173. 5: *cer*-za.232.

Different bioinformatic tools were applied to study the characteristics of the gene product of *HORVU5Hr1G089230.1* and to identify impacts of the mutational events. Initially, transmembrane domains were annotated with TMHMM (Krogh *et al.* 2001). The algorithm predicted a TM helix formed by AAs of positions 391-413 at the C-terminal end of the Morex peptide sequence (Figure 24). Accordingly, these domains were missing in the truncated polypeptides predicted for *cer*-za.227, *cer*-za.232 and *cer*-za.318 because they carry premature stop codons after amino acids 153, 253 and 153, respectively. Next, peptide sequences were screened for the presence of N-terminal signal peptides for the secretory pathway, mitochondria, chloroplasts or thylakoids using TargetP 2.0 (Table 13, Armenteros *et al.* 2019). In summary, the likelihood for N-terminal signal peptides was very low, indicating that the protein localisation will likely be mediated by the C-terminal transmembrane domains (Figure 24). DeepLoc 1.0 was applied to study the subcellular localization (Armenteros *et al.* 2017). The algorithm predicted the endoplasmic reticulum as most likely destination for the Morex protein HORVU5Hr1G089230, as well as for the altered polypeptide from *cer*-za.173. Further, it was suggested that the protein is membrane bound. The truncated proteins from *cer*-za.227, *cer*-za.232 and *cer*-za.318, lacking the predicted TM domain, were predicted to localize to the cytosol.

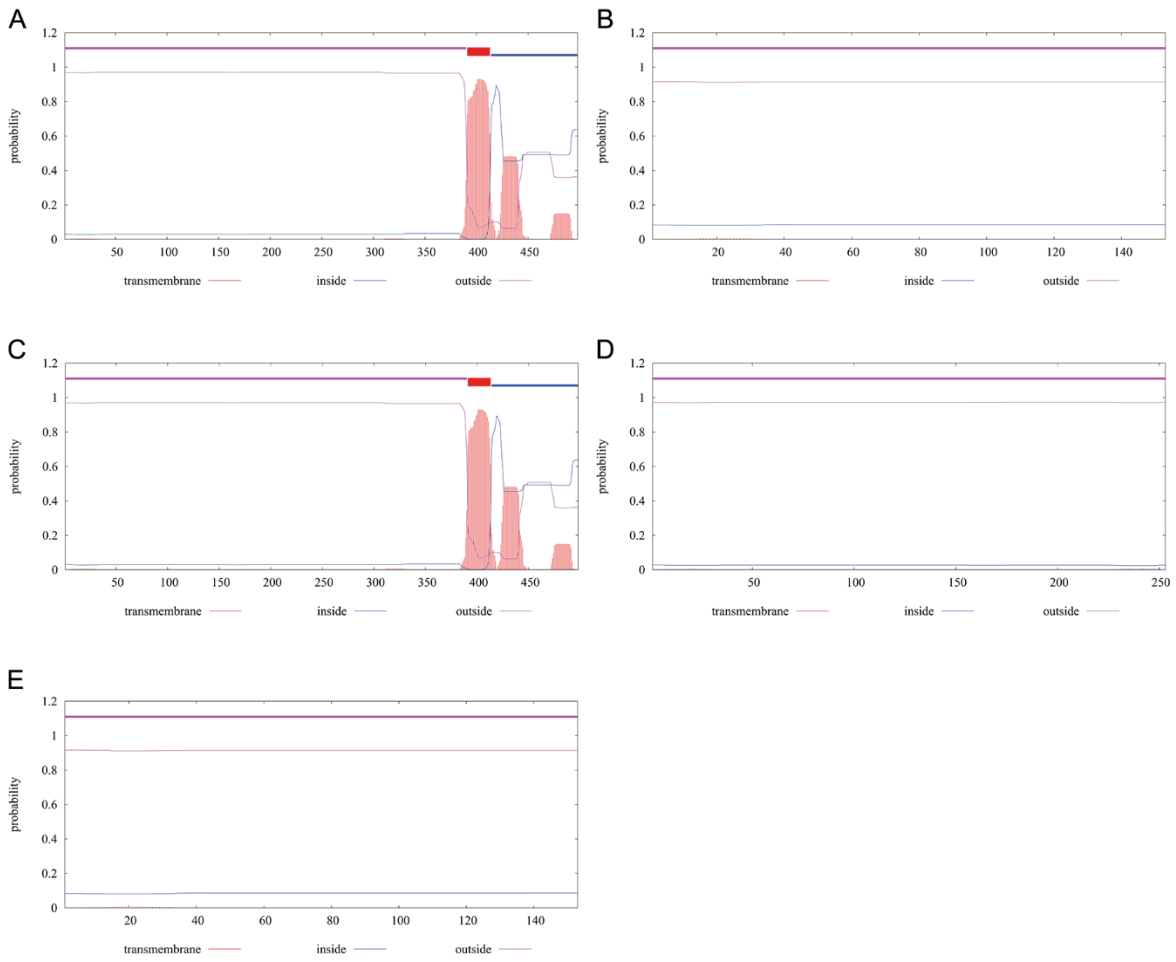

Figure 24: Posterior probabilities of transmembrane helices calculated for HORVU5Hr1G089230.1 by TMHMM 2.0. Mutated polypeptide sequences of different *cer*-za lines were studied. The Morex sequence served as reference. A: Reference Morex. B: *cer*-za.227. C: *cer*-za.173. D: *cer*-za.232. E: *cer*-za.318.

Table 13: Likelihood of N-terminal signal sequences for different subcellular locations for HORVU5Hr1G089230 predicted by TargetP-2.0. SP: Signal Peptide for the secretory pathway. mTP: Mitochondrial transfer peptide. cTP: Chloroplast transfer peptide. lTP: Thylakoid luminal transfer peptide.

Line	Other	SP	mTP	cTP	lTP
Morex	0.993951	0.000096	0.003802	0.001894	0.000257
cer-za.227	0.990887	0.000134	0.005531	0.002709	0.000738
cer-za.173	0.994264	0.000097	0.003560	0.001819	0.000260
cer-za.232	0.993951	0.000096	0.003802	0.001894	0.000257
cer-za.318	0.990887	0.000134	0.005531	0.002709	0.000738

Table 14: Prediction of the subcellular localisation of the different HORVU5Hr1G089230.1 polypeptides by DeepLoc 1.0.

Line	Subcellular localisation	Type
Morex	ER	membrane bound
cer-za.227	Cytosol	soluble
cer-za.173	ER	membrane bound
cer-za.232	Cytosol	soluble
cer-za.318	Cytosol	soluble

Next, cofactor binding sites were predicted using Cofactory (Table 15, Geertz-Hansen *et al.* 2014). The algorithm can identify Rossmann-fold sequences, which are functional motifs formed by secondary structures able to bind dinucleotides. A Rossmann-fold was predicted to be formed by the AAs of the positions 11-57. Since these AAs are not affected in any of the *cer*-za lines, all proteins are predicted to include the Rossmann-fold. Further, a weak specificity for NAD and an enhanced specificity for NADP were predicted, but no binding to FAD.

Table 15: Predicted cofactor binding sites for the polypeptide variants of HORVU5Hr1G089230. Cofactory 1.0 was utilised to identify Rossmann fold sequences and predict the cofactor specificity. A probability score was provided for each cofactor, FAD, NAD and NADP. Values above 0.5 indicate a reasonable binding specificity.

Line	Domain	FAD	NAD	NADP	Cofactor(s)	AAs
Morex	1	0.006	0.553	0.716	NAD/NADP	11-57
cer-za.227	1	0.006	0.553	0.716	NAD/NADP	11-57
cer-za.173	1	0.006	0.553	0.716	NAD/NADP	11-57
cer-za.232	1	0.006	0.553	0.716	NAD/NADP	11-57
cer-za.318	1	0.006	0.553	0.716	NAD/NADP	11-57

Figure 25: Results of the domain prediction approach for HORVU5Hr1G089230.1 using Pfam. Two significant matches for domains were annotated, i.e. an NAD binding domain and a sterile family domain.

Similarly, Pfam (Mistry *et al.* 2021) predicted a NAD binding domain based on database-supported alignments (Figure 25). The NAD_binding_4 family domain is associated with SDR-like proteins (short-chain dehydrogenases/reductases) which are Rossmann-fold NAD(P)H-binding proteins. Further, a male sterile family domain was annotated at the C-terminal end of the peptide sequence.

Table 16: Sequence search results for the peptide sequence of HORVU5Hr1G089230.1 annotated by Pfam. The database driven algorithm screens for related sequences and predicts domains based on these results.

			Alignment		HMM	
Family	**Description**	**Clan**	**Start**	**End**	**From**	**To**
NAD binding 4	Male sterility protein	CL0063	12	320	1	256
Sterile	Male sterility protein	n/a	395	490	2	89

Finally, a protein-protein-BLAST was performed to identify closely related sequences. based on the full sequence of the predict protein of HORVU5Hr1G089230.1 from Morex. BLAST search was performed without restrictions to taxa. The 20 highest ranked sequences are listed in Table 17. These sequences were closely related and derived from family members of the *Poaceae* and the subfamily *Pooideae*. The barley HORVU5Hr1G089230.1 protein itself was annotated as putative fatty acyl-CoA reductase 1. Most of the related sequences are predicted to encode similar enzymes. Mutational impacts on the tertiary structure of proteins were modelled and illustrated with Phyre2 and NGL-Viewer (Figure 26). The 498 AA sequence of the Morex protein HORVU5Hr1G089230.1 includes several secondary structures (Figure 26A). The predicted TM domain at the C-terminal end was also annotated by Phyre2 and NGL-Viewer. Consequently, the structures of *cer*-za.227 and *cer*-za.318 are highly degenerated caused by the premature stop codons (Figure 26B/E). The presumed splicing error in the nucleotide sequence of *cer*-za.232 also reduces the protein size (Figure 26D). In contrast, the polypeptide chain is not shortened in the *cer*-za.173 protein and the amino acid exchange is located outside of the TM helix (Table 16). In the tertiary structure, several alterations in the orientation of some secondary structures are indicated. The amino acid exchange of *cer*-za.173 at position 138 therefore occurs in the predicted NAD_4_binding domain. This could affect the activity of the protein. In conclusion, important mutational events were identified for the *cer*-za alleles in the exon structure of *HORVU5Hr1G089230.1*. Predicted gene products of three of the *cer*-za alleles are truncated. Several independent bioinformatic algorithms predicted a C-terminal transmembrane domain and the presence of a functional Rossmann-fold domain for the HORVU5Hr1G089230.1 peptide. A pBLAST search of the protein indicated a close relationship to acyl-CoA reductases from *Poaceae*. These results indicate that HORVU5Hr1G089230.1 might harbour acyl-CoA reductase activity.

Table 17: Top 20 results of a pBLAST (protein-protein BLAST) search for the peptide sequence of HORVU5Hr1G089230.1. The algorithm was targeting non-redundant protein sequences (nr) without taxa restrictions.

#	Description	Species	Max Score	AAs	Accession
1	Fatty acyl-CoA reductase 1	*Hordeum vulgare*	1036	498	KAE8808760.1
2	Fatty acyl-CoA reductase 1	*Aegilops tauschii subsp. strangulata*	1012	498	XP_020161393.1
3	Fatty acyl-CoA reductase 1-like	*Triticum dicoccoides*	999	498	XP_037435869.1
4	Unnamed protein product	*Triticum turgidum subsp. durum*	995	498	VAI21127.1
5	Fatty acyl-CoA reductase 1	*Brachypodium distachyon*	936	497	XP_003578640.1
6	Hypothetical protein	*Triticum aestivum*	913	497	KAF7047074.1
7	Fatty acyl-coenzyme A reductase 3	*Aegilops tauschii*	906	497	AIZ97194.1
8	Unnamed protein product	*Triticum turgidum subsp. durum*	893	497	VAI00664.1
9	Unnamed protein product	*Triticum turgidum subsp. durum*	892	497	VAI00665.1
10	Fatty acyl-CoA reductase 1-like	*Triticum dicoccoides*	890	497	XP_037428610.1
11	Putative fatty acyl-CoA reductase 7	*Brachypodium distachyon*	888	496	XP_003578641.1
12	unnamed protein product	*Triticum turgidum subsp. durum*	887	497	VAI00670.1
13	Hypothetical protein	*Triticum aestivum*	886	497	KAF7047075.1
14	Hypothetical protein	*Triticum aestivum*	867	494	KAF7106214.1
15	Unnamed protein product	*Triticum turgidum subsp. durum*	855	484	VAI00669.1
16	Hypothetical protein	*Brachypodium distachyon*	832	438	PNT65134.1
17	Unnamed protein product	*Triticum turgidum subsp. durum*	818	441	VAI00666.1
18	Putative fatty acyl-CoA reductase 4	*Triticum urartu*	796	496	EMS46840.1
19	Unnamed protein product	*Triticum turgidum subsp. durum*	783	450	VAI00671.1
20	Fatty acyl-CoA reductase 1	*Triticum urartu*	749	596	EMS63229.1

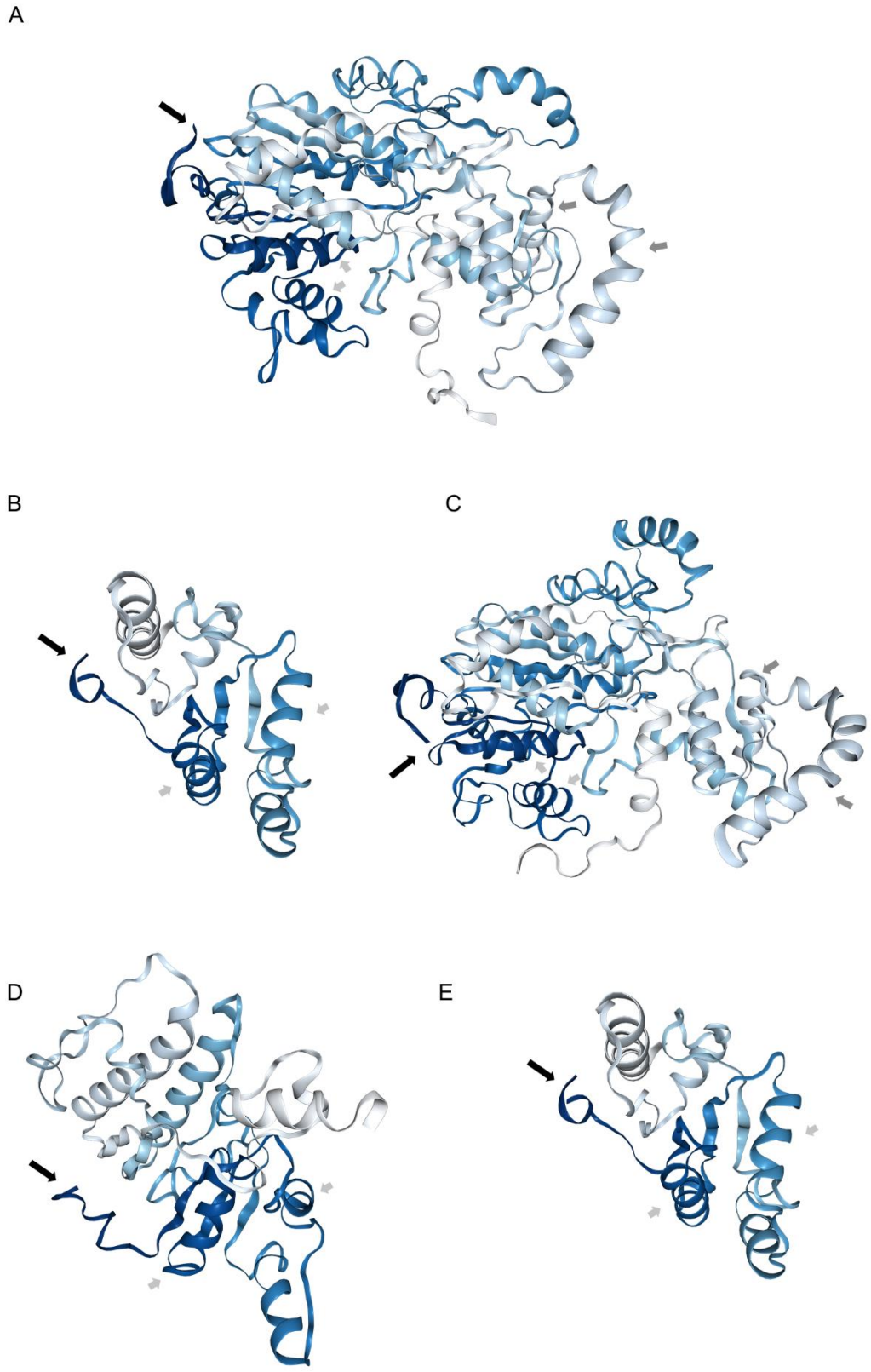

Figure 26: Tertiary structures calculated by Phyre2 and visualized with the NGL-Viewer for the different predicted polypeptides of *cer*-za alleles of the HORVU5Hr1G089230.1 protein. A reference structure was plotted based on the Morex sequence. Black arrow: N-terminal end. Light grey arrows: Rossmann-fold domain. Dark grey arrow: Transmembrane domain. A: Reference. B: *cer*-za.227. C: *cer*-za.173. D: *cer*-za.232. E: *cer*-za.318.

3.3.3 Phylogenetic classification of CER-ZA

Phylogenetic classification is a powerful strategy to generate hypotheses about the function and characteristics of a protein. A wide range of annotated FAR sequences was included in the phylogenetic analysis This involved sequences derived from the pBLAST search as well as the eight FAR sequences from *A. thaliana* and 21 putative paralogs from *H. vulgare*, both derived from EnsemblePlants. Further, annotated sequences from well-described monocot FARs and dicot FARs were included. The selected sequences were aligned with ClustalW and a Maximum-Likelihood tree was calculated using the Bootstrap method with 500 replicates to enhance the quality of the result. The tree was finally rooted to a FAR from the protist *Euglena gracilis* and widely grounded on high bootstrap confidence intervals. Three overall clusters became visible (Figure 27). The dominant clusters were split into monocot and dicot sequences. The third cluster was heterogeneously formed by the previously characterised *At*FAR2, *At*FAR6 and *Os*FAR2 proteins, as well as the two *H. vulgare* sequences HORVU2Hr1G086620.1 and HORVU4Hr1G074700.1. Since the two *At*FARs and *Os*FAR2 were shown to be chloroplast localized, a similar target sequence would be expected for the two barley sequences. While most of the barley sequences formed dense subclusters, the CER-ZA protein was more closely associated with proteins from more ancestral taxa of *Aegiliposis* and *Brachypodium*. Most of the barley paralogous sequences formed separate clusters indicating that some of these sequences were derived from gene duplication events.

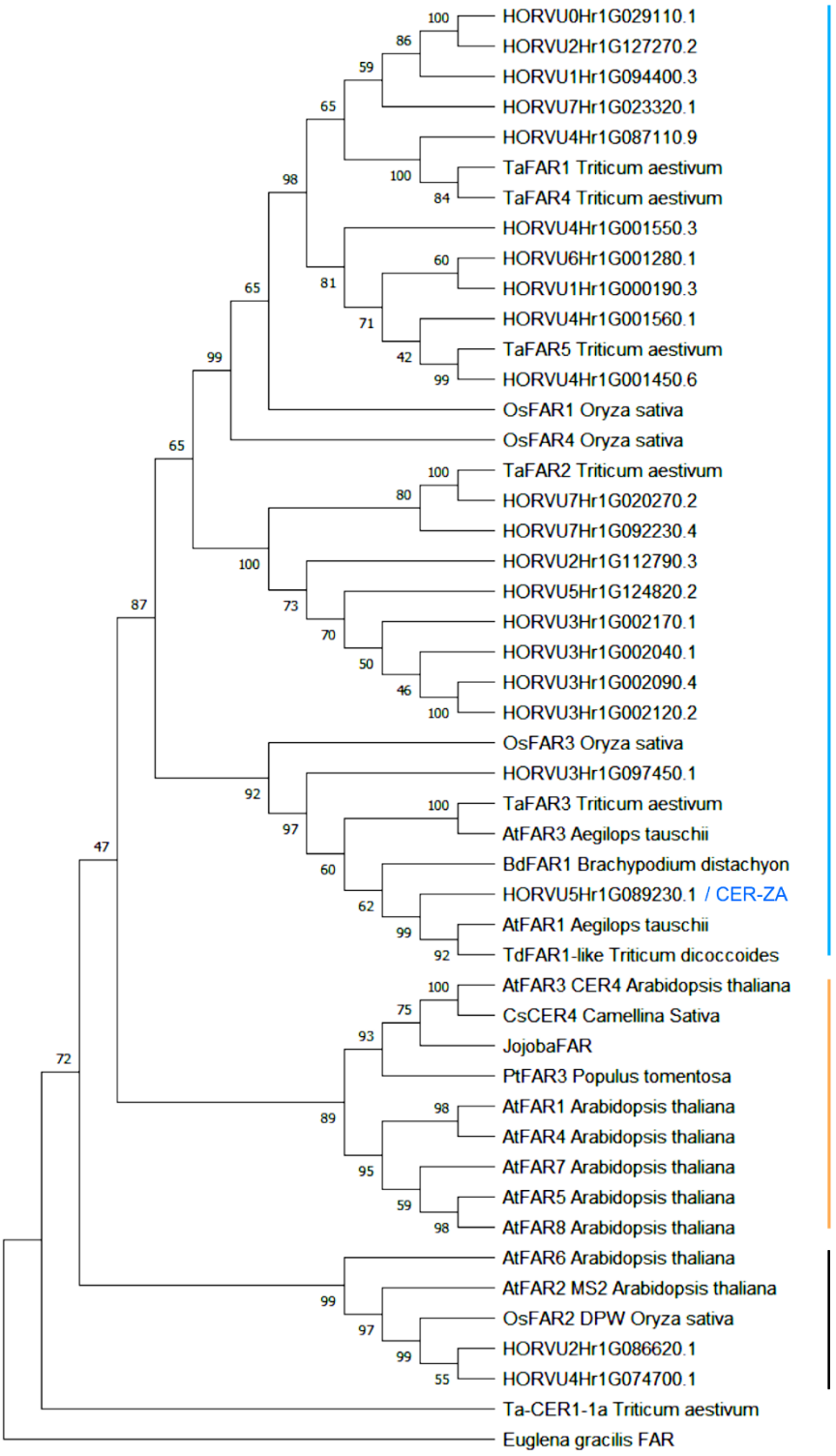

Figure 27: Phylogenetic relationship of annotated FAR sequences of different plant species. All eight *A. thaliana* FARs and the 21 annotated *H. vulgare* FAR sequences were included. Three clusters can be differentiated. Blue: Monocotyledons. Orange: Dicotyledons. Black: Putative chloroplast-localised proteins. Calculations were based on the Maximum-Likelihood method with 500 Bootstrap replicas. CER, *eceriferum*. DPW, defective pollen wall. FAR, fatty acyl-CoA reductase. MS, male sterility. The tree was rooted to an acyl-CoA reductase from the protist *Euglena gracilis*.

3.3.4 The *cer*-ye plants carry a mutation in the gene *HORVU4Hr1G063420*

The segregating F2 generation of a cross between Bowman and an eight-times backcrossed *cer*-ye.267 line was screened for the visible phenotype of the leaf cuticle mutation with the water-droplet test (3.1), and a pool of samples from eighteen *cer*-like plants (presumably homozygous for *cer*-ye.267) was collected. Additionally, 40 samples showing the wild-type phenotype (presumably heterozygous for *cer*-ye.267 or WT genotype) were pooled. The pooled RNA samples were subjected to RNA-Seq analysis. Three additional allelic lines, *cer*-ye.582, *cer*-ye.792 and *cer*-ye.1395, were included in the RNA-Seq analysis. After consideration of the expression levels derived from RNA-Seq data, *HORVU4Hr1G063420* was identified as candidate gene. The coding sequence is restricted to the first exon of this gene. During the mapping approach, a single SNP between the Morex sequence and *cer*-ye.267 was identified at position 531213539 of *HORVU4Hr1G063420* (Figure 28).

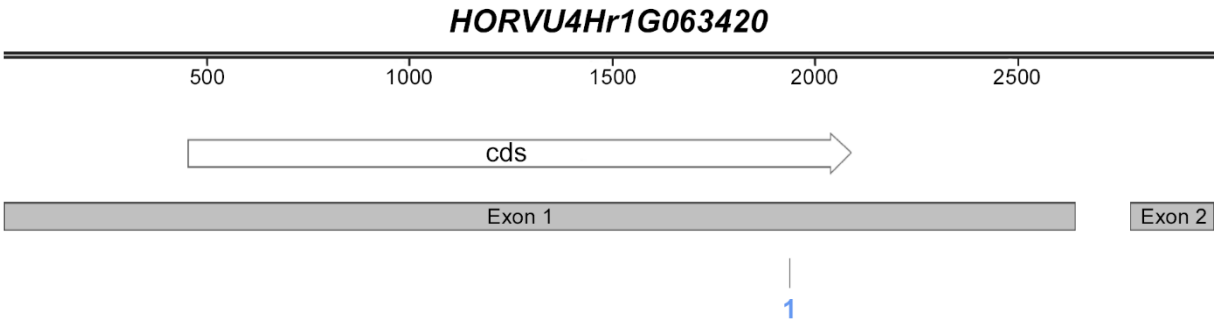

Figure 28: Gene map of *HORVU4Hr1G063420* indicating the predicted mutational site in the coding sequence based on the performed BSR-Seq analyses. A single SNP between the Morex and *cer*-ye.267 sequences was identified (1). Details about the SNP are listed in Table 18.

This SNP causes the nucleotide exchange of thymine to adenine in the coding sequence localised on exon 1 (Table 18).

Table 18: Results of the BSR analysis for *cer*-ye.267. A single SNP was identified at the C-terminal end of the coding sequence of *HORVU4Hr1G063420*.

			SNP		
Gene-ID	**#**	**Position**	**Morex**	***cer*-ye.267**	**Localisation**
HORVU4Hr1G063420	1	531213539	T	A	Exon 1, cds

Similarly, SNP calling was performed for the three additional alleles *cer*-ye.582, *cer*-ye.792 and *cer*-ye.1395 in comparison with the Morex sequence. No SNP could be identified for *cer*-ye.582. This could be due to the limitation of the RNA-Seq approach to the transcriptome; therefore, if a mutation occurs in an intron or sequences at the 5' or 3' ends of the gene, this

would not be captured and would require a genome-based sequencing approach to be covered.

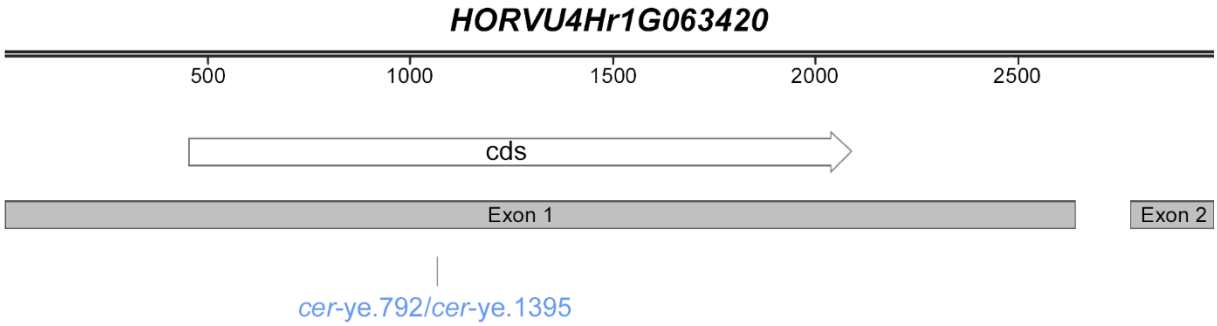

Figure 29: Gene map of *HORVU4Hr1G063420* indicating the mutational sites for the *cer*-ye.792 and *cer*-ye.1395 alleles based on the BSR-Seq analyses. A single SNP was found between Morex and *cer*-ye.792 and *cer*-ye.1395. For *cer*-ye.582, no SNP was captured. Details about the mutational events are listed in Table 19.

In contrast, *cer*-ye.792 and *cer*-ye.1395 shared a SNP at position 531212667 in the coding sequence of *HORVU4Hr1G063420* (Figure 29). The mutation caused the replacement of cytosine with adenine.

Table 19: Results of the BSR-Seq analysis for *cer*-ye alleles (Figure 29). For *cer*-ye.582 no mutational event was identified (n. I.). The *cer*-ye.792 and *cer*-ye.1395 mutants shared a single SNP in the candidate gene *HORVU4Hr1G063420*.

			SNP		
Gene-ID	**Allele**	**Position**	**Morex.**	***cer*-ye**	**Localisation**
	cer-ye.582	n. I.	n. I.	n. I.	n. I.
HORVU4Hr1G063420	*cer*-ye.792	531212667	C	A	Exon 1, cds
	cer-ye.1395	531212667	C	A	Exon 1, cds

3.3.5 Protein predictions and modelling of CER-YE variants

The impact of base pair exchanges in the different *cer*-ye alleles were studied by calculating the translated protein sequences for *HORVU4Hr1G063420.1* from Morex and from the *cer*-ye mutants (Table 20).

Table 20: Overview of the amino acid changes based on SNP calling in *cer*-ye alleles. The Morex genome served as reference.

	Position	Mutational event SNP		Amino acid exchange		Polypeptide length
Genotype	**[AA_n]**	**Morex**	***cer***	**Morex**	***cer***	**[AAs]$_n$**
cer-ye.267	495	T	A	F	Y	545
cer-ye.582	n. I.	n. I.	n. I.	n. I.	n. I.	n. I.
cer-ye.792	204	C	A	C	premature stop	204
cer-ye.1395	204	C	A	C	premature stop	204

The reference protein from Morex contains 545 AAs. For *cer*-ye.267, the exchange from thymine to adenine is predicted to result in the exchange of phenylalanine by tyrosine. Both amino acids are structurally related since tyrosine is the hydroxylated form of phenylalanine. In contrast, no mutational event was found based on the BSR-Seq analysis for *cer*-ye.582. Conclusively, the transcript sequence of *cer*-ye.582 does not seem to be affected. However, it is possible that mutations in the introns or in the 5' or 3' sequences of the gene affect the expression of cer-ye.582. The single-nucleotide replacement of cytosine by adenine shared by *cer*-ye.792 and *cer*-ye.1395 results in the formation of a premature-stop codon. The resulting gene products would consequently be truncated to 204 AAs. The variant polypeptides were aligned to the reference sequence and plotted in Figure 30.

Figure 30: Alignment of the HORVU4Hr1G063420.1 protein sequences of the four *cer*-ye alleles to the reference sequence from Morex. The level of consensus is indicated by grey bars. 1: Reference sequence. 2: *cer*-ye.267. 3: *cer*-ye.582. 4: *cer*-ye.792. 5: *cer*-ye.1395.

The TMHMM tool was utilised to predict transmembrane domains (Figure 31). Two TM domains were predicted formed by the AA sequences of 65-87 and 94-116. These TM domains occur in the first third of the protein sequence, outside of the region where the SNPs were found. Therefore, the SNPs do not affect the TM domain formation. Next, the polypeptide chains of the Morex protein and of the *cer*-ye alleles were screened for N-terminal signal peptides using TargetP (Table 21). The likelihood of a signal peptide was extremely low for the *cer*-ye polypeptides indicting another mechanism to mediate the subcellular localisation. The deep-learning platform DeepLoc 1.0 was utilised to predict the subcellular localisation of the polypeptides. The algorithm indicated a membrane bound localization at the ER (Table 22).

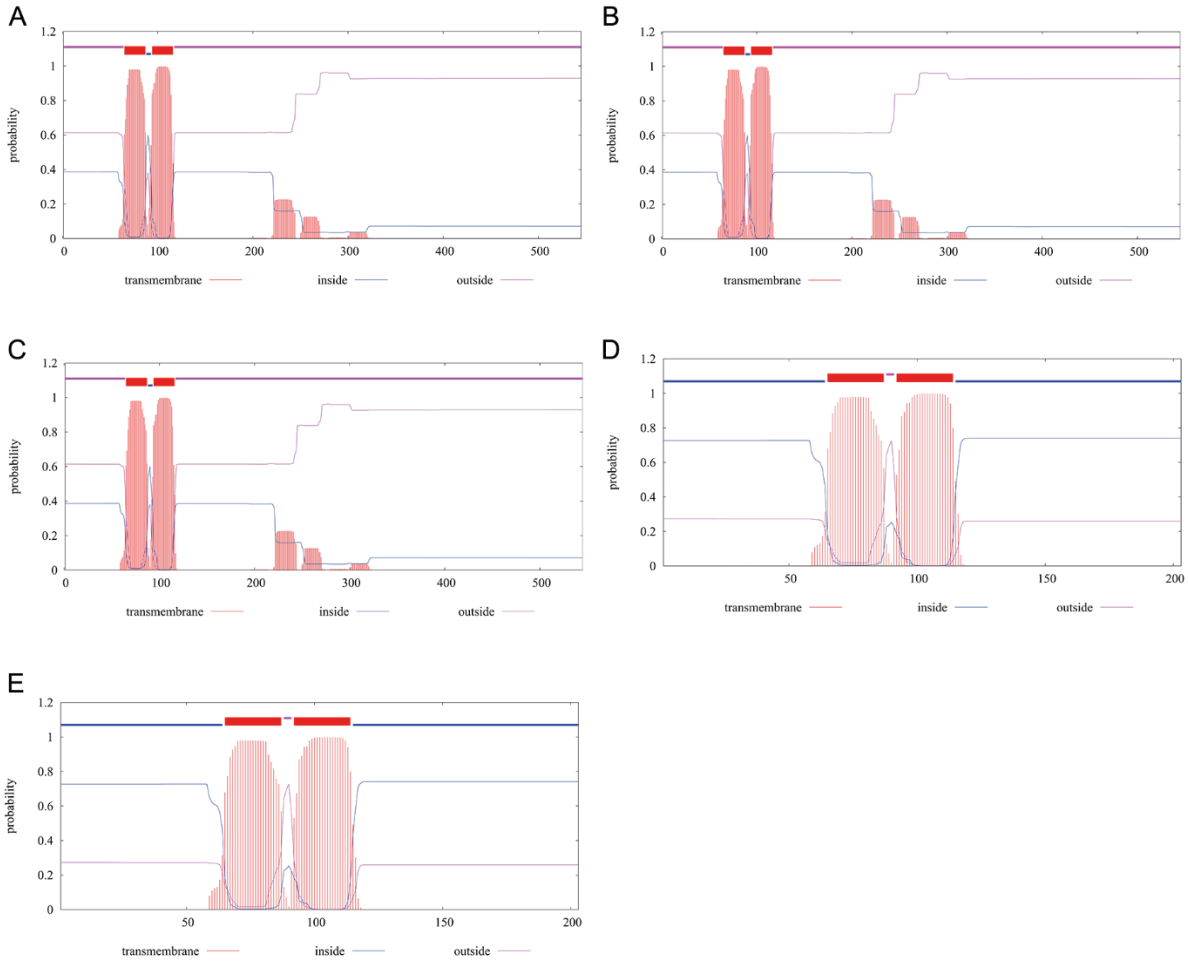

Figure 31: Posterior probabilities of transmembrane helices calculated by TMHMM 2.0 for HORVU4Hr1G063420.1 reference from Morex and *cer*-ye sequences. A: Reference peptide from Morex. B: *cer*-ye.267. C: *cer*-ye.582. D: *cer*-ye.792. E: *cer*-ye.1395. Two transmembrane domains were predicted for the different polypeptides.

Table 21: Likelihood of N-terminal pre-peptides for different subcellular locations of HORVU4Hr1G063420.1 from Morex and *cer*-ye variants by TargetP-2.0. SP: Signal peptide for the secretory pathway. mTP: Mitochondrial transfer peptide. cTP: Chloroplast transfer peptide. lTP: Thylakoid luminal transfer peptide.

Line	Other	SP	mTP	cTP	lTP
Reference	0.999924	0.000016	0.000017	0.000025	0.000020
cer-ye.267	0.999924	0.000016	0.000017	0.000025	0.000020
cer-ye.582	0.999924	0.000016	0.000017	0.000025	0.000020
cer-ye.792	0.999924	0.000016	0.000017	0.000025	0.000020
cer-ye.1395	0.999924	0.000016	0.000017	0.000025	0.000020

Table 22: Prediction of the subcellular localisation of the different polypeptides of HORVU4Hr1G063420.1 from Morex and *cer*-ye variants by DeepLoc 1.0.

Line	Subcellular localisation	Type
Reference	ER	membrane bound
cer-ye.267	ER	membrane bound
cer-ye.582	ER	membrane bound
cer-ye.792	ER	membrane bound
cer-ye.1395	ER	membrane bound

The Pfam algorithm was utilised to annotate family domains of functional motifs (Figure 32). Two sequences of significance of domains were matched. First, a typical family domain of 3-ketoacyl-CoA synthases was predicted (FAE1/Type III polyketide synthase-like proteins). Additionally, a C-terminal domain was suggested formed by the amino acids 419-504 which is commonly annotated with acyl-carrier protein synthases III (Table 23).

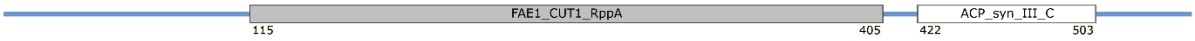

Figure 32: Domains in the peptide sequence of HORVU4Hr1G063420 predicted by Pfam. An FAE1/Type III synthase like family domain as well as an acyl-carrier-protein synthase III domain were predicted.

Table 23: Results of the Pfam approach to identify domains in the protein sequence of *HORVU4Hr1G063420.*

			Alignment		**HMM**	
Family	Description	Clan	Start	End	From	To
FAE1_CUT1_RppA	FAE1/Type III polyketide synthase-like protein	CL0046	115	404	1	289
ACP_syn_III_C	3-Oxoacyl-[acyl-carrier-protein (ACP)]-synthase III C-terminal	CL0046	422	503	11	89

Concomitantly, the pBLAST approach especially found monocot 3-ketoacyl-CoA synthase sequences (Table 24). The first 20 matches including the Morex reference sequence are listed in Table 24; sequences from *Poaceae* dominated the results with high score values and query coverages.

Table 24: Top 20 results of a pBLAST (protein-protein BLAST) search for the peptide sequence of HORVU4Hr1G063420.1. The algorithm was targeting non-redundant protein sequences (nr) without taxa restrictions.

#	Description	Scientific Name	Max Score	Acc. Length	Accession
1	Predicted protein	*Hordeum vulgare subsp. vulgare*	1127	545	BAJ85769.1
2	3-ketoacyl-CoA synthase 1	*Hordeum vulgare*	1111	556	KAE8798945.1
3	3-ketoacyl-CoA synthase 1-like	*Triticum dicoccoides*	1091	546	XP_037425588.1
4	Hypothetical protein	*Triticum aestivum*	1090	546	KAF7066481.1
5	3-ketoacyl-CoA synthase 1	*Aegilops tauschii subsp. strangulata*	1070	539	XP_020197814.1
6	3-ketoacyl-CoA synthase 1-like	*Triticum dicoccoides*	1068	541	XP_037420221.1
7	Unnamed protein product	*Triticum turgidum subsp. durum*	1029	513	VAI07770.1
8	Hypothetical protein	*Zizania palustris*	1002	541	KAG8074250.1
9	3-ketoacyl-CoA synthase 1	*Oryza sativa Japonica Group*	996	596	XP_015627774.2
10	3-ketoacyl-CoA synthase 1	*Brachypodium distachyon*	993	547	XP_003558380.1
11	Senescence-associated protein 15	*Oryza sativa Japonica Group*	992	532	ABF94942.1
12	Hypothetical protein	*Oryza meyeriana var. granulata*	985	532	KAF0913358.1
13	Unnamed protein product	*Miscanthus lutarioriparius*	975	550	CAD6210414.1
14	Hypothetical protein	*Eragrostis curvula*	974	542	TVU47751.1
15	3-ketoacyl-CoA synthase 1-like	*Oryza brachyantha*	974	532	XP_040378280.1
16	3-ketoacyl-CoA synthase 1	*Zea mays*	973	547	NP_001351905.1
17	Hypothetical protein	*Digitaria exilis*	973	540	KAF8718474.1
18	3-ketoacyl-CoA synthase 1-like	*Panicum miliaceum*	972	537	RLN17971.1
19	3-ketoacyl-CoA synthase 1	*Setaria italica*	971	544	XP_004985020.1
20	Hypothetical protein	*Panicum hallii var. hallii*	971	537	PUZ41948.1

Finally, tertiary structures were studied for the *cer*-ye alleles using the deep-learning platform Phyre2 (Figure 33). Previously annotated transmembrane domains were labelled. Since no SNP was identified in the coding sequence of *cer*-ye.582 (Figure 33C), the polypeptide sequence and the protein structure are predicted to be identical with that of the Morex protein (Figure 33A). The single amino acid change in the *HORVU4Hr1G063420* protein of *cer*-ye.267 could severely alter the tertiary structure and affect the stability of the transmembrane domains (Figure 33B). In the *cer*-ye.267 protein structure, the α-helixes of the TM domains are predicted to be oppositely orientated compared to the reference protein from Morex. The early stop codon shared by the HORVU4Hr1G063420 proteins from *cer*-ye.792 and *cer*-ye.1395 leads to a strongly truncated polypeptide with altered protein structure (Figure 33D/E).

In summary, mutational events localised to the coding sequence of *HORVU4Hr1G063420* were identified in three of the *cer*-ye alleles. The *cer*-ye.792 and *cer*-ye.1395 proteins carry the same mutational event which causes premature stop codons. For *cer*-ye.582, no mutational event was identified in the transcript sequence. The *cer*-ye.267 sequence carries an amino acid exchange at position 495 which is localised in the annotated C-terminal 3-oxoacyl-ACP synthase domain. The Morex protein was predicted to be a membrane bound, ER localised protein. BLAST search and Pfam predictions indicated an activity as β-ketoacyl-CoA synthase.

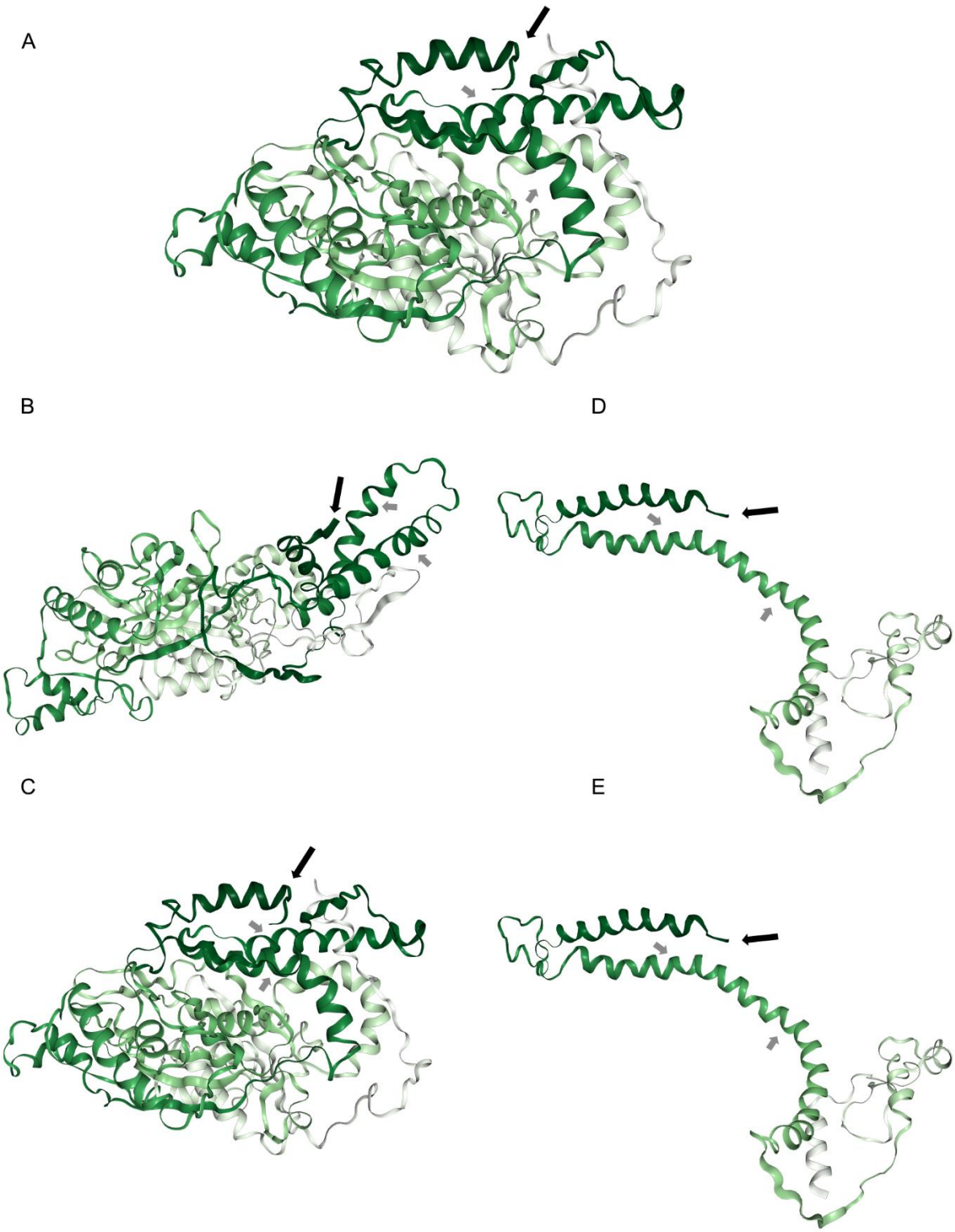

Figure 33: Tertiary structures calculated by Phyre2 and visualized with the NGL-Viewer for the different predicted polypeptides of HORVU4Hr1G063420 from Morex and the *cer*-ye lines. Black arrow: N-terminal end. Grey arrows: Transmembrane domains. A reference structure was plotted based on the Morex sequence. A: Reference structure from Morex. B: *cer*-ye.267. C: *cer*-ye.582. D: *cer*-ye.792. E: *cer*-ye.1395.

3.3.6 Phylogenetic classification of CER-YE

In the Arabidopsis genome sequence, 21 entries have been annotated as *KCS* sequences forming the *KCS* family (Joubès *et al.* 2008). Furthermore, 34 sequences were annotated as *KCS* orthologs in the genome of *H. vulgare* Morex (Tong *et al.* 2021). The putative CER-YE protein HORVU4Hr1G063420 was annotated as *Hv*KCS1 within the KCS protein family in *H. vulgare*. KCS sequences from both species were aligned and their phylogenetic relationships were predicted using the Maximum-Likelihood algorithm. A KCS sequence from the protist *Trypanosoma brucei* was used to root the tree. Bootstrap replicates enhanced confidence intervals of the phylogenetic prediction. The tree is shown in Figure 34. Although Arabidopsis and barley are distantly related, several of the sequences form heterogenic clusters. This clustering also includes HORVU4Hr1G063420 (CER-YE), which forms a clade with *At*KCS1, *At*KCS13 and *At*KCS14 with confidence interval values above 70%.

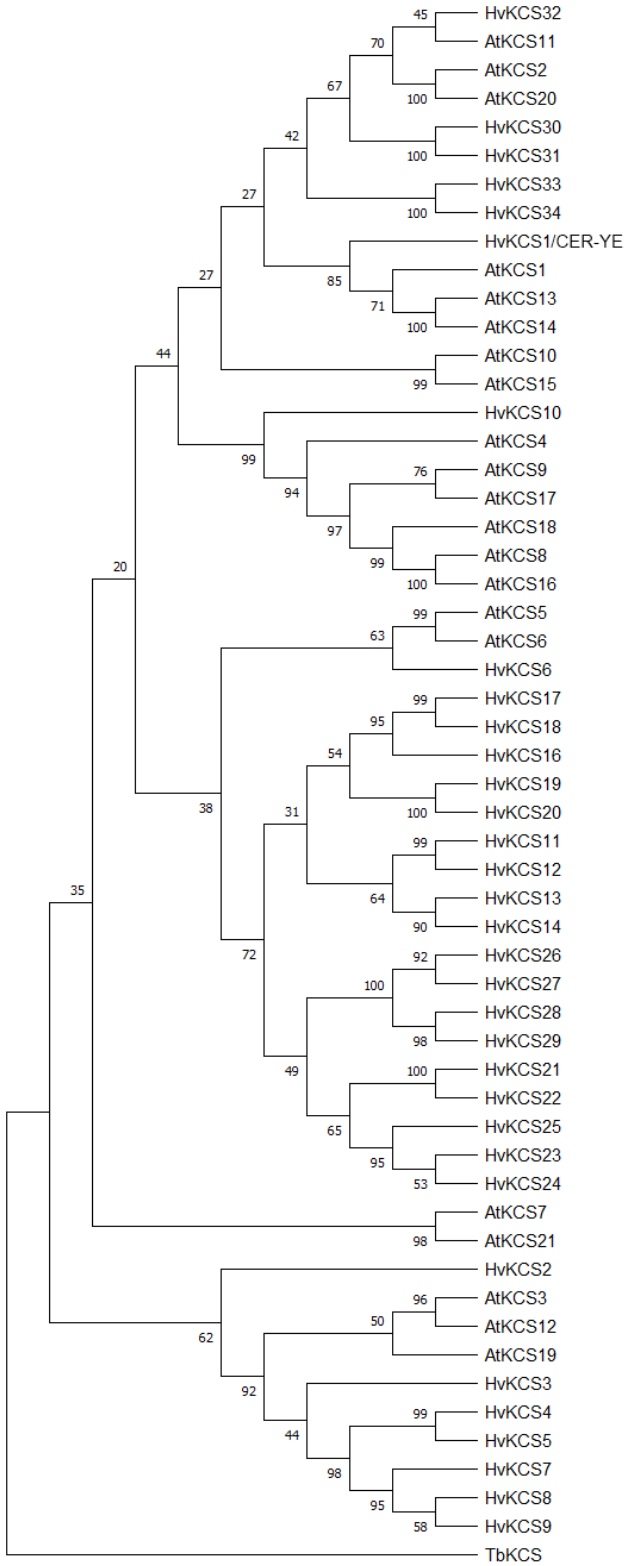

Figure 34: Maximum-Likelihood tree based on 21 annotated *A. thaliana* and 33 annotated *H. vulgare* KCS protein sequences. The relationship was calculated based on 1000 bootstrap consensus replicates and statistical probabilities are labelled on the axes. The tree was rooted to a KCS sequence from the protist *Trypanosoma brucei*.

3.4 Allelism test of the mutants *cer*-ye.267 and *cer*-zh.54 demonstrate that they are *Hv*KCS1 alleles

The results of the BSR-Seq approach indicated that the *cer*-ye mutants carry mutations in the locus *HORVU4Hr1G063420.* Previously, the *H. vulgare eceriferum* line *cer*-zh.54 was mapped to the same gene (Li *et al.* 2018). Therefore, it was possible that the two mutant lines, *cer*-ye and *cer*-zh, carry mutations in the same locus. For this reason, the two bowman introgression lines *cer*-ye.267 (BC8) and *cer*-zh.54 (BC7) were crossed to perform an allelism test. The underlying principle is based on the Mendelian laws; non-allelic lines should result in heterozygous F1 offspring which do not retain the recessive *cer* phenotype, while a cross of homozygous allelic plants would generate homozygous (or heteroallelic) F1 *cer* mutant plants. After crossing, the F1 plants were screened for the mutant phenotype using the water droplet repellence test on the leaves. The results of the allelism test are depicted in Figure 35.

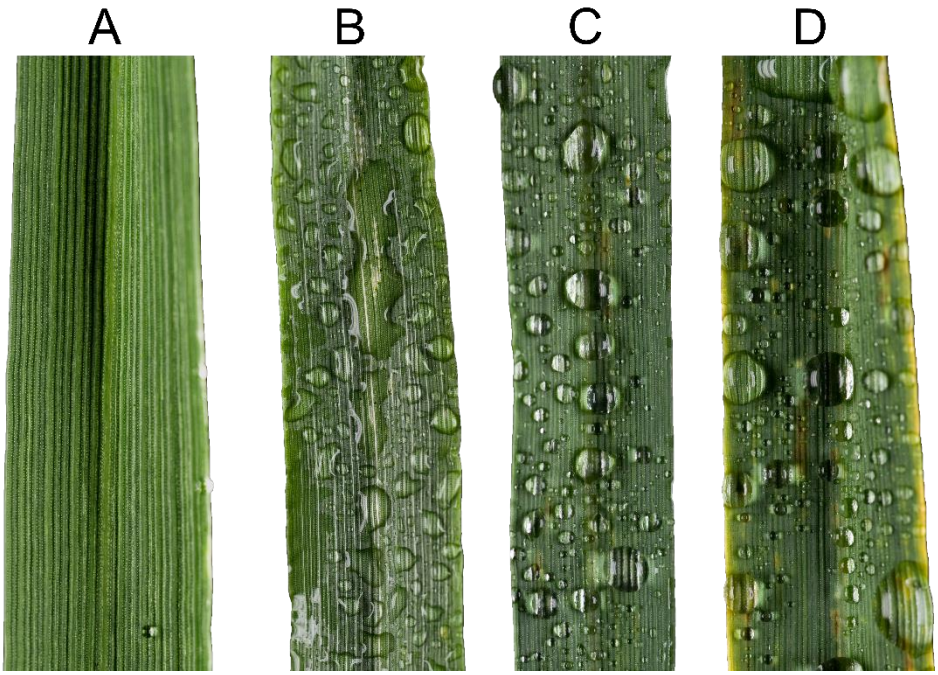

Figure 35: Water-repellence phenotypes of F1 plants derived from the cross of the *cer*-ye.267 and *cer*-zh.54 bowman introgression mutants. A: Bowman. B: *cer*-ye.267. C: *cer*-zh.54. D: Leaf of a *cer*-ye.267 x *cer*-zh.54 F1 plant. Water droplets were not retained on the surface of the reference cultivar Bowman, while droplets formed on the leaves of the *eceriferum* lines *cer*-ye.267, *cer*-zh.54 and of the F1 plant of *cer*-ye.267 x *cer*-zh.54.

The F1 generation was screened for a *cer*-like phenotype by wetting of the leaves. Water droplets repelled from the wild-types tissue. The individual *cer* lines *cer*-ye.267, *cer*-zh.54 showed the previously described hydrophilicity (Figure 35B/C). A similar phenotype was observed for the F1 progenitor generation of *cer*-ye.267 x *cer*-zh.54 (Figure 35D).

3.5 The expression of *Cer-za* and *Cer-ye* is tissue-specific

Based on the results described in the previous paragraphs, the *Cer-za* and *Cer-ye* genes are predicted to code for an acyl-CoA reductase and a β-ketoacyl-CoA synthase, respectively. Both genes appear to be involved in the synthesis of cuticular wax compounds. It is known that wax synthesis is associated with epidermal cells. Therefore, the two genes might be expressed in epidermal tissue. Semiquantitative RT-PCRs were performed using cDNA from isolated epidermal cells, stripped leaf material with partially removed epidermis, as well as from root tissue. *ACT2* was selected as housekeeping gene.

3.5.1 Gene expression of *Cer-za* is detectable in epidermal leaf tissue

HORVU5Hr1G089230 (*Cer-za*) is predicted to produce up to seven different transcripts; however, the primers used were designed to exclusively bind to the largest transcript *HORVU5Hr1G089230.1* and amplify a 196 bp amplicon. Different PCR settings were tested to find the optimal reaction conditions allowing the amplification of both the transcript of *HORVU5Hr1G089230* as well as the *ACT2* gene, without oversaturating the signal intensity of *ACT2*. Finally, a T_A of 56°C and 33 cycles of 15 s elongation time turned out to be sufficient (Figure 36). The applied reaction settings did exclusively lead to a detectable signal with the cDNA generated from epidermal tissue as template, while no amplicons could be generated from cDNA obtained from stripped leaves or roots.

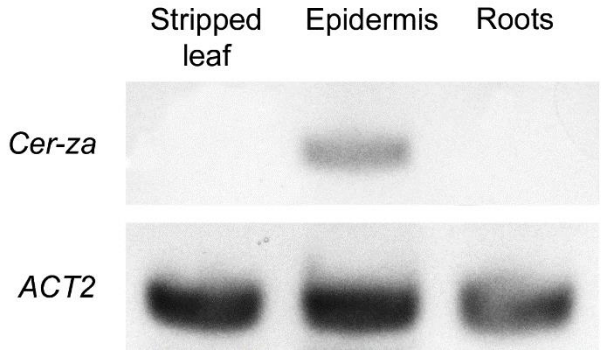

Figure 36: Expression of *Cer-za* in different barley tissues. Relative RT-PCR was performed to demonstrate the expression of *Cer-za* in leaves lacking the epidermis (stripped leaf), in epidermis and roots. Template concentrations were normalized according to *ACT2* expression. The agarose gel was stained with Midori Green. The presented picture was inverted.

3.5.2 Gene expression of *Cer-ye* is restricted to epidermal tissue

The primer pair used was designed to uniquely bind in the coding sequence of *HORVU4Hr1G063420 (Cer-ye),* and the RT-PCR generated an amplicon of 238 bp. Different reaction settings were tested and a T_A of 56°C was sufficient, accompanied with 32 cycles of 15 s elongation time each. A band was just detectable in the agarose gel after the reaction with epidermal tissue as template (Figure 37). Both, the stripped leaf sample and root tissue, showed no expression of *Cer-ye*.

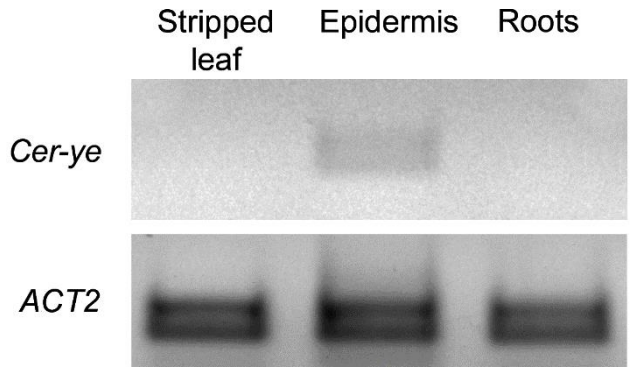

Figure 37: Expression of *Cer-ye* in different barley tissues. RT-PCR was performed to demonstrate the expression of *Cer*-ye in stripped leaves, epidermis or roots. Template concentrations were normalised utilising *ACT2* as housekeeping gene. The inverted picture shows an agarose gel stained with Midori Green.

3.6 Localisation to CER-ZA to the ER

Several proteins involved in the biosynthesis of cuticular waxes have been localised to the ER. To study the subcellular localization of CER-ZA, a GFP-tag was fused to the N-terminal protein sequence of CER-ZA. This construct and an ER targeting DsRED-HDEL marker were agroinfiltrated into *Nicotiana benthamiana* leaves. The area around the infiltration site was carefully screened for expression-associated fluorescence signals. Only cells that showed signals for both channels (GFP and DsRED) were considered. This is especially important with regard to the autofluorescence of chlorophyll or fluorescence signals emitted from aromatic compounds (e.g. wound suberin) which are increasingly produced and released as stress reaction to the infiltration. Therefore, each considered cell was confirmed to be fully intact before being further investigated. Wavelengths were specifically filtered to allow the suppression of chlorophyll autofluorescence and to observe the fluorescence protein emission at a maximum extent. A signal occurred in a neighbouring epidermal cell of the infiltration site (Figure 38). The GFP signal (Figure 38A) occurred in a net-like structure all over the cell with an increased intensity close to an oval shade presumably derived from the nucleus. The ER marker-associated DsRed signal (Figure 38B) was observed with a similar net-like structure and the same nucleus shade. Finally, both signals were merged (Figure 38C), and the resulting

overlay showed a clear overlap of the GFP-tagged CER-ZA protein and the ER associated DsRed marker.

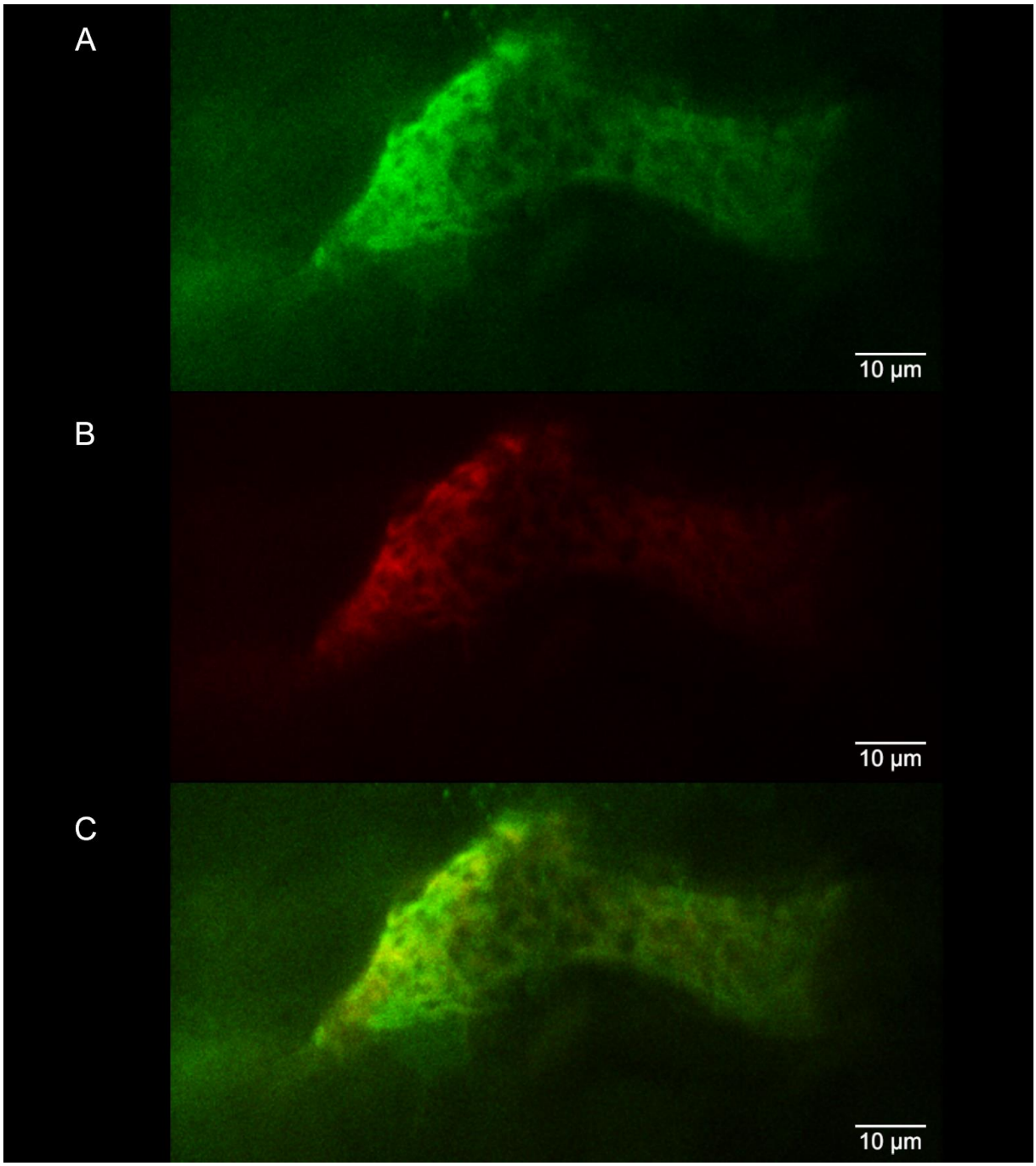

Figure 38: Localisation of GFP-tagged CER-ZA in epidermal cells of transgenic *N. benthamiana* leaves with a confocal microscope. A: GFP emission (488 nm) with GFP-tagged CER-ZA filtered at a center wavelength of 525.3 nm. B: DsRED emission (521 nm) of DsRED fused to an ER-marker filtered at a center wavelength of 607.36 nm. C: Merge of both channels.

3.7 Primary alcohols accumulate after expression of CER-ZA in *E. coli*

E. coli provides a well-established heterologous system suitable for the expression of different proteins. CER-ZA was expressed under the inducible T7 promotor to accumulate high amounts of protein. The empty vector was used as negative control. Since no additional substrates were provided, the putative acyl-CoA reductase was restricted to use substrates from the endogenous acyl-CoA pool of *E. coli*. The expression of CER-ZA was confirmed by protein isolation and separation on SDS PAGE in combination with Coomassie Blue staining (Figure 39). A strong band close to 55 kDa became visible for the CER-ZA expression construct. The position of the CER-ZA band corresponds to the calculated molecular weight of 56.77 kDa for the His-tagged CER-ZA protein. Low-molecular weight proteins increased concomitantly after expression of CER-ZA and were suspected to be degradation products.

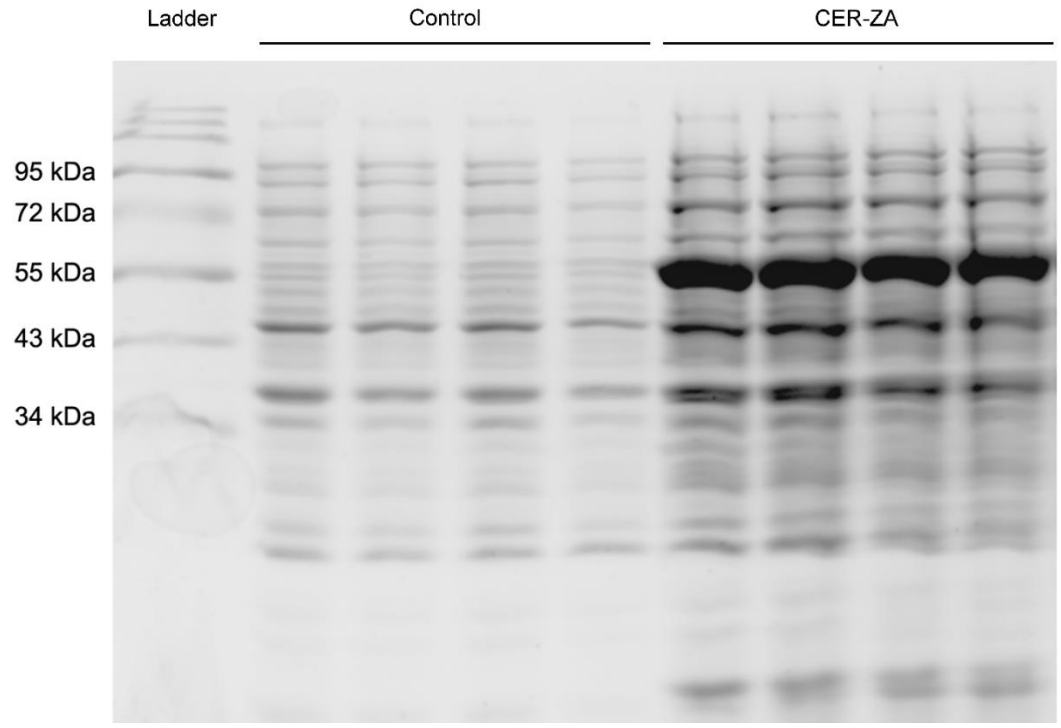

Figure 39: Separation of proteins from *E. coli* expressing CER-ZA by SDS PAGE in comparison to the empty vector control. A pre-stained protein marker was added as molecular weight reference. A strong band was observed at approximately 55 kDa after expression of CER-ZA. Control: pET-15b. CER-ZA: pET-15b-CER-ZA. n = 4.

In addition, a Western Blot was performed to confirm that the observed protein at 55 kDa corresponds to the His-tagged CER-ZA protein. His-tagged proteins were detected with the His detector kit followed by recording the chemiluminescence (Figure 40). Again, strong signals were detected at a molecular weight of approximately 55 kDa for the CER-ZA expressing samples, while the control lacked this signal. Some low molecular-weight proteins were observed and might be derived from protein degradation.

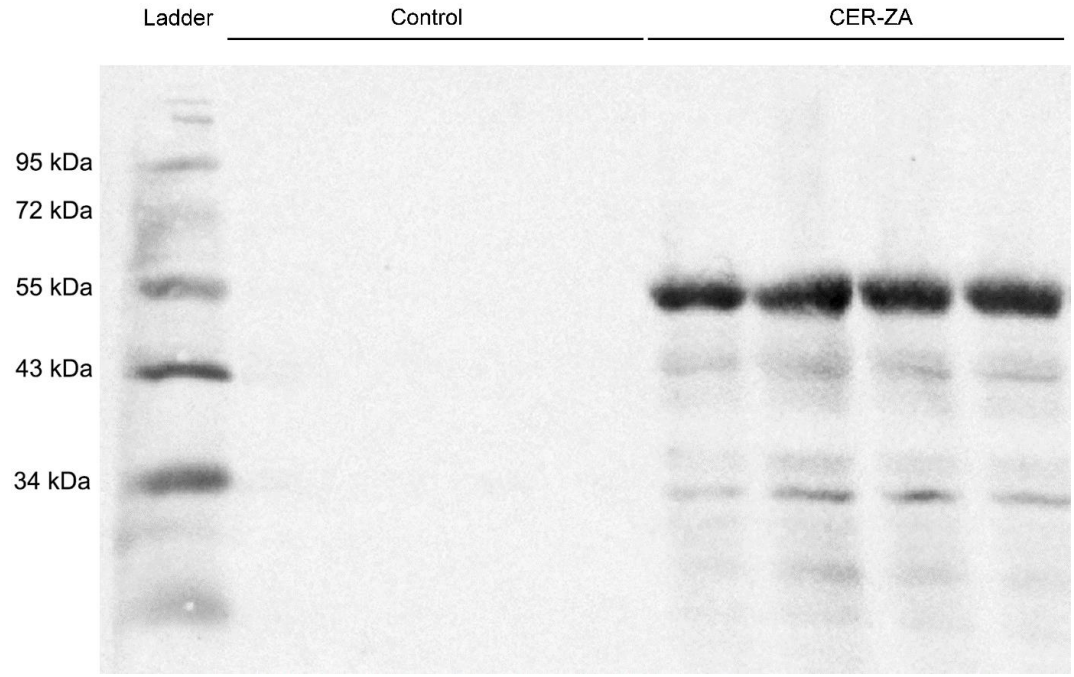

Figure 40: Identification of His-tagged CER-ZA by Western Blot after expression in *E. coli*. A protein marker was added as molecular weight reference. A strong signal was observed at approximately 55 kDa after expression of CER-ZA. Control: pET-15b. CER-ZA: pET-15b-CER-ZA. n = 4.

Next, alcohol production in the CER-ZA expressing cells was studied via GC after silylation of lipids extracted from the cells. The chromatograms were screened for the presence of saturated primary alcohols. Indeed, compared to the negative control, an additional peak appeared in chromatograms derived from samples that expressed the CER-ZA protein. The new peak was clearly identified as silylated hexadecanol based on its mass spectrum. An overall accumulation of primary alcohols was noticed after expression of CER-ZA: The total amount of primary alcohols was strongly increased from 3.49 ± 1.90 nmol/100 mL (cell culture with OD600 = 1) to 27.18 ± 3.61 nmol/100 mL (Figure 41A). The primary alcohols were saturated and were composed of chain lengths of $C_{14:0}$-ol, $C_{16:0}$-ol and $C_{18:0}$-ol. While $C_{14:0}$-ol and $C_{16:0}$-ol were not detectable in control samples, $C_{18:0}$-ol was present in control and CER-ZA expressing cells at similar levels (Figure 41B). In contrast a strong accumulation of $C_{16:0}$-ol (16.12 ± 5.91 nmol/100 mL) and $C_{14:0}$-ol (7.51 ± 2.46 nmol/100 mL) was observed in CER-ZA expressing cells.

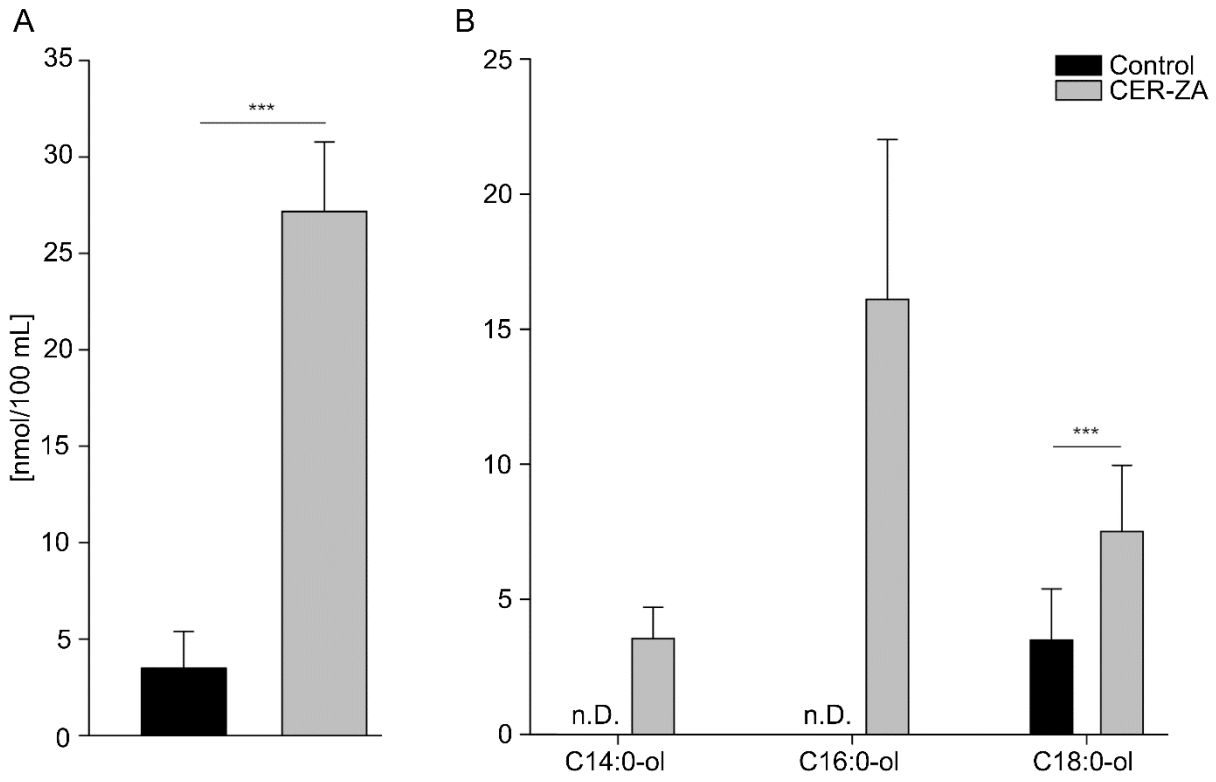

Figure 41: Quantification of primary alcohols after expression of CER-ZA in *E. coli* by GC-FID. A: Summarized total amount of alcohols. B: Individual primary alcohols. n.D., Not detectable. The amounts of alcohols were normalised to nmol per 100 mL of culture with an OD600 = 1. n = 3. Student's *t*-test; $p^{***} \leq 0.01$. $p^{**} \leq 0.03$. $p^{*} \leq 0.05$.

3.8 Primary alcohols accumulate after expression of CER-ZA in *S. cerevisiae*

In addition to the expression in *E. coli* as a prokaryotic system, CER-ZA was expressed in eukaryotic cells (*S. cerevisiae)*. Total lipids were extracted and analysed via GC/MS after silylation. Heptadecanol was added as internal standard for quantification. $C_{16:0}$-ol and $C_{18:0}$-ol were identified in the control as well as in the CER-ZA expression cultures. In the latter, an additional peak uniquely appeared at a retention time of 29.8 min that was clearly identified as the TMS derivative of hexacosanol ($C_{26:0}$-ol) (Figure 43). While in average 0.37 ±0.07 nmol/L culture with OD600 = 1 of primary alcohols were measured in the control cells, the amount increased about 4-fold after expression of CER-ZA (1.73 ± 0.42 nmol/L, Figure 42A). This increase was mainly based on a strong increase of $C_{16:0}$-ol from 0.04 ± 0.04 nmol/L to 0.27 ± 0.09 nmol/L, as well as on the striking accumulation of $C_{26:0}$-ol (1.01 ± 0.22 nmol/L) in the CER-ZA expression cells (Figure 42B). In the control chromatogram, an unknown low abundant substance was detected that co-migrated with $C_{26:0}$-ol. Therefore, the presence of $C_{26:0}$-ol in the control could not be excluded; however, the fragmentation pattern of the peak eluting at 29.8 min in the control chromatogram differed from the one of the CER-ZA expressing cells, and only the latter corresponded to the mass spectrum of $C_{26:0}$-ol.

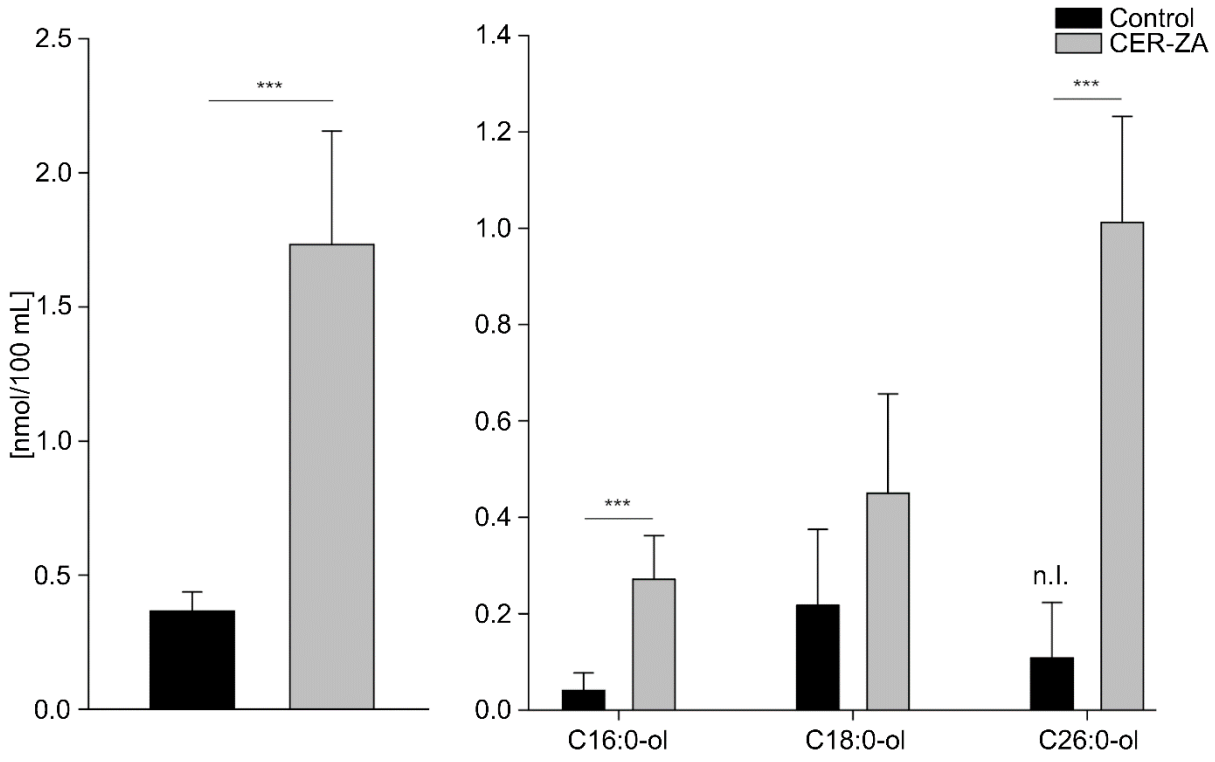

Figure 42: Quantification of primary alcohols after expression of CER-ZA in *S. cerevisiae*. A: Total amount of alcohols. B: Individual primary alcohols. The amounts of alcohols were normalised to nmol per 100 mL of culture with an OD600 = 1. n.l., not identified. $n_{Control}$: 3. $n_{CER\text{-}ZA}$: 9. Student's *t*-test; $p^{***} \leq 0.01$. $p^{**} \leq 0.03$. $p^{*} \leq 0.05$.

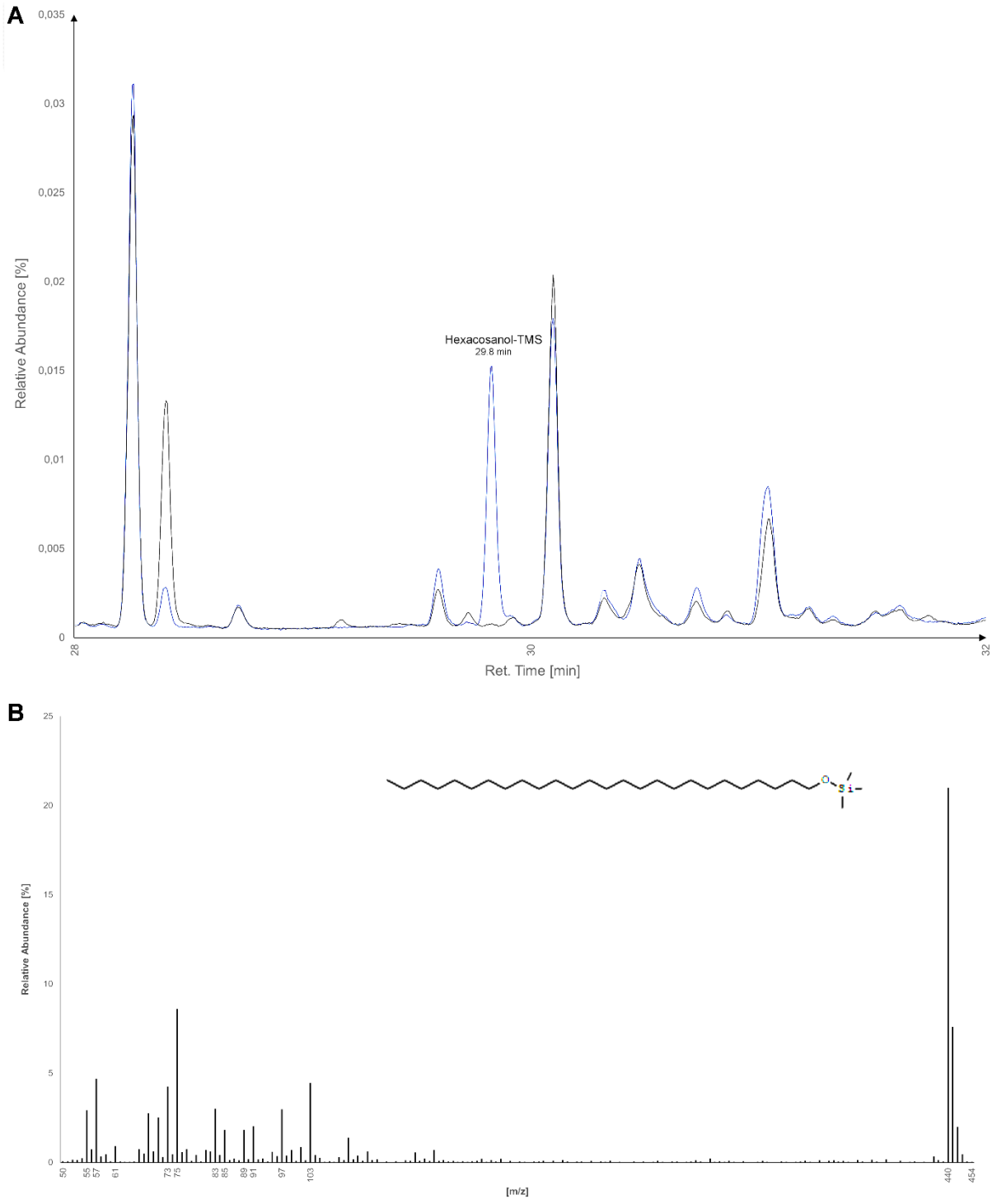

Figure 43: Identification of C_{26}-ol production in yeast cells expression CER-ZA. Overlaid GC/MS chromatograms comparing the vector control (black) and CER-ZA expressing cells (blue) between the retention times of 28 and 32 min (A). The chromatogram of the CER-ZA sample harboured an additional peak at 29.8 min. (B). The mass spectrum of the peak eluting at 29.8 revealed a molecular weight of M_r: 454.88, corresponding to hexacosanol-TMS. Its detection was restricted to samples expressing CER-ZA.

3.9 Expression of CER-ZA in the wax-deficient *A. thaliana cer*4-3 mutant

Phylogenetic analysis indicated that the acyl-CoA reductase *At*CER4/FAR3 is a co-ortholog to CER-ZA in Arabidopsis. *At*FAR3 was shown to produce primary alcohols from acyl-CoAs with NADPH as cofactor (Rowland *et al.* 2006). Expression of *At*FAR3 in yeast resulted in the accumulation of C_{24} and C_{26} primary alcohols, and the cuticular waxes of *cer*4 alleles were shown to be deficient in primary alcohols and esters. In Arabidopsis as in barley, C_{26} represents the dominant chain length of primary alcohols. To address the question whether CER-ZA is a functional ortholog of *At*CER4/FAR3, CER-ZA was expressed in the cuticular wax deficient *A. thaliana cer*4-3 allele under the native *At*CER4 promotor. After transformation, four independent *A. thaliana cer*4-3+CER-ZA lines were selected in the T1 generation. The plants were grown and after selfing, homozygous plants were obtained in the T3 generation. Cuticular waxes of stem sections from the *cer*4-3+CER-ZA T3 plants as well as from Col-0 and *A. thaliana cer*4-3 mutant plants were extracted and analysed by GC. Since independent transgenic lines harbour insertions at different loci, the intensity of the protein expression can differ. Therefore, the null hypothesis was initially tested within this group with ANOVA to identify uniform variations. Afterwards, significant differences between the group of *cer*4-3+CER-ZA lines against Col-0 and *cer*4-3 were tested. Values calculated for *cer*4-3+CER-ZA line 3 will be referred to in the following since the standard deviations for this line were generally low. Initially, the total wax loads of the different genotypes were compared (Figure 44A). Col-0 (13.92 ± 0.56 µg/cm²) and *cer*4-3 (11.48 ± 0.32 µg/cm²) differed significantly from each other. The total wax load of the *cer*4-3+CER-ZA lines (14.03 ± 1.84 µg/cm², line 3) was not statistically different from Col-0 but was significantly increased compared to *cer*4-3. Moving on to the distribution to individual substance classes, the strongest variations were observed for primary alcohols and esters. Primary alcohols (even numbered carbon atoms) were analysed separately from the more dominant secondary alcohols (odd numbered) because changes in primary alcohols might be masked by secondary alcohols (Figure 44H/I). The primary alcohol content of *cer*4-3 (0.15 ± 0.00 µg/cm²) was reduced to approximately 10% of Col-0 levels (1.45 ± 0.12 µg/cm²). After expression of CER-ZA, the primary alcohol content approximately duplicated compared to *cer*4-3 to 0.27 ± 0.04 µg/cm² in *cer*4-3+CER-ZA line 3 (Figure 44F/H). Similarly, the ester content in *cer*4-3+CER-ZA (0.31 ± 0.08 µg/cm², line 3) increased significantly by 67% compared to *cer*4-3 (0.21 ± 0.03 µg/cm²) but did not reach Col-0 levels (0.44 ± 0.07 µg/cm²). No variations from Col-0 and *cer*4-3 were found for ketones, triterpenoids, and secondary alcohols (Figure 44E/G/I). Variants tests for acids and aldehydes showed strong variations between the four *cer*4-3+CER-ZA lines in these substance groups, but a tendency of increase was observed for aldehydes (Figure 44C/D).

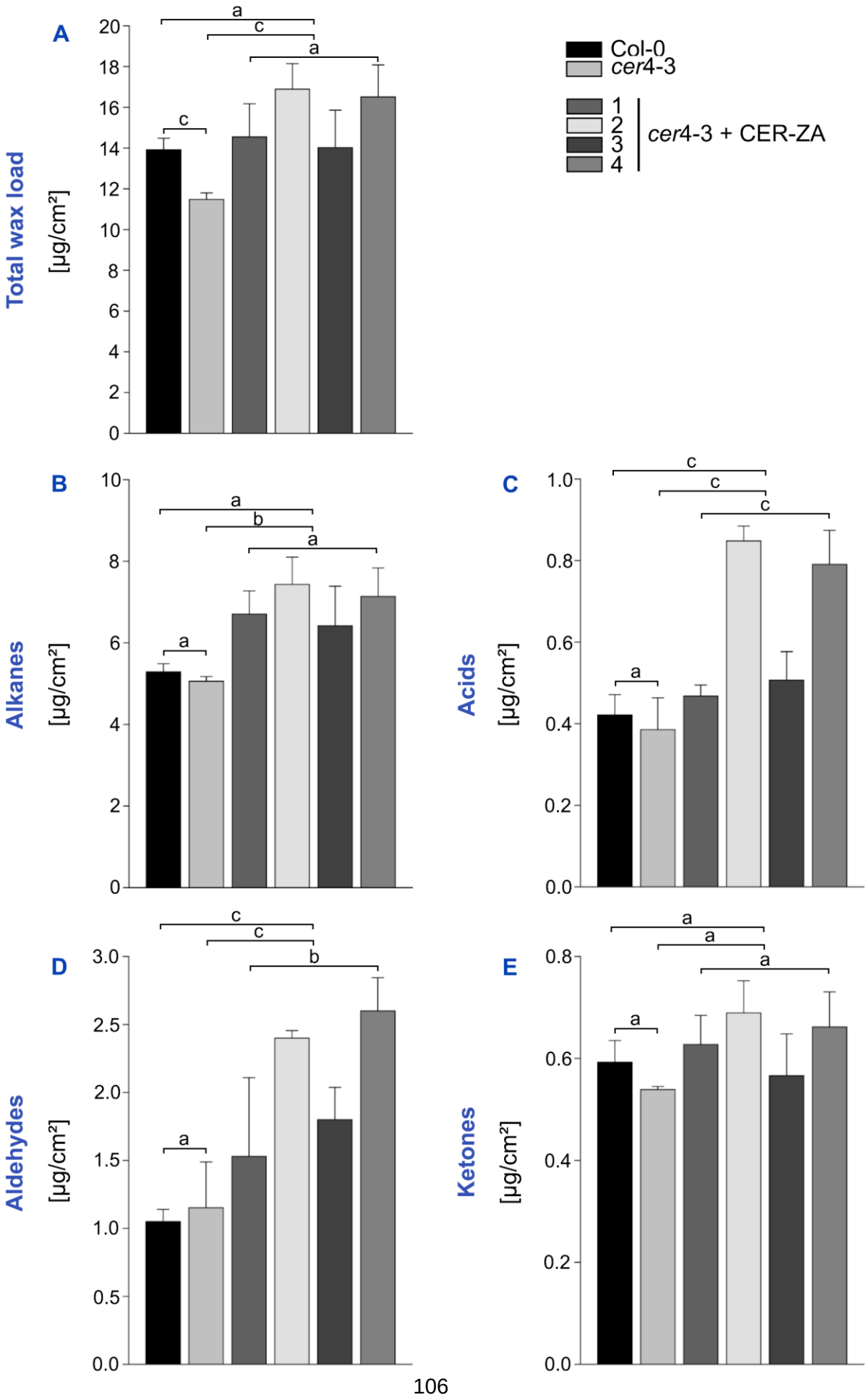
A
Total wax load
[µg/cm²]
B
Alkanes
[µg/cm²]
C
Acids
[µg/cm²]
D
Aldehydes
[µg/cm²]
E
Ketones
[µg/cm²]
Col-0
cer4-3
1
2
3
4
cer4-3 + CER-ZA

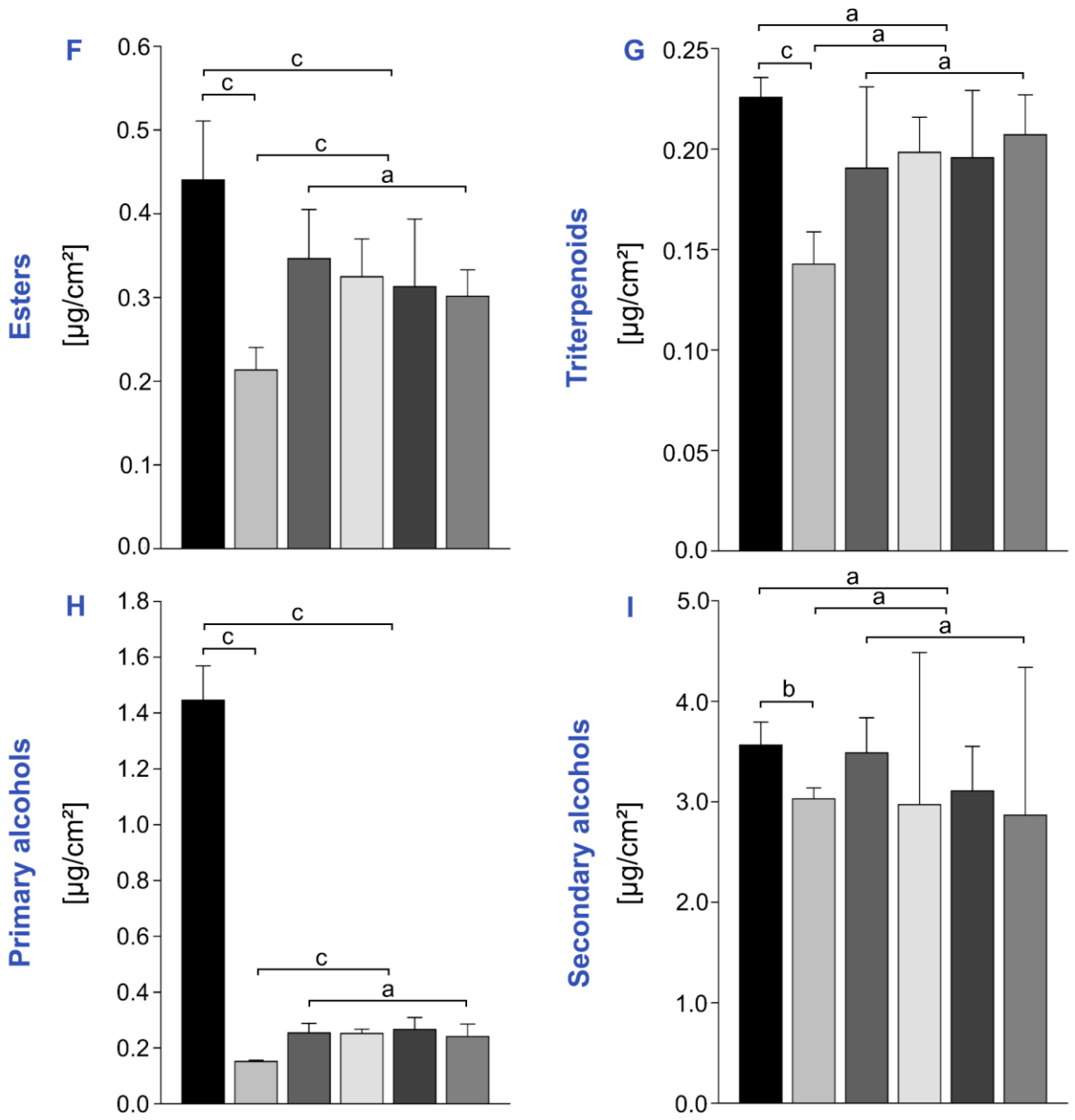

Figure 44: Quantification of cuticular waxes extracted from *A: thaliana* Col-0, *cer*4-3 and four independent *cer*4-3+CER-ZA lines. A: Total wax load. B-I: Distribution to substance classes. B: Alkanes. C: Fatty acids. D: Aldehydes. E: Ketones. F: Esters. G: Triterpenoids. H: Primary alcohols. I: Secondary alcohols. n = 4. ANOVA was used to test the null hypothesis for the four independent *cer*4-3+CER-ZA lines. The group was further tested against Col-0 and *cer*4-3; $p_c \leq 0.01$. $p_b \leq 0.03$.

3.10 Cuticular barrier properties of the *cer*-za.227 *and cer*-ye.267 mutants

3.10.1 Water-flow permeability barrier

The data presented here were generated in collaboration with Prof. Lukas Schreiber's group (IZMB, University of Bonn). A porometer was used to determine the total transpiration for Bowman, *cer*-za.227 and *cer*-ye.267 (both mutants with Bowman background) under well-watered conditions (Figure 45). Stomata are expected to be wide opened under these conditions, and their transpiration is dominating in the measured values. The transpiration flow rates differed strongly between the adaxial and abaxial leaf sides in all measured genotypes. On the adaxial leaf side of Bowman, a transpiration flow rate of $4.59 \times 10^{-8} \pm 1.07 \times 10^{-8}$ m/s was calculated, while the flow rate on the abaxial site was $1.61 \times 10^{-8} \pm 6.07 \times 10^{-9}$ m/s. No significant differences were found for the flow rates in *cer*-za.227 and *cer*-ye.267 in the stomatal dominated transpiration flow rate compared to the reference Bowman.

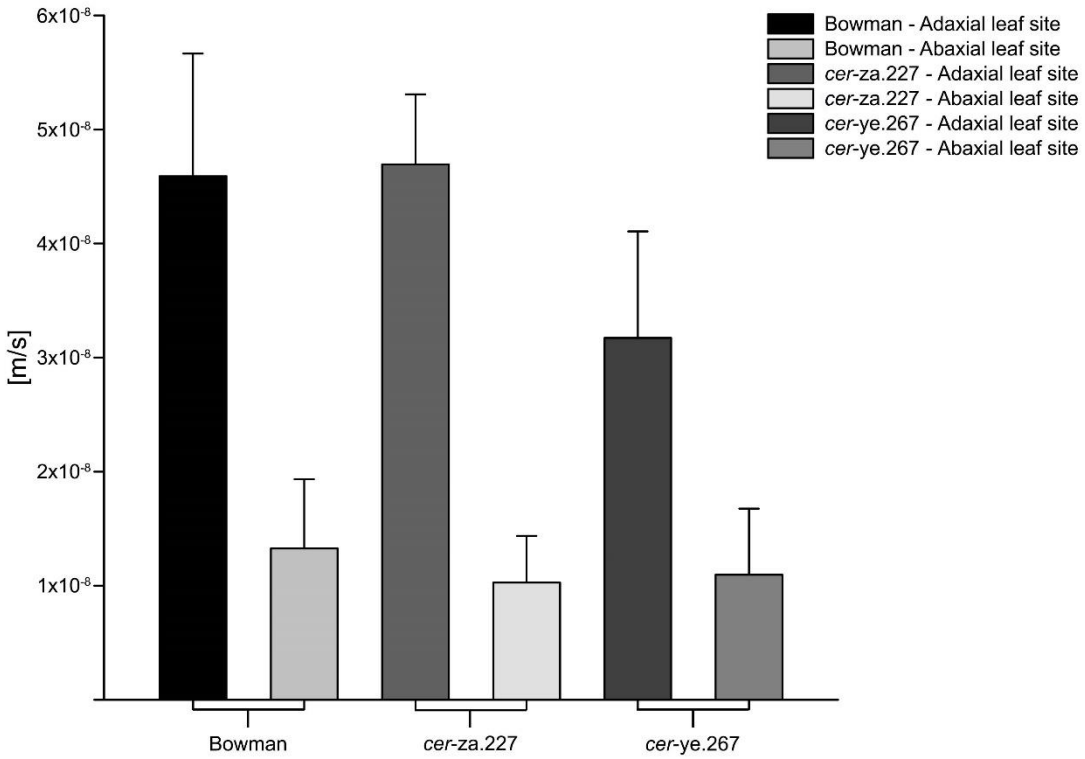

Figure 45: Stomata transpiration flow rates measured for *H. vulgare* leaves with a porometer and calculated in [m/s]. Five replicates of the second leaf each of Bowman, *cer*-za.227 and *cer*-ye.267 lines were measured on the adaxial and abaxial leaf sides. Student's *t*-test; no significant differences between the lines were detected.

The minimal water permeability, in the following designated as P_{min}, was gravimetrically determined and plotted in [m/s] against the relative water deficit (RWD, Figure 46). P_{min} is defined as the residual, water flow which mostly occurs across the cuticle and which persists

after closure of all intact stomata. After an initial rapid decline, during which the leaf stomata were closed, the P_{min} values reached stable levels. Regression lines were calculated and plotted for the linear section. Further permeabilities were calculated based on this linear section. After comparing the calculated values of the minimal water permeability (Table 25) to the stomatal transpiration flow rates, a close approximation of the initially measured water permeability was noticed. After reaching P_{min}, the transpiration flow rate decreased by roughly 95% in all three genotypes. For the reference Bowman, a permeability rate of $1.61 \times 10^{-9} \pm 5.58 \times 10^{-10}$ m/s was determined. P_{min} calculated for the *eceriferum* lines did not differ significantly from the Bowman cultivar, but *cer*-za.227 showed high standard deviation.

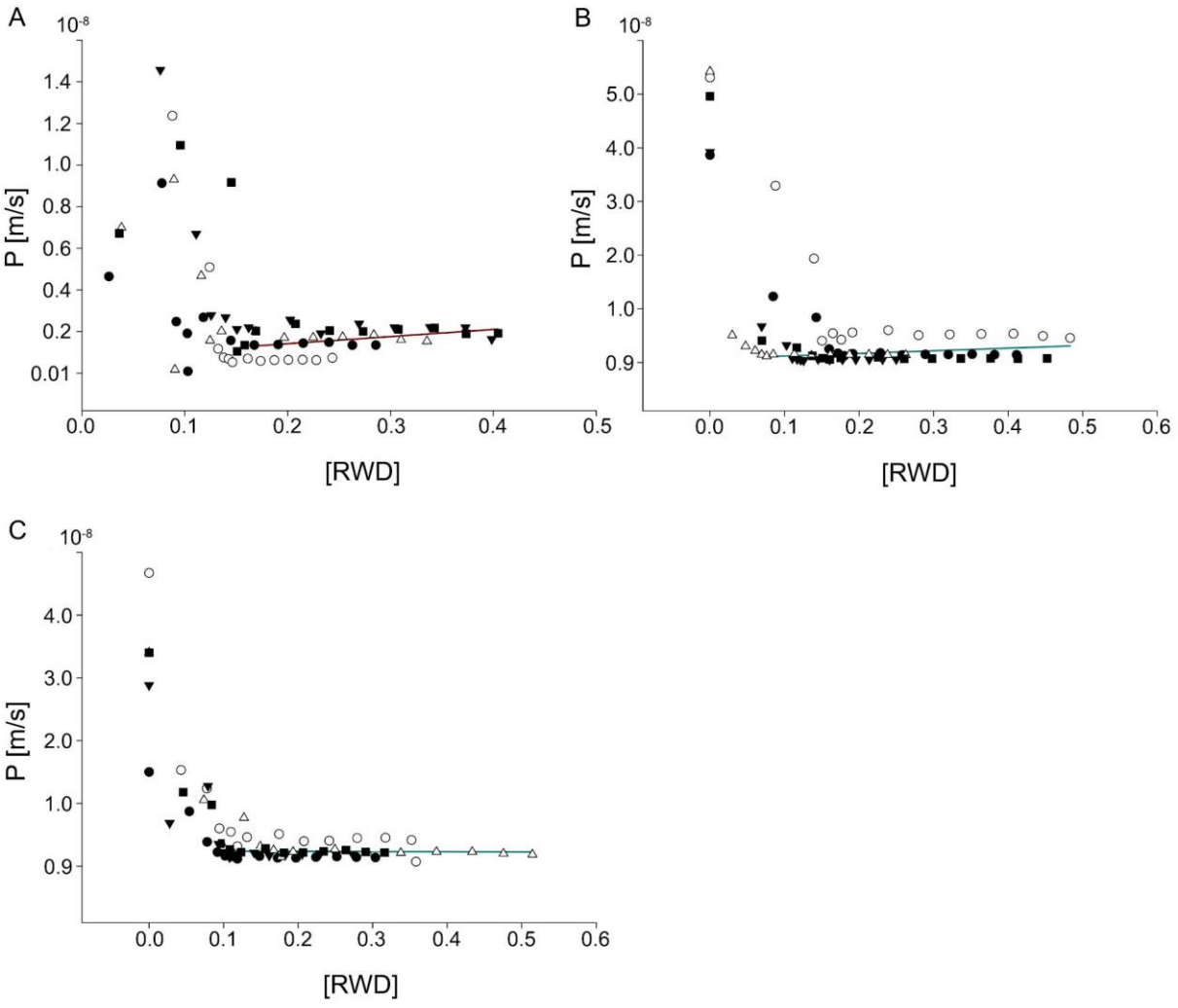

Figure 46: Gravimetric determination of the minimal water permeability measured in [m/s] as flow rate plotted against the relative water deficit (RWD). Each data point series (filled/open circles, squares, triangles) represents one replicate (n = 5). Regression lines were plotted after the values reached a plateau. A: Bowman. B: *cer*-za.227. C: *cer*-ye.267.

Table 25: Water permeabilities determined for Bowman, *cer*-za.227 and *cer*-ye.267 given in [m/s]. The initial measured water permeability prior to stomata-closure and the minimal water permeability P_{min} measured after stomata-closure were calculated based on gravimetrically measured water-loss.

	Initial water permeability		**Minimal water permeability (P_{min})**	
Genotype	**AVG**	**SD**	**AVG**	**SD**
Bowman	45.9×10^{-9}	11.8×10^{-9}	1.61×10^{-9}	0.56×10^{-9}
cer-za.227	46.9×10^{-9}	6.72×10^{-9}	1.89×10^{-9}	1.69×10^{-9}
cer-ye.267	31.7×10^{-9}	10.2×10^{-9}	2.35×10^{-9}	0.89×10^{-9}

3.10.2 Permeation barrier properties

Permeation barrier properties of the cuticles were studied utilising the herbicide metribuzin. Metribuzin is a photosynthesis inhibitor, and its effect on the photosynthetic apparatus of leaf mesophyll cells can be recorded by measuring chlorophyll fluorescence. 50 µmol of metribuzin were dissolved in a defined volume of 0.1% Brij 4. The solution was equally sprayed onto the leaf surface of barley plants at the three-leaf developmental stage. Metribuzin penetration was indirectly monitored by tracking of the photochemical efficiency measured over time with a PAM fluorometer (Figure 47). Control treatments with water or 0.1% Brij 4 solution did not affect the photosynthetic quantum yield II (PY(II)) which fluctuated around a value of 0.7. Metribuzin application caused a decrease of PY(II) in all three genotypes over the first 25 min after treatment. The reduction to a minimum PY(II) of 0.49 ± 0.07 was measured for *cer*-za.227 which was comparable to the decrease for Bowman (0.47 ± 0.06). In stark contrast, the reduction for *cer*-ye.267 was significantly stronger with a PY(II) decreasing to 0.23 ± 0.10. Regression lines were calculated to determine the factor of reduction compared to Bowman; accordingly, the effect of the treatment was increased by a factor 2.3 in *cer*-ye.267, indicating that metribuzin increasingly penetrated the epidermal cell layer of *cer*-ye.267.

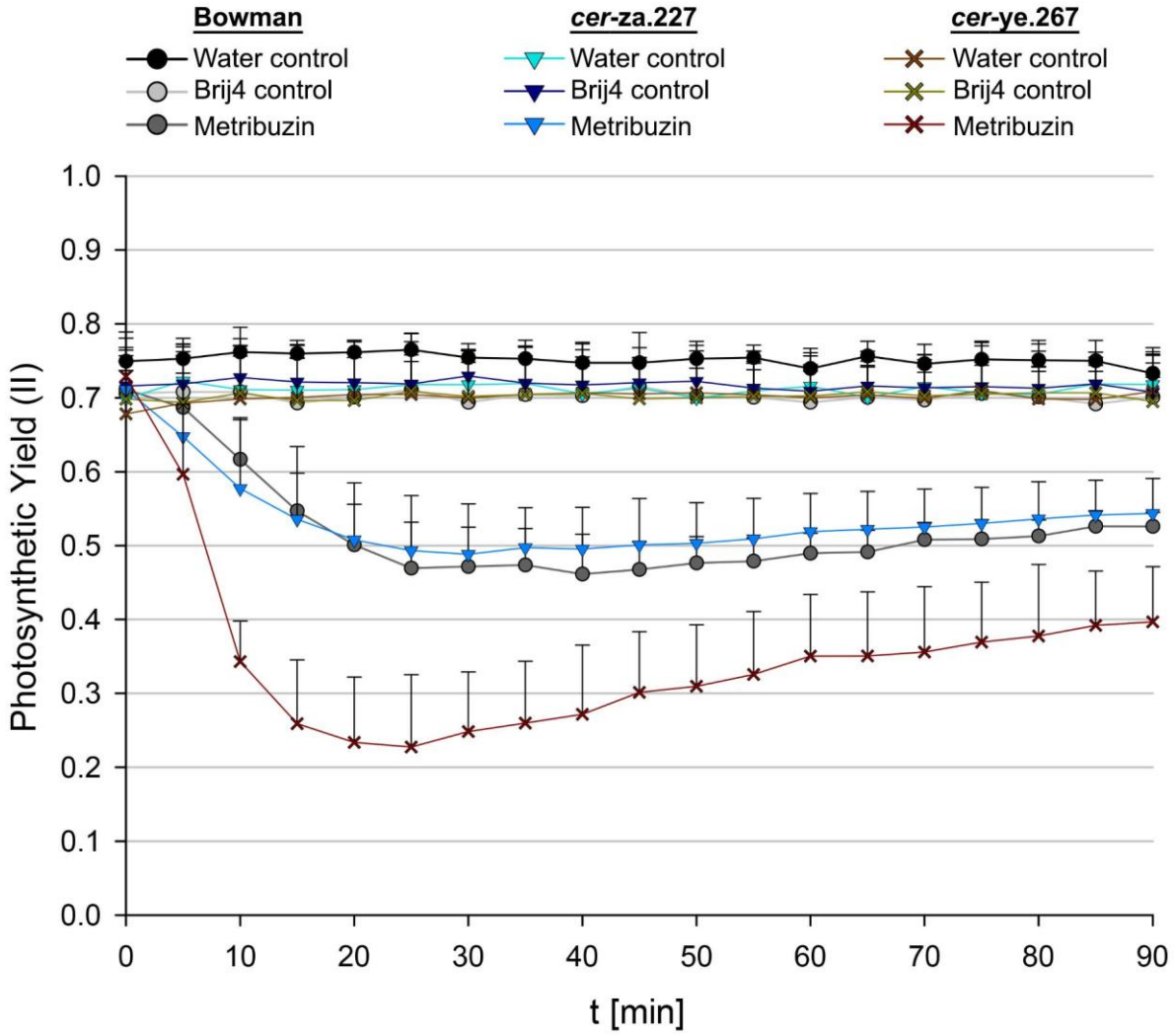

Figure 47: Photosynthetic quantum yield (II) after treatment of leaves of the barley lines Bowman, *cer*-za.227 and *cer*-ye.267 with 50 µmol metribuzin dissolved in 0.1% Brij 4. Treatments with water and 0.1% Brij 4 solutions were used as controls. Data points were collected at 5 min intervals for 90 min.

4 Discussion

The establishment of cuticular wax biosynthesis was a crucial adaptation to the novel environment during the colonisation of the terrestrial habitat. Changing climatic conditions accompanied with a growing human world population represents a challenge for mankind's food security. In view of this problem, a complex strategy combining several key factors to improve agricultural yield is required. One of these factors could be the enhancement of drought resistance by strengthening the physiological barrier provided by the cuticle. Cuticles of extant plants evolved to their current complexity over millions of years, but the current climate change occurs in unprecedented speed and will require a fast adaptation of the crop plants to the new conditions. Modern genetic modification tools allow breeders the increasingly efficient generation of novel cultivars. A deep knowledge about the genetic background is crucial for targeted modifications of complex structures as the cuticle. Consequently, the role of key enzymes as well as the impact of biochemical changes on the properties of the cuticular barrier must be clarified. To contribute to this knowledge base, the genetic background of the two *eceriferum* mutant lines *cer*-za and *cer*-ye in *H. vulgare* was studied. A BSR-Seq approach allowed the identification of candidate genes for the two mutations. The protein sequences were used to identify orthologous proteins in other species, and catalytic functions for the synthesis of cuticular waxes were analysed.

4.1 *cer-za* carries mutations in the locus *HORVU5Hr1G089230*

The first part of the study describes the identification of the locus *HORVU5Hr1G089230* which carries mutations in the *cer*-za mutant alleles (3.3.1). Different mutational events in the transcripts of *cer*-za.227, *cer*-za.318 and *cer*-za.232 cause premature stop codons which were predicted to lead to non-functional protein products (3.3.1). Since *cer*-za.227 and *cer*-za.318 shared the very same deletion, it is possible that the two lines are derived from the same mutagenesis event and that the seed batches were split and occur two times in the seed stock. The SNP found in the coding sequence of *cer*-za.173 was localised to the NAD_4_binding domain (3.3.2). Protein structure modelling suggested that the amino acid exchange might lead to a steric change in the tertiary structure and disable the binding of cofactors (3.3.2). The presence of different domain sequences as well as sequence comparison to proteins with known functions strongly indicated that the CER-ZA protein harbours fatty acyl-CoA reductase activity (3.3.2). Two common family domains were predicted by independent algorithms and were similarly present in FARs from *Triticum aestivum* (Wang *et al.* 2015, Wang *et al.* 2015, Wang *et al.* 2016, Chai *et al.* 2018). Both domains are generally annotated as sterility protein domains based on the early description of *Male Sterility 2* in Arabidopsis. *MS2* encodes the chloroplast localised alcohol-forming acyl-CoA reductase *At*FAR2 that is involved in the formation of sporopollenin and was identified as male sterility protein (Chen *et al.* 2011);

however, the annotation of this domain as male sterility sequence is misleading since these domains are shared by several reductases which are not necessarily male sterile proteins. In the course on this study, no indication of degenerated anthers or reduced yield was noticed. The phylogenetic tree of CER-ZA related sequences revealed a distinct formation of separated monocot and dicot clusters for putative alcohol forming acyl-CoA reductases. The results indicated that the FAR family members were strongly diversified after separation of the angiosperms. Within the monocots, CER-ZA clustered closer with sequences from ancestral *Poaceae* species, while most of its paralogs formed a cluster with *Tritium aestivum* proteins (3.3.3). This finding raised the hypothesis that CER-ZA might represent an ancestral protein in *H. vulgare*, while most of its paralogs are derived from gene duplications later during species development. However, the large number of putative FAR sequences in *H. vulgare* could be a result of adaptation to different habitats and changing evolutionary pressures, but detailed studies on the evolution of the reductase family are required.

4.2 *Cer-za* encodes an alcohol-forming acyl-CoA reductase

Sequence homology analysis strongly indicated a function of CER-ZA as alcohol-forming acyl-CoA reductase (3.3.2). Taking this into account, the protein coding sequence was expressed in *E. coli* and lipids extracted. The lipids were enriched in saturated C_{16} primary alcohols (0). These results were similar to the expression of a variety of *At*FARs by Doan *et al.* (2009), but in their study, unsaturated alcohols were additionally detected. On the other hand, expression of *Ta*FAR5 in *E. coli* also exclusively resulted in the production of saturated alcohols (Wang *et al.* 2015). Since these FAR proteins are in part involved in different pathways, the results indicate a broader substrate spectrum of FARs depending on their biosynthetic function (Domergue *et al.* 2010). In this experiment, the pool of usable acyl-CoAs was restricted to endogenous resources from *E. coli*. To expand the substrate spectrum, CER-ZA was additionally expressed in *S. cerevisiae* whose lipidome contains fatty acids up to chain lengths of C_{26}. The approach resulted in the strong accumulation of the C_{26} primary alcohol (hexacosanol, 3.8) while no shorter-chain alcohols with chain lengths between C_{18} and C_{24} were identified. Since the C_{26} primary alcohol represents the main lipid of waxes in *H. vulgare,* CER-ZA is presumably specific for very long-chain acyl-CoAs. Rowland *et al.* (2006) reported a similar result after expression of *At*FAR3 in yeast, but they noticed additionally a low accumulation of C_{24} alcohols. The complementation of *A. thaliana cer*4-1 with *At*FAR3 led to the accumulation of C_{24}-C_{30} primary alcohols, but not only of C_{26} primary alcohol (Rowland *et al.* 2006). Eight FARs from the close barley relative *Triticum aestivum* have been described. All enzymes have been associated with cuticular wax synthesis and reported to produce primary alcohols with different chain-length specificities. *Ta*FAR2 produced C_{18} primary alcohols while the heterologous expression of *Ta*FAR1 and *Ta*FAR5 in yeast caused the

accumulation of C_{22} primary alcohols (Wang *et al.* 2015; Wang *et al.* 2015). *Ta*FAR3, *Ta*FAR4, *Ta*FAR6, *Ta*FAR7 and *Ta*FAR8 were reported to produce C_{24}-C_{26} primary alcohols in yeast. However, transgenic expression of *Ta*FAR5 in *Solanum lycopersicum* did not lead to an accumulation of C_{22} but C_{26}-C_{30} primary alcohols (Wang *et al.* 2015). Similarly, Chai *et al.* (2018) reported the generation of even-chained primary alcohols up to C_{30} caused by the transgenic expression of *Ta*FAR6, *Ta*FAR7 and *Ta*FAR8 in *Oryza sativa* and *Solanum lycopersicum*. Wang *et al.* (2018) described three FARs from *Brachypodium distachyon* which showed high sequence similarities with FARs from *Tritium aestivium* but differed in the substrate specificies. Substrate specificities can presumably not be estimated from the protein sequence. Therefore, the factors determining substrate specificities are not restricted to the individual FAR but may also be based on the presence of species-specific factors. These interactions have not yet been clarified and require more research.

4.3 *Cer-za* is required for the reductive pathway of cuticular wax biosynthesis in *H. vulgare*

A function of CER-ZA in the biosynthesis pathway of cuticular waxes in *H. vulgare* was concluded. The expression of *Cer-za* is high in the epidermal cell layer where the cuticular wax synthesis is localized, supporting the role of CER-ZA in wax biosynthesis (3.5.1). Similarly, the wax-related gene *AtCER6* is exclusively expressed in epidermal tissues (Hooker, Millar, and Kunst 2002). The closely related *Ta*FAR5 enzyme was also expressed in reproductive organs such as anthers, pistils and seed coats which were not included in this study and could be looked at in the future (Wang *et al.* 2015). Most wax-related proteins are targeted to the ER as the site of the cuticular wax biosynthesis (Greer *et al.* 2007; Li *et al.* 2008; Kunst and Samuels 2009; Wang *et al.* 2015). In agreement with these findings, the localisation studies clearly showed that CER-ZA is localised to the ER. The prediction of the C-terminal transmembrane domain (3.3.2) suggests that this domain of CER-ZA could be integrated into the membrane of the ER with the N-terminal protein sequence orientated to the ER lumen. These transmembrane domains have not been predicted for Arabidopsis FARs, but Wang *et al.* (2015) reported a similar TM domain structure for *Ta*FAR5. It is possible that the presence of the TM domain is based on an independent evolutionary diversification after the split of the angiosperms. Experimental confirmation of such strong structural deviations however is still awaiting.

Plant surfaces are often covered with three-dimensional crystalline platelet-shaped wax crystals. Within the *Poaceae,* these structures are predominantly formed by primary alcohols which also strongly dominate the cuticular waxes of *H. vulgare* (Koch *et al.* 2006). Especially the primary alcohols are strongly affected in cuticular waxes of the *cer*-za alleles. Therefore, CER-ZA is most likely performing the initial step of the reductive pathway, reducing VLCFA-

CoA thioesters to primary alcohols, which are further used for wax ester synthesis by an - in *H. vulgare* unidentified - wax ester synthase. The expression of CER-ZA in the wax-deficient FAR mutant *A. thaliana cer*4-3 led to the duplication in the cuticular accumulation of primary alcohols in four independent lines (3.9). The amounts of alcohols that accumulated in *cer*4-3+CER-ZA were less striking compared to the complementation of *A. thaliana cer4-1* with *At*CER4/FAR3 performed by Rowland *et al.* (2006), but this could be based on the previously discussed strong structural differences between the monocot and dicot acyl-CoA reductases. The results support the function of CER-ZA as primary alcohol producing enzyme in the reductive pathway. Inhibition of this step could cause an accumulation of VLCFA which increases the substrate flow into the decarbonylating pathway and would provide an explanation for the observed accumulation of alkanes in *cer*-za.227 (3.2.1). Since the *cer*-za.227 mutant is still capable to synthesise primary alcohols and esters, it is likely that other - not yet described - FARs are actively taking part in this pathway in *H. vulgare*. A total of 21 *Hv*FAR paralogs were annotated. Some of those will may be involved in the deposition of suberin in roots and seeds as reported for *At*FAR1, *At*FAR4 and *At*FAR7 (Domergue *et al.* 2010). Root transcriptome data could already highlight possible candidates of barley FARs involved in the suberin biosynthesis. The two barley protein sequences HORVU2Hr1G086620 and HORVU4Hr1G074700 were found to cluster with *A. thaliana At*FAR2/MS2 and *O. sativa* DPW that were shown to be plastidial localized and share a function in the formation of anther cuticle and sporopollenin (Shi *et al.* 2011; Chen *et al.* 2011). Localisation studies of both genes could indicate similar functions of the two putative barley orthologs. A further observation was the concomitantly decrease of aldehydes in the *cer*-za.227 mutant. Until now, aldehyde-forming acyl-CoA reductases involved in this pathway were postulated to exist but not identified yet, rising the idea that there could be a mechanism that leads to the release of the intermediate aldehyde from the acyl-CoA reductase. The acyl-CoA reductase *At*FAR6 was found to be not involved in the cuticular wax biosynthesis but was observed to be able to produce both fatty alcohols and aldehydes in dependence of substrate chain-lengths and concentrations in *in vitro* assays (Doan *et al.* 2012). Thus, it would be possible that CER-ZA is involved both in the production of alcohols and aldehydes from acyl-CoAs. More studies are needed targeting this still open question that offers a new perspective on the biosynthesis pathway of cuticular waxes. Conclusively, it can be stated that the alcohol-forming acyl-CoA reductase CER-ZA is a key enzyme in the reductive pathway of cuticular waxes in *H. vulgare*. CER-ZA converts VLCFA-CoAs into primary alcohols and crucially contributes to the overall wax synthesis (Figure 48). Therefore, the CER-ZA protein should be designated as *Hv*FAR1.

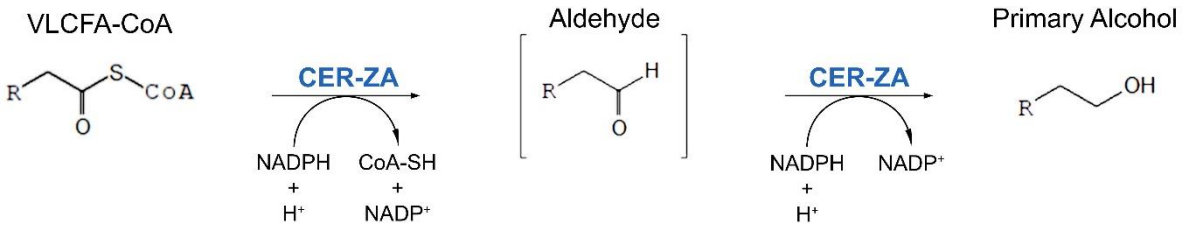

Figure 48: Reduction of very long-chain fatty acyl-CoAs to primary alcohols catalysed by CER-ZA. NADPH presumably serves as cofactor for the two-step reaction under formation of an intermediate aldehyde.

4.4 *Cer-ye* is allelic to *Cer-zh* which was annotated as *HvKCS1*

Since the *cer*-ye.267 line used in this study had been backcrossed several times (BC_8) to the cultivar Bowman, the locus of interest, originally derived from Foma, was introgressed into a uniform Bowman background. This circumstance allowed to apply a BSR-Seq strategy of plants derived from a cross of *cer*-ye.267 to Bowman, using only a small number of plants in each pool. Mapping and SNP calling resulted in the identification of mutational events in the coding sequence of *HORVU4Hr1G063420* (3.3.4) for most of the *cer*-ye alleles. The *HORVU4Hr1G063420* gene was annotated to encode a β-ketoacyl-CoA synthase. Premature stop codons cause the formation of truncated proteins in *cer*-ye.792 and *cer*-ye.1395. Both lines shared the very same SNP. It is possible that the two lines are derived from the same mutagenic event and the seeds were split during the seed bank establishment. The *HORVU4Hr1G063420* sequence is annotated as C-terminal 3-oxoacyl-carrier-protein (ACP) synthase III protein family domain (3.3.5). This sequence is one of two highly conserved domains which were described by Guo *et al.* (2016). The authors found that these domains are shared by a total of 475 examined β-ketoacyl-CoA synthases. Jasinski *et al.* (2012) demonstrated that already single amino acid exchanges can have tremendous effects on the catalytic binding pocket size and can prevent substrate binding. A similar effect of the amino acid exchange in the functional domain of *cer*-ye can be expected. Nuclear magnetic resonance (NMR) spectroscopy could be used in future experiments to confirm the structural changes in the overall conformation which were predicted by Phyre2 (3.3.2). The BSR-Seq approach did not point out a mutational event in the genome of *cer*-ye.592. Li *et al.* (2018) described similar results in course of a comparable BSR approach and traced it back to the restriction of the method to the transcriptome. Sequencing of the up- and downstream located regulatory regions would be required to identify the unknown mutational event; however, the results for the remaining *cer*-ye alleles indicated that the *cer*-ye mutations are localized in the gene *HORVU4Hr1G063420*. The *HORVU4Hr1G063420* protein family (*Hv*KCS1) commonly share an intron-less coding sequence. This characteristic was suggested to be derived from ancestral sequences (Guo *et al.* 2016). Database-driven algorithms predicted that CER-YE is

ER localised and membrane bound, in agreement with the presence of two predicted transmembrane domains, (3.3.5). Several authors reported that KCS from other plants are membrane bound, ER localized and expressed in the epidermis (3.5.2) (Shepherd and Griffiths 2006; Guo *et al.* 2016; Wang *et al.* 2017). The gene *HORVU4Hr1G063420* from barley was already described by Li *et al.* (2018) who identified it in a similar approach in another *H. vulgare eceriferum* line designated as *cer*-zh.54. According to the seed stock database, the two NILs were listed as independent and non-allelic lines (Druka *et al.* 2011). The results of this study instead indicated that the lines *cer*-ye and *cer*-zh are alleles. Consequently, the two lines *cer*-ye and *cer*-zh were expected to show similar phenotypes. The cuticular waxes in the *cer*-ye and *cer*-zh alleles revealed significant reductions over the full spectrum of aliphatic substance classes already occurring for C_{20} lipids (3.2.3, 3.2.4). Chain length dependent reductions across substance classes were reported for other KCS mutants. *At*KCS1 for instance was shown to produce VLCFA longer than C_{26}, and *At*KCS6 and its functional ortholog *Hv*FAR6 generate VLCFA with chain lengths from C_{24}-C_{26} (Hooker, Millar, and Kunst 2002; Weidenbach *et al.* 2014; Gan *et al.* 2017). Further, the decrease in C_{20} lipids, the shortest chain lipids evaluated in this study, indicated that the initial substrates of *Cer-ye* must be the freshly generated from C_{16} and C_{18} acyl-CoAs derived from the *de novo* synthesis in the chloroplasts. In agreement with this scenario, Li *et al.* (2018) came to a similar conclusion for *Cer-zh*. The two NILs *cer*-ye.267 and *cer*-zh.54 are affected in the same locus and share a similar biochemical phenotype. Finally, *cer*-ye.267 and *cer*-zh.54 were crossed, and the analysis of the F1 plants corroborated their allelic relationship (3.4). Further, since the cuticular wax biosynthesis is just partially affected in *cer*-ye.267 and *cer*-zh.54, there must be at least one other KCS in barley with partially overlapping substrate specificities. The existence of several FAE complexes with partially similar functions has been described (Joubès *et al.* 2008; Haslam and Kunst 2013). Novel methods like gene editing allow the rapid generation of new *cer* mutants with one or several simultaneously inhibited *Hv*KCS paralogous lines in reverse genetic strategies. Such mutants could strongly support the analysis of the specificities and interactions of KCS enzymes as well as their use in industrial production of VLC fatty acids.

4.5 Primary alcohols do not contribute to the barrier properties of the cuticle of *H. vulgare*

Biochemical data showed that the *H. vulgare cer*-za.227 and *cer*-ye.267 lines resemble each other with regard to the total cuticular wax load on their leaves, and in both lines epicuticular waxes were altered (3.2). But the affected aliphatic substances, contributing to the individual cuticular waxes, differed strongly. This allowed the direct consideration of effects on the cuticular barrier linked to the respective composition. The experiments were focused on properties favouring the reduction of uncontrolled water-loss (3.10.1) and the permeability of small, soluble molecules. To exclude that the variations were derived from differences in stomatal transpiration, the permeabilities were measured initially and shown to not differ between the Bowman, *cer*-za.227 and *cer*-ye.267 plants (Figure 46). The measured values corresponded to a stomatal conductance of 4 x 10^{-3} m/s which was determined for the growing third barley leaf by Richardson *et al.* (2007). The observed strong deviations between the adaxial and abaxial sides of the leaves in the permeabilities are suggested to be derived from differences in the stomatal density. Bi *et al.* (2017) confirmed an increased stomatal density on the adaxial side of the leaves of the close relative *T. aestivum*. The residual cuticular conductance was measured after closure of the stomata and was calculated as 4.9 x 10^{-4} m/s for *H. vulgare* leaves by Fricke *et al.* (2004). Data used in this study were calculated for the cuticular permeability, but after conversion, the calculated permeability was similar to the value found by Fricke *et al.* (2004). Minor differences between the Bowman and *cer*-za.227 and *cer*-ye.267 plants were statistically not significant. Therefore, these results do not allow to conclude that the decrease in the total wax in *cer*-za.227 and *cer*-ye.267 plants does not affect the barrier function in general. In contrast Li *et al.* (2018) reported a slight decrease in the water-holding barrier for the *cer*-ye allele *cer*-zh.54. However, under the applied conditions, the remaining waxes in the mutants are still sufficient to establish a functional barrier against water-loss. Several studies reported a correlation between wax load and grain yield for barley and wheat especially under drought conditions (Gonzalez and Ayerbe 2010; Monnevoux *et al.* 2004; Zhang *et al.* 2013). It must be considered that the application of stress or experiments at different ontological stages could result in deviating results. Interestingly, the monitoring of the diffusion of metribuzin, a soluble photosynthetic inhibitor, across the cuticle, showed a different result (2.9.3). Here, the barrier of *cer*-ye.267 was clearly less capable of restraining the movement of metribuzin through the cuticle, while the data for *cer*-za.227 were not different from Bowman. Given that the overall wax load was comparable for *cer*-za.227 and *cer*-ye.267, these differences can be explained by variations in the wax composition. Cuticular waxes of *cer*-ye.267 were found to be equally reduced in all compounds. Consequently, the enhanced permeability of metribuzin cannot be based on changes in the biochemical composition but rather on the reduction of the wax load itself. The ratio between the barrier-forming wax layer

and wax-unrelated polar paths of diffusion (e.g. trichomes) shifts towards the polar sites and consequently opens more pathways across the cuticle (Schreiber 2005, Fernández *et al.* 2017). Further, a reduced thickness of the cuticle shortens the distance that a molecule needs to travel across the wax layer and could allow more metribuzin do penetrate through the barrier within the same timeframe compared to Bowman. In contrast *cer*-za.227 line is especially reduced in primary alcohols and esters, while the amounts of alkanes were increased. Some authors reported striking increases in alkanes under drought and suggested, that alkanes might provide enhanced barrier properties (Panikashvili *et al.* 2007; Bi *et al.* 2017). The incorporation of alkanes and the lack of alcohols might render the cuticular wax layer in *cer*-za.227 more non-polar. As a consequence, the permeability for polar substances like metribuzin might be affected in agreement with previous studies (Fernández *et al.* 2017). On the other side, the results indicate that especially primary alcohols, which form the dominating group in the cuticle, do not primarily contribute to the permeability barrier. Accordingly, biochemical data generated in this study (3.2.1, 3.2.3) highlighted the contribution of primary alcohols especially to the crystalline epicuticular wax structures. However, the epicuticular wax crystals were suggested not to be the fraction important for establishing the permeability barrier (Zeisler-Diehl, Müller, and Schreiber 2018). The precise function of the primary alcohols cannot be clarified at this point. Because of importance of primary alcohols for wax crystal formation, it is assumed, that the UV reflecting properties of the dense epicuticular wax crystals provide UV-B protection (Long *et al.* 2003). Further studies will be necessary to provide experimental evidence for this hypothesis. Besides, it was shown that the water-repellence properties were strongly affected by the two mutations *cer*-za.227 and *cer*-ye.267 (3.1). The Lotus effect observed for the reference cultivar Bowman provides self-cleaning benefits which also correlate with protection against certain pathogens (Barthlott and Neinhuis 1997; Zeisler-Diehl, Barthlott, and Schreiber 2020). On the other hand, compounds like C_{26} aldehydes and C_{26} alcohols were shown to trigger the germination of powdery mildew (Zabka *et al.* 2008; Hansjakob *et al.* 2010; Hansjakob, Riederer, and Hildebrandt 2011); consequently, the *cer*-za.227 and *cer*-ye.267 lines could be less susceptible to this pathogen. It was suggested that *Blumeria* did specify on C_{26} aldehydes and C_{26} alcohols after diversification of the angiosperm progenitors into monocots and dicots (Chaw *et al.* 2004; Weidenbach *et al.* 2014). However, whether the mutations provide benefits or disadvantages during plant pathogen interactions, would need to be tested in specific experiments.

5 Summary

Changing environmental conditions demand the expansion of the genetic resources to enable the rapid adaption and development of novel crop species. The cuticle as direct interface between plants and their environment is thereby of a special interest. This study aimed to contribute to the knowledge about the genetic background of the cuticular wax biosynthesis in barley (*Hordeum vulgare)* with the characterisation of the two wax-deficient *eceriferum* mutants *cer*-za.227 and *cer*-ye.267. Both lines showed reduced water-repellence properties due to the reduction of epicuticular wax crystals on the leaf surfaces. Biochemical analysis showed strong reductions of the cuticular wax load on leaves of both *eceriferum* lines. The *cer*-za.227 mutant was particularly affected in primary alcohols and esters while in *cer*-ye.267, the amounts of all cuticular wax substances were reduced. A bulked segregant RNA-sequencing approach led to the identification of the two genes *HORVU5Hr1G089230* and *HORVU4Hr1G063420* which carry mutations in the lines *cer*-za.227 and *cer*-ye.267, respectively. Consideration of additional allelic *cer*-za and *cer*-ye lines revealed that these allelic mutants carry mutations in the same two genes. The gene product of *HORVU5Hr1G089230*, CER-ZA, was confirmed to harbour fatty acyl-CoA reductase (FAR) activity. Its heterologous expression in *E. coli*, yeast and the wax-deficient *A. thaliana cer*4-3 mutant resulted in the accumulation of primary alcohols. CER-ZA is the first protein of the FAR family that has been characterised in *H. vulgare*. Accordingly, CER-ZA was named *Hv*FAR1. The CER-ZA enzyme catalyses the reduction of very long chain acyl-CoAs to primary alcohols and contributes crucially to the biosynthesis of cuticular waxes in *H. vulgare*. The protein was localised to the ER. The *cer*-ye.267 mutant carries a mutation in the gene *HORVU4Hr1G063420*. This gene codes for a protein with sequence similarity to for a β-ketoacyl-CoA synthase (KCS). KCS enzymes generate very long chain fatty acids as precursors for the synthesis of different wax lipids. The same gene has previously been described as *Cer-zh*. Within this study, it was confirmed that *cer*-ye.267 and *cer*-zh.54 are allelic mutants. The protein affected in *cer*-ye.267 and *cer*-zh.54 was named *Hv*KCS1 and it catalyses the elongation of C_{16} and C_{18} acyl-CoAs to very long-chain fatty acids as part of a fatty acid elongation complex. Comparisons of the barrier properties of *cer*-za.227 and *cer*-ye.267 with Bowman indicated that the dominant compounds in barley, i.e. primary alcohols, do not contribute to the formation of a functional water-loss and penetration barrier, but that this barrier function rather depends on the ratio of polar and non-polar compounds.

6 List of references

Aarts, M. G. M., R. Hodge, K. Kalantidis, D. Florack, Z. A. Wilson, B. J. Mulligan, W. J. Stiekema, R. Scott, and A. Pereira. 1997. 'The Arabidopsis MALE STERILITY 2 Protein Shares Similarity with Reductases in Elongation/Condensation Complexes'. *The Plant Journal* 12 (3): 615–23. https://doi.org/10.1046/j.1365-313X.1997.00615.x.

Adamson, A. W., and A. P. Gast. 1990. 'Contact Angle'. In *Physical Chemistry of Surfaces*: 385–88. John Wiley & Sons, Inc., New York.

Armenteros, A. J. J., M. Salvatore, O. Emanuelsson, O. Winther, G. von Heijne, A. Elofsson, and H. Nielsen. 2019. 'Detecting Sequence Signals in Targeting Peptides Using Deep Learning'. *Life Science Alliance* 2 (5): e201900429. https://doi.org/10.26508/lsa.201900429.

Armenteros, A. J. J., C. K. Sønderby, S. K. Sønderby, H. Nielsen, and O. Winther. 2017. 'DeepLoc: Prediction of Protein Subcellular Localization Using Deep Learning'. *Bioinformatics* 33 (21): 3387-3395. https://doi.org/10.1093/bioinformatics/btx548.

Armenteros A. J. J., K. D. Tsirigos, C. K. Sønderby, T. N. Petersen, O. Winther, S. Brunak, G. von Heijne, and H. Nielsen. 2019. 'SignalP 5.0 Improves Signal Peptide Predictions Using Deep Neural Networks'. *Nature Biotechnology* 37: 420–423. https://doi.org/10.1038/s41587-019-0036-z.

Baldotto, L. E. B., and F. L. Olivares. 2008. 'Phylloepiphytic Interaction between Bacteria and Different Plant Species in a Tropical Agricultural System'. *Canadian Journal of Microbiology* 54 (11): 918–31. https://doi.org/10.1139/W08-087.

Barnes, P. W., S. D. Flint, and M. M. Caldwell. 1987. 'Photosynthesis Damage and Protective Pigments in Plants from a Latitudinal Arctic/Alpine Gradient Exposed to Supplemental UV-B Radiation in the Field'. *Arctic and Alpine Research* 19 (1): 21–27. https://doi.org/10.1080/00040851.1987.12002573.

Barthlott, W., and C. Neinhuis. 1997. 'Purity of the Sacred Lotus, or Escape from Contamination in Biological Surfaces'. *Planta* 202 (1): 1–8. https://doi.org/10.1007/s004250050096.

Barthlott, W., C. Neinhuis, D. Cutler, F. Ditsch, I. Meusel, I. Theisen, and H. Wilhemli. 1998. 'Classification and Terminology of Plant Epicuticular Waxes'. *Botanical Journal of the Linnean Society* 126 (3): 237–60. https://doi.org/10.1111/j.1095-8339.1998.tb02529.x.

Barthlott, W., T. Schimmel, S. Wiersch, K. Koch, M. Brede, M. Barczewski, S. Walheim, A. Weis, A. Kaltenmeier, A. Leder, and H. F. Bohn. 2010. 'The Salvinia Paradox: Superhydrophobic Surfaces with Hydrophilic Pins for Air Retention Under Water'. *Advanced Materials* 22 (21): 2325–28. https://doi.org/10.1002/adma.200904411.

Barua, U. M., K. J. Chalmers, C. A. Hackett, W. T. B. Thomas, W. Powell, and R. Waugh. 1993. 'Identification of RAPD Markers Linked to a Rhynchosporium Secalis Resistance Locus in Barley Using Near-Isogenic Lines and Bulked Segregant Analysis'. *Heredity* 71 (2): 177–84. https://doi.org/10.1038/hdy.1993.122.

Batt, R. F., and J. T. Martin. 1960. 'The Cuticles of Apple Fruits.' In *The Annual Report of the Agricultural and Horticultural Research Station*: 106-111. The National Fruit and Cider Institute Long Ashton, Bristol. https://doi.org/10.1007/978-1-4020-4443-4_13.

Bernard, A., F. Domergue, S. Pascal, R. Jetter, C. Renne, J.-D. Faure, R. P. Haslam, J. A. Napier, R. Lessire, and J. Joubès. 2012. 'Reconstitution of Plant Alkane Biosynthesis in Yeast Demonstrates That Arabidopsis ECERIFERUM1 and ECERIFERUM3 are Core Components of a Very-Long-Chain Alkane Synthesis Complex'. *The Plant Cell* 24 (7): 3106–18. https://doi.org/10.1105/tpc.112.099796.

Bernard, A., and J. Joubès. 2013. 'Arabidopsis Cuticular Waxes: Advances in Synthesis, Export and Regulation'. *Progress in Lipid Research* 52 (1): 110–29. https://doi.org/10.1016/j.plipres.2012.10.002.

Bhardwaj, V., P. Sharma, and S. Chauhan. 2013. 'Thermo-Acoustic Investigation in Alcohol–Water Mixtures: Impact of Lipophilic Antioxidant on Anionic Surfactant Properties for Potential Cosmeceutical Application'. *Thermochimica Acta* 566: 155–61. https://doi.org/10.1016/j.tca.2013.05.037.

Bhushan, B., and Y. C. Jung. 2007. 'Wetting Study of Patterned Surfaces for Superhydrophobicity'. *Ultramicroscopy* 107 (10-11): 1033–41. https://doi.org/10.1016/j.ultramic.2007.05.002.

Bhushan, B., and Y. C. Jung. 2008. 'Wetting, Adhesion and Friction of Superhydrophobic and Hydrophilic Leaves and Fabricated Micro/Nanopatterned Surfaces'. *Journal of Physics: Condensed Matter* 20 (22). https://doi.org/10.1088/0953-8984/20/22/225010.

Bi, H., N. Kovalchuk, P. Langridge, P. J. Tricker, S. Lopato, and N. Borisjuk. 2017. 'The Impact of Drought on Wheat Leaf Cuticle Properties'. *BMC Plant Biology* 17 (1): 1-13. https://doi.org/10.1186/s12870-017-1033-3.

Bird, D., F. Beisson, A. Brigham, J. Shin, S. Greer, R. Jetter, L. Kunst, X. Wu, A. Yephremov, and L. Samuels. 2007. 'Characterization of Arabidopsis ABCG11/WBC11, an ATP Binding Cassette (ABC) Transporter That Is Required for Cuticular Lipid Secretion'. *The Plant Journal* 52 (3): 485–98. https://doi.org/10.1111/j.1365-313X.2007.03252.x.

Blokker, P., P. Boelen, R. Broekman, and J. Rozema. 2006. 'The Occurrence of p-Coumaric Acid and Ferulic Acid in Fossil Plant Materials and Their Use as UV-Proxy'. In *Plants and Climate Change*, edited by J. Rozema, R. Aerts, and H. Cornelissen, (41): 197–208. Tasks for Vegetation Science. Springer, Dordrecht. https://doi.org/10.1007/978-1-4020-4443-4_13.

Bonaventure, G., J. J. Salas, M. R. Pollard, and J. B. Ohlrogge. 2003. 'Disruption of the FATB Gene in Arabidopsis Demonstrates an Essential Role of Saturated Fatty Acids in Plant Growth'. *The Plant Cell* 15 (4): 1020–33. https://doi.org/10.1105/tpc.008946.

Brownsey, R. W., A. N. Boone, J. E. Elliott, J. E. Kulpa, and W. M. Lee. 2006. 'Regulation of Acetyl-CoA Carboxylase'. *Biochemical Society Transactions* 34 (2): 223–27. https://doi.org/10.1042/BST0340223.

Bunster, L., N. J. Fokkema, and B. Schippers. 1989. 'Effect of Surface-Active Pseudomonas spp. on Leaf Wettability'. *Applied and Environmental Microbiology* 55 (6): 1340–45. https://doi.org/10.1128/aem.55.6.1340-1345.1989.

Burch, A. Y., V. Zeisler, K. Yokota, L. Schreiber, and S. E. Lindow. 2014. 'The Hygroscopic Biosurfactant Syringafactin Produced by *Pseudomonas syringae* Enhances Fitness on Leaf Surfaces during Fluctuating Humidity'. *Environmental Microbiology* 16 (7): 2086–98. https://doi.org/10.1111/1462-2920.12437.

Burke, E. J., S. J. Brown, and N. Christidis. 2006. 'Modeling the Recent Evolution of Global Drought and Projections for the Twenty-First Century with the Hadley Centre Climate Model'. *Journal of Hydrometeorology* 7 (5): 1113–25. https://doi.org/10.1175/JHM544.1.

Cai, S., G. Chen, Y. Wang, Y. Huang, D. B. Marchant, Y. Wang, Q. Yang, F. Dai, A. Hills, P. J. Franks, E. Nevo, D. E. Soltis, P. S. Soltis, E. Sessa, P. G. Wolf, D. Xue, G. Zhang, B. J. Pogson, M. R. Blatt, and Z.-H. Chen. 2017. 'Evolutionary Conservation of ABA Signaling for Stomatal Closure'. *Plant Physiology* 174 (2): 732–47. https://doi.org/10.1104/pp.16.01848.

Chai, G., C. Li, F. Xu, Y. Li, X. Shi, Y. Wang, and Z. Wang. 2018. 'Three Endoplasmic Reticulum-Associated Fatty Acyl-Coenzyme A Reductases were Involved in the Production of Primary Alcohols in Hexaploid Wheat (*Triticum aestivum* L.)'. *BMC Plant Biology* 18 **(**41). https://doi.org/10.1186/s12870-018-1256-y

Chaw, S.-M., C.-C. Chang, H.-L. Chen, and W.-H. Li. 2004. 'Dating the Monocot–Dicot Divergence and the Origin of Core Eudicots Using Whole Chloroplast Genomes'. *Journal of Molecular Evolution* 58 (4): 424–41. https://doi.org/10.1007/s00239-003-2564-9.

Chen, W., X.-H. Yu, K. Zhang, J. Shi, S. De Oliveira, L. Schreiber, J. Shanklin, and D. Zhang. 2011. 'Male Sterile2 Encodes a Plastid-Localized Fatty Acyl Carrier Protein Reductase Required for Pollen Exine Development in Arabidopsis'. *Plant Physiology* 157 (2): 842–53. https://doi.org/10.1104/pp.111.181693.

Chen, Z.-H., G. Chen, F. Dai, Y. Wang, A. Hills, Y.-L. Ruan, G. Zhang, P- J. Franks, E. Nevo, and M.-R. Blatt. 2017. 'Molecular Evolution of Grass Stomata'. *Trends in Plant Science* 22 (2): 124–39. https://doi.org/10.1016/j.tplants.2016.09.005.

Chloupek, O., V. Dostál, T. Středa, V. Psota, and O. Dvořáčková. 2010. 'Drought Tolerance of Barley Varieties in Relation to Their Root System Size'. *Plant Breeding* 129 (6): 630–36. https://doi.org/10.1111/j.1439-0523.2010.01801.x.

Cupp, D., J. P. Kampf, and A. M. Kleinfeld. 2004. 'Fatty Acid−Albumin Complexes and the Determination of the Transport of Long Chain Free Fatty Acids across Membranes'. *Biochemistry* 43 (15): 4473–81. https://doi.org/10.1021/bi036335l.

Day, T. A., G. Martin, and T. C. Vogelmann. 1993. 'Penetration of UV-B Radiation in Foliage: Evidence That the Epidermis Behaves as a Non-Uniform Filter'. *Plant, Cell & Environment* 16 (6): 735–41. https://doi.org/10.1111/j.1365-3040.1993.tb00493.x.

Doan, T. T. P., A. S. Carlsson, M. Hamberg, L. Bülow, S. Stymne, and P. Olsson. 2009. 'Functional Expression of Five Arabidopsis Fatty Acyl-CoA Reductase Genes in *Escherichia coli*'. *Journal of Plant Physiology* 166 (8): 787–96. https://doi.org/10.1016/j.jplph.2008.10.003.

Doan, T. T. P., F. Domergue, A. E. Fournier, S. J. Vishwanath, O. Rowland, P. Moreau, C. C. Wood, A. S. Carlsson, M. Hamberg, and P. Hofvander. 2012. 'Biochemical Characterization of a Chloroplast Localized Fatty Acid Reductase from *Arabidopsis thaliana*'. *Biochimica et Biophysica Acta (BBA) - Molecular and Cell Biology of Lipids* 1821 (9): 1244–55. https://doi.org/10.1016/j.bbalip.2011.10.019.

Domergue, F., S. J. Vishwanath, J. Joubès, J. Ono, J. A. Lee, M. Bourdon, R. Alhattab, C. Lowe, S. Pascal, R. Lessire, and O. Rowland. 2010. 'Three Arabidopsis Fatty Acyl-Coenzyme A

Reductases, FAR1, FAR4, and FAR5, Generate Primary Fatty Alcohols Associated with Suberin Deposition'. *Plant Physiology* 153 (4): 1539–54. https://doi.org/10.1104/pp.110.158238.

Dong, W., D. Wu, G. Li, D. Wu, and Z. Wang. 2018. 'Next-Generation Sequencing from Bulked Segregant Analysis Identifies a Dwarfism Gene in Watermelon'. *Scientific Reports* 8 (1): 2908. https://doi.org/10.1038/s41598-018-21293-1.

Druka, A., J. Franckowiak, U. Lundqvist, N. Bonar, J. Alexander, K. Houston, S. Radovic, F. Shahinnia, V. Vendramin, M. Morgante, N. Stein, and R. Wough. 2011. 'Genetic Dissection of Barley Morphology and Development'. *Plant Physiology* 155 (2): 617–27. https://doi.org/10.1104/pp.110.166249.

Edwards, D., G. D. Abbott, and J. A. Raven. 1996. 'Cuticles of Early Land Plants: A Palaeoecophysiological Evaluation'. In *Plant Cuticles: An Integrated Functional Approach*, edited by G. Kerstiens: 1-31. BIOS Scientific Publishers Ltd., Oxford.

Extrand, C. W.. 2005. 'Modeling of Ultralyophobicity: Suspension of Liquid Drops by a Single Asperity'. *Langmuir* 21 (23): 10370–74. https://doi.org/10.1021/la0513050.

Febrero, A., S. Fernández, J. L. Molina-Cano, and J. L. Araus. 1998. 'Yield, Carbon Isotope Discrimination, Canopy Reflectance and Cuticular Conductance of Barley Isolines of Differing Glaucousness'. *Journal of Experimental Botany* 49 (326): 1575–81. https://doi.org/10.1093/jxb/49.326.1575.

Fernández, V., H. A. Bahamonde, J. J. Peguero-Pina, E. Gil-Pelegrín, D. Sancho-Knapik, L. Gil, H. E. Goldbach, and T. Eichert. 2017. 'Physico-Chemical Properties of Plant Cuticles and Their Functional and Ecological Significance'. *Journal of Experimental Botany* 68 (19): 5293–5306. https://doi.org/10.1093/jxb/erx302.

Fernández, V., P. Guzmán-Delgado, J. Graça, S. Santos, and L. Gil. 2016. 'Cuticle Structure in Relation to Chemical Composition: Re-Assessing the Prevailing Model'. *Frontiers in Plant Science* 7: 427. https://doi.org/10.3389/fpls.2016.00427.

Forbes, P.. 2008. 'Self-Cleaning Materials'. *Scientific American* 299 (2): 88–95. http://www.jstor.org/stable/26000766.

Fukuda, S., A. Satoh, H. Kasahara, H. Matsuyama, and Y. Takeuchi. 2008. 'Effects of Ultraviolet-B Irradiation on the Cuticular Wax of Cucumber (*Cucumis sativus*) Cotyledons'. *Journal of Plant Research* 121 (2): 179–89. https://doi.org/10.1007/s10265-007-0143-7.

Gan, L., S. Zhu, Z. Zhao, L. Liu, X. Wang, Z. Zhang, X. Zhang, J. Wang, J. Wang, X. Guo, J. Wan. 2017. 'Wax Crystal-Sparse Leaf 4, Encoding a β-Ketoacyl-Coenzyme A Synthase 6, Is Involved in Rice Cuticular Wax Accumulation'. *Plant Cell Reports* 36 (10): 1655–66. https://doi.org/10.1007/s00299-017-2181-5.

Geertz-Hansen H. M., N. Blom, A. M. Feist, S. Brunak, and T. N. Petersen. 2014. 'Cofactory: Sequence-Based Prediction of Cofactor Specificity of Rossmann Folds'. *Proteins* 82 (9):1819-28. https://doi.org/10.1002/prot.24536.

Genty, B., J.-M. Briantais, and N. R. Baker. 1989. 'The Relationship between the Quantum Yield of Photosynthetic Electron Transport and Quenching of Chlorophyll Fluorescence'. *Biochimica et Biophysica Acta (BBA) - General Subjects* 990 (1): 87–92. https://doi.org/10.1016/S0304-4165(89)80016-9.

Genzer, J., and A. Marmur. 2008. 'Biological and Synthetic Self-Cleaning Surfaces'. *MRS Bulletin* 33 (8): 742–46. https://doi.org/10.1557/mrs2008.159.

Gietz, R. D., and R. H. Schiestl. 2007. 'High-Efficiency Yeast Transformation Using the LiAc/SS Carrier DNA/PEG Method'. *Nature Protocols* 2 (1): 31–34. https://doi.org/10.1038/nprot.2007.13.

Godfray, H. C. J., J. R. Beddington, I. R. Crute, L. Haddad, D. Lawrence, J. F. Muir, J. Pretty, S. Robinson, S. M. Thomas, and C. Toulmin. 2010. 'Food Security: The Challenge of Feeding 9 Billion People'. *Science* 327 (5967): 812–18. https://doi.org/10.1126/science.1185383.

Gorb, E., K. Haas, A. Henrich, S. Enders, N. Barbakadze, and S. Gorb. 2005. 'Composite Structure of the Crystalline Epicuticular Wax Layer of the Slippery Zone in the Pitchers of the Carnivorous Plant Nepenthes Alata and Its Effect on Insect Attachment'. *Journal of Experimental Biology* 208 (24): 4651–62. https://doi.org/10.1242/jeb.01939.

Graham, L. E.. 1993. *Origin of Land Plants.* John Wiley & Sons, Inc., New York.

Greenberg, B. M., V. Gaba, A. K. Mattoo, and M. Edelman. 1989. 'Degradation of the 32 kDa Photosystem II Reaction Center Protein in UV, Visible and Far Red Light Occurs Through a Common 23.5 kDa Intermediate'. *Zeitschrift für Naturforschung C* 44 (5–6): 450–52. https://doi.org/10.1515/znc-1989-5-618.

Greer, S., M. Wen, D. Bird, X. Wu, L. Samuels, L. Kunst, and R. Jetter. 2007. 'The Cytochrome P450 Enzyme CYP96A15 is the Midchain Alkane Hydroxylase Responsible for Formation of Secondary Alcohols and Ketones in Stem Cuticular Wax of Arabidopsis'. *Plant Physiology* 145 (3): 653–67. https://doi.org/10.1104/pp.107.107300.

Gubatz, S., V. J. Dercksen, C. Brüß, W. Wenschke, and U. Wobus. 2007. 'Analysis of Barley (*Hordeum vulgare*) Grain Development Using Three-Dimensional Digital Models'. *The Plant Journal* 52 (4): 779-790. https://doi.org/10.1111/j.1365-313X.2007.03260.x.

Guo, H.-S., Y.-M. Zhang, X.-Q. Sun, M.-M. Li, Y.-Y. Hang, and J.-Y. Xue. 2016. 'Evolution of the KCS Gene Family in Plants: The History of Gene Duplication, Sub/Neofunctionalization and Redundancy'. *Molecular Genetics and Genomics* 291 (2): 739–52. https://doi.org/10.1007/s00438-015-1142-3.

Hansjakob, A., S. Bischof, G. Bringmann, M. Riederer, and U. Hildebrandt. 2010. 'Very-Long-Chain Aldehydes Promote in vitro Prepenetration Processes of *Blumeria graminis* in a Dose- and Chain Length-Dependent Manner'. *New Phytologist* 188 (4): 1039–54. https://doi.org/10.1111/j.1469-8137.2010.03419.x.

Hansjakob, A., M. Riederer, and U. Hildebrandt. 2011. 'Wax Matters: Absence of Very-Long-Chain Aldehydes from the Leaf Cuticular Wax of the Glossy11 Mutant of Maize Compromises the Prepenetration Processes of Blumeria Graminis'. *Plant Pathology* 60 (6): 1151–61. https://doi.org/10.1111/j.1365-3059.2011.02467.x.

Harwood, J. L.. 2005. 'Fatty Acid Biosynthesis'. In *Plant Lipids*, edited by D. J. Murphy: 27-66. Blackwell Publishing, Oxford.

Harwood, W. A.. 2019. 'An Introduction to Barley: The Crop and the Model'. In *Barley: Methods and Protocols* 1900. Springer Protocols, New York.

Haslam, T. M., A. Mañas-Fernández, L. Zhao, and L. Kunst. 2012. 'Arabidopsis ECERIFERUM2 Is a Component of the Fatty Acid Elongation Machinery Required for Fatty Acid Extension to Exceptional Lengths'. *Plant Physiology* 160 (3): 1164–74. https://doi.org/10.1104/pp.112.201640.

Haslam, T. M., and L. Kunst. 2013. 'Extending the Story of Very-Long-Chain Fatty Acid Elongation'. *Plant Science* 210 (September): 93–107. https://doi.org/10.1016/j.plantsci.2013.05.008.

Haslam, T. M., and L. Kunst. 2020. 'Arabidopsis ECERIFERUM2-LIKEs Are Mediators of Condensing Enzyme Function'. *Plant and Cell Physiology* 61 (12): 2126–38. https://doi.org/10.1093/pcp/pcaa133.

Hegebarth, D., and R. Jetter. 2017. 'Cuticular Waxes of *Arabidopsis thaliana* Shoots: Cell-Type-Specific Composition and Biosynthesis'. *Plants* 6 (3): 27. https://doi.org/10.3390/plants6030027.

Hirano, S. S., and C. D. Upper. 2000. 'Bacteria in the Leaf Ecosystem with Emphasis On *Pseudomonas syringae* - a Pathogen, Ice Nucleus, and Epiphyte'. *Microbiology and Molecular Biology Reviews* 64 (3): 624–53. https://doi.org/10.1128/MMBR.64.3.624-653.2000.

Holloway, P. J.. 1969. 'The Effects of Superficial Wax on Leaf Wettability'. *Annals of Applied Biology* 63 (1): 145–53. https://doi.org/10.1111/j.1744-7348.1969.tb05475.x.

Holloway, P. J.. 1971. 'Chemical and Physical Characteristics of Leaf Surfaces'. In *Ecology of Leaf Surface Micro Organisms*, edited by T. F. Preece and C. H. Dickinson: 39-53. Academic press, London.

Hooker, T. S., A. A. Millar, and L. Kunst. 2002. 'Significance of the Expression of the CER6 Condensing Enzyme for Cuticular Wax Production in Arabidopsis'. *Plant Physiology* 129 (4): 1568–80. https://doi.org/10.1104/pp.003707.

Israelachvili, J. N.. 1992. 'Adhesion Forces between Surfaces in Liquids and Condensable Vapours'. *Surface Science Reports* 14 (3): 109–59. https://doi.org/10.1016/0167-5729(92)90015-4.

Jacobs, J. F., G. J. M. Koper, and W. N. J. Ursem. 2007. 'UV Protective Coatings: A Botanical Approach'. *Progress in Organic Coatings*, Coatings Science International 2006, 58 (2): 166–71. https://doi.org/10.1016/j.porgcoat.2006.08.023.

Jasinski, S., A. Lécureuil, M. Miquel, O. Loudet, S. Raffaele, M. Froissard, and P. Guerche. 2012. 'Natural Variation in Seed Very Long Chain Fatty Acid Content is Controlled by a New Isoform of KCS18 in *Arabidopsis thaliana*'. *PLOS ONE* 7 (11): e49261. https://doi.org/10.1371/journal.pone.0049261.

Jeffree, C. E.. 1986. 'The Cuticle, Epicuticular Waxes and Trichomes of Plants, with Reference to Their Structure, Functions and Evolution'. In *Insects on the Plant Surface*, edited by B. E. Juniper and T. R. E. Southwood: 23–64. Edward Arnold Publishers Ltd., London.

Jeffree, C. E., E. A. Baker, and P. J. Holloway. 1975. 'Ultrastructure and Recrystallization of Plant Epicuticular Waxes'. *New Phytologist* 75 (3): 539–49. https://doi.org/10.1111/j.1469-8137.1975.tb01417.x.

Jenks, M. A., S. D. Eigenbrode, and B. Lemieux. 2002. 'Cuticular Waxes of Arabidopsis'. *The Arabidopsis Book* 1: e0016. https://dx.doi.org/10.1199%2Ftab.0016.

Jetter, R., and M. Riederer. 1994. 'Epicuticular Crystals of Nonacosan-10-ol: In-Vitro Reconstitution and Factors Influencing Crystal Habits'. *Planta* 195 (2): 257–70. https://doi.org/10.1007/BF00199686.

Jetter, R., and S. Schäffer. 2001. 'Chemical Composition of the *Prunus laurocerasus* Leaf Surface. Dynamic Changes of the Epicuticular Wax Film during Leaf Development'. *Plant Physiology* 126 (4): 1725–37. https://doi.org/10.1104/pp.126.4.1725.

Jetter, R., and L. Kunst. 2008. 'Plant Surface Lipid Biosynthetic Pathways and Their Utility for Metabolic Engineering of Waxes and Hydrocarbon Biofuels'. *The Plant Journal* 54 (4): 670–83. https://doi.org/10.1111/j.1365-313X.2008.03467.x.

Jetter, R., and M. Riederer. 2016. 'Localization of the Transpiration Barrier in the Epi- and Intracuticular Waxes of Eight Plant Species: Water Transport Resistances Are Associated with Fatty Acyl Rather Than Alicyclic Components'. *Plant Physiology* 170 (2): 921–34. https://doi.org/10.1104/pp.15.01699.

Jordan, B. R., J. He, W. S. Chow, and J. M. Anderson. 1992. 'Changes in mRNA Levels and Polypeptide Subunits of Ribulose 1,5-Bisphosphate Carboxylase in Response to Supplementary Ultraviolet-B Radiation'. *Plant, Cell & Environment* 15 (1): 91–98. https://doi.org/10.1111/j.1365-3040.1992.tb01461.x.

Jordan, W. R., P. J. Shouse, A. Blum, F. R. Miller, and R. L. Monk. 1984. 'Environmental Physiology of Sorghum. II. Epicuticular Wax Load and Cuticular Transpiration'. *Crop Science* 24 (6): 1168-1173. https://doi.org/10.2135/cropsci1984.0011183X002400060038x.

Joubès, J., and F. Domergue. 2020. 'Biosynthesis of the Plant Cuticle'. In *Hydrocarbons, Oils and Lipids: Diversity, Origin, Chemistry and Fate*, edited by H. Wilkes: 139-157. Springer International Publishing, Basel. https://doi.org/10.1007/978-3-319-54529-5_ 8-1.

Joubès, J., S. Raffaele, B. Bourdenx, C. Garcia, J. Laroche-Traineau, P. Moreau, F. Domergue, and R. Lessire. 2008. 'The VLCFA Elongase Gene Family in *Arabidopsis thaliana*: Phylogenetic Analysis, 3D Modelling and Expression Profiling'. *Plant Molecular Biology* 67 (5): 547–66. https://doi.org/10.1007/s11103-008-9339-z.

Kelley, L. A., S. Mezulis, C. M. Yates, M. N. Wass, and M. J. E. Sternberg. 2015. 'The Phyre2 Web Portal for Protein Modelling, Prediction and Analysis'. *Nat. Protocols* 10: 845–858. https://doi.org/10.1038/nprot.2015.053.

Kenrick, P., and P. R. Crane. 1997. 'The Origin and Early Evolution of Plants on Land'. *Nature* 389 (6646): 33–39. https://doi.org/10.1038/37918.

Kim, H., S. B. Lee, H. J. Kim, M. K. Min, I. Hwang, and M. C. Suh. 2012. 'Characterization of Glycosylphosphatidylinositol-Anchored Lipid Transfer Protein 2 (LTPG2) and Overlapping Function between LTPG/LTPG1 and LTPG2 in Cuticular Wax Export or Accumulation in *Arabidopsis thaliana'*. *Plant and Cell Physiology* 53 (8): 1391–1403. https://doi.org/10.1093/pcp/pcs083.

Kinkel, L. L.. 1997. 'Microbial Population Dynamics on Leaves'. *Annual Review of Phytopathology* 35 (1): 327–47. https://doi.org/10.1146/annurev.phyto.35.1.327.

Knoll, D., and L. Schreiber. 1998. 'Influence of Epiphytic Micro-Organisms on Leaf Wettability: Wetting of the Upper Leaf Surface of Juglans Regia and of Model Surfaces in Relation to Colonization by Micro-Organisms'. *The New Phytologist* 140 (2): 271–82. https://doi.org/10.1046/j.1469-8137.1998.00269.x.

Knowles, J. R.. 1989. 'The Mechanism of Biotin-Dependent Enzymes'. *Annual Review of Biochemistry* 58 (1): 195–221. https://doi.org/10.1146/annurev.bi.58.070189.001211.

Koch, K., W. Barthlott, S. Koch, A. Hommes, K. Wandelt, W. Mamdouh, S. De-Feyter, and P. Broekmann. 2006. 'Structural Analysis of Wheat Wax (*Triticum aestivum*, c.v. "Naturastar" L.): From the Molecular Level to Three Dimensional Crystals'. *Planta* 223 (2): 258–70. https://doi.org/10.1007/s00425-005-0081-3.

Koch, K., and W. Barthlott. 2009. 'Superhydrophobic and Superhydrophilic Plant Surfaces: An Inspiration for Biomimetic Materials'. *Philosophical Transactions of the Royal Society A: Mathematical, Physical and Engineering Sciences* 367 (1893): 1487–1509. https://doi.org/10.1098/rsta.2009.0022.

Koch, K., B. Bhushan, and W. Barthlott. 2008. 'Diversity of Structure, Morphology and Wetting of Plant Surfaces'. *Soft Matter* 4 (10): 1943–63. https://doi.org/10.1039/B804854A.

Koch, K., B. Bhushan, Y. C. Jung, and W. Barthlott. 2009. 'Fabrication of Artificial Lotus Leaves and Significance of Hierarchical Structure for Superhydrophobicity and Low Adhesion'. *Soft Matter* 5 (7): 1386–93. https://doi.org/10.1039/B818940D.

Kosma, D. K., and M. A. Jenks. 2007. 'Eco-Physiological and Molecular-Genetic Determinants of Plant Cuticle Function in Drought and Salt Stress Tolerance'. In *Advances in Molecular Breeding Toward Drought and Salt Tolerant Crops*, edited by M. A. Jenks, P. M. Hasegawa, and S. M. Jain: 91–120. Springer Netherlands, Dordrecht. https://doi.org/10.1007/978-1-4020-5578-2_5

Kosma, D. K., B. Bourdenx, A. Bernard, E. P. Parsons, S. Lü, J. Joubès, and M. A. Jenks. 2009. 'The Impact of Water Deficiency on Leaf Cuticle Lipids of Arabidopsis'. *Plant Physiology* 151 (4): 1918–29. https://doi.org/10.1104/pp.109.141911.

Kramer, D. M., G. Johnson, O. Kiirats, and G. E. Edwards. 2004. 'New Fluorescence Parameters for the Determination of QA Redox State and Excitation Energy Fluxes'. *Photosynthesis Research* 79 (2): 209. https://doi.org/10.1023/B:PRES.0000015391.99477.0d.

Krauss, P., C. Markstädter, and M. Riederer. 1997. 'Attenuation of UV Radiation by Plant Cuticles from Woody Species'. *Plant, Cell & Environment* 20 (8): 1079–85. https://doi.org/10.1111/j.1365-3040.1997.tb00684.x.

Krogh, A., B. Larsson, G. von Heijne, and E. L. Sonnhammer. 2001. 'Predicting Transmembrane Protein Topology with a Hidden Markov Model: Application to Complete Genomes'. *Journal of Molecular Biology 305* (3): 567-580. https://doi.org/10.1006/jmbi.2000.4315.

Kunst, L., and L. Samuels. 2009. 'Plant Cuticles Shine: Advances in Wax Biosynthesis and Export'. *Current Opinion in Plant Biology* 12 (6): 721–27. https://doi.org/10.1016/j.pbi.2009.09.009.

Laemmli, U. K.. 1970. 'Cleavage of Structural Proteins During the Assembly of the Head of Bacteriophage T4'. *Nature* 227 (5259): 680–85. https://doi.org/10.1038/227680a0.

Lai, C., L. Kunst, and R. Jetter. 2007. 'Composition of Alkyl Esters in the Cuticular Wax on Inflorescence Stems of *Arabidopsis thaliana* Cer Mutants'. *The Plant Journal* 50 (2): 189–96. https://doi.org/10.1111/j.1365-313X.2007.03054.x.

Langridge, P.. 2018. 'Economic and Academic Importance of Barley'. In *The Barley Genome*, edited by N. Stein and G. Mühlbauer: 1-10. Springer, Cham. https://doi.org/10.1007/978-3-319-92528-8_1.

Lawrenson, T., O. Shorinola, N. Stacey, C. Li, L. Østergaard, N. Patron, C. Uauy, and W. Harwood. 2015. 'Induction of Targeted, Heritable Mutations in Barley and *Brassica oleracea* Using RNA-Guided Cas9 Nuclease'. *Genome Biology* 16 (1): 258. https://doi.org/10.1186/s13059-015-0826-7.

Lee, S. B., Y. S. Go, H.-J. Bae, J. H. Park, S. H. Cho, H. J. Cho, D. S. Lee, O. K. Park, I. Hwang, and M. C. Suh. 2009. 'Disruption of Glycosylphosphatidylinositol-Anchored Lipid Transfer Protein Gene Altered Cuticular Lipid Composition, Increased Plastoglobules, and Enhanced Susceptibility to Infection by the Fungal Pathogen *Alternaria brassicicola*'. *Plant Physiology* 150 (1): 42–54. https://doi.org/10.1104/pp.109.137745.

Lee, S. B., S.-J. Jung, Y.-S. Go, H.-U. Kim, J.-K. Kim, H.-J. Cho, O. K. Park, and M.-C. Suh. 2009. 'Two Arabidopsis 3-Ketoacyl CoA Synthase Genes, KCS20 and KCS2/DAISY, Are Functionally Redundant in Cuticular Wax and Root Suberin Biosynthesis, but Differentially Controlled by Osmotic Stress'. *The Plant Journal* 60 (3): 462–75. https://doi.org/10.1111/j.1365-313X.2009.03973.x.

Lee, S. B., and M. C. Suh. 2015. 'Cuticular Wax Biosynthesis is Up-Regulated by the MYB94 Transcription Factor in Arabidopsis'. *Plant and Cell Physiology* 56 (1): 48–60. https://doi.org/10.1093/pcp/pcu142.

Lei, L., L. Yang, B. Cui, H. Liu, J. Wang, H. Zheng, W. Xin, and D. Zou. 2021. 'Combined Gene Family Characterization and RNA-Seq to Study the Response of ß-Ketoacyl-CoA Synthase to Abiotic Stress in Rice (*Oryza sativa* L.)'. *Plant Growth Regulation* 95 (1): 97–110. https://doi.org/10.1007/s10725-021-00728-2.

Li, F., X. Wu, P. Lam, D. Bird, H. Zheng, L. Samuels, R. Jetter, and L. Kunst. 2008. 'Identification of the Wax Ester Synthase/Acyl-Coenzyme A: Diacylglycerol Acyltransferase WSD1 Required for Stem Wax Ester Biosynthesis in Arabidopsis'. *Plant Physiology* 148 (1): 97–107. https://doi.org/10.1104/pp.108.123471.

Li, G., L. Li, R. Tarozo, W. M. Longo, K. J. Wang, H. Dong, and Y. Huang. 2018. 'Microbial Production of Long-Chain n-Alkanes: Implication for Interpreting Sedimentary Leaf Wax Signals'. *Organic Geochemistry* 115: 24–31. https://doi.org/10.1016/j.orggeochem.2017.10.005.

Li, C., T. M. Haslam, A. Krüger, L. M. Schneider, K. Mishina, L. Samuels, H. Yang, L. Kunst, U. Schaffrath, C. Nawrath, G. Chem, T. Komatsuda, and P. von Wettstein-Knowles. 2018. 'The β-Ketoacyl-CoA Synthase HvKCS1, Encoded by Cer-zh, Plays a Key Role in Synthesis of Barley Leaf Wax and Germination of Barley Powdery Mildew'. *Plant and Cell Physiology* 59 (4): 811–27. https://doi.org/10.1093/pcp/pcy020.

Lindow, S. E., G. Andersen, and G. A. Beattie. 1993. 'Characteristics of Insertional Mutants of *Pseudomonas syringae* with Reduced Epiphytic Fitness'. *Applied and Environmental Microbiology* 59 (5): 1593–1601. https://doi.org/10.1128/aem.59.5.1593-1601.1993.

Lindow, S. E., and M. T. Brandl. 2003. 'Microbiology of the Phyllosphere'. *Applied and Environmental Microbiology* 69 (4): 1875–83. https://doi.org/10.1128/AEM.69.4.1875-1883.2003.

Lindsey, B. E., L. Rivero, C. S. Calhoun, E. Grotewold, and J. Brkljacic. 2017. 'Standardized Method for High-Throughput Sterilization of Arabidopsis Seeds'. *Journal of Visualized Experiments* 128: e56587. https://doi.org/10.3791/56587.

Liu, S., C.-T. Yeh, H. M. Tang, D. Nettleton, and P. S. Schnable. 2012. 'Gene Mapping via Bulked Segregant RNA-Seq (BSR-Seq)'. *PLOS ONE* 7 (5): e36406. https://doi.org/10.1371/journal.pone.0036406.

Long, L. M., H. P. Patel, W. C. Cory, and A. E. Stapleton. 2003. 'The Maize Epicuticular Wax Layer Provides UV Protection'. *Functional Plant Biology* 30 (1): 75–81. https://doi.org/10.1071/fp02159.

Lundqvist, U.. 2014. 'Scandinavian Mutation Research in Barley – a Historical Review'. *Hereditas* 151 (6): 123–31. https://doi.org/10.1111/hrd2.00077.

Lundqvist, U., and P. von Wettstein-Knowles. 1982. 'Dominant Mutations at Cer-yy Change Barley Spike Wax into Leaf Blade Wax'. *Carlsberg Research Communications* 47 (1): 29–43. https://doi.org/10.1007/BF02907795.

Mansour, E., E. S. A. Moustafa, N. Qabil, A. Abdelsalam, H. A. Wafa, A. E. Kenawy, A. M. Casas, and E. Igartua. 2018. 'Assessing Different Barley Growth Habits under Egyptian Conditions for Enhancing Resilience to Climate Change'. *Field Crops Research* 224: 67–75. https://doi.org/10.1016/j.fcr.2018.04.016.

McFarlane, H. E., A. Döring, and S. Persson. 2014. 'The Cell Biology of Cellulose Synthesis'. *Annual Review of Plant Biology* 65 (1): 69–94. https://doi.org/10.1146/annurev-arplant-050213-040240.

Mekhedov, S., O. M. de Ilárduya, and J. Ohlrogge. 2000. 'Toward a Functional Catalog of the Plant Genome. A Survey of Genes for Lipid Biosynthesis'. *Plant Physiology* 122 (2): 389-402. https://doi.org/10.1104/pp.122.2.389.

Metz, J. G., M. R. Pollard, L. Anderson, T. R. Hayes, and M. W. Lassner. 2000. 'Purification of a Jojoba Embryo Fatty Acyl-Coenzyme A Reductase and Expression of Its cDNA in High Erucic Acid Rapeseed'. *Plant Physiology* 122 (3): 635–44. https://doi.org/10.1104/pp.122.3.635.

Meyer, A., S. Eskandari, S. Grallath, and D. Rentsch. 2006. 'AtGAT1, a High Affinity Transporter for Gamma-Aminobutyric Acid in *Arabidopsis thaliana*'. *The Journal of Biological Chemistry* 281 (11): 7197–7204. https://doi.org/10.1074/jbc.M510766200.

Mikkelsen, J. D.. 1979. 'Structure and Biosynthesis of β-Diketones in Barley Spike Epicuticular Wax'. *Carlsberg Research Communications* 44 (3): 133-147. https://doi.org/10.1007/BF02906294.

Millar, A. A., and L. Kunst. 1997. 'Very-Long-Chain Fatty Acid Biosynthesis Is Controlled through the Expression and Specificity of the Condensing Enzyme'. *The Plant Journal* 12 (1): 121–31. https://doi.org/10.1046/j.1365-313X.1997.12010121.x.

Millar, A. A., S. Clemens, S. Zachgo, E. M. Giblin, D. C. Taylor, and L. Kunst. 1999. 'CUT1, an Arabidopsis Gene Required for Cuticular Wax Biosynthesis and Pollen Fertility, Encodes a Very-Long-Chain Fatty Acid Condensing Enzyme'. *The Plant Cell* 11 (5): 825–38. https://doi.org/10.1105/tpc.11.5.825.

Mistry, J., S. Chuguransky, L. Williams, M. Qureshi, G. A. Salazar, E. L. L. Sonnhammer, S. C. E. Tosatto, L. Paladin, S. Raj, L. J. Richardson, R. D. Finn, and A. Bateman. 2021. 'Pfam: The Protein Families Database in 2021'. *Nucleic Acids Research* 49 (D1): 412–419. https://doi.org/10.1093/nar/gkaa913.

Monat, C., S. Padmarasu, T. Lux, T. Wocker, H. Gundlach, A. Himmelbach, J. Ens, C. Li, G. J. Muehlbauer, Al. H. Schulman, R. Waugh, I. Braumann, C. Pozniak, W. Scholz, K. F. X. Mayer, M. Spannagl, N. Stein, and M. Mascher. 2019. 'TRITEX: Chromosome-Scale Sequence Assembly of Triticeae Genomes with Open-Source Tools'. *Genome Biology* 20 (284): https://doi.org/10.1186/s13059-019-1899-5.

Morris, C. E., J.-M. Monier, and M.-A. Jacques. 1998. 'A Technique to Quantify the Population Size and Composition of the Biofilm Component in Communities of Bacteria in the Phyllosphere'. *Applied and Environmental Microbiology* 64 (12): 4789–95. https://doi.org/10.1128/AEM.64.12.4789-4795.1998.

Morris, C. E., and J.-M. Monier. 2003. 'The Ecological Significance of Biofilm Formation by Plant-Associated Bacteria'. *Annual Review of Phytopathology* 41 (1): 429–53. https://doi.org/10.1146/annurev.phyto.41.022103.134521.

Newton, A. C., A. J. Flavell, T. S. George, P. Leat, B. Mullholland, L. Ramsay, C. Revoredo-Giha, J. Russell, B. J. Steffenson, J. S. Swansten, W. T. B. Thomas, R. Waugh, P. J. White, and I. J. Bingham. 2011. 'Crops That Feed the World 4. Barley: A Resilient Crop? Strengths and Weaknesses in the Context of Food Security'. *Food Security* 3 (141). https://doi.org/10.1007/s12571-011-0126-3.

Niklas, K. J, E. D. Cobb, and A. J. Matas. 2017. 'The Evolution of Hydrophobic Cell Wall Biopolymers: From Algae to Angiosperms'. *Journal of Experimental Botany* 68 (19): 5261–69. https://doi.org/10.1093/jxb/erx215.

Nosonovsky, M., and B. Bhushan. 2008. 'Roughness-Induced Superhydrophobicity: A Way to Design Non-Adhesive Surfaces'. *Journal of Physics: Condensed Matter* 20 (22): 225009. https://doi.org/10.1088/0953-8984/20/22/225009.

Oeffner, J., J.-P. Jalkanen, S. Walheim, and T. Schimmel. 2020. 'From Nature to Green Shipping: Assessing the Economic and Environmental Potential of AIRCOAT on Low-Draught Ships'. *Proceedings of the 8th Transport Research Arena*, TRA (10).

Ohlrogge, J., and J. Browse. 1995. 'Lipid Biosynthesis'. *The Plant Cell 7* (7): 957. https://doi.org/10.1105/tpc.7.7.957.

Pang, Q., and J. B. Hays. 1991. 'UV-B-Inducible and Temperature-Sensitive Photoreactivation of Cyclobutane Pyrimidine Dimers in *Arabidopsis thaliana'*. *Plant Physiology* 95 (2): 536–43. https://doi.org/10.1104/pp.95.2.536.

Panikashvili, D., S. Savaldi-Goldstein, T. Mandel, T. Yifhar, R. B. Franke, R. Höfer, L. Schreiber, J. Chory, and A. Aharoni. 2007. 'The Arabidopsis DESPERADO/AtWBC11 Transporter is Required for Cutin and Wax Secretion'. *Plant Physiology* 145 (4): 1345–60. https://doi.org/10.1104/pp.107.105676.

Panikashvili, D., J. X. Shi, L. Schreiber, and A. Aharoni. 2011. 'The Arabidopsis ABCG13 Transporter is Required for Flower Cuticle Secretion and Patterning of the Petal Epidermis'. *New Phytologist* 190 (1): 113–24. https://doi.org/10.1111/j.1469-8137.2010.03608.x.

Patwari, P.. 2019. 'Cuticular Waxes Contribute to Drought Tolerance in Arabidopsis and Barley'. Rheinische Friedrich-Wilhelms-Universität Bonn.

Patwari, P., V. Salewski, K. Gutbrod, T. Kreszies, B. Dresen-Scholz, H. Peisker, U. Steiner, A. J. Meyer, L. Schreiber, and P. Dörmann. 2019. 'Surface Wax Esters Contribute to Drought Tolerance in Arabidopsis'. *The Plant Journal* 98 (4): 727–44. https://doi.org/10.1111/tpj.14269.

Pighin, J. A., H. Zheng, L. J. Balakshin, I. P. Goodman, T. L. Western, R. Jetter, L. Kunst, and A. L. Samuels. 2004. 'Plant Cuticular Lipid Export Requires an ABC Transporter'. *Science* 306 (5696): 702–4. https://doi.org/10.1126/science.1102331.

Pitois, O., and X. Chateau. 2002. 'Small Particle at a Fluid Interface: Effect of Contact Angle Hysteresis on Force and Work of Detachment'. *Langmuir* 18 (25): 9751–56. https://doi.org/10.1021/la020300p.

Pulsifer, I. P., S. Kluge, and O. Rowland. 2012. 'Arabidopsis LONG-CHAIN ACYL-COA SYNTHETASE 1 (LACS1), LACS2, and LACS3 Facilitate Fatty Acid Uptake in Yeast'. *Plant Physiology and Biochemistry* 51: 31–39. https://doi.org/10.1016/j.plaphy.2011.10.003.

Qiu, W., J.-W. Park, and H. B. Scholthof. 2002. 'Tombusvirus P19-Mediated Suppression of Virus-Induced Gene Silencing is Controlled by Genetic and Dosage Features That Influence Pathogenicity'. *Molecular Plant-Microbe Interactions* 15 (3): 269–80. https://doi.org/10.1094/MPMI.2002.15.3.269.

Reicosky, D. A., and J. W. Hanover. 1978. 'Physiological Effects of Surface Waxes: I. Light Reflectance for Glaucous and Nonglaucous *Picea pungens'*. *Plant Physiology* 62 (1): 101–4. https://doi.org/10.1104/pp.62.1.101.

Reynhardt, E. C., and M. Riederer. 1994. 'Structures and Molecular Dynamics of Plant Waxes'. *European Biophysics Journal* 23 (1): 59–70. https://doi.org/10.1007/BF00192206.

Reyssat, M., L. Courbin, E. Reyssat, and H. A. Stone. 2008. 'Imbibition in Geometries with Axial Variations'. *Journal of Fluid Mechanics* 615: 335–44. https://doi.org/10.1017/S0022112008003996.

Richards, R. A., H. M. Rawson, and D. A. Johnson. 1986. 'Glaucousness in Wheat: Its Development and Effect on Water-Use Efficiency, Gas Exchange and Photosynthetic Tissue Temperatures'. *Australian Journal of Plant Physiology* 13 (4): 465–73. https://doi.org/10.1071/pp9860465.

Richardson, A., R. Franke, G. Kerstiens, M. Jarvis, L. Schreiber, and W. Fricke. 2005. 'Cuticular Wax Deposition in Growing Barley (*Hordeum vulgare*) Leaves Commences in Relation to the Point of Emergence of Epidermal Cells from the Sheaths of Older Leaves'. *Planta* 222**:** 472–483. https://doi.org/10.1007/s00425-005-1552-2.

Richardson, A., A. Boscari, L. Schreiber, G. Kerstiens, M. Jarvis, P. Herzyk, and W. Fricke. 2007. 'Cloning and Expression Analysis of Candidate Genes Involved in Wax Deposition along the Growing Barley (*Hordeum vulgare*) Leaf'. *Planta* 226 (6): 1459–73. https://doi.org/10.1007/s00425-007-0585-0.

Richardson, A., T. Wojciechowski, R. Franke, L. Schreiber, G. Kerstiens, M. Jarvis, and W. Fricke. 2007. 'Cuticular Permeance in Relation to Wax and Cutin Development along the Growing Barley (*Hordeum vulgare*) Leaf'. *Planta* 225 (6): 1471–81. https://doi.org/10.1007/s00425-006-0456-0.

Riederer, M., and L. Schreiber. 2001. 'Protecting Against Water Loss: Analysis of the Barrier Properties of Plant Cuticles'. *Journal of Experimental Botany* 52 (363): 2023–32. https://doi.org/10.1093/jexbot/52.363.2023.

Riederer, M., and C. Müller, (eds). 2008. *Annual Plant Reviews, Biology of the Plant Cuticle*. John Wiley & Sons, New York.

Roach, P., N. J. Shirtcliffe, and M. I. Newton. 2008. 'Progess in Superhydrophobic Surface Development'. *Soft Matter* 4 (2): 224–40. https://doi.org/10.1039/B712575P.

Rose, A. S., A. R. Bradley, Y. Valasatava, J. M. Duarte, A. Prlić, and P. W. Rose. 2018. 'NGL Viewer: Web-Based Molecular Graphics for Large Complexes'. *Bioinformatics* 34 (21): 3755–3758. https://doi.org/10.1093/bioinformatics/bty419.

Rowland, O., H. Zheng, S. R. Hepworth, P. Lam, R. Jetter, and L. Kunst. 2006. 'CER4 Encodes an Alcohol-Forming Fatty Acyl-Coenzyme A Reductase Involved in Cuticular Wax Production in Arabidopsis'. *Plant Physiology* 142 (3): 866–77. https://doi.org/10.1104/pp.106.086785.

Rowland, O., and F. Domergue. 2012. 'Plant Fatty Acyl Reductases: Enzymes Generating Fatty Alcohols for Protective Layers with Potential for Industrial Applications'. *Plant Science* 193–194: 28–38. https://doi.org/10.1016/j.plantsci.2012.05.002.

Rozema, J., A. J. Noordijk, R. A. Broekman, A. van Beem, B. M. Meijkamp, N. V. J. de Bakker, J. W. M. van de Staaij, A. von Beem, F. Ariese, and S. M. Kars. 2001. '(Poly)Phenolic Compounds in Pollen and Spores of Antarctic Plants as Indicators of Solar UV-B – A New Proxy for the Reconstruction of Past Solar UV-B?'. *Plant Ecology* 154 (1): 9–26. https://doi.org/10.1023/A:1012913608353.

Rozema, J., P. Blokker, M. A. Mayoral Fuertes, and R. Broekman. 2009. 'UV-B Absorbing Compounds in Present-Day and Fossil Pollen, Spores, Cuticles, Seed Coats and Wood: Evaluation of a Proxy for Solar UV Radiation'. *Photochemical & Photobiological Sciences* 8 (9): 1233–43. https://doi.org/10.1039/b904515e.

Ruinen, J.. 1961. 'The Phyllosphere: I. An Ecologically Neglected Milieu'. *Plant and Soil* 15 (2): 81–109.

Saito, N., and H. Werbin. 1969. 'Evidence for a DNA-Photoreactivating Enzyme in Higher Plants'. *Photochemistry and Photobiology* 9 (4): 389–93. https://doi.org/10.1111/j.1751-1097.1969.tb07304.x.

Salas, J. J., and J. B. Ohlrogge. 2002. 'Characterization of Substrate Specificity of Plant FatA and FatB Acyl-ACP Thioesterases'. *Archives of Biochemistry and Biophysics* 403 (1): 25–34. https://doi.org/10.1016/S0003-9861(02)00017-6.

Schönherr, J.. 1976. 'Water Permeability of Isolated Cuticular Membranes: The Effect of Cuticular Waxes on Diffusion of Water'. *Planta* 131 (2): 159–64. https://doi.org/10.1007/BF00389989.

Schönherr, J., and M. Riederer. 1989. 'Foliar Penetration and Accumulation of Organic Chemicals in Plant Cuticles'. In *Reviews of Environmental Contamination and Toxicology*, edited by G. W. Ware: 1–70. Springer, New York. https://doi.org/10.1007/978-1-4613-8850-0_1.

Schönherr, J., and L. Schreiber. 2004. 'Size Selectivity of Aqueous Pores in Astomatous Cuticular Membranes Isolated from *Populus canescens* (Aiton) Sm. Leaves'. *Planta* 219 (3): 405–11. https://doi.org/10.1007/s00425-004-1239-0.

Schönherr, J.. 2006. 'Characterization of Aqueous Pores in Plant Cuticles and Permeation of Ionic Solutes'. *Journal of Experimental Botany* 57 (11): 2471–91. https://doi.org/10.1093/jxb/erj217.

Schreiber, L., and M. Riederer. 1996. 'Ecophysiology of Cuticular Transpiration: Comparative Investigation of Cuticular Water Permeability of Plant Species from Different Habitats'. *Oecologia* 107 (4): 426–32. https://doi.org/10.1007/BF00333931.

Schreiber, L., T. Kirsch, and M. Riederer. 1997. 'Transport Properties of Cuticular Waxes of *Fagus sylvatica* (L.) and *Picea abies* (L.) Karst.: Estimation of Size Selectivity and Tortuisity from Diffusion Coefficients of Aliphatic Molecules'. *Planta* 198: 104-109. https://doi.org/10.1007/BF00197592.

Schreiber, L.. 2005. 'Polar Paths of Diffusion across Plant Cuticles: New Evidence for an Old Hypothesis'. *Annals of Botany* 95 (7): 1069–73. https://doi.org/10.1093/aob/mci122.

Schreiber, L., U. Krimm, D. Knoll, M. Sayed, G. Auling, and R. M. Kroppenstedt. 2005. 'Plant–Microbe Interactions: Identification of Epiphytic Bacteria and Their Ability to Alter Leaf Surface Permeability'. *New Phytologist* 166 (2): 589–94. https://doi.org/10.1111/j.1469-8137.2005.01343.x.

Schreiber, L., and J. Schönherr. 2009. 'Chemistry and Structure of Cuticles as Related to Water and Solute Permeability'. In *Water and Solute Permeability of Plant Cuticles: Measurement and Data Analysis*, 1–29. Berlin, Heidelberg: Springer. https://doi.org/10.1007/978-3-540-68945-4_1.

Schultz, D. J., and J. B. Ohlrogge. 2002. 'Metabolic Engineering of Fatty Acid Biosynthesis'. In *Lipid Biotechnology*, edited by T. M. Kuo, and H. Gardner: 1-29. CRC Press, New York.

Segado, P., E. Domínguez, and A. Heredia. 2016. 'Ultrastructure of the Epidermal Cell Wall and Cuticle of Tomato Fruit (*Solanum lycopersicum* L.) during Development'. *Plant Physiology* 170 (2): 935–46. https://doi.org/10.1104/pp.15.01725.

Seo, P. J., and C.-M. Park. 2011. 'Cuticular Wax Biosynthesis as a Way of Inducing Drought Resistance'. *Plant Signaling & Behavior* 6 (7): 1043–45. https://doi.org/10.4161/psb.6.7.15606.

Serrano-Vega, M. J., R. Garcés, and E. Martínez-Force. 2005. 'Cloning, Characterization and Structural Model of a FatA-Type Thioesterase from Sunflower Seeds (*Helianthus annuus* L.)'. *Planta* 221 (6): 868–80. https://doi.org/10.1007/s00425-005-1502-z.

Sheldon, P. S., R. G. O. Kekwick, C. G. Smith, C. Sidebottom, and A. R. Slabas. 1992. '3-Oxoacyl-[ACP] Reductase from Oilseed Rape (*Brassica napus*)'. *Biochimica et Biophysica Acta* 1120 (2): 151–59. https://doi.org/10.1016/0167-4838(92)90263-D.

Shepherd, T., and D. W. Griffiths. 2006. 'The Effects of Stress on Plant Cuticular Waxes'. *The New Phytologist* 171 (3): 469–99. https://doi.org/10.1111/j.1469-8137.2006.01826.x.

Shi, J., H. Tan, X.-H. Yu, Y. Liu, W. Liang, K. Ranathunge, R. B. Franke, L. Schreiber, Y. Wang, G. Kai, J. Shanklin, H. Ma and D. Zhang. 2011. 'Defective Pollen Wall Is Required for Anther and Microspore Development in Rice and Encodes a Fatty Acyl Carrier Protein Reductase'. *The Plant Cell* 23 (6): 2225–2246. https://doi.org/10.1105/tpc.111.087528

Solovchenko, A., and M. Merzlyak. 2003. 'Optical Properties and Contribution of Cuticle to UV Protection in Plants: Experiments with Apple Fruit'. *Photochemical & Photobiological Sciences* 2 (8): 861–66. https://doi.org/10.1039/B302478D.

Somerville, C. and J. Browse. 1991. 'Plant Lipids: Metabolism, Mutants, and Membranes'. *Science* 252 (5002): 80-87. https://doi.org/10.1126/science.252.5002.80.

Sreenivasulu, N, B. Usadel, A. Winter, V. Radchuk, U. Scholz, N. Stein, W. Weschke, M. Strickert, T. J. Close, M. Stitt, A. Graner, and U. Wobus. 2008. 'Barley Grain Maturation and Germination: Metabolic Pathway and Regulatory Network Commonalities and Differences Highlighted by New MapMan/PageMan Profiling Tools'. *Plant Physiology* 146 (4): 1738–1758. https://doi.org/10.1104/pp.107.111781.

Srivastava, K., and G. L. B. Wiesenberg. 2018. 'Severe Drought-Influenced Composition and $\delta^{13}C$ of Plant and Soil n-Alkanes in Model Temperate Grassland and Heathland Ecosystems'. *Organic Geochemistry* 116: 77–89. https://doi.org/10.1016/j.orggeochem.2017.11.002.

Steinmüller, D., and M. Tevini. 1985. 'Action of Ultraviolet Radiation (UV-B) upon Cuticular Waxes in Some Crop Plants'. *Planta* 164 (4): 557–64. https://doi.org/10.1007/BF00395975.

Strid, Å., W. S. Chow, and J. M. Anderson. 1990. 'Effects of Supplementary Ultraviolet-B Radiation on Photosynthesis in *Pisum sativum'*. *Biochimica et Biophysica Acta* 1020 (3): 260–68. https://doi.org/10.1016/0005-2728(90)90156-X.

Suh, M. C., A. L. Samuels, R. Jetter, L. Kunst, M. Pollard, J. Ohlrogge, and F. Beisson. 2005. 'Cuticular Lipid Composition, Surface Structure, and Gene Expression in Arabidopsis Stem Epidermis'. *Plant Physiology* 139 (4): 1649–65. https://doi.org/10.1104/pp.105.070805.

Tecon, R., and J. H. J. Leveau. 2012. 'The Mechanics of Bacterial Cluster Formation on Plant Leaf Surfaces as Revealed by Bioreporter Technology'. *Environmental Microbiology* 14 (5): 1325–32. https://doi.org/10.1111/j.1462-2920.2012.02715.x.

Tevini, M., and A. H. Teramura. 1989. 'UV-B Effects on Terrestrial Plants'. *Photochemistry and Photobiology* 50 (4): 479–87. https://doi.org/10.1111/j.1751-1097.1989.tb05552.x.

The Arabidopsis Genome Initiative. 2000. 'Analysis of the Genome Sequence of the Flowering Plant *Arabidopsis thaliana*'. *Nature* 408: 796-815. https://doi.org/10.1038/35048692.

Tong, T., Y.-X. Fang, Z. Zhang, J. Zheng, X. Zhang, J. Li, C. Niu, D. Xue, and X. Zhang. 2021. 'Genome-Wide Identification and Expression Pattern Analysis of the KCS Gene Family in Barley'. *Plant Growth Regulation* 93 (1): 89–103. https://doi.org/10.1007/s10725-020-00668-3.

Towbin, H., T. Staehelin, and J. Gordon. 1979. 'Electrophoretic Transfer of Proteins from Polyacrylamide Gels to Nitrocellulose Sheets: Procedure and Some Applications'. *Proceedings of the National Academy of Sciences of the United States of America* 76 (9): 4350–54. https://doi.org/10.1073/pnas.76.9.4350.

Turner, N. C.. 2017. 'Turgor Maintenance by Osmotic Adjustment, an Adaptive Mechanism for Coping with Plant Water Deficits'. *Plant, Cell & Environment* 40 (1): 1–3. https://doi.org/10.1111/pce.12839.

Vogg, G., S. Fischer, J. Leide, E. Emmanuel, R. Jetter, A. A. Levy, and M. Riederer. 2004. 'Tomato Fruit Cuticular Waxes and Their Effects on Transpiration Barrier Properties: Functional Characterization of a Mutant Deficient in a Very-Long-Chain Fatty Acid ß-ketoacyl-CoA Synthase'. *Journal of Experimental Botany* 55 (401): 1401–10. https://doi.org/10.1093/jxb/erh149.

Voisin, D., C. Nawrath, S. Kurdyukov, R. B. Franke, J. J. Reina-Pinto, N. Efremova, I. Will, L. Schreiber, and A. Yephremov. 2009. 'Dissection of the Complex Phenotype in Cuticular Mutants of Arabidopsis Reveals a Role of SERRATE as a Mediator'. *PLoS Genetics* 5 (10). https://doi.org/10.1371/journal.pgen.1000703.

von Mohl H.. 1847. 'Untersuchungen Der Frage: Bildet die Cellulose die Grundlage Sämtlicher Vegetabilischen Membranen'. *Botanische Zeitung* 5: 497–505.

Vorholt, J. A.. 2012. 'Microbial Life in the Phyllosphere'. *Nature Reviews Microbiology* 10 (12): 828–40. https://doi.org/10.1038/nrmicro2910.

Walton, T. J.. 1990. 'Waxes, Cutin and Suberin'. *Methods in Plant Biochemistry* 4 (11): 5–158.

Wang, Y., M. Wang, Y. Sun, D. Hegebarth, T. Li, R. Jetter and Z. Wang. 2015. 'Molecular Characterization of TaFAR1 Involved in Primary Alcohol Biosynthesis of Cuticular Wax in Hexaploid Wheat'. *Plant and Cell Physiology* 56 (10): 1944–1961. https://doi.org/10.1093/pcp/pcv112

Wang, Y., M. Wang, Y. Sun, Y. Wang, T. Li, G. Chai, W. Jiang, L. Shan, C. Li, E. Xiao, and Z. Wang. 2015. 'FAR5, a Fatty Acyl-Coenzyme A Reductase, Is Involved in Primary Alcohol Biosynthesis of the Leaf Blade Cuticular Wax in Wheat (*Triticum aestivum* L.)'. *Journal of Experimental Botany* 66 (5): 1165–78. https://doi.org/10.1093/jxb/eru457.

Wang, W., Y. Zhang, C. Xu, J. Ren, X. Liu, K. Black, X. Gai, Q. Wang, and H. Ren. 2015. 'Cucumber ECERIFERUM1 (CsCER1), Which Influences the Cuticle Properties and Drought Tolerance of Cucumber, Plays a Key Role in VLC Alkanes Biosynthesis'. *Plant Molecular Biology* 87 (3): 219–33. https://doi.org/10.1007/s11103-014-0271-0.

Wang, M., Y. Wang, H. Wu, J. Xu, T. Li, D. Hegebarth, R. Jetter, L. Chen and Z. Wang. 2016. 'Three TaFAR Genes Function in the Biosynthesis of Primary Alcohols and the Response to Abiotic Stresses in *Triticum aestivum*'. *Scientific Reports* 6 (25008). https://doi.org/10.1038/srep25008

Wang, X., Y. Guan, D. Zhang, X. Dong, L. Tian, and L. Q. Qu. 2017. 'A β-Ketoacyl-CoA Synthase is Involved in Rice Leaf Cuticular Wax Synthesis and Requires a CER2-LIKE Protein as a Cofactor'. *Plant Physiology* 173 (2): 944–55. https://doi.org/10.1104/pp.16.01527.

Wang, Y., Y. Sun, Q. You, W. Luo, C. Wang, S. Zhao, G. Chai, T. Li, X. Shi, C. Li, R. Jetter and Z. Wang. 2018. 'Three Fatty Acyl-Coenzyme A Reductases, BdFAR1, BdFAR2 and BdFAR3, are Involved in Cuticular Wax Primary Alcohol Biosynthesis in *Brachypodium distachyon*'. *Plant and Cell Physiology* 59 (3): 527–543. https://doi.org/10.1093/pcp/pcx211

Weidenbach, D., M. Jansen, R. B. Franke, G. Hensel, W. Weissgerber, S. Ulferts, I. Jansen, L. Schreiber, V. Korzun, R. Pontzen, J. Kumlehn, K. Pillen, and U. Schaffrath. 2014. 'Evolutionary Conserved Function of Barley and Arabidopsis 3-KETOACYL-CoA SYNTHASES in Providing Wax Signals for Germination of Powdery Mildew Fungi'. *Plant Physiology* 166 (3): 1621–33. https://doi.org/10.1104/pp.114.246348.

Wettstein-Knowles, P., and A. G. Netting. 1976. 'Composition of Epicuticular Waxes on Barley Spikes'. *Carlsberg Research Communications* 41 (5): 225. https://doi.org/10.1007/BF02906259.

Wood, C. C., J. R. Petrie, P. Shrestha, M. P. Mansour, P. D. Nichols, A. G. Green, and S. P. Singh. 2009. 'A Leaf-Based Assay Using Interchangeable Design Principles to Rapidly Assemble Multistep Recombinant Pathways'. *Plant Biotechnology Journal* 7 (9): 914–24. https://doi.org/10.1111/j.1467-7652.2009.00453.x.

Wu, P., J. Xie, J. Hu, D. Qiu, Z. Liu, J. Li, M. Li, H. Zhang, L. Yang, H. Liu, Y. Zhou, Z. Zhang, and H. Li. 2018. 'Development of Molecular Markers Linked to Powdery Mildew Resistance Gene Pm4b by Combining SNP Discovery from Transcriptome Sequencing Data with Bulked Segregant Analysis (BSR-Seq) in Wheat'. *Frontiers in Plant Science* 9: 95. https://doi.org/10.3389/fpls.2018.00095.

Xu, S.-J., P.-A. Jiang, Z.-W. Wang, and Y. Wang. 2009. 'Crystal Structures and Chemical Composition of Leaf Surface Wax Depositions on the Desert Moss Syntrichia Caninervis'. *Biochemical Systematics and Ecology* 37 (6): 723–30. https://doi.org/10.1016/j.bse.2009.12.012.

Xue, D., X. Zhang, X. Lu, G. Chen, and Z.-H. Chen. 2017. 'Molecular and Evolutionary Mechanisms of Cuticular Wax for Plant Drought Tolerance'. *Frontiers in Plant Science* 8: 621. https://doi.org/10.3389/fpls.2017.00621.

Yeats, T. H., W. Huang, S. Chatterjee, H. M.-F. Viart, M. H. Clausen, R. E. Stark, and J. K. C. Rose. 2014. 'Tomato Cutin Deficient 1 (CD1) and Putative Orthologs Comprise an Ancient Family of Cutin Synthase-like (CUS) Proteins That Are Conserved among Land Plants'. *The Plant Journal* 77 (5): 667–75. https://doi.org/10.1111/tpj.12422.

Zabka, V., M. Stangl, G. Bringmann, G. Vogg, M. Riederer, and U. Hildebrandt. 2008. 'Host Surface Properties Affect Prepenetration Processes in the Barley Powdery Mildew Fungus'. *New Phytologist* 177 (1): 251–63. https://doi.org/10.1111/j.1469-8137.2007.02233.x.

Zeisler, V., and L. Schreiber. 2016. ‘Epicuticular Wax on Cherry Laurel (*Prunus laurocerasus*) Leaves Does Not Constitute the Cuticular Transpiration Barrier’. *Planta* 243 (1): 65–81. https://doi.org/10.1007/s00425-015-2397-y.

Zeisler-Diehl, V., Y. Müller, and L. Schreiber. 2018. ‘Epicuticular Wax on Leaf Cuticles Does Not Establish the Transpiration Barrier, Which is Essentially Formed by Intracuticular Wax’. *Journal of Plant Physiology* 227: 66–74. https://doi.org/10.1016/j.jplph.2018.03.018.

Zeisler-Diehl, V. V., W. Barthlott, and L. Schreiber. 2020. ‘Plant Cuticular Waxes: Composition, Function, and Interactions with Microorganisms’. In *Hydrocarbons, Oils and Lipids: Diversity, Origin, Chemistry and Fate*, edited by Heinz Wilkes: 123–38. Springer International Publishing, Basel. https://doi.org/10.1007/978-3-319-90569-3_7.

Zhang, X., and X. Cai. 2011. ‘Climate Change Impacts on Global Agricultural Land Availability’. *Environmental Research Letter* 6 (1). https://doi.org/10.1088/1748-9326/6/1/014014.

Zhang, Z., W. Wei, H. Zhu, G. S. Challa, C. Bi, H. N. Trick, and W. Li. 2015. ‘W3 Is a New Wax Locus That Is Essential for Biosynthesis of β-Diketone, Development of Glaucousness, and Reduction of Cuticle Permeability in Common Wheat’. *PLOS ONE* 10 (10). https://doi.org/10.1371/journal.pone.0140524.

Zhao, J., H. Sun, H. Dai, G. Zhang, and F. Wu. 2010. ‘Difference in Response to Drought Stress among Tibet Wild Barley Genotypes’. *Euphytica* 172 (3): 395–403. https://doi.org/10.1007/s10681-009-0064-8.

7 Appendix

7.1 Vector maps

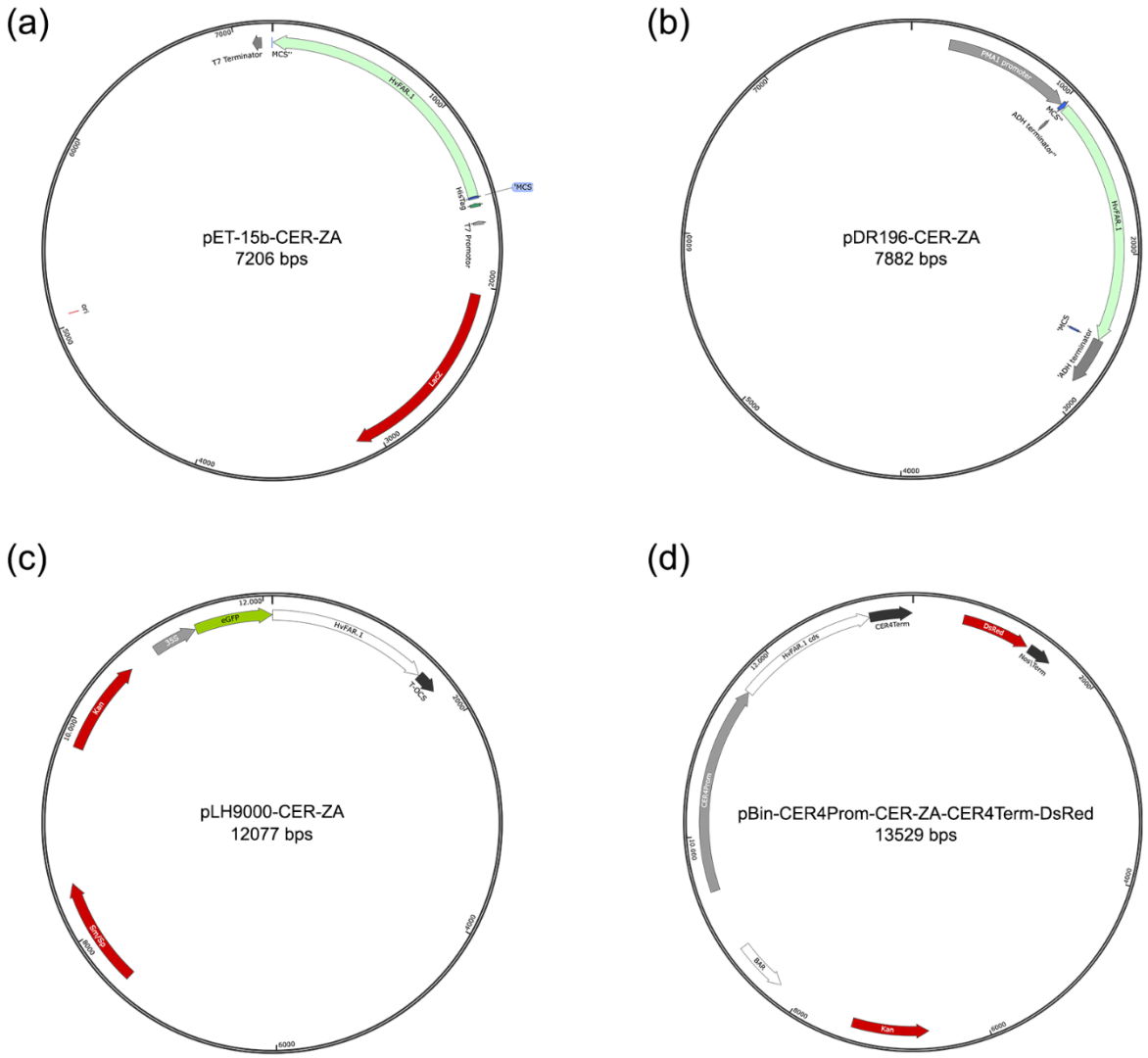

Figure 49: Vector maps of utilised constructs. (a) pET-15b-CER-ZA: Heterologous expression in *E. coli*. (b) pDR196-CER-ZA: Heterologous expression in *S. cerevisiae*. (c): pLH9000-CER-ZA: Localisation studies in *N. benthamiana* of CER-ZA by GFP fusion. (d): pBin-CER4PROM-CER-ZA-CER4TERM with DsRed marker: Expression of CER-ZA in *A. thaliana cer*4-3.

7.2 List of oligonucleotides

Restriction sites are highlighted in red or blue colours.

Stock number	Template	Purpose	Acceptor vector	Restriction site	Sequence
Expression in *E. coli* of CER-ZA					
bn4160	*HORVU5Hr1G089230.1*	Expression of *Cer-za*	pET-15b	XhoI	cgcctcgagAATGGACGCTGGCGCGGT
bn4161	*HORVU5Hr1G089230.1*	Expression of *Cer-za*	pET-15b	BamHI	cgcggatccCTATACGCTTCCCTTATTTTTGCGGCCGTA
bn4176	pET-15b	Control Primer			AAGGAATGGTGCATGCAAGG
bn4080	*HORVU5Hr1G089230.1*	Control Primer	-	-	ACACTTCTTTGCAAATTC
Expression in *S. cerevisiae* of CER-ZA					
bn4277	*HORVU5Hr1G089230.1*	Expression of *Cer-za*	pDR196	EcoRI	cgcgaattcAATGGACGCTGGCGCGGT
bn4171	*HORVU5Hr1G089230.1*	Expression of *Cer-za*	pDR196	SalI	cgcgtcgacCTATACGCTTCCCTTATTTTTGCGGCCGTA
bn4174	pDR196	Control Primer	-	-	ATGGTGGGTACCGCTTATGC
bn4175	pDR196-HvFAR	Control Primer	-	-	ATCCGCGCGTAATACGACTC
Subcellular localization of CER-ZA					
bn4045	*HORVU5Hr1G089230.1*	Subcellular localisation of *Cer-za*	pLH9000	BamHI	aaaggatccATGGACGCTGGCGCG
bn4046	*HORVU5Hr1G089230.1*	Subcellular localisation of *Cer-za*	pLH9000	SalI	aaagtcgacCTATACGCTTCCCTTATTTT
Sequencing					
bn 3707	*HORVU5Hr1G089230*	Sequencing section I			ACAAAACAAACTCTGGTGGCTA
bn 3708	*HORVU5Hr1G089230*	Sequencing section I			AAGAGAACATCAAAGAAAAACTG

bn 3709	*HORVU5Hr1G089230*	Sequencing section II	TTCTCTTTCTTCC TTATATAGGT
bn 3710	*HORVU5Hr1G089230*	Sequencing section II	TGATTTTTGATAC ATCACACTCT
bn 3711	*HORVU5Hr1G089230*	Sequencing section III	AAGTAAGCGAAT CTCTTGAACAG
bn 3712	*HORVU5Hr1G089230*	Sequencing section III	ACTTCTTTTTTAA GTTGGTACGG
bn 3713	*HORVU5Hr1G089230*	Sequencing section IV	AAAATGGCAAGC CCTTCAACAA
bn 3714	*HORVU5Hr1G089230*	Sequencing section IV	AAAAACATATCTG AAAGGCTTTTA
bn 3715	*HORVU5Hr1G089230*	Sequencing section V	AAACATGCAAAAT AATTCATACTG
bn 3716	*HORVU5Hr1G089230*	Sequencing section V	ACAAGGGACAAG TTTATGTCAC
bn 3717	*HORVU5Hr1G089230*	Sequencing section VI	ATGATTTTTTTTT CTGTTAGCAAAG
bn 3718	*HORVU5Hr1G089230*	Sequencing section VI	AAATTGGATCAC AACAGAAATAAAT A
bn3883	*HORVU5Hr1G089230*	Sequencing section VII	TGTCGTCCCAGC ACCACATC
bn3884	*HORVU5Hr1G089230*	Sequencing section VII	CTGGTTACAGCT CAAGGCCC
bn3967	*HORVU5Hr1G089230*	Sequencing section VIII	GCCTAGTTGACG AAGAAAGGAAAT G
bn3968	*HORVU5Hr1G089230*	Sequencing section VIII	CAAGCTACCGTG ATAATAAGGGC
bn3987	*HORVU4Hr1G063420*	Sequencing section I	AACCACCGCCAT TAATAG
bn3988	*HORVU4Hr1G063420*	Sequencing section I	AGATCTTGTTCTG GTCC
bn3989	*HORVU4Hr1G063420*	Sequencing section II	ATCTACCTCTCCA TCGAC
bn3990	*HORVU4Hr1G063420*	Sequencing section II	ACTTGAGGAACT TGAGC
bn3991	*HORVU4Hr1G063420*	Sequencing section III	AGTGCTTCAACT GCGT

bn3992	*HORVU4Hr1G063420*	Sequencing section III			ACGTTACCAAACGAAAC
bn3993	*HORVU4Hr1G063420*	Sequencing section IV			AGTGCCGTTGTTTTCAG
bn3994	*HORVU4Hr1G063420*	Sequencing section IV			ACCGTTTCCAATTTATCTC
bn4064	*HORVU4Hr1G063420*	Sequencing section V			AACTCACGCTTCCGGTTC
bn4065	*HORVU4Hr1G063420*	Sequencing section V			AGATCTTGTTCTGGTCCTCC
bn4066	*HORVU4Hr1G063420*	Sequencing section VI			AGACCAAGATCACCACCCG
bn4067	*HORVU4Hr1G063420*	Sequencing section VI			AGCGACTTGAGGAACTTGAG
Expression of CER-ZA in *A. thaliana cer4-3*					
bn3955	*HORVU5Hr1G089230*	Expression of *Cer-za*	pBin-35s-GG-DsRed	BsaI	GCGGGTCTCAAATTATGGACGCTGGCGCGGTGG
bn3956	*HORVU5Hr1G089230*	Expression of *Cer-za*	pBin-35s-GG-DsRed	BsaI	CGCGGTCTCAATTACTATACGCTTCCCTTATTTTT
bn3957	*At4g33790*	CER4 Promotor	pBin-35s-GG-DsRed	BsaI	GCGGATCTGAGACCTTTCCTTGTAGCCGCCTTTA
bn3958	*At4g33790*	CER4 Promotor	pBin-35s-GG-DsRed	BsaI	CGCGGTCTCAAATTTATGTTTGTATATACGTT
bn3959	*At4g33790*	CER4 Terminator	pBin-35s-GG-DsRed	BsaI	GCGGGTCTCTTAATTTTAGTTGTATAATCTT
bn3960	*At4g33790*	CER4 Terminator	pBin-35s-DsRed	BsaI	CGCCTAGAGAGACCAAACTTTACATGGGGGCAATG
Semi-quantitative RT-PCR					
bn3698	*AY145451.1*	Housekeeping gene, *ACT2*			CACCCTGAGCAACTCATCAG
bn3699	*AY145451.1*	Housekeeping gene, *ACT2*			TCCAAGCACAGATCAACAATC

bn4254	*HORVU5Hr1G089230.1*	Expression levels of *Cer-za*	AACAACAGGTGG CTACTCGA
bn4255	*HORVU5Hr1G089230.1*	Expression levels of *Cer-za*	ACCGTGATAATA AGGGCCGA
bn4275	*HORVU4Hr1G063420*	Expression levels of *Cer-ye*	TGTTTCTCTTCTG GTCGCCT
bn4276	*HORVU4Hr1G063420*	Expression levels of *Cer-ye*	CGAACCACCACA CCAACATT

7.3 Supplemental data

7.3.1 Cuticular wax composition of *cer*-za.227

Table 26: Total amount of cuticular waxes extracted from barley leaves given in [µg/cm²].

Bowman		*cer*-za.227	
AVG	SD	AVG	SD
6.082	1.117	2.387	0.462

Table 27: Composition of aliphatic lipids in cuticular waxes from barley leaves in [µg/cm²].

	Bowman		*cer*-za.227	
	AVG	SD	AVG	SD
Alkanes	0.049	0.006	0.126	0.016
Acids	0.179	0.156	0.166	0.078
Alcohols	4.872	0.801	1.506	0.319
Aldehydes	0.038	0.041	0.008	0.008
Esters	0.944	0.113	0.581	0.124

Table 28: Chain length composition of cuticular waxes from barley leaves in [µg/cm²].

	Bowman		*cer*-za.227	
	AVG	SD	AVG	SD
C_{22}	0.014	0.019	0.019	0.020
C_{24}	0.319	0.139	0.210	0.075
C_{26}	4.634	0.703	1.412	0.258
C_{27}	0.040	0.023	0.004	0.002
C_{28}	0.082	0.067	0.034	0.028
C_{33}	0.049	0.006	0.126	0.016
C_{38}	0.005	0.001	0.005	0.003
C_{40}	0.018	0.002	0.016	0.003
C_{42}	0.122	0.018	0.122	0.008
C_{44}	0.168	0.018	0.130	0.011
C_{46}	0.276	0.034	0.130	0.060
C_{48}	0.275	0.028	0.130	0.016
C_{50}	0.080	0.011	0.049	0.022

7.3.2 Cuticular wax composition of epicuticular and intracuticular wax fractions of *cer*-za.227

Table 29: Total amount of cuticular waxes from barley leaves given in [µg/cm²]. IW, EW, intracuticular and epicuticular wax.

	IW		EW		Total	
	AVG	SD	AVG	SD	AVG	SD
Bowman	2.343	0.328	9.139	0.865	11.482	1.070
cer-za.227	1.413	0.299	1.775	0.249	3.187	0.175

Table 30: Composition of aliphatic lipids in cuticular waxes from barley leaves in [µg/cm²]**.** IW, EW, intracuticular and epicuticular wax.

	Bowman				*cer*-za.227			
	IW		EW		IW		EW	
	AVG	SD	AVG	SD	AVG	SD	AVG	SD
Alkanes	0.024	0.003	0.052	0.004	0.063	0.008	0.068	0.006
Acids	0.030	0.024	0.049	0.012	0.020	0.003	0.027	0.006
Alcohols	1.926	0.262	7.878	0.775	0.893	0.215	1.115	0.146
Aldehydes	0.014	0.003	0.120	0.027	0.044	0.012	0.080	0.020
Esters	0.349	0.064	1.041	0.114	0.393	0.071	0.485	0.085

Table 31: Chain length composition of cuticular waxes from barley leaves in [µg/cm²]. IW, EW, intracuticular and epicuticular wax.

	Bowman				*cer*-za.227			
	IW		EW		IW		EW	
	AVG	SD	AVG	SD	AVG	SD	AVG	SD
C_{20}	0.003	0.001	0.019	0.003	0.002	0.000	0.006	0.001
C_{22}	0.027	0.007	0.033	0.009	0.021	0.005	0.016	0.003
C_{24}	0.093	0.012	0.230	0.016	0.058	0.009	0.056	0.010
C_{26}	1.775	0.250	7.479	0.718	0.775	0.191	1.004	0.131
C_{27}	0.001	0.001	0.026	0.020	0.002	0.002	0.004	0.001
C_{28}	0.071	0.017	0.260	0.049	0.098	0.022	0.137	0.026
C_{33}	0.024	0.003	0.052	0.004	0.063	0.008	0.068	0.006
C_{38}	0.001	0.002	0.014	0.001	0.002	0.002	0.006	0.001
C_{40}	0.025	0.004	0.097	0.007	0.037	0.007	0.057	0.010
C_{42}	0.053	0.007	0.174	0.017	0.047	0.009	0.067	0.010
C_{44}	0.098	0.014	0.300	0.034	0.063	0.015	0.089	0.013
C_{46}	0.090	0.013	0.257	0.028	0.051	0.011	0.068	0.012
C_{48}	0.017	0.013	0.059	0.006	0.025	0.003	0.025	0.005
C_{50}	0.064	0.011	0.140	0.021	0.168	0.024	0.173	0.034

7.3.3 Cuticular wax composition of *cer*-za alleles

Table 32: Total amount of cuticular waxes from Bowman and *cer*-ye.267 in [µg/cm²].

Bowman		*cer*-za.173		*cer*-za.232		*cer*-za.318	
AVG	SD	AVG	SD	AVG	SD	AVG	SD
13.048	3.022	3.285	0.674	13.048	3.022	3.285	0.674

Table 33: Composition of aliphatic lipids in cuticular waxes in [µg/cm²].

	Bowman		*cer*-za.173		*cer*-za.232		*cer*-za.318	
	AVG	SD	AVG	SD	AVG	SD	AVG	SD
Alkanes	0.099	0.021	0.155	0.029	0.111	0.045	0.105	0.024
Acids	0.203	0.071	0.157	0.050	0.092	0.034	0.102	0.085
Alcohols	10.545	2.222	2.184	0.542	2.037	0.594	1.666	0.863
Aldehydes	0.818	0.351	0.169	0.036	0.112	0.027	0.121	0.085
Esters	1.384	0.372	0.621	0.059	0.709	0.013	0.666	0.249

Table 34: Chain length composition of cuticular waxes in [µg/cm²].

	Bowman		*cer*-za.173		*cer*-za.232		*cer*-za.318	
	AVG	SD	AVG	SD	AVG	SD	AVG	SD
C_{20}	0.000	0.000	0.000	0.000	0.000	0.000	0.000	0.000
C_{22}	0.051	0.014	0.015	0.014	0.023	0.032	0.010	0.009
C_{24}	0.290	0.066	0.083	0.052	0.048	0.014	0.043	0.019
C_{25}	0.019	0.012	0.013	0.013	-	-	0.018	0.025
C_{26}	10.843	2.416	2.099	0.493	1.892	0.539	1.587	0.878
C_{27}	0.077	0.018	0.086	0.009	0.093	0.006	0.073	0.033
C_{28}	0.207	0.142	0.140	0.082	0.144	0.039	0.133	0.089
C_{30}	0.080	0.022	0.074	0.031	0.042	0.015	0.026	0.014
C_{33}	0.099	0.021	0.155	0.029	0.111	0.045	0.105	0.024
C_{38}	0.079	0.067	0.034	0.021	0.013	0.006	0.137	0.167
C_{40}	0.024	0.005	0.018	0.002	0.020	0.001	0.011	0.008
C_{42}	0.163	0.042	0.169	0.010	0.215	0.015	0.150	0.043
C_{44}	0.256	0.079	0.140	0.008	0.164	0.005	0.119	0.037
C_{46}	0.466	0.119	0.114	0.009	0.131	0.012	0.114	0.033
C_{48}	0.396	0.099	0.146	0.016	0.167	0.010	0.136	0.047

7.3.4 Cuticular wax composition of *cer*-ye.267

Table 35: Total amount of cuticular waxes from Bowman and *cer*-ye.267 given in [µg/cm²].

Bowman		*cer*-ye.267	
AVG	SD	AVG	SD
8.672	1.012	3.276	0.412

Table 36: Composition of aliphatic lipids in cuticular waxes in [µg/cm²].

	Bowman		*cer*-ye.267	
	AVG	SD	AVG	SD
Alkanes	0.060	0.013	0.023	0.005
Acids	7.843	0.897	2.757	0.376
Alcohols	0.163	0.044	0.084	0.060
Aldehydes	0.237	0.033	0.140	0.071
Esters	0.370	0.186	0.336	0.252

Table 37: Chain length composition of cuticular waxes in [µg/cm²].

	Bowman		*cer*-ye.267	
	AVG	SD	AVG	SD
C_{22}	0.002	0.000	0.002	0.004
C_{24}	0.031	0.004	0.032	0.047
C_{26}	0.288	0.028	0.104	0.016
C_{27}	7.578	0.881	2.672	0.373
C_{28}	0.128	0.026	0.029	0.017
C_{33}	0.193	0.023	0.065	0.010
C_{38}	0.060	0.013	0.023	0.005
C_{40}	0.009	0.003	0.012	0.006
C_{42}	0.058	0.027	0.201	0.131
C_{44}	0.080	0.040	0.018	0.014
C_{46}	0.104	0.055	0.034	0.033
C_{48}	0.072	0.040	0.044	0.046
C_{50}	0.017	0.006	0.013	0.010

7.3.5 Cuticular wax composition of epicuticular and intracuticular wax fractions of *cer*-ye.267

Table 38: Total amount of cuticular waxes from Bowman and *cer*-ye.267 given in [µg/cm²]. IW, EW, intracuticular and epicuticular wax.

	IW		EW		Total	
	AVG	SD	AVG	SD	AVG	SD
Bowman	2.343	0.328	9.139	0.865	11.482	1.070
cer-ye.267	1.076	0.166	2.353	0.344	3.429	0.496

Table 39: Composition of aliphatic lipids in cuticular waxes in [µg/cm²]. IW, EW, intracuticular and epicuticular wax.

	Bowman				*cer*-ye.267			
	IW		EW		IW		EW	
	AVG	SD	AVG	SD	AVG	SD	AVG	SD
Alkanes	0.024	0.003	0.052	0.004	0.010	0.001	0.017	0.002
Acids	0.030	0.024	0.049	0.012	0.013	0.001	0.042	0.018
Alcohols	1.926	0.262	7.878	0.775	0.828	0.111	1.787	0.315
Aldehydes	0.014	0.003	0.120	0.027	0.007	0.005	0.055	0.034
Esters	0.349	0.064	1.041	0.114	0.218	0.052	0.452	0.063

Table 40: Chain length composition of cuticular waxes in [µg/cm²]. IW, EW, intracuticular and epicuticular wax.

	Bowman				*cer*-ye.267			
	IW		EW		IW		EW	
	AVG	SD	AVG	SD	AVG	SD	AVG	SD
C_{20}	0.003	0.001	0.019	0.003	0.001	0.001	0.008	0.003
C_{22}	0.027	0.007	0.033	0.009	0.019	0.008	0.022	0.007
C_{24}	0.093	0.012	0.230	0.016	0.038	0.004	0.074	0.002
C_{26}	1.775	0.250	7.479	0.718	0.758	0.100	1.701	0.325
C_{27}	0.001	0.001	0.026	0.020	0.000	0.000	0.004	0.001
C_{28}	0.071	0.017	0.260	0.049	0.033	0.006	0.077	0.029
C_{33}	0.024	0.003	0.052	0.004	0.010	0.001	0.017	0.002
C_{38}	0.001	0.002	0.014	0.001	0.003	0.002	0.013	0.002
C_{40}	0.025	0.004	0.097	0.007	0.093	0.012	0.230	0.029
C_{42}	0.053	0.007	0.174	0.017	0.012	0.002	0.025	0.003
C_{44}	0.098	0.014	0.300	0.034	0.032	0.006	0.058	0.009
C_{46}	0.090	0.013	0.257	0.028	0.047	0.008	0.075	0.011
C_{48}	0.017	0.013	0.059	0.006	0.011	0.008	0.020	0.003
C_{50}	0.064	0.011	0.140	0.021	0.020	0.014	0.032	0.006

7.3.6 Cuticular wax composition of *cer*-ye alleles

Table 41: Total amount of cuticular waxes from Bowman and *cer*-ye.267 given in [µg/cm²].

Bowman		*cer*-ye.582		*cer*-ye.792		*cer*-ye.1395	
AVG	SD	AVG	SD	AVG	SD	AVG	SD
13.048	3.022	3.285	0.674	13.048	3.022	3.285	0.674

Table 42: Composition of aliphatic lipids in cuticular waxes in [µg/cm²].

	Bowman		*cer*-ye.582		*cer*-ye.792		*cer*-ye.1395	
	AVG	SD	AVG	SD	AVG	SD	AVG	SD
Alkanes	0.099	0.021	0.155	0.029	0.111	0.045	0.105	0.024
Acids	0.203	0.071	0.157	0.050	0.092	0.034	0.102	0.085
Alcohols	10.545	2.222	2.184	0.542	2.037	0.594	1.666	0.863
Aldehydes	0.818	0.351	0.169	0.036	0.112	0.027	0.121	0.085
Esters	1.384	0.372	0.621	0.059	0.709	0.013	0.666	0.249

Table 43: Chain length composition of cuticular waxes in [µg/cm²].

	Bowman		*cer*-ye.582		*cer*-ye.792		*cer*-ye.1395	
	AVG	SD	AVG	SD	AVG	SD	AVG	SD
C_{20}	0.000	0.000	0.000	0.000	0.000	0.000	0.000	0.000
C_{22}	0.051	0.014	0.015	0.014	0.023	0.032	0.010	0.009
C_{24}	0.290	0.066	0.083	0.052	0.048	0.014	0.043	0.019
C_{25}	0.019	0.012	0.013	0.013	-	-	0.018	0.025
C_{26}	10.843	2.416	2.099	0.493	1.892	0.539	1.587	0.878
C_{27}	0.077	0.018	0.086	0.009	0.093	0.006	0.073	0.033
C_{28}	0.207	0.142	0.140	0.082	0.144	0.039	0.133	0.089
C_{30}	0.080	0.022	0.074	0.031	0.042	0.015	0.026	0.014
C_{33}	0.099	0.021	0.155	0.029	0.111	0.045	0.105	0.024
C_{38}	0.079	0.067	0.034	0.021	0.013	0.006	0.137	0.167
C_{40}	0.024	0.005	0.018	0.002	0.020	0.001	0.011	0.008
C_{42}	0.163	0.042	0.169	0.010	0.215	0.015	0.150	0.043
C_{44}	0.256	0.079	0.140	0.008	0.164	0.005	0.119	0.037
C_{46}	0.466	0.119	0.114	0.009	0.131	0.012	0.114	0.033
C_{48}	0.396	0.099	0.146	0.016	0.167	0.010	0.136	0.047

7.3.7 Expression of CER-ZA in wax deficient *A. thaliana cer*4-3

Table 44: Total amount of cuticular waxes from Arabidopsis Col-0, *cer*4-3 and four independent lines of *cer*4-3+CER-ZA in [µg/cm²].

				*cer*4-3+CER-ZA							
Col-0		*cer*4-3		Line 1		Line 2		Line 3		Line 4	
AVG	SD	AVG	SD	AVG	SD	AVG	SD	AVG	SD	AVG	SD
13.92	0.56	11.48	0.32	14.55	1.63	16.89	1.26	14.03	1.84	16.52	1.56

Table 45: Composition of aliphatic lipids in cuticular waxes from Arabidopsis Col-0, *cer*4-3 and four independent lines of *cer*4-3+CER-ZA in [µg/cm²].

					*cer*4-3+CER-ZA							
	Col-0		*cer4-3*		Line 1		Line 2		Line 3		Line 4	
	AVG	SD	AVG	SD	AVG	SD	AVG	SD	AVG	SD	AVG	SD
Alkanes	5.29	0.20	5.06	0.12	6.71	0.57	7.43	0.67	6.42	0.97	7.14	0.70
Acids	0.42	0.05	0.39	0.08	0.47	0.03	0.85	0.04	0.51	0.07	0.79	0.08
Ketones	1.48	0.11	1.35	0.02	1.57	0.14	1.72	0.16	1.42	0.20	1.65	0.17
Aldehydes	1.05	0.09	1.15	0.34	1.53	0.58	2.40	0.06	1.80	0.24	2.60	0.24
Esters	0.44	0.07	0.21	0.03	0.35	0.06	0.33	0.05	0.31	0.08	0.30	0.03
Triterpenoids	0.23	0.01	0.14	0.02	0.19	0.04	0.20	0.02	0.20	0.03	0.21	0.02
2-Alcohols	3.57	0.23	3.03	0.11	3.49	0.35	2.97	1.51	3.11	0.44	2.87	1.47
1-Alcohols	1.45	0.12	0.15	0.01	0.25	0.03	0.25	0.02	0.27	0.04	0.24	0.05

Table 46: Chain length composition in cuticular waxes from Col-0 and *cer*4-3 in [µg/cm²].

	Col-0		*cer4-3*	
	AVG	SD	AVG	SD
C_{22}	0.02	0.01	0.03	0.01
C_{24}	0.05	0.01	0.01	0.00
C_{26}	0.44	0.04	0.10	0.02
C_{27}	0.10	0.01	0.05	0.01
C_{28}	0.98	0.07	0.33	0.06
C_{29}	10.17	0.52	9.29	0.24
C_{30}	1.34	0.14	1.17	0.35
C_{31}	0.15	0.02	0.16	0.01
C_{38}	0.01	0.00	0.00	0.00
C_{40}	0.03	0.01	0.01	0.00
C_{42}	0.11	0.01	0.03	0.00
C_{44}	0.11	0.04	0.03	0.01
C_{46}	0.11	0.03	0.11	0.03
C_{48}	0.08	0.01	0.04	0.01
Cyclic	0.23	0.01	0.14	0.02

Table 47: Chain length composition in cuticular waxes from four independent *cer*4-3+CER-ZA lines in [µg/cm²].

	*cer*4-3+CER-ZA							
	Line 1		Line 2		Line 3		Line 4	
	AVG	SD	AVG	SD	AVG	SD	AVG	SD
C_{22}	0.03	0.01	0.02	0.00	0.01	0.01	0.02	0.01
C_{24}	0.02	0.00	0.02	0.00	0.02	0.00	0.02	0.01
C_{26}	0.18	0.02	0.16	0.00	0.15	0.03	0.21	0.05
C_{27}	0.08	0.01	0.12	0.01	0.09	0.01	0.11	0.01
C_{28}	0.45	0.12	0.71	0.01	0.54	0.07	0.70	0.10
C_{29}	11.63	1.05	12.70	1.14	10.79	1.57	12.20	1.20
C_{30}	1.48	0.49	2.46	0.06	1.77	0.14	2.55	0.23
C_{31}	0.15	0.01	0.20	0.03	0.15	0.04	0.20	0.03
C_{38}	0.00	0.00	0.00	0.00	0.00	0.00	0.00	0.00
C_{40}	0.01	0.00	0.01	0.00	0.01	0.00	0.02	0.00
C_{42}	0.07	0.01	0.06	0.00	0.07	0.01	0.06	0.01
C_{44}	0.06	0.01	0.06	0.01	0.05	0.01	0.07	0.02
C_{46}	0.17	0.03	0.15	0.02	0.13	0.03	0.10	0.05
C_{48}	0.04	0.01	0.04	0.01	0.05	0.03	0.05	0.03
Cyclic	0.19	0.04	0.20	0.02	0.20	0.03	0.21	0.02

7.3.8 Expression of CER-ZA in *E. coli* and *S. cerevisiae*

Table 48: Quantification of alcohols after the expression of CER-ZA in *E. coli*. Averages and standard deviations were calculated in nmol per 100 mL culture with an OD600 = 1.

	Control cells		CER-ZA expressing cells	
Chain length	AVG	SD	AVG	SD
14:0-ol	n. D.	-	3.548	1.163
16:0-ol	n. D.	-	16.119	5.914
18:0-ol	3.490	1.902	7.510	2.457
Total amount	3.490	1.902	27.176	3.605

Table 49: Quantification of alcohols after the expression of CER-ZA in *S. cerevisiae*. Averages and standard deviations are presented in nmol per 100 mL culture of an OD600 = 1.

	Control		CER-ZA expressing cells	
Chain length	AVG	SD	AVG	SD
16:0-ol	0.041	0.036	0.271	0.091
18:0-ol	0.217	0.158	0.450	0.206
26:0-ol	0.108	0.115	1.012	0.220
Total amount	0.366	0.071	1.733	0.423

7.3.9 Leaf water permeability measurement

Table 50: Calculated predominant stomatal transpiration measured with a porometer from five replicates each.

	Adaxial leaf site		Abaxial leaf site	
Genotype	AVG	SD	AVG	SD
Bowman	4.59×10^{-8}	1.07×10^{-8}	1.61×10^{-8}	6.07×10^{-9}
cer-za.227	4.69×10^{-8}	6.14×10^{-9}	1.03×10^{-8}	4.10×10^{-9}
cer-ye.267	3.17×10^{-8}	9.34×10^{-9}	1.10×10^{-8}	5.80×10^{-9}

7.3.10 Photosynthetic inhibition by metribuzin treatment

Table 51: Data points of the photosynthetic quantum yield, Y(II), measured in five minutes intervals over 90 minutes after application of 50 µmol metribuzin dissolved in 0.1% Brij 4.

t	Bowman		*cer*-za.227		*cer*-ye.267	
[min]	AVG	SD	AVG	SD	AVG	SD
0	0.711	0.070	0.711	0.026	0.729	0.020
5	0.687	0.070	0.648	0.086	0.597	0.095
10	0.617	0.054	0.577	0.096	0.343	0.055
15	0.547	0.051	0.536	0.098	0.259	0.086
20	0.501	0.055	0.508	0.077	0.234	0.089
25	0.470	0.062	0.493	0.074	0.227	0.098
30	0.472	0.053	0.488	0.068	0.248	0.081
35	0.474	0.049	0.497	0.054	0.260	0.084
40	0.462	0.054	0.496	0.056	0.272	0.094
45	0.468	0.037	0.501	0.063	0.301	0.082
50	0.477	0.036	0.503	0.055	0.310	0.083
55	0.479	0.031	0.509	0.055	0.326	0.085
60	0.490	0.027	0.519	0.052	0.350	0.083
65	0.492	0.029	0.522	0.051	0.351	0.087
70	0.508	0.023	0.525	0.051	0.356	0.088
75	0.509	0.026	0.530	0.049	0.369	0.081
80	0.513	0.022	0.536	0.050	0.378	0.097
85	0.526	0.021	0.542	0.047	0.392	0.074
90	0.526	0.019	0.544	0.047	0.397	0.075

7.3.11 Sequences for the calculation of phylogenetic trees

7.3.11.1 CER-ZA

Table 52: Sequences used for the calculation of a Maximum Likelihood tree. Representatives of monocot and dicot plants were chosen for the phylogenetic tree. Accession numbers were extracted from the National Center for Biotechnology Information.

Species	Sequence ID	Accession Number
Hordeum vulgare	CER-ZA	KAE8808760.1
Arabidopsis thaliana	*At*FAR1	NP_197642.1
Arabidopsis thaliana	*At*FAR2	NP_187805.1
Arabidopsis thaliana	*At*FAR3	NC_003075.7
Arabidopsis thaliana	*At*FAR4	NP_190040.3
Arabidopsis thaliana	*At*FAR5	NC_003074.8
Arabidopsis thaliana	*At*FAR6	OAP02756.1
Arabidopsis thaliana	*At*FAR7	NC_003076.8
Arabidopsis thaliana	*At*FAR8	NC_003074.8
Arabidopsis thaliana	*At*CER1	AAC24374.1
Arabidopsis thaliana	*At*CER3	CAA65198.1
Arabidopsis thaliana	*At*MAH1	OAP19740.1
Arabidopsis thaliana	*At*WSD1	OAO89882.1
Oryza sativa	*Os*FAR1	NC_029262.1
Oryza sativa	*Os*FAR2	XM_015776819.2
Oryza sativa	*Os*FAR3	XM_015779646.2
Oryza sativa	*Os*CER1	AF143746.1
Tritium aestivum	*Ta*FAR1	ACK44495.1
Tritium aestivum	*Ta*FAR2	KJ675403.1
Tritium aestivum	*Ta*FAR3	AMR68893.1
Tritium aestivum	*Ta*FAR4	AMR68894.1
Tritium aestivum	*Ta*FAR5	AID81988.1
Tritium aestivum	*Ta*CER1	
Camelina sativa	*Cs*CER3	AAD38039.1
Camelina sativa	*Cs*CER4	AAD38039.1
Camelina sativa	*Cs*MAH1	AAD38039.1
Simmondsia chinensis	*Sc*FAR	AAD38039.1
Populus tomentosa	*Pt*FAR3	AEV53412.1
Euglena gracilis	*Eg*FAR	ADI60057.1

Table 53: 21 paralogous sequences to *HORVU5Hr1G089230* were annotated by UniProt/EMBL.

Gene Name	Transcript	Target ID	Query ID
HORVU3Hr1G097450	*HORVU3Hr1G097450.1*	80.61 %	79.32 %
HORVU6Hr1G001280	*HORVU6Hr1G001280.1*	44.25 %	46.39 %
HORVU2Hr1G127270	*HORVU2Hr1G127270.2*	46.48 %	47.79 %
HORVU4Hr1G001450	*HORVU4Hr1G001450.6*	40.82 %	50.00 %
HORVU4Hr1G001560	*HORVU4Hr1G001560.1*	52.63 %	14.06 %
HORVU0Hr1G029110	*HORVU0Hr1G029110.1*	46.29 %	47.59 %
HORVU7Hr1G092230	*HORVU7Hr1G092230.4*	53.24 %	52.81 %
HORVU7Hr1G020270	*HORVU7Hr1G020270.2*	49.33 %	51.61 %
HORVU5Hr1G124820	*HORVU5Hr1G124820.2*	52.30 %	52.41 %
HORVU3Hr1G002040	*HORVU3Hr1G002040.1*	50.40 %	50.40 %
HORVU7Hr1G023320	*HORVU7Hr1G023320.1*	47.80 %	45.78 %
HORVU3Hr1G002120	*HORVU3Hr1G002120.2*	49.01 %	49.80 %
HORVU2Hr1G112790	*HORVU2Hr1G112790.3*	48.80 %	48.80 %
HORVU3Hr1G002090	*HORVU3Hr1G002090.4*	49.90 %	51.00 %
HORVU3Hr1G002170	*HORVU3Hr1G002170.1*	50.68 %	52.21 %
HORVU1Hr1G094400	*HORVU1Hr1G094400.3*	42.54 %	46.39 %
HORVU4Hr1G001550	*HORVU4Hr1G001550.3*	43.08 %	33.13 %
HORVU4Hr1G087110	*HORVU4Hr1G087110.9*	48.60 %	52.21 %
HORVU1Hr1G000190	*HORVU1Hr1G000190.3*	46.64 %	48.80 %
HORVU2Hr1G086620	*HORVU2Hr1G086620.1*	33.47 %	16.06 %
HORVU4Hr1G074700	*HORVU4Hr1G074700.1*	20.97 %	28.51 %

7.3.11.2 CER-YE

Table 54: Currently annotated 33 members of the KCS gene family in *H. vulgare* used for the calculation of phylogenetic trees.

Gene	Loci	Transcript	Annotated by…
KCS1	*HORVU4Hr1G063420*	*HORVU4Hr1G063420.1*	Tong *et al.* 2020; Li *et al.* 2018
KCS2	*HORVU5Hr1G056870*	*HORVU5Hr1G056870.5*	Tong *et al.* 2020
KCS3	*HORVU1Hr1G040420*	*HORVU1Hr1G040420.4*	Tong *et al.* 2020
KCS4	*HORVU7Hr1G022690*	*HORVU7Hr1G022690.1*	Tong *et al.* 2020
KCS5	*HORVU7Hr1G022610*	*HORVU7Hr1G022610.1*	Tong *et al.* 2020
KCS6	*HORVU4Hr1G067340*	*HORVU4Hr1G067340.2*	Tong *et al.* 2020
KCS7	*HORVU2Hr1G122150*	*HORVU2Hr1G122150.1*	Tong *et al.* 2020
KCS8	*HORVU1Hr1G086360*	*HORVU1Hr1G086360.3*	Tong *et al.* 2020
KCS9	*HORVU7Hr1G018420*	*HORVU7Hr1G018420.1*	Tong *et al.* 2020
KCS10	*HORVU1Hr1G089710*	*HORVU1Hr1G089710.3*	Tong *et al.* 2020
KCS11	*HORVU6Hr1G073300*	*HORVU6Hr1G073300.1*	Tong *et al.* 2020
KCS12	*HORVU1Hr1G086760*	*HORVU1Hr1G086760.1*	Tong *et al.* 2020
KCS13	*HORVU7Hr1G006910*	*HORVU7Hr1G006910.1*	Tong *et al.* 2020
KCS14	*HORVU0Hr1G038430*	*HORVU0Hr1G038430.1*	Tong *et al.* 2020
KCS16	*HORVU3Hr1G069880*	*HORVU3Hr1G069880.2*	Tong *et al.* 2020
KCS17	*HORVU5Hr1G122360*	*HORVU5Hr1G122360.1*	Tong *et al.* 2020
KCS18	*HORVU5Hr1G087530*	*HORVU5Hr1G087530.1*	Tong *et al.* 2020
KCS19	*HORVU3Hr1G097570*	*HORVU3Hr1G097570.1*	Tong *et al.* 2020
KCS20	*HORVU6Hr1G082270*	*HORVU6Hr1G082270.1*	Tong *et al.* 2020
KCS21	*HORVU7Hr1G023280*	*HORVU7Hr1G023280.1*	Tong *et al.* 2020
KCS22	*HORVU7Hr1G023280*	*HORVU7Hr1G023280.1*	Tong *et al.* 2020
KCS23	*HORVU7Hr1G022780*	*HORVU7Hr1G022780.1*	Tong *et al.* 2020
KCS24	*HORVU2Hr1G112840*	*HORVU2Hr1G112840.1*	Tong *et al.* 2020
KCS25	*HORVU7Hr1G030880*	*HORVU7Hr1G030880.1*	Tong *et al.* 2020
KCS26	*HORVU7Hr1G042050*	*HORVU7Hr1G042050.1*	Tong *et al.* 2020
KCS27	*HORVU6Hr1G004830*	*HORVU6Hr1G004830.1*	Tong *et al.* 2020
KCS28	*HORVU7Hr1G042040*	*HORVU7Hr1G042040.1*	Tong *et al.* 2020
KCS29	*HORVU6Hr1G094160*	*HORVU6Hr1G094160.2*	Tong *et al.* 2020
KCS30	*HORVU1Hr1G090730*	*HORVU1Hr1G090730.1*	Tong *et al.* 2020
KCS31	*HORVU1Hr1G090730*	*HORVU1Hr1G090730.1*	Tong *et al.* 2020
KCS32	*HORVU6Hr1G036950*	*HORVU6Hr1G036950.4*	Tong *et al.* 2020
KCS33	*HORVU4Hr1G073840*	*HORVU4Hr1G073840.2*	Tong *et al.* 2020
KCS34	*HORVU7Hr1G023530*	*HORVU7Hr1G023530.2*	Tong *et al.* 2020

Table 55: Currently annotated 21 members of the KCS gene family in *A. thaliana* used for the calculation of phylogenetic trees.

Gene	Loci	Transcript	Annotated by…
KCS1	*AT1G01120*	*AT1G01120.1*	Joubes *et al.* 2008
KCS2	*AT1G04220*	*AT1G04220.1*	Joubes *et al.* 2008
KCS3	*AT1G07720*	*AT1G07720.1*	Joubes *et al.* 2008
KCS4	*AT1G19440*	*AT1G19440.1*	Joubes *et al.* 2008
KCS5	*AT1G25450*	*AT1G25450.1*	Joubes *et al.* 2008
KCS6	*AT1G68530*	*AT1G68530.1*	Joubes *et al.* 2008
KCS7	*AT1G71160*	*AT1G71160.1*	Joubes *et al.* 2008
KCS8	*AT2G15090*	*AT2G15090.1*	Joubes *et al.* 2008
KCS9	*AT2G16280*	*AT2G16280.1*	Joubes *et al.* 2008
KCS10	*AT2G26250*	*AT2G26250.1*	Joubes *et al.* 2008
KCS11	*AT2G26640*	*AT2G26640.1*	Joubes *et al.* 2008
KCS12	*AT2G28630*	*AT2G28630.1*	Joubes *et al.* 2008
KCS13	*AT2G46720*	*AT2G46720.1*	Joubes *et al.* 2008
KCS14	*AT3G10280*	*AT3G10280.1*	Joubes *et al.* 2008
KCS15	*AT3G52160*	*AT3G52160.2*	Joubes *et al.* 2008
KCS16	*AT4G34250*	*AT4G34250.1*	Joubes *et al.* 2008
KCS17	*AT4G34510*	*AT4G34510.1*	Joubes *et al.* 2008
KCS18	*AT4G34520*	*AT4G34520.1*	Joubes *et al.* 2008
KCS19	*AT5G04530*	*AT5G04530.1*	Joubes *et al.* 2008
KCS20	*AT5G43760*	*AT5G43760.1*	Joubes *et al.* 2008
KCS21	*AT5G49070*	*AT5G49070.1*	Joubes *et al.* 2008

7.4 List of tables

7.5 List of figures